Myocardial infarct healing : rupture and remodeling

Myocardial Infarct Healing

Rupture and Remodeling

ISBN 978 90 5278 817 3
Design en Layout: Monique van den Borne
Printing: Datawyse | Universitaire Pers Maastricht

Myocardial Infarct Healing

Rupture and Remodeling

PROEFSCHRIFT

ter verkrijging van de graad van doctor aan de Universiteit Maastricht,
op gezag van de Rector Magnificus, Prof. mr G.P.M.F. Mols
volgens het besluit van het College van Decanen,
in het openbaar te verdedigen
op vrijdag 17 april 2009 om 14.00 uur

door

Susanna Wilhelmina Maria van den Borne
geboren op 14 februari 1976 te Tilburg

UNIVERSITAIRE PERS MAASTRICHT

Promotores
Prof. dr. J.F.M. Smits
Prof. dr. M.J.A.P. Daemen

Copromotor
Dr. W.M. Blankesteijn

Beoordelingscommissie
Prof. dr. H.J.G.M. Crijns (voorzitter)
Prof. dr. D.J.G.M. Duncker, Erasmus Universiteit, Rotterdam
Prof. dr. J.M.A. van Engelshoven
Prof. dr. F.C.S. Ramaekers
Prof. dr. F.M.A.C. van Roy, Universiteit Gent, België

Financial support by the Netherlands Heart Foundation and by Stichting Hartsvrienden Rescar for the publication of this thesis is gratefully acknowledged.

Additional support was granted by the J.E. Jurriaanse Stichting, Schering-Plough, Pfizer, AstraZeneca, Merck Sharp & Dohme, Bristol Myers Squibb, PharmaTarget and Teva Nederland.

CONTENTS

1 General Introduction

INTRODUCTION

Cardiovascular diseases comprise the most important cause of morbidity and mortality worldwide.[1] They are common in developing and developed nations and afflict both men and women. Most notably, atherosclerosis, leading to ischemic heart disease, ventricular remodeling and heart failure, accounts for the major share of cardiovascular diseases. The increasing life expectancy of the population contributes to the increased burden. In addition, advances in diagnosis and treatment of various cardiovascular diseases have improved the survival of patients with residual myocardial dysfunction, thereby increasing prevalence of manifest heart failure. Most available treatment strategies alleviate symptoms but do not cure, let alone prevent, ischemic heart disease. Major challenges for cardiovascular research in the ensuing years will be to develop strategies for early recognition of individuals at risk of ischemic heart disease and its complications so that early prevention and treatment measures may be initiated.

The structure of the heart

The heart consists of cardiomyocytes and non-myocytes. The cardiomyocytes account for approximately 70% of the volume of the myocardium, but constitute only about 33% of the cell population.[2] The non-myocytes consist of several different cell types like fibroblasts, endothelial cells and vascular smooth muscle cells and are found in the cardiac interstitium.

The extracellular matrix of the heart

The structural backbone of the heart is provided by the extracellular matrix comprising various proteins, such as collagens. Type I, III and VI collagen are present in and around the coronary arteries and within the interstitium; type IV collagen is present in the basement membrane surrounding the cardiomyocytes and other cells, such as endothelial cells and pericytes. Collagen is produced by (myo-)fibroblasts as soluble pro-collagen, which crosslinks extracellularly to mature collagen. In a normal adult, interstitial collagen makes up to 1–2% of the volume of the heart.[3] Under pathological conditions, such as after myocardial infarction (MI), in addition to the replacement fibrosis (infarct wound healing), there is excessive deposition of interstitial collagen in the infarct border and the remote myocardium. The increased interstitial fibrosis may constitute up to 10% of the volume of the heart.[4]

The wound healing process after myocardial infarction

Myocardial infarction usually results from coronary atherosclerosis with superimposed coronary thrombosis, which leads to myocardial necrosis involving the full (transmural) or partial ventricular wall thickness subtended by the affected coronary artery.[5]

The wound healing after myocardial infarction mimics the wound healing processes observed in other tissues, such as the skin. However, cardiac wound healing has some distinctive features. The adult cardiomyocytes are terminally differentiated cells that have lost, at least to a great extent, the capacity to divide and regenerate.[6] Therefore, adequate cardiac wound healing is mainly determined by the factors that control the formation of granulation tissue. Furthermore, there is the rhythmic contraction of the non-infarcted myocardium, which imposes a cyclic stretch on the healing wound. In addition, the architectural changes in the infarct are tightly controlled in order to maintain cardiac function after infarction.

The process of cardiac wound healing after myocardial infarction can be divided into four overlapping phases, which are schematically represented in Figure 1.1. Phase 1 is characterized by the death of cardiomyocytes, either by apoptosis, necrosis or both. Various intracellular macromolecules are released into the bloodstream, for example creatine kinase (CK), CK isoenzymes and cardiac-specific troponins.[5] Elevated circulating levels of these cardiomyocyte biomarkers can be measured as indicators of the severity of myocardial damage.

Phase 2 of the healing process embodies an early inflammatory response. Since the majority of the apoptotic cells after infarction cannot be phagocytosed by neighboring cells, secondary necrosis occurs from 12 hours to 4 days after infarction,[7] stimulating the influx of inflammatory cells. One of the first features of the inflammatory response is activation of the complement system, and release of several cytokines, such as interleukins-6 and -8.[8-10] Within 6–8 hours after the onset of myocardial infarction neutrophilic granulocytes (PMN) migrate into the infarcted area, reaching their peak number within 24–48 hours after infarction. The granulocytes help to remove the dead cardiomyocytes. Granulocyte infiltration is followed by the influx of other inflammatory cells, like lymphocytes, plasma cells and macrophages at 3-7 days post-MI.[3]

Phase 3 of the cardiac wound healing process constitutes the formation of granulation tissue. Simultaneously with the activation of collagen synthesis, collagen degradation is activated. In the first week after myocardial infarction, specific matrix metalloproteinases (MMP) are activated, that cleave interstitial collagens.[11, 12] Increased collagenolytic activity can result in loss of structural support, distortion of tissue architecture, reduction of cardiac stiffness, wall thinning and even rupture of the myocardium. Two to three days after infarction, new extracellular matrix proteins are being deposited, first in the infarct border zone and later in the infarct center. The granulation tissue increases the tensile strength of the infarct and prevents cardiac rupture. During this phase, fibrin is deposited followed by other extracellular matrix proteins, e.g. fibronectin and tenascin.[13, 14] Within approximately one week after infarction, myofibroblasts

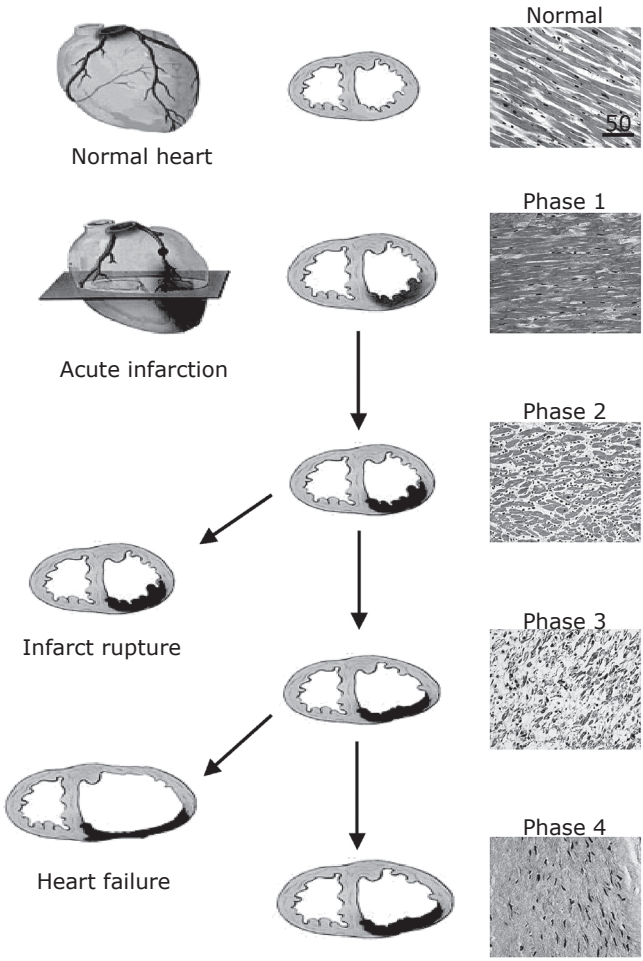

Figure 1.1 The different phases of wound healing post-myocardial infarction

The top row shows a normal heart, a transverse heart section, and associated normal heart histology. Acute myocardial infarction occurs when there is occlusion of one of the coronary arteries (occlusion of the left anterior descending coronary artery is represented by a black dot over the artery). The first phase of the wound healing process (12-18 hours post-infarction) is characterized by eosinophilia and nuclear pyknosis (second row, far right panel). Between days 1 and 4 post infarction the nuclei may disappear and polymorphonuclear leukocytes infiltrate into the infarcted area with removal of necrotic fibers (third row, phase 2). At this time, when the infarct wall is weakest, the myocardium may rupture, often leading to sudden death. In the hearts that do not rupture, there is matrix remodeling and granulation tissue formation that by 3 weeks includes removal of necrotic debris, mononuclear cell infiltration, increased numbers of fibroblasts and capillaries, and an increase in collagen deposition (fourth row, phase 3). After three months, the infarcted region thins and is replaced by scar tissue (bottom row, phase 4). The remaining viable myocardium may remodel and become dysfunctional, leading to heart failure. Scale bar length is indicated in micrometers. Figure adapted from: E. Creemers and J. Cleutjens. For full color illustration, see page 152.

surround the infarcted area, producing interstitial collagens. The peak of type III collagen production is followed by a lower and slower developing peak of type I collagen. Complete collagen cross-linking takes another couple of weeks to occur. Collagen turnover in a normal adult non-infarcted heart may take approximately 4 months to complete, but may be much faster in the early phase of cardiac wound healing in the infarcted zone.[15]

Granulation tissue is also characterized by the presence of many blood vessels, starting to appear within a few days after infarction. The new blood vessels are derived from pre-existent blood vessels (angiogenesis) or from endothelial progenitor cells that migrate from the border zone into the infarct (neovascularization).[3] A 2–3 week old granulation tissue in an infarcted region is characterized as a cell-rich tissue, containing (partly) cross-linked interstitial collagens, macrophages, blood vessels, and (myo) fibroblasts.

Phase 4 of cardiac wound healing is characterized by the formation of scar tissue. During this phase, cells disappear from the wound and collagen becomes almost completely cross-linked. The cardiac scar tissue has a permanent nature because of the lack of cardiomyocyte regeneration. A well healed myocardial infarct consists of a strong replacement scar and little interstitial fibrosis in the non-infarcted areas. However, the loss of functional myocardium creates additional biomechanical stress on the remaining viable heart muscle. This can lead to adverse myocardial remodeling leading to dilatation of the heart, thinning of the walls of the ventricles and eventually heart failure.[16] The above mentioned time line of post-infarction wound healing is generalized for humans, and is observed to be significantly accelerated in smaller animals, like rats and mice.[3]

Changes in the non-infarcted myocardium after myocardial infarction

As mentioned above, structural changes after infarction are not limited to the infarcted area, but also extend into the non-infarcted myocardium. Although the changes in the non-infarcted region are not as outspoken as in the infarct area, they contribute significantly to the ventricular remodeling. Changes in the non-infarcted myocardium include hypertrophy of the cardiomyocytes, growth of the capillary network, and an increase in interstitial collagen. Myocardial hypertrophy starts within several days after infarction and cardiomyocyte volume may increase by 110% in humans.[17] Capillary endothelial cells proliferate, but usually not enough to fully compensate for the extent of cardiomyocyte hypertrophy; this results in an increase of oxygen diffusion distance and hence relative ischemia. Besides heart muscle and endothelial cells, changes in the interstitial collagen content are apparent in the non-infarcted ventricle. As mentioned above, interstitial collagens double within 1 week after infarction.[4] Similar to the infarct zone, type III collagen deposition precedes type I collagen. The increase in interstitial collagen deposition may be beneficial to the heart in that

it helps to prevent dilatation. Increased amounts of interstitial collagens will, on the other hand, increase the stiffness of the heart and result in a reduced cardiac function.[18]

Major complications of infarct healing

The process of myocardial infarct healing is very complex and can lead to several complications. In this thesis we will focus on two common complications of myocardial infarction, associated with the healing process. The first complication is myocardial infarct rupture which occurs early, usually within a week after MI. The second complication is heart failure post-MI, a complication that typically occurs in a later stage (months to years) after MI.

1. Infarct Rupture

Myocardial infarct rupture is a usually lethal complication of acute myocardial infarction for which no adequate treatment is available. The overall incidence of infarct rupture is approximately 2-7%; however, infarct rupture accounts for 15% of the in-hospital mortality post-MI.[19] The acute presentation of myocardial infarct rupture of the ventricular free wall results from the subsequent tamponade that develops. Symptoms are severe, persistent chest pain, hypotension, restlessness and agitation, pulsus paradoxus, cardiogenic shock and eventually electro-mechanical dissociation.[20] Infarct rupture is associated with increasing age, transmural infarction, the first episode of myocardial infarction and the absence of a history of ischemic heart disease.[19] Almost 80% of free wall ruptures occur within the first week after the onset of myocardial infarction.[21] This period corresponds well with healing phase 2, in which there are dead cardiomyocytes in the infarct area without adequate replacement fibrosis.[3]

Research in animal models demonstrated that inhibition of plasminogen activation[22, 23] or targeted deletion of MMP-2[24] or MMP-9[23] reduced the influx of inflammatory cells in the infarct area and reduced the incidence of infarct rupture. Sheikh et al.[25] have demonstrated an important role for cellular adhesion proteins in the development of rupture. They described that αE-catenin conditional knockout mice showed an increased incidence of cardiac rupture post-MI.[25] However, the molecular mechanisms involved in infarct rupture in humans have not been described so far.

2. Heart Failure

A more frequent complication of myocardial infarction associated with adverse remodeling is heart failure. Heart failure is the condition in which the heart is unable to maintain sufficient cardiac output to meet the metabolic and oxygen demands of the peripheral tissue.[26] One of the most important causes of heart failure is myocardial infarction. Due to the improved survival post-MI, more and more people are at risk to develop heart failure. Within six years of the

clinical event of acute myocardial infarction, 22% of male and 46% of female patients develop heart failure.[27] The loss of ventricular muscle during the episode of acute ischemic heart disease, and the complex architectural alterations involving both the infarcted and non-infarcted myocardium contribute to the evolution of heart failure. Dilatation and infarct expansion are the most prominent changes in the infarct region,[28] and can lead to both systolic (decreased contraction) and diastolic (decreased relaxation) dysfunction.[29] The ventricular dilatation may initially serve as a compensatory mechanism to maintain stroke volume after the loss of contractile tissue. However, this precarious balance can be exceeded in which increased cavity volume with insufficient compensatory hypertrophy results in loading conditions promoting further enlargement and dysfunction. Patients showing extensive infarct expansion after myocardial infarction are more likely to develop heart failure.[30] Recently a role for myofibroblasts was proposed in the prevention of dilatation post-MI. Myofibroblasts have contractile properties and can persist in human infarcts for decades post-MI[13] and may prevent infarct expansion (see chapter 2).

Molecular imaging

Since heart failure is a progressive and invalidating disease for which no cure is available, it is of utmost importance to detect patients at risk of heart failure as early as possible before the clinical symptoms become manifest. That way, high risk patients can be treated aggressively in order to prevent the development of heart failure. The current imaging modalities, such as echocardiography and cardiovascular magnetic resonance imaging provide excellent information on left ventricular chamber dimensions and function post-MI (see Figure 1.2). However, these changes represent delayed, and often irreversible, consequences of remodeling. Furthermore, these techniques do not provide biological or molecular information on the development of heart failure or processes involved in the progression of heart failure.

Molecular imaging is broadly defined as the in vivo assessment of biological processes at the cellular and molecular level.[31] Recent insight in molecular mechanisms of disease on the one hand and imaging technologies on the other hand, have merged to allow monitoring of disease processes at their most fundamental levels, i.e. the molecular pathways involved. The impact of molecular imaging on ischemic heart disease can be envisioned in several ways. First, patients at risk for complications after MI may be identified before they develop symptoms. Furthermore, emerging molecular imaging tools can provide markers of therapy success or failure before clinical effects become manifest. Imaging will also provide important information on the optimal timing and dosing of drugs. So whereas conventional diagnostic imaging detects the outcome of disease processes, molecular imaging provides an opportunity to monitor the development of these processes in an early stage.

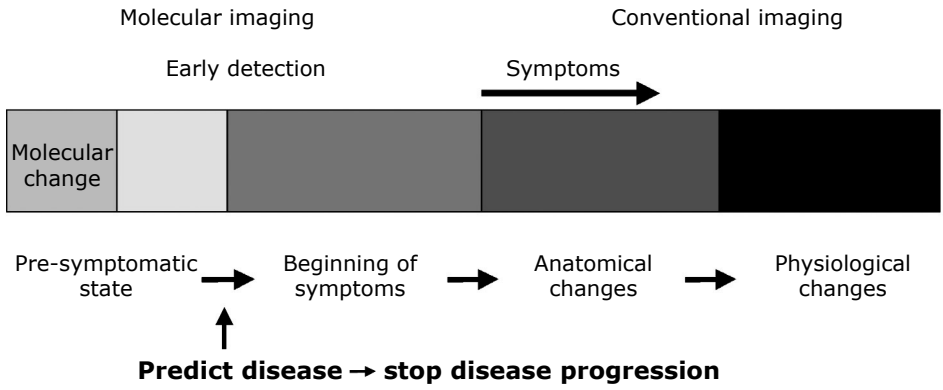

Figure 1.2 Molecular imaging versus conventional, anatomical imaging

Molecular imaging detects early changes on a molecular level, at a pre-symptomatic stage. Detecting molecular changes at an early stage can help in patient stratification and prevention of disease progression by earlier and more aggressive treatment. Moreover, molecular imaging may be a tool to study the effect of treatment. Conventional imaging detects anatomical changes, usually when the patient already has symptoms of the disease.

Outline of this thesis

As described in the previous paragraphs, the wound healing after myocardial infarction is a very complex process and if this does not occur properly, it can lead to several complications such as ventricular rupture in the early stage or adverse cardiac remodeling and heart failure in later stages post-MI.

The first hypothesis of the present thesis is that cell adhesion molecules, especially αE-catenin, and upregulation of MMP's are involved in the process of infarct rupture in humans. Second, we hypothesized that molecular imaging is a tool to study the process of heart failure and the effects of heart failure treatment post-MI.

Therefore, the aims of this thesis were twofold:

1. To study molecular mechanisms of myocardial infarct rupture post-MI, focusing on adhesion molecules and matrix metalloproteinases.
2. To study adverse myocardial remodeling and heart failure post-MI, using a molecular imaging tool.

We started with a study in a mouse model of myocardial infarction (Chapter 3), in which we studied infarct healing post-MI in 5 different strains frequently used in cardiovascular research. We studied incidence of rupture and heart failure and mechanisms contributing to these complications. Since it is known from literature that members of the matrix metalloproteinase family play an important role

in development of cardiac rupture post-MI in mouse models, we studied the role of these MMP's in post mortem heart samples of patients who died of cardiac rupture post-MI in chapter 4. Furthermore, we studied the role of the cellular adhesion proteins in cardiomyocytes and their role in cardiac rupture post-MI in chapter 5, and described a possible molecular mechanism that can lead to infarct rupture post-MI in humans.

Molecular imaging was used to visualize cardiac remodeling post-MI in an early stage in chapter 6. Furthermore, in chapter 7 we investigated whether this molecular imaging probe for heart failure can detect the efficacy of pharmacological intervention after myocardial infarction, thereby creating the possibility of following up on treatment and offering individualized therapy. In chapter 8, the findings of the experimental chapters are discussed and put into a broader context.

Molecular Imaging of Myocardial Remodeling: Targeting the Myofibroblasts

2

submitted

ABSTRACT

The adverse cardiac remodeling after acute myocardial infarction (MI) is an inexorable process that continues to occur even after the initial injury has abated and leads to development of heart failure (HF). Since 22% of men and 46% of women develop heart failure within 6 years after their first episode of MI, the importance of a better understanding of the process of remodeling after MI can hardly be overemphasized. For development of an effective preventive strategy it will be necessary to identify a subset of MI patients who are at higher risk for development of HF. It is expected that novel biomarkers and/or morphological and molecular imaging tools will offer this discriminatory prognostic information.

Adverse cardiac remodeling refers to geometric changes and inexorable functional deterioration, typically after acute myocardial infarction (MI).[32, 33] During the earlier healing phase, there is an efficient removal of necrotic debris and collagen is deposited; the replacement fibrosis initially supports ventricular function. This process involves a complex interplay among different cell types, including inflammatory cells, endothelial cells of newly forming blood vessels and fibroblast-like cells. With the passage of time, numerous changes also occur in myocytic and interstitial compartments in the unaffected remote myocardial regions. There is substantial myocyte hypertrophy and significant interstitial fibrosis that eventually contribute to functional compromise. The process of wound healing and adverse remodeling after MI has been studied predominantly in rodent models, wherein a coronary artery is surgically ligated for induction of MI. The development of transgenic and knockout mouse models has allowed the study of the effect of individual genes and pathogenetic cascades on the remodeling process.

Targeted imaging of various components of the infarct healing and remodeling process, in both injured and remote areas, should allow identification of susceptible post-MI patients before clinically manifest heart failure (HF). Such an imaging strategy may also provide important information on the efficacy and adequacy of therapeutic intervention. One of the prominent cell types in the healing infarct, useful for imaging purposes, is the myofibroblast. This cell type combines characteristics of fibroblasts (ECM production) with smooth muscle cells (contractile properties), and appears to play a crucial role in infarct healing and scar contraction. We will discuss the role of the myofibroblast in infarct healing, define molecular targets on myofibroblasts, and discuss the feasibility of molecular imaging of these cells for early detection and treatment of patients at risk for developing heart failure post-MI.

Origin, proliferation and characteristics of myocardial myofibroblasts

The wound healing process and fibroblast-like cells

The wound healing after MI involves a complex cascade of events. Cardiomyocyte death during acute injury invokes recruitment of inflammatory cells at the infarct border, which remove the necrotic cell debris by phagocytosis; and granulation tissue formation begins around the fourth day after MI, depending on the species. The granulation tissue consists of inflammatory cells, newly formed blood vessels for restoration of blood supply and fibroblast-like cells which deposit collagen. Eventually, this granulation tissue matures into a scar which is devoid of inflammatory cells but rich in extracellular matrix and fibroblast-like cells.[3] Tacitly, the scar tissue in the infarct has been perceived as a passive replacement for the lost cardiomyocytes with little biological activity. However, the scar tissue is now being increasingly recognized as an active playground

wherein ongoing activity of fibroblast-like cells maintain a process of collagen turnover and scar tissue contraction.[3, 34] The persistence of fibroblast-like cells in the infarct area is a prerequisite to ensure maintenance of the extracellular matrix in the scar, which is subjected to mechanical stress, and wear and tear in the beating heart. Since the fibroblasts-like cells remain for a long time in the myocardial scar tissue and their quantitative extent is proportional to the collagen deposition, such cells and their characteristics should comprise worthy targets for molecular imaging for the early detection of adverse remodeling.

Origin of myofibroblasts

The most intriguing fibroblasts-like cells in the granulation tissue are myofibroblasts, which may be derived from multiple sources (Figure 2.1).[35] In addition to pre-existing local fibroblasts which can differentiate into myofibroblasts, epithelial and endothelial cells may evolve into myofibroblasts by the process of epithelial-mesenchymal transition (EMT)[36] and endothelial-mesenchymal transition (EndMT).[37] Further, circulating fibroblast-like cells may be derived from bone marrow stem cells; these blood-borne mesenchymal stem cell progenitors have a fibroblast/myofibroblasts-like phenotype and are called fibrocytes.[38] It is believed that myofibroblasts of different origins participate with the resident mesenchymal cells in the reparative process, although the relative contribution of each of these populations remains to be established. There is a growing interest in dissecting the role of the various myofibroblast subpopulations in tissue regeneration and fibroproliferative diseases.[35]

Myofibroblast differentiation after MI

Under normal circumstances, the resident cardiac fibroblasts have no contractile microfilaments or stress fibers, and exhibit few or no actin-associated cell-to-cell and cell-to-matrix contacts and have minimal extracellular matrix production.[39] In aftermath of MI, fibroblasts are activated to differentiate as myofibroblasts, which converge into the damaged region and accelerate extracellular matrix protein synthesis, such as collagen, fibronectin and laminin[40] to replace necrotic cardiomyocytes by a scar.

An important stimulus for the phenotypic transition of fibroblast to myofibroblast is the change in the mechanical microenvironment. In intact tissue, fibroblasts are generally stress shielded within the framework of the cross linked extracellular matrix (ECM). When the architectural integrity is lost in the injured region, fibroblasts exposed to mechanical stress transform into proto-myofibroblasts.[41] The proto-myofibroblasts are characterized by the presence of stress fibers containing cytoplasmic β- and γ-actins. Subsequent exposure to transforming growth factor β1 (TGF-β1), and ED-A splice variant of fibronectin result in the evolution of proto-myofibroblasts into differentiated myofibroblasts.[42, 43] This fully differentiated cell type is characterized by the expression of alpha smooth

muscle actin (ASMA) and other smooth muscle differentiation markers.[44-46] Indeed, mice lacking the ED-A exon of fibronectin have been shown to display abnormal skin wound healing.[47]

The reconstructed ECM enables the repaired tissue to take over the mechanical load again and myofibroblasts disappear by apoptosis. Stress release is a potent promoter of myofibroblasts apoptosis in vivo.[48] Therefore, interrupting the mechanical feedback loop of myofibroblasts contraction and gradually increasing ECM tension may constitute a strategy to prevent excessive collagen deposition in the heart.

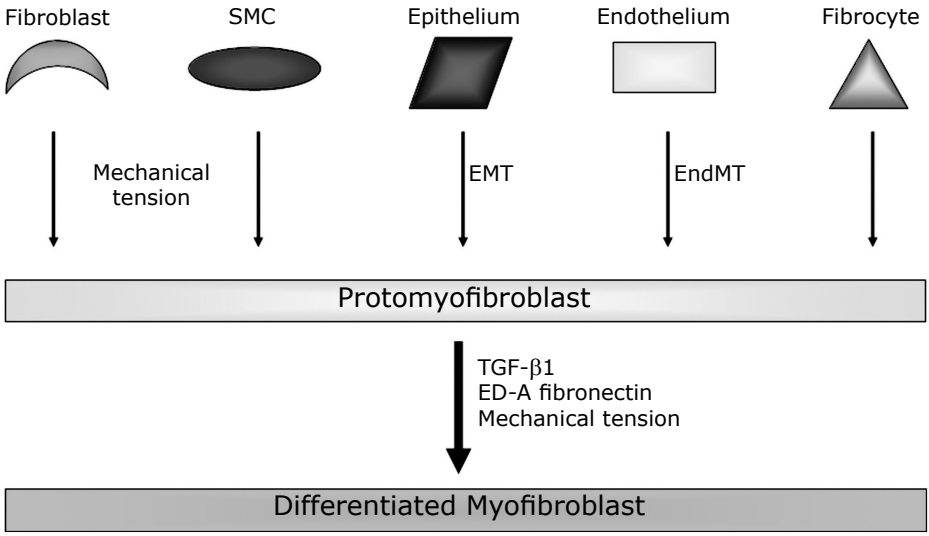

Figure 2.1 Origin of cardiac myofibroblasts

Myofibroblasts may be derived from different cell types. Besides the residential fibroblasts, they can also evolve from smooth muscle cells (SMC), epithelial and endothelial cells and blood-borne mesenchymal stem cell progenitors (called fibrocytes). Upon specific stimuli these cells can transform into proto-myofibroblasts, which in turn can differentiate into myofibroblasts in response to TGF-β1, ED-A fibronectin and mechanical stretch.

Contractile properties of myofibroblasts

During the skin wound healing, myofibroblasts align perpendicular to the wound rim and their contractile properties bring wound margins closer, a phenomenon which is know as wound contraction and which minimizes the scar size.[49] The reduction in size is stabilized by extracellular matrix deposition and subsequently the myofibroblasts disappear from the scar area.[44] This explains why a scar is generally considered to be an ECM-rich acellular entity. However, unlike wound healing in the skin,[50] myofibroblasts persist for up to 20 years even in healed

human infarcts[13] proposing a continued role for myofibroblasts for the stability of the infarct area which is under repetitive stress in a beating heart. Not only are the myofibroblasts persistent in the infarct scar, they continue to produce type I and III fibrillar collagen long after the scar tissue has replaced the necrotic myocytes indicative of their role in the stability of the scar.

The nature of contraction generated by the myofibroblasts is fundamentally distinct from that generated by the cardiomyocytes. Whereas myofibroblasts typically generate a sustained contraction resembling smooth muscle cells (such as in vasculature), cardiomyocytes contract and relax cyclically. Cardiomyocytes contract upon a stimulus from the cardiac conduction system, whereas the sustained contraction of myofibroblasts is modulated by circulating factors and neurohormones, like angiotensin II.[39] Given the high electrical resistance of the connective tissue in the infarct area,[51] smooth muscle-like cells, such as the myofibroblasts, are better suited for tonic contraction than cardiomyocytes; myofibroblast contraction is also more favorable energetically in relatively poorly-perfused scarred tissue.

ECM deposition, scar formation and adverse myocardial remodeling

Collagen deposition, replacement and interstitial fibrosis

It is well established that well-healed infarcts contain large amounts of ECM, which may occupy up to 80% of the infarct area.[3] On the other hand, collagen deposition in uninfarcted remote myocardial region occurs predominantly in the interstitium and contributes to ventricular stiffness and dysfunction. Various neurohumoral substances such as angiotensin II and transforming growth factor beta-1 (TGF-β1), which are preferentially overexpressed within the cardiomyocytes in the infarct border, traverse the common interstitial space and enhance collagen synthesis at sites distant from the MI. The fibrosis that develops over time in regions remote to the infarct represents the majority of connective tissue found in ischemic cardiomyopathy, and contributes to adverse structural remodeling in the failing human heart.[52] It seems reasonable to presume that an optimally healed infarcted heart comprises a strong ECM-rich replacement scar, but minimal remote fibrosis. Summarily, whereas resident interstitial fibroblasts are responsible for minimal normal collagen deposition in healthy myocardium, phenotypically transformed myofibroblasts are central to fibrogenesis at sites of remodeling after MI.

Molecular targets in myofibroblasts amenable to imaging

The myofibroblast as a target for molecular imaging of infarct healing

From the foregoing discussion, one can surmise that assessment of the extent of myofibroblast presence and collagen deposition would be a useful tool for identification of patients likely to develop heart failure after MI. In these pa-

tients, one would expect either a low amount of myofibroblasts in the infarct area (predicting poor ECM maintenance and excessive scar dilatation) or excessive amounts of fibroblasts in the uninjured parts of the heart (indicative for fibrosis of the non-infarcted myocardium). For development of useful imaging techniques within this context, it would be desirable to define moieties that are exclusively expressed by myofibroblasts. Although myofibroblasts express several markers, both intracellular and extracellular, unfortunately none of these targets are sufficiently exclusive to be highly specific for myofibroblasts.[53]

Worthy markers for identification of myofibroblasts

Myofibroblasts share the expression of ASMA with smooth muscle cells, which is an early differentiation marker of vascular smooth muscle cells (SMC) (see Figure 2.2). Unlike SMC however, myofibroblasts express relatively low amounts of smooth muscle myosin heavy chain and do not express smoothelin, a late differentiation marker.[48] Expression of various (trans) membrane moieties on myofibroblasts may, however, comprise better targets. The migration and differentiation of myofibroblasts are partially determined by expression of frizzled-2, a tissue polarity gene with a seven transmembrane structure.[54] Frizzled-2 is upregulated in the myofibroblasts during their migration into the infarct area. Frizzled-2 receptors are located on the plasma membrane and should be easily accessible, provided that specific ligands would be available (see Figure 2.2).

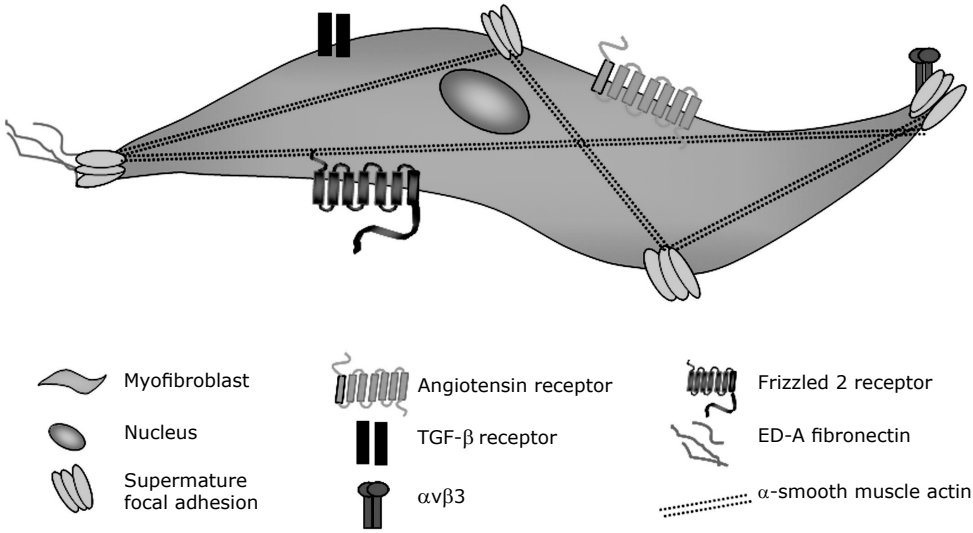

Figure 2.2 Potential targets for myofibroblast imaging

The myofibroblasts expresses several targets that might be of interest for molecular imaging. Angiotensin receptor, Frizzled-2 receptor and TGF-β receptors are reasonable candidates and easily accessible to targeting tracer molecules because of their extracellular localization. αvβ3 integrins are expressed in the supermature focal adhesions and may constitute yet another candidate. However, specificity and efficacy of these targets needs to be determined because these targets are presented on numerous other cell types. For full color illustration, see page 153.

Myofibroblasts also express renin, angiotensin converting enzyme (ACE) and angiotensin receptors.[51] Because renin and ACE are excreted, they are not very suitable as targets for molecular imaging. Angiotensin II perpetuates collagen synthesis by induction of TGF-β1 expression which is abrogated by angiotensin II type 1 receptor (AT1) antagonists. An ongoing expression of angiotensin II and AT1 receptors and active TGF-β1 and TGF-β1 receptors is observed in the infarcted rodent heart months after MI and underscores persistent metabolic activity of activated myofibroblasts.[51] Angiotensin II, produced locally by activated macrophages, cardiomyocytes and myofibroblasts exerts its effect by directly inducing NADPH oxidase activity in myofibroblasts stimulating TGFβ1 production, and triggering fibroblast proliferation and differentiation into collagen secreting myofibroblasts. Because of the persistent expression of AT1 receptors on myofibroblasts, they can serve as suitable targets for molecular imaging.

TGFβ1 augments production of interstitial collagens, fibronectin and proteoglycans by cardiac myofibroblasts (see Figure 2.2). It also stimulates its own production in myofibroblasts, thereby establishing an autocrine cycle of myofibroblastic differentiation and activation.[35] Studies have shown that overexpression of TGFβ1 in transgenic mice can lead to cardiac hypertrophy, characterized by both interstitial fibrosis and hypertrophic growth of cardiac myocytes.[55] Therefore, TGF-β1 receptors could be a potential target for molecular imaging. The components of the RAS system and TGF-β1 signaling, although expressed at high levels on myofibroblasts, are not specific for these cells as they can be found on other cells as well.

Analysis of myofibroblasts in fibrotic and granulation tissue reveals extensive cell-matrix contacts called fibronexi; such fibronexi are not observed in fibroblasts isolated from normal connective tissue. Cultured myofibroblasts develop specialized focal adhesions (FA) that have been termed 'supermature FA' to account for their significantly longer appearance compared with classical FA of ASMA-negative fibroblasts. In addition, supermature FA exhibit a specific molecular composition by coexpressing high levels of vinculin, paxillin, tensin and the integrins αvβ3 and α5β1[56] (see Figure 2.2). αvβ3 integrin expression in myocardium is generally rare in adults, but it is seen on endothelial cells during angiogenesis in response to angiogenic growth factors such as βFGF, and is fundamental for endothelial cell proliferation, adhesion and survival. Since neoangiogenesis and myofibroblastic proliferation occur together in post-MI remodeling, integrin targeting may be a reasonable approach for molecular imaging.

In addition to relatively exclusive (trans) membrane markers, it may also be prudent to target the company myofibroblasts keep. In the infarct area, for instance, the presence of myofibroblasts leads to collagen deposition and colla-

gen crosslinking is mediated by lysyl oxidase family enzymes.[57] Lysyl oxidase is upregulated during the first weeks of infarct healing, remains elevated up to 90 days after MI,[57] its expression is responsive to connective tissue growth factor (CTGF) and TGF-β,[58] and could probably be used as a surrogate marker for the extent of myofibroblast proliferation.

Imaging of upregulation of receptors for growth factors on myofibroblasts

As discussed above, myocardial upregulation of the RAS system contributes prominently to ventricular remodeling. Myocardial angiotensin II (AT) type 1 receptor overexpression is associated with interstitial fibrosis[59] and AT type 1 receptor deficient transgenic mice exhibit minimal structural remodeling after MI.[60] Angiotensin receptor blockers in myocardial infarction prevent and restrict ventricular remodeling, and reduce morbidity and mortality after MI regardless of LV functional deterioration.[61-65] It is therefore conceivable that a novel diag-

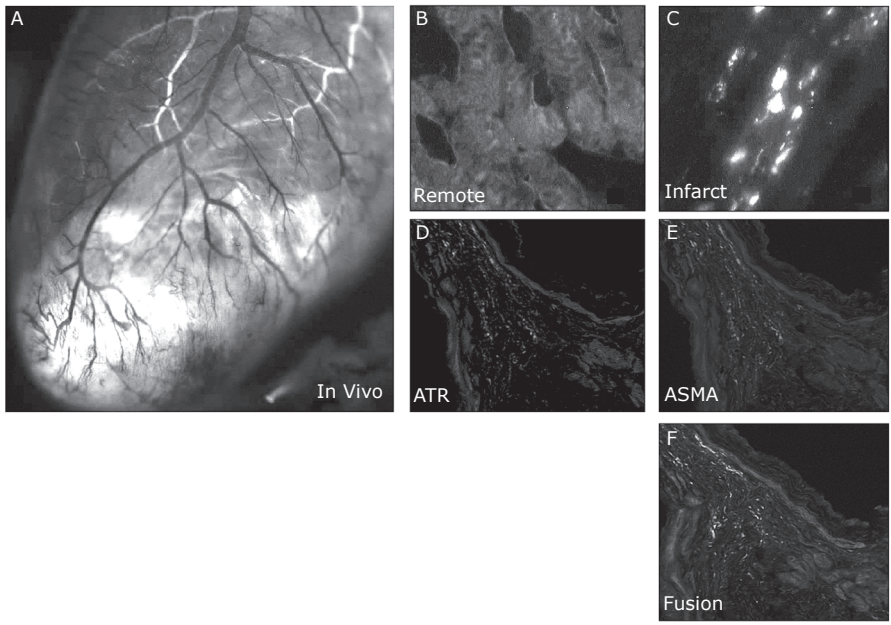

Figure 2.3 Optical imaging of angiotensin receptors

In vivo microscopic imaging shows a 3-week old myocardial infarction in a mouse model for myocardial infarction. After administration of green fluorescent angiotensin peptide analog (APA) increased uptake in the infarct area is observed (A). Sections show no uptake of APA in the remote zone (B) and clear uptake in non-myocytic cells in the infarct region (C). The angiotensin receptor positive cells (D, green), also stained positive for ASMA (E, red) showing colocalization (F, yellow) indicating that AT receptors are present on myofibroblasts. For full color illustration, see page 154.

nostic strategy targeted at detecting the extent of myocardial AT receptor expression would allow identification of patients at risk of developing HF, and allow optimization of pharmacologic therapy in HF patients. For this purpose, employing molecular imaging techniques, an angiotensin peptide analogue (APA) was labeled with a fluorescent tracer, which targeted both angiotensin type 1 and 2 receptors with high affinity (Ki= 3 pM).[66] Intravital fluorescence imaging was performed to determine the myocardial upregulation of AT receptors in a murine MI model. To more specifically target type 1 receptors, radionuclide imaging with Tc-99m-labeled losartan, an AT type 1 receptor blocker, was performed using microSPECT/microCT. For this purpose, AT receptor imaging was performed in a large number of mice at various time points after permanent coronary artery ligation as well as in controls using a fluoresceinated or radiolabeled targeting probe, followed by pathological characterization using confocal and ex vivo 2-photon microscopy. No or little tracer uptake was observed in control animals or in infarct region up to the first day. Distinct uptake occurred in the infarct area at 1 to 12 weeks after MI, with maximum uptake at 3 weeks; uptake markedly resolved at 12 weeks after MI. Pre-mortem echocardiographic characterization confirmed left ventricular remodeling and pathologic characterization revealed localization of the tracer with collagen producing myofibroblasts, and co-localization with alpha smooth muscle actin (Figure 2.3). ^{99m}Tc-labeled losartan uptake in the infarct region was 2.5-fold higher than the control animals.[66] This study has demonstrated the feasibility of in vivo imaging through targeting of myocardial angiotensin receptors. It is eminently important for the development of a strategy for prevention of HF, to recognize the subjects that are prone to develop HF from those with no apparent structural LV abnormality (stage A) and asymptomatic post-MI patients (stage B).[67] Although angiotensin receptor upregulation in kidney has been observed earlier by a carbon-11 labeled AT1 antagonist,[68] the hypothesis of the role of targeting neurohumoral upregulation for ventricular remodeling was initially proposed by imaging of ACE with F-18 fluoro-benzoyl lisinopril,[69] by incubating short-axis myocardial slices explanted from cardiac allograft recipients with end-stage ischemic cardiomyopathy. There was specific binding of radiotracer to ACE which, expressed as luminescence/mm2, was highest in infarct border zone, followed by infarct and remote segments and the uptake reduced to half after the segments pre-incubated with cold lisinopril. The targeting studies presented here, demonstrated that ACE (and probably AT II, also) upregulation may induce proliferation of myofibroblasts, which have increased angiotensin receptor density and contribute to collagen deposition.[66] However, it remains to be seen whether imaging targeted to AT receptors and/or ACE will result in clinically robust imaging strategy.

Imaging of surface moieties on myofibroblasts in the infarct area

Besides upregulation of angiotensin receptors, integrin moieties are overexpressed on myofibroblasts, which enhance promoter activity of collagen genes

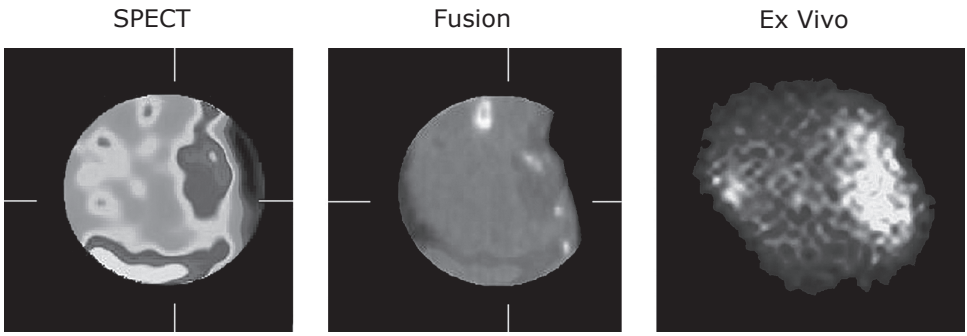

Figure 2.4 **In and Ex vivo images of radiolabeled CRIP imaging**

In vivo imaging with radiolabeled CRIP showed intense uptake in the infarct area two weeks post MI. The uptake decreased over time. The cardiac localization is confirmed in CT fusion image and ex vivo images. For full color illustration, see page 154.

and reduce metalloproteinase genes, an effect reversible by abrogation of autocrine TGF-β signaling.[70] The RGD probes that bind to integrins such as αvβ3 have been used to identify myofibroblastic proliferation in post-infarct animal models[71] as well as in clinical studies.[72] It has been proposed that the uptake of RGD probe indirectly represents the rate of fibrogenesis or collagen deposition. The first animal study demonstrating myofibroblasts by integrin targeting used Cy5.5-RGD imaging peptide (CRIP) labeled with technetium-99m (Tc) in a murine model of ventricular dysfunction after MI. The fluorescent moiety of the targeting peptide was exploited for immunoelectron microscopic characterization of the probe localization. Similar to ATII receptor imaging, MI was induced in Swiss-Webster mice by coronary artery occlusion and imaging performed 2, 4, and 12 weeks after MI. MicroSPECT-microCT imaging was performed after intravenous administration of Tc-99m labeled CRIP (Figure 2.4); scrambled CRIP was used for comparison to demonstrate specificity of the targeting agent. A subset of animals received either captopril or captopril combined with losartan up to 4 weeks after MI to evaluate the impact of neurohumoral antagonists on myofibroblasts population and collagen deposition, and hence their role in modifying myocardial remodeling. Maximum CRIP uptake was observed in the infarct area; quantitative uptake, expressed as percent injected dose per gram (%ID/g) was highest at 2 weeks, 6-fold higher than the myocardium of unmanipulated mice. The CRIP uptake resolved by 50% in the infarct zone at 3 months and almost entirely disappeared at one year. However, the uptake was higher at 12 weeks in the peri-infarct zone and remote areas. The uptake was histologically traced to myofibroblasts by fluorescent microscopic localization of CRIP and concurrent staining with ASMA. Ultrastructural analysis by immunogold labeled anti-Cy antibody, confirmed CRIP uptake in myofibroblasts. In vitro experiments revealed CRIP binding to activated αvβ3/5 with an affinity of 1-3nM, but did not bind to integrins working as collagen receptors (e.g. α1β1 or

$\alpha 5\beta 1$) or platelet receptor (e.g. $\alpha IIb\beta 3$). Histologic characterization of the infarcts revealed maximum myofibroblasts infiltration (expressing ASMA) at 2 weeks post MI, which decreased over time. Picrosirius red polarization microscopy revealed that although the total collagen content of the infarct region remained similar over time, the thin, newly formed, yellow-green collagen fibers were reduced and correlated directly with the radiotracer uptake. Compared to the infarct zone, collagen deposition was substantially less in the remote myocardium, but overall collagen content and yellow-green thin collagen fibers increased substantially in the remote region with passage of time; there was again a direct correlation between tracer uptake and the thin collagen fiber deposition in the remote myocardium. In addition, there was a directly proportional relationship between radiotracer uptake and ASMA-positive myofibroblasts. Correlation between radiotracer uptake and ASMA as well as thin collagen fiber areas suggests that the neocollagen production is decreased in the infarct zone and increased in remote zone over time.[71]

Treatment with captopril alone reduced the CRIP uptake by 50% and combination therapy with losartan further reduced the uptake by 75%. Pharmacological intervention decreased collagen deposition by about 15% in the infarct and simultaneously induced maturation of collagen deposition as represented by substantial increase in proportion of red-orange collagen fibers. On the other hand, there was a 50% reduction in collagen deposition in the remote myocardium by combination therapy.[71]

An RGD imaging peptide (RIP) directed against integrin expression, which is similar to CRIP but not fluorophore-labeled, has been used in a clinical study to assess the feasibility and safety of noninvasive imaging of interstitial alterations after myocardial infarction (MI).[72] RIP-based early integrin imaging, in patients with their first episode of myocardial infarction, was compared to the extent of fibrotic scar formation verified by late gadolinium enhanced cardiovascular magnetic resonance (CMR) imaging one year after MI. This preliminary imaging study was performed in 10 patients (ages 39-72 years, 6 male) at 3 and 8 weeks after MI. Technetium-99m labeled RIP was injected intravenously and SPECT images were acquired 2 hours later. Myocardial perfusion imaging was performed within one week after MI for delineation of infarct size prior to discharge. One year later all patients underwent CMR for the assessment of scar size. Image fusion and analysis software allowed comparison of both early RIP uptake and subsequent scar formation, and comparison of myocardial perfusion and RIP uptake. The RIP uptake was observed in 7 of the 10 patients at both 3 and 8 weeks. Although the RIP uptake corresponded to areas of perfusion defects, it almost always extended beyond the infarct zone. In all positive cases, RIP uptake co-localized with the extent of the scar demonstrated by MR imaging one year later (Figure 2.5). This study provided a proof of concept that imaging

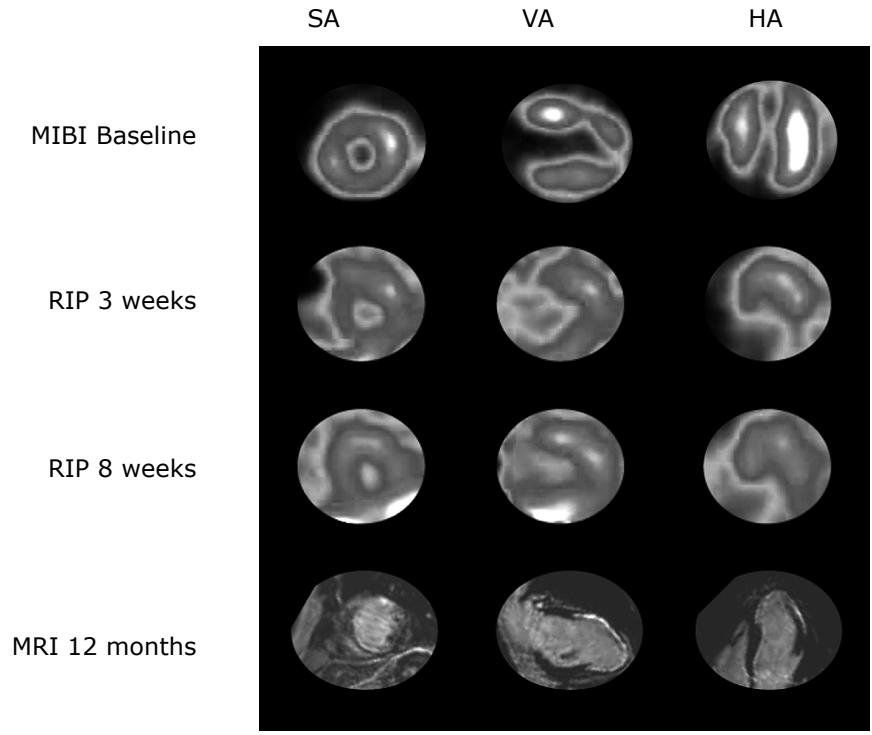

Figure 2.5 **MIBI at baseline, RIP imaging at 3 and 8 week post-MI and cardiac MRI 1 year post-MI**

The MIBI scan (first row) shows apical perfusion defects in the short axis (SA), vertical axis (VA) and horizontal axis (HA) at baseline. RIP imaging at 3 and 8 weeks post MI (row 2 and 3) show uptake corresponding to the infarct area and borderzone delineated by the MIBI scan. The cardiac MR one year post-MI shows scar formation corresponding to RIP uptake (row 4). For full color illustration, see page 155.

of myofibroblasts is a feasible proposal. We do expect that such and similar strategies would allow risk stratification in the aftermath of MI and may also allow optimization of pharmacological intervention.

The good and the bad of myofibroblasts and collagen deposition after myocardial infarction

Myofibroblast in the infarct region replace the lost cardiomyocytes which are not able to regenerate, and help produce a strong scar tissue. They also possess contractile properties and are associated with a smaller scar area which helps to prevent infarct expansion and ventricular dilatation. On the other hand, the inexorable production of collagen from the myofibroblasts in the remote area contributes to adverse ventricular remodeling and unfavorable outcomes. Unlike in skin and other organs, myofibroblasts persist for a long time in the heart with net balance in favor of remodeling. It is of paramount importance that we

understand the process of myofibroblast proliferation better and modulate the process to subdue the disadvantages without compromising the advantages. As such, there has been a growing interest in dissecting the role of the various myofibroblasts subpopulations in tissue regeneration and fibroproliferative diseases. Could myofibroblasts from different locations behave differently and may pharmacological intervention influence the healing characteristics favorably? We have observed the favorable impact of captopril-losartan therapy on infarct healing, that contributes to maturation of collagen tissue in the infarct zone but preferentially reduces the extent of collagen deposition in the remote myocardium. This allows for a balanced influence on ventricular mechanics, and vindicates clinical outcomes in patients appropriately treated by RAS antagonists.

Conclusions

Myofibroblast presence happens to be a prominent phenomenon in myocardial healing after myocardial infarction. Myofibroblasts produce collagen which is expected to stabilize the lost tissue, prevent infarct expansion and ventricular dysfunction after deposition in the myocardial void. However, concurrent proliferation of fibroblasts in the non-injured myocardial regions results in adverse ventricular remodeling and evolution of heart failure over time. An ability to image myofibroblasts before the onset of clinically manifest HF should allow identification of patients likely to develop heart failure and institution of aggressive preventive strategies. Although there are no obvious candidates for molecular imaging of myofibroblasts, as they at least partially share antigenic properties with other surrounding cellular population (such as fibroblasts and smooth muscle cells), overexpression of integrin moieties and upregulation of receptors for growth factors comprise potential targets for imaging. Successful use of RGD-based imaging in both experimental and clinical settings may offer encouraging avenues for individualization of heart failure prevention and management. The study of the impact of pharmacological intervention on the processes of infarct healing and remodeling, as evaluated by RGD imaging, may also allow better explanation of their favorable clinical role.

Mouse strain determines the outcome of woundhealing post-MI

3

submitted

ABSTRACT

Aim: To study the effect of the genetic background on the wound healing process after myocardial infarction (MI) in mice.

Methods: In five different mouse strains (BalbC, C57Bl6, FVB, 129S6 and Swiss) MI was induced. At 3, 14, and 28 days after MI cardiac dimensions were monitored by echocardiography and histology, whereas cardiac function was determined by direct intraventricular pressure measurements (dP/dt). Furthermore, matrix metalloproteinases (MMP) were measured by zymography, and mRNA expression by QPCR.

Results: Infarct rupture, which typically occurred at 3-6 days post-MI, was most frequent in 129S6 mice (62%), followed by C57Bl6 (36%), FVB (29%), Swiss (23%) and BalbC (5%). The high incidence of infarct rupture in 129S6 mice was associated with high systolic blood pressures and increased influx of inflammatory cells. Cardiac dilatation was most marked in Swiss mice and least prominent in 129S6 mice. The degree of dilatation was associated with a reduced ejection fraction and decreased dP/dt values at 14 and 28 days post-MI. At day 14 and 28 post-MI, secondary thinning of the infarct area was marked in BalbC, FVB and Swiss, but absent in C57Bl6 and 129S6. In the latter two groups, this was paralleled by the highest number of myofibroblasts at day 14 post-MI.

Conclusion: The outcome of infarct healing in mice strongly depends on genetic background. Based on our results we suggest that for studies on infarct rupture, 129S6 is the background of choice, whereas BalbC and Swiss mice are the preferred models to study infarct thinning post-MI.

INTRODUCTION

The process of cardiac wound healing after myocardial infarction (MI) is complex and, if not occurring optimally, may result in severe complications such as infarct rupture[73] and infarct thinning leading to heart failure.[30] To better understand the process of infarct healing, rodent models of MI have extensively been studied. These studies have yielded invaluable information on the molecular mechanisms involved in infarct healing. The availability of genetically altered mice, allowing the study of the effect of individual genes on infarct healing, has intensified this research even further.

When constructing a transgenic or knockout mouse, the choice of the genetic background can have a significant effect on the observed phenotype.[74] This implies that the selection of the mouse strain can be of vital importance for the outcomes of the study. Although strain effects have been reported in different cardiovascular studies on hemostasis and thrombosis[75] and stroke,[76] surprisingly little is known about the effects of the genetic background on the wound healing process after MI. To our knowledge, only a single study on differences in the frequency of infarct rupture after MI in three different mouse strains has been published.[77] In this study the incidences of infarct rupture were 3, 27 and 59% in male FVB/N, C57Bl/6J and 129sv mice, respectively, illustrating the major impact of the genetic background on cardiac pathology.[77]
The aim of the present study was to perform a systematic comparison of the wound healing post-MI in five different mouse strains that are commonly used in cardiovascular research. We hypothesized that the genetic background of the mice has a profound effect on either early (infarct rupture) or late (infarct thinning and heart failure) complications of MI. The results of the present study allow us to formulate recommendations regarding the choice of the genetic background in studies on specific aspects of the wound healing process post-MI.

MATERIALS AND METHODS

Experimental protocol

The design and number of animals that were included in the study are given in Figure 3.1 and Table 3.1, respectively. In total, 354 mice of five strains were included (BalbC n=64, C57Bl6 n=73, FVB n=73, 129S6 n=80 and Swiss n=64). All mice underwent baseline echocardiography at their entry into the study, before the surgical intervention. Of these 354 mice, 40 mice were subjected to sham surgery. In the sham animals echocardiographic measurements were repeated on days 3, 14 and 28 after sham surgery and direct intraventricular hemodynamic pressure measurements (see below) were performed 28 days after sham surgery immediately before sacrifice. All remaining (n=314) mice were

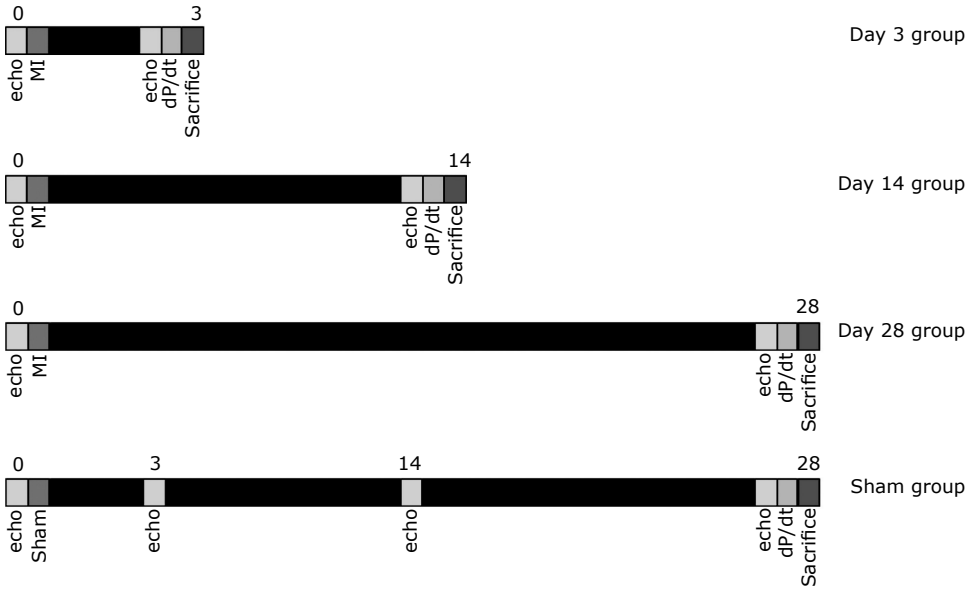

Figure 3.1 **Flow chart of the experimental protocols**

Of each mouse strain, mice were divided into 4 groups. All MI mice were subjected to baseline echocardiography, MI surgery and echo and hemodynamic measurements at the experimental time point. As a control, sham operated mice of every strain were used. They underwent echocardiography before MI and at day 3, 14 and 28. Hemodynamic measurements were executed at day 28. For full color illustration, see page 156.

subjected to coronary artery ligation on day 0 to produce MI as described below. Of these, 37 mice died during the surgical intervention or within 24 hours after MI. Within 10 days after MI 21 mice died of acute heart failure, diagnosed by pulmonary edema, and 55 mice died of infarct rupture, diagnosed by hematothorax. The surviving mice were divided into 3 groups and sacrificed on post-MI day 3 (n=39), 14 (n=40) or 28 (n=38). Terminal echocardiographic and hemodynamic measurements were performed on the day of sacrifice (Figure 3.1). Fifty-six mice were excluded because of no or small MI (<15%) or incomplete measurements. The area at ischemic risk was assessed in 28 animals from five strains.

Animals

Male mice, 10-12 weeks old were obtained from the following suppliers; FVB/NJ, Balb/cJ and C57Bl/6J mice from Jackson Labs (Bar Harbor, Maine, USA), 129S6/SvEv mice from Taconic (Germantown, NY, USA) and outbred Swiss mice from Charles River (Wilmington, MA, USA). All experimental procedures were approved by the Animal Care and Use Committee of Maastricht University and

were in accordance with the Guide for the Care and Use of Laboratory Animals, published by the US National Institutes of Health (NIH Publication No. 85-23, revised 1996).

Table 3.1 Number of animals used in the study

	n	AAR	sham	day 3	day 14	day 28	infarct Rupture	acute heart failure	surgical death	excluded*
BalbC	64	5	9	7	8	9	1	2	9	14
C57Bl6	73	7	7	7	7	7	9	2	12	15
FVB	73	6	9	8	6	8	11	13	4	8
129S6	80	5	7	8	9	6	28	2	5	10
Swiss	64	5	8	9	10	8	6	2	7	9
	354									

** excluded due to no or small (<15%) infarction*

Experimental myocardial infarction

Myocardial infarction was induced as previously described.[78] In short, mice were anesthetized with xylazine (2.5 mg/kg s.c.) and ketamine (50 mg/kg i.m.), and maintained on isoflurane (1.5-2.5%). Mice were laid on their back and the trachea was intubated with a stainless steel tube connected to a respirator (Hugo Sachs Electronic rodent ventilator type 845, March-Hugstetten, Germany) set at a stroke volume of 250μL at a rate of 210 strokes/min. Body temperature was monitored with a rectal probe and maintained at 37 °C using a heating pad and lamp. After opening the chest through the left 4th intercostal space, a ligature (6-0 prolene) was tied around the main left coronary artery. Chest and skin were closed in layers using 5-0 silk sutures. Animals recovered overnight in an incubator (30 °C). Sham surgery was performed identically, except that the ligature around the coronary artery was not tied.

All interventions and measurements were performed by the same technician to minimize variation in infarct size and measurement procedures.

Evaluation of ischemic area at risk

To evaluate if differences in coronary architecture may influence the outcome of the study, the area of the left ventricle that was at risk after left coronary artery ligation was compared in 5 BalbC, 7 C57Bl6, 6 FVB, 5 129S6 and 5 Swiss mice. Directly after the MI procedure, the abdomen was opened and 250 μl of 2.5% trypan blue was injected through the inferior vena cava to delineate the non-ischemic tissue and to quantify the area at risk (AAR). Hearts were excised, briefly washed in isotonic saline, frozen at -20 °C and cut into 2 mm thick sections in a transverse orientation. Well-perfused parts of the myocardium stained blue whereas the AAR remained unstained. Using a computerized morphometry system (Qwin version 3.2.0, Leica, Cambridge, UK), the AAR was calculated and expressed as percentage of the left ventricular area.

Echocardiography
Echocardiographic measurements were performed under light (1-2%) isoflurane anesthesia. One recording was taken prior to surgical procedures (baseline) and final recordings were made at 3, 14 or 28 days after MI surgery (Figure 3.1). Serial measurements were performed on days 0, 3, 14 and 28 in the sham-operated control animals. Transthoracic echocardiography was performed using a Hewlett-Packard 15-MHz linear array transducer (15-6L) interfaced with a Sonos 5500 echocardiography system (Phillips, Eindhoven, The Netherlands). Two-dimensional B-Mode images were captured at a rate of 90-120 Hz from the parasternal long-axis views and from the mid-papillary short axis view of the left ventricle. Data were obtained from at least 3 different images taken in end-diastole and end-systole using EnConcert software (Agilent Technologies, Andover, MA, USA). Infarct size, LV cavity dimensions and ventricular function were assessed.

Evaluation of left ventricular contractility (dP/dt)
The LV contractility was determined on post-MI day 3, 14 or 28 in the 3 experimental groups and on day 28 in the sham MI group. Mice were anesthetized with urethane (2.5 mg/g body weight i.p., Sigma-Aldrich, St Louis, MO, USA). Body temperature and respiration were controlled as described above. A high-fidelity catheter tip micromanometer (Mikro-tip, 1.4F, SPR-671; Millar Instruments, Houston, Tx, USA) was inserted through the right carotid artery into the left ventricular cavity. Ventricular pressure was measured and sampled at a rate of 2 kHz. Maximal positive and negative pressure development (+dP/dt, -dP/dt) and heart rate were determined on a beat to beat basis and one-second averages were stored on disk. dP/dt values were determined at baseline and during maximal stimulation with dobutamine (Sigma). For this purpose, the maximal effect of dobutamine was determined during an i.v. ramp-infusion of dobutamine using a micro injection pump (model 200 series, KdScientific, Boston, MA, USA). The infusion rate of dobutamine was increased every 2 minutes by 0.5 ng/g/min until the final rate of 5 ng/g/min.

Tissue preparation
At the end of the experiment, hearts and lungs were excised and weighed. Hearts were divided longitudinally; one halve was incubated in 4% paraformaldehyde for 24 hours, processed and embedded in paraffin for immunohistochemical stainings. The other halve was subdivided in right ventricle, left ventricle, infarct and septum and snap-frozen in liquid nitrogen until further used for protein and RNA isolation.

Histology and Immunohistochemistry
Sections of 4 μm were cut from the paraffin embedded heart halves and stained with the AZAN technique. Infarct size (percentage of the left ventricular area) as

well as infarct and septum thickness were measured using a computerized morphometry system (Qwin, Leica). For Sirius Red staining, sections were treated with 0.2% aqueous phosphomolybdic acid for 5 min and subsequently incubated for 60 min with 0.1% Sirius Red F3BA (C.I. 35780, Polysciences, Northhampton, UK) in saturated picric acid and washed for 2 min with 0.01 N HCl. Sections were then rinsed in 70% alcohol for 30 seconds, dehydrated and mounted with cover-slip. The relative collagen areas in the infarct and septum were quantified as percentage of total tissue surface using the Qwin morphometry system. Alpha smooth muscle actin (ASMA) was used to identify myofibroblasts in the infarct area. For this purpose, after deparaffination, rehydration and blocking of endogenous peroxidase, sections were incubated for 2 hours at room temperature using anti-alpha smooth muscle actin (ASMA monoclonal antibody, Sigma, dilution 1:2000). After washing in PBS, sections were incubated with secondary antibody (rabbit anti mouse HRP 1:500, DakoCytomation, Glostrup, Denmark) for 1 hour at room temperature. Sections were briefly counterstained with haematoxylin. Myofibroblast areas were determined using the Qwin morphometry system and were expressed as myofibroblast area/total tissue area (%). In addition, haematoxylin and eosin-stained sections were used to identify inflammatory cells by cytological characteristics and counted in four randomly chosen fields (90.000 μm^2 per field) of the border zone of day 3 post-MI infarct samples in all five strains.

Zymography

Proteins were isolated from the infarct area of the day 3 group for all strains as previously described.[22] Latent and active MMP activity was detected using zymography, as previously described.[11] Briefly, gelatin (final concentration of 0.66 mg/ml) was added to a 10% standard Laemmli[79] acrylamide polymerization mixture. Ten µg of non-denatured protein was loaded per lane.[80] A protein standard with proven MMP-2 and -9 activity was loaded on each gel as a control. Following electrophoresis, gels were rinsed two times 15 minutes in 2.5% Triton X-100 and incubated overnight at 37 °C in substrate buffer (50 mmol/L Tris HCl pH 8.5, 5 mmol/L CaCl2, and 0.02% NaN3). After incubation, gels were stained with 0.1% Coomassie Blue R 250 (BioRad, Hercules, CA, USA) in acetic acid: methanol:water (1:4:5) and destained in the same solvent. The zones of proteolytic activity were visualized as clear bands against a dark background. The gels were digitized and analyzed with image analysis software (Qwin, Leica). The integrated optical density of the individual bands was determined and normalized against the value of a standard sample that was run on every gel.

Real time PCR

Real time PCR was performed as previously described.[81] In short, septal tissue was homogenized with a PRO200 tissue homogenizer (PRO Scientific, Monroe, CT, USA) and RNA was isolated using the RNeasy Fibrous Tissue mini kit (Qiagen,

Maryland, USA) according to the manufacturer's instructions. RNA was further purified by DNase digestion using the DNA-Free RNA kitTM (Zymo Research, Orange, CA, USA) to remove any residual genomic DNA. First strand cDNA was synthesized by adding 100 ng of DNase-treated total RNA to Ready-To-Go You Prime First-Strand Beads (Amersham Biosciences Europe, Freiburg, Germany). Random hexamers were used as primers. The reactions were incubated for 10 minutes at 65 °C, 1 hour at 37 °C and 2 minutes at 95 °C. The resulting cDNA was either used immediately as template for real-time PCR or stored at −20 °C. Real-time PCR primers were designed, using Primer Express software (version 1.5; Applied Biosystems, Foster City, CA, USA). The designed primers were used to quantify the expression of mRNA levels of atrial natriuretic factor (ANF) and brain natriuretic peptide (BNP). The expression was determined by measuring the binding of the fluorescent dye SYBR Green I, using SYBRGreen PCR Master Mix kit (Eurogentec, Seraing, Belgium). Real-time PCR was performed in a MyIQ system (Biorad). Cardiac gene expression was normalized to the housekeeping gene Cyclophilin. All samples were run in duplicates. Data analyses were performed using the MyIQ System software (Biorad, USA). The following primers were used for real time PCR:

ANF:	forward: 'CATCATGGGCTCCTTCTCCAT'
	reverse: 'TGTACACAGGATTTGGTCCAATATG'
BNP:	forward: 'AGGACCAAGGCCTCACAAAA'
	reverse: 'TTGAGATATGTGTCACCTTGGAATTT'
cyclophilin:	forward: 'TTCCTCCTTTCACAGAATTATTCCA'
	reverse: 'CCACCAGTGCCATTATGG'

Statistical analysis

All data are presented as mean±SEM. Survival was analyzed by a Kaplan Meier curve with a log-rank test for differences between groups. Statistical analysis was performed using ANOVA with Bonferroni posthoc t-tests to identify between strain differences or time-dependent changes. Specifically, in sham-MI mice, the echocardiographic data were compared between strains using a 2-way ANOVA with strain as a between factor and time (days after MI) as a within factor. For the between strain comparison of the echocardiographic data after MI, the same procedure was applied with time as between factor. The hemodynamic (+dP/dt) data were compared using a 3-way ANOVA with strain and time as between factors and the response to dobutamine (baseline and maximal values) as within factor. In the figures the p-values of the various Bonferonni post-hoc comparisons are given. A P-value of <0.05 was considered to indicate statistical significance.

RESULTS

A total of 354 mice were used for this study. Thirty-seven mice died during or shortly (<24 h) after surgery because of complications of anesthesia, arrhythmia or bleeding and were not included in the analysis. In the first week post-MI fifty-five mice died of cardiac rupture, as diagnosed by hematothorax. Twenty-one mice died of heart failure, diagnosed by a more than 270% increase in LW/BW ratio and clear fluid in the thoracic cavity, and fifty-six mice were excluded from the study due to small infarct size (<15%) or incomplete measurements. Twenty-eight mice were used to determine the area at risk and 157 mice were included in the experimental protocol (Table 3.1).

Area at risk

The mean left ventricular AAR values were not different between mouse strains. The following AARs were observed: BalbC 46±4%, C57Bl6 50±5%, FVB 48±6%, 129S6 48±2% and Swiss 48±4% (p=0.97). This indicates similar infarct sizes in all mouse strains at the time of surgery.

Survival of the different mouse strains

After induction of MI, only 33% of the 129S6 mice were alive at 28 days post-MI, as compared to 85% of the BalbC mice (Figure 3.2A). Kaplan Meier analysis demonstrated significant differences in mortality between the five mouse strains (p=0.004). All mice died of either infarct rupture or acute heart failure. Infarct rupture, diagnosed by massive blood loss in the thoracic cavity, occurred in 62% of the 129S6 mice, 36% in C57Bl6, 29% in FVB, 23% in Swiss and in 5% of the BalbC mice (Figure 3.2B). The timing of infarct rupture differed between the groups. 129S6 mice typically ruptured between day 3 and 4 post-MI, C57Bl6 mice ruptured on day 4 and 5 and FVB mice ruptured on day 5 and 6. Early lethal heart failure (between day 2-7 post-MI), occurred mainly in the FVB mice (28%) whereas in the other strains this complication occurred in less than 10% of the cases (Figure 3.2B).

Post-mortem characteristics of the five different mouse strains

In Table 2 the post-mortem characteristics of the different mouse strains at the different time points are summarized. At baseline there was a variation in body weight between the five strains and this variation was maintained over time (see sham groups). The Swiss mice weighed significantly more than the other mouse strains; all strains gained weight during the study.

Heart weight normalized for body weight increased in all mouse strains after MI surgery compared to sham operated animals. The 129S6 mice had the highest heart weight to body weight ratio. Lung weight normalized for body weight (LW/BW) also tended to increase in all strains after MI surgery. Over

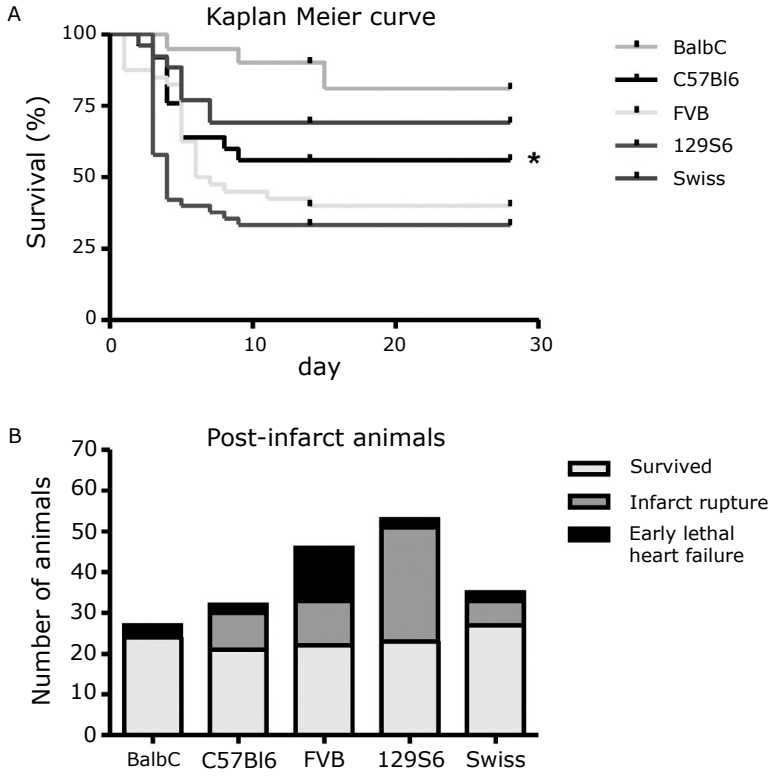

Figure 3.2 **Survival and causes of death between 5 different mouse strains**

A: *Kaplan Meier curve analysis of 5 different mouse strains showed significant differences in survival (p=0.004). BalbC mice showed the highest survival, 85% of these mice were still alive at day 28 post-MI. The BalbC mice were followed by Swiss (69%), C57Bl6 (56%) FVB (37%) whereas only 33% of the 129S6 mice were still alive at 28 days post-MI.* **B:** *The causes of death in the post-MI mice were infarct rupture and early heart failure in the first week post-MI. Of the 129S6 mice, 62% died of infarct rupture, as compared to only 5% of the BalbC mice. Death due to acute heart failure in the first week post-MI mainly occurred in the FVB mice (28%). For full color illustration, see page 156.*

time, post-MI LW/BW increased significantly in BalbC and Swiss mice, but not in the other strains, suggesting the development of pulmonary edema in these two strains.

Cardiac dimensions by echocardiography

Echocardiographic analysis showed similar baseline characteristics in all five strains. In sham operated mice, echocardiographic parameters were not significantly different between strains and remained similar over the 28 day time course of the study. In the sham groups the end systolic volume (ESV) ranged from 0.02-0.05 cm^3, the end diastolic volume (EDV) from 0.05-0.09 cm^3, the

ejection fraction (EF) from 39-57% and the fractional shortening (FS) ranged from 25-31%. The range of values observed in the sham group is indicated by grey areas in Figure 3.3. After MI, differences between strains became more pronounced: all strains showed an increase in both ESV and EDV after MI (Figure 3.3A-B), but the ESV and EDV were significantly greater in Swiss mice than in other strains. There was a decrease in EF and FS after MI in all mouse strains, with the lowest values in Swiss and BalbC mice and the best preserved values in FVB mice (Figure 3.3C-D).

Cardiac function

Left ventricular function was evaluated at day 3, 14 and 28 post-MI, as well as in sham operated mice at day 28 (Figure 3.4). Direct intraventricular measurements were made at baseline conditions and during maximal stimulation with dobutamine. Baseline and dobutamine-stimulated systolic blood pressures were highest in 129S6 mice, in both the sham and MI groups (Figure 3.4A-B). Lowest systolic blood pressures were observed in Swiss mice at all time points after MI. C57Bl6 mice had significantly higher systolic blood pressures than FVB and Swiss mice. Diastolic blood pressures were not different between mouse strains, neither in sham nor at any point of time post-MI (data not shown). Mean heart rates varied from 492 to 584 beats/min with the highest heart rate in C57Bl6 mice and the lowest heart rate in BalbC mice (data not shown).

Maximal ventricular contractility (+dP/dt) was reduced post-MI in all mouse strains except in 129S6 (Figure 3.4C). Dobutamine stimulation increased the +dP/dt values in all mouse strains (Figure 3.4D). The +dP/dt was highest in 129S6 mice and differed significantly from BalbC, FVB and Swiss mice. The lowest +dP/dt was observed in Swiss mice, which was significantly different from all other strains. In BalbC and Swiss mice LV +dP/dt was higher at 3 and

Table 3.2 Post mortem characteristics of the 5 different mouse strains

Parameter	Group	Day	BalbC	C57Bl6	FVB	129S6	Swiss	p value#
BW (g)	MI	day 0	24.2±0.4	25.2±0.3	27.8±0.3	23.6±0.4	36.5±0.3	<0.0001
	MI	day 3	25.8±0.7	26.4±1.2	26.7±0.4	25.9±1.0	35.2±0.5	<0.0001
	MI	day 14	24.6±1.1	26.9±1.3	28.3±0.9	25.5±1.3	36.1±0.8	<0.0001
	MI	day 28	26.6±0.7	28.4±0.6	30.1±0.2	26.8±0.5	37.8±0.6	<0.0001
	Sham	day 28	26.8±0.5	26.7±0.8	29.2±0.3	23.7±1.5	37.9±0.7	<0.0001
HW/BW (%)	MI	day 3	0.62±0.03	0.67±0.03	0.61±0.02	0.70±0.03	0.63±0.02	0.0850
	MI	day 14	0.62±0.05	0.64±0.03	0.63±0.06	0.69±0.02	0.55±0.02	0.1977
	MI	day 28	0.58±0.03	0.66±0.03	0.59±0.02	0.65±0.02	0.59±0.02	0.1984
	Sham	day 28	0.49±0.02	0.49±0.01	0.45±0.02	0.54±0.01	0.47±0.01	0.0004
LW/BW (%)	MI	day 3	0.62±0.03	0.55±0.02	0.65±0.04	0.65±0.04	0.58±0.01	0.1098
	MI	day 14	0.91±0.14	0.88±0.13	0.67±0.07	0.56±0.02	0.94±0.11	0.1033
	MI	day 28	0.89±0.13	0.53±0.01	0.55±0.02	0.54±0.04	0.82±0.07	0.0026
	Sham	day 28	0.55±0.02	0.55±0.02	0.50±0.01	0.54±0.02	0.54±0.02	0.1396

P values show comparison between the groups for the given parameter (one-way ANOVA)

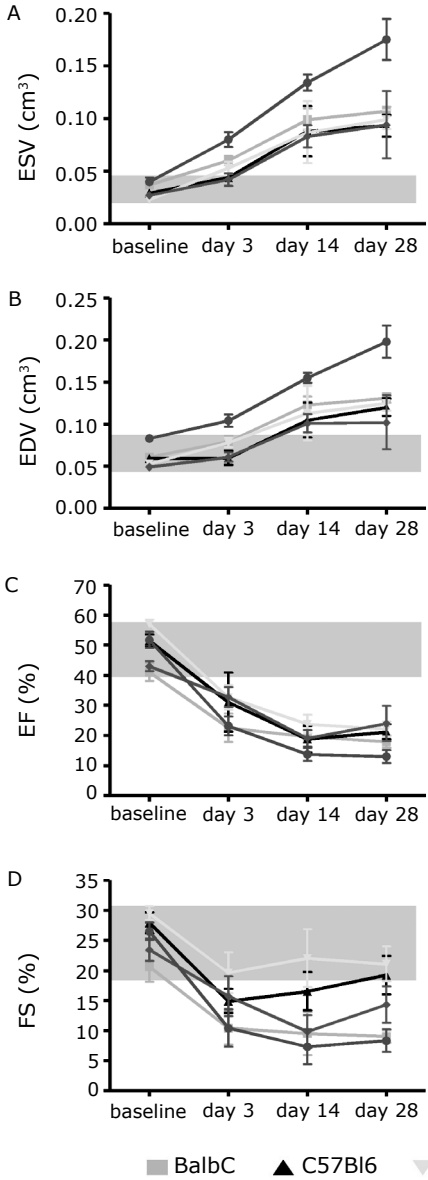

Strain			p-value
BalbC	>	C57Bl6	ns
BalbC	>	FVB	ns
BalbC	>	129S6	ns
C57Bl6	>	129S6	ns
FVB	>	C57Bl6	ns
FVB	>	129S6	ns
Swiss	>	BalbC	0.0001
Swiss	>	C57Bl6	<0.0001
Swiss	>	FVB	<0.0001
Swiss	>	129S6	<0.0001

Strain			p-value
BalbC	>	C57Bl6	ns
BalbC	>	FVB	ns
BalbC	>	129S6	0.0128
C57Bl6	>	129S6	ns
FVB	>	C57Bl6	ns
FVB	>	129S6	ns
Swiss	>	BalbC	<0.0001
Swiss	>	C57Bl6	<0.0001
Swiss	>	FVB	<0.0001
Swiss	>	129S6	<0.0001

Strain			p-value
BalbC	>	Swiss	ns
C57Bl6	>	BalbC	0.0038
C57Bl6	>	129S6	ns
C57Bl6	>	Swiss	<0.0001
FVB	>	BalbC	0.0001
FVB	>	C57Bl6	ns
FVB	>	129S6	ns
FVB	>	Swiss	<0.0001
129S6	>	BalbC	0.0076
129S6	>	Swiss	0.0001

Strain			p-value
BalbC	>	Swiss	ns
C57Bl6	>	BalbC	0.0002
C57Bl6	>	FVB	ns
C57Bl6	>	129S6	ns
C57Bl6	>	Swiss	<0.0001
FVB	>	BalbC	<0.0001
FVB	>	129S6	0.0269
FVB	>	Swiss	<0.0001
129S6	>	BalbC	ns
129S6	>	Swiss	0.0320

Figure 3.3 Echocardiographic measurements

Echocardiographic measurements were performed in sham operated and in post-MI mice. The values measured at baseline in the sham operated mice remained similar over time and are represented by the grey rectangle. Post-MI, end systolic volume (ESV) and end diastolic volume (EDV) increased in all mouse strains, with the highest increase in Swiss mice (Fig. 3.3 A,B). The ejection fraction (EF) and fractional shortening (FS) decreased after MI surgery in all mouse strains with the highest decrease in Swiss and BalbC mice. BalbC (green), C57Bl6 (black), FVB (yellow), 129S6 (red), Swiss (blue). For full color illustration, see page 157.

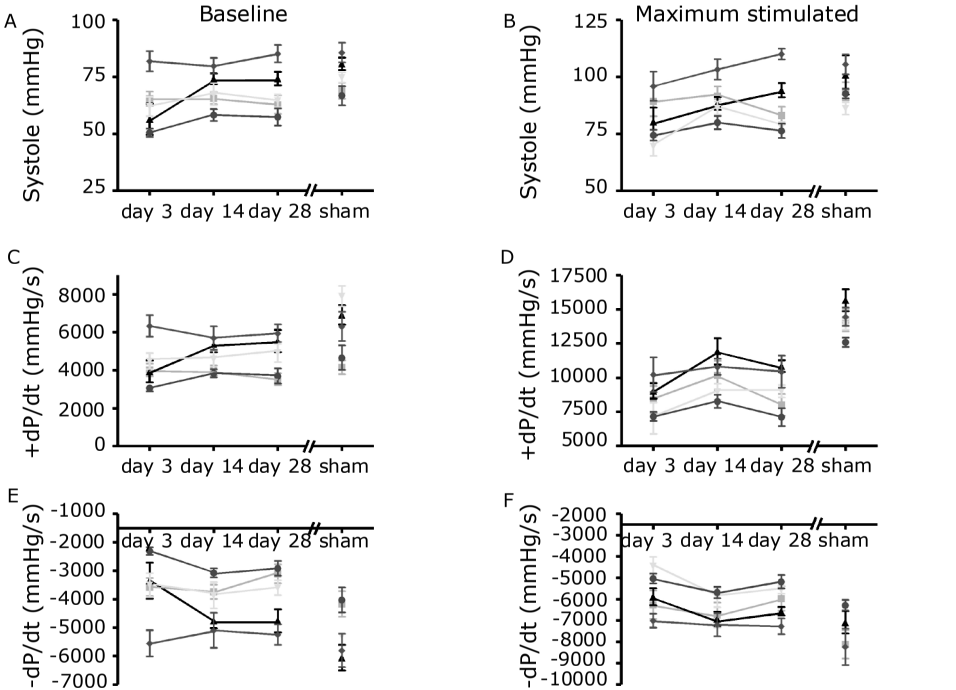

Strain			p-value
BalbC	>	FVB	ns
BalbC	>	Swiss	ns
C57Bl6	>	BalbC	ns
C57Bl6	>	FVB	0.0433
C57Bl6	>	Swiss	<0.0001
FVB	>	Swiss	ns
129S6	>	BalbC	<0.0001
129S6	>	C57Bl6	<0.0001
129S6	>	FVB	<0.0001
129S6	>	Swiss	<0.0001

Strain			p-value
BalbC	>	Swiss	ns
C57Bl6	>	BalbC	<0.0001
C57Bl6	>	FVB	ns
C57Bl6	>	Swiss	<0.0001
FVB	>	BalbC	0.0195
FVB	>	Swiss	<0.0001
129S6	>	BalbC	<0.0001
129S6	>	C57Bl6	ns
129S6	>	FVB	0.0028
129S6	>	Swiss	<0.0001

Strain			p-value
BalbC	>	C57Bl6	ns
BalbC	>	129S6	<0.0001
C57Bl6	>	129S6	0.0045
FVB	>	BalbC	ns
FVB	>	C57Bl6	0.0327
FVB	>	129S6	<0.0001
Swiss	>	BalbC	0.0256
Swiss	>	C57Bl6	<0.0001
Swiss	>	FVB	ns
Swiss	>	129S6	<0.0001

Figure 3.4 Hemodynamic measurements

Hemodynamic measurements were taken in sham-operated mice at day 28 and in post-MI mice either at day 3, 14 or 28 depending on the group. Hemodynamic measurements were taken under physiological (baseline) conditions (A,C,E) and after maximal stimulation with dobutamine (B, D, F). Results from the three-way ANOVA are presented in the tables. Systolic blood pressure was significantly higher in 129S6 mice compared to the other strains. Also, systolic blood pressure was significantly higher in C57Bl6 mice compared to FVB and Swiss mice (Figure 4A-B). The +dP/dt, a measurement of contraction strength, was highest in 129S6 mice and was significantly different from BalbC, FVB and Swiss mice. The lowest +dP/dt values were measured in Swiss mice (Figure 4C,D). The ventricular relaxation (–dP/dt), was best in 129S6 mice both at baseline and after maximum dobutamine stimulation. BalbC (green ■), C57Bl6 (black ▲), FVB (yellow ▼), 129S6 (red ◆), Swiss (blue ●). For full color illustration, see page 158.

14 days post-MI than at day 28 post-MI, suggesting that cardiac performance is deteriorating. Furthermore, the strain differences regarding the +dP/dt values were maintained when normalized for systolic blood pressure (data not shown).

The strongest maximal ventricular relaxation (-dP/dt) at baseline was observed in 129S6 mice and the weakest in Swiss mice (Figure 3.4E). The relaxation values increased after maximum dobutamine stimulation in all strains with again the best relaxation in 129S6 mice and the lowest in Swiss mice (Figure 3.4F). The combined data show that cardiac function after MI was best preserved in 129S6 and C57Bl6 mice, whereas BalbC, FVB and Swiss mice showed more deterioration of cardiac function.

Morphometry, ASMA and collagen content

Infarct size, as measured in AZAN-stained sections, was not different between the five mouse strains and values were also comparable over time (see Table 3.3). In the sham groups there were no strain-dependent differences in septal and anterior wall thickness. The thickness of the infarcted left ventricular anterior wall decreased after MI in all five mouse strains compared to the left ventricular anterior wall in sham operated mice. Over time the thickness of the infarct decreased further in BalbC, Swiss and FVB mice. In contrast, the thickness of the infarcted wall remained relatively constant over time in C56Bl6 and 129S6 mice. Septum wall thickness did not change in BalbC mice post-MI, while in the other strains septum wall thickness increased with the most prominent increase in C57Bl6 and FVB mice (Table 3.3).

Table 3.3 Histological and Immunohistochemical characterisation

Parameter	Group	Day	BalbC	C57Bl6	FVB	129S6	Swiss	p-value[#]
AAR/LV (%)			46±4	50±5	48±6	48±2	48±4	0.973
Infarct size (%)	MI	day 14	39±2	46±3	41±7	46±3	43±2	0.3299
	MI	day 28	42±3	42±2	42±5	37±5	44±2	0.6345
Infarct wall thickness (μm)	MI	day 14	385±20	409±21	480±64	517±36	498±48	0.0546
	MI	day 28	262±11	402±13	300±22	484±33	333±26	<0.0001
	Sham[*]	day 28	968±75	1192±106	1061±52	1093±165	1119±69	0.5313
Septum wall thickness (μm)	MI	day 14	1039±58	1407±125	1374±116	1152±180	1281±59	0.1888
	MI	day 28	1059±98	1313±66	1429±225	1168±278	1121±68	0.2490
	Sham	day 28	1084±61	1113±102	1174±35	1061±96	1006±36	0.4874
Myofibroblasts (%)[†]	MI	day 14	4.8±1.2	8.1±2.0	5.5±3.0	9.9±1.6	3.4±0.8	0.0209
	MI	day 28	3.2±1.0	2.0±0.5	2.9±0.8	4.1±1.5	2.2±0.4	0.3886
Collagen infarct (%)	MI	day 14	73.5±3.3	75.3±3.7	71.4±7.2	79.4±1.8	73.0±3.1	0.5078
	MI	day 28	80.9±1.1	81.9±2.1	83.8±1.9	80.9±4.4	79.8±1.6	0.6857
	Sham[*]	day 28	1.29±0.4	0.41±0.1	0.31±0.1	0.98±0.2	0.84±0.2	0.0133
Collagen septum (%)	MI	day 14	3.29±0.5	1.44±0.4	1.28±0.2	2.21±0.4	1.64±0.2	0.007
	MI	day 28	4.1±0.9	0.96±0.4	3.04±1.4	1.52±0.4	3.14±0.4	0.2019
	Sham	day 28	1.19±0.4	0.59±0.2	0.57±0.1	0.96±0.2	0.99±0.2	0.2443

[†]measured in the infarct area, [*]anterior wall without infarction, [#]P values show comparison between the groups for the given parameter (one-way ANOVA)

Myofibroblasts were stained using an anti-ASMA antibody and the percentage of the infarct area that was populated by myofibroblasts was quantified. At day 14 post-MI the area covered by myofibroblasts was significantly larger in 129S6 mice than in Swiss mice ($p<0.05$) (Table 3.3).The percentage of the infarct area populated by myofibroblasts decreased in all mouse strains between day 14 and 28 post-MI.

The total collagen content in the anterior left ventricular wall differed between sham operated mice. BalbC mice had significantly more collagen in the anterior wall than FVB mice ($p<0.05$). After MI, total collagen content of the left anterior wall increased significantly in all five mouse strains. The magnitude of this increase was not different between strains. Also in the septum, remote from the infarcted area, the collagen content increased over time after MI in all five mouse strains. At day 14 post-MI BalbC mice had significantly more collagen in the septum than C57Bl6, FVB and Swiss mice ($p<0.05$) (Table 3.3).

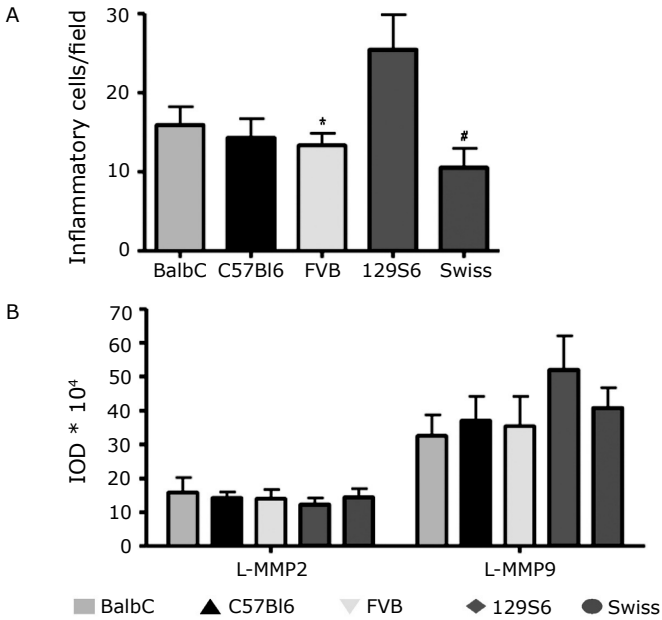

Figure 3.5 **Inflammatory cell influx and MMP-activity at day 3 post-myocardial infarction**

Inflammatory cells were counted at the infarct borderzone 3 days post-MI. **A:** *Quantitative analysis showed a significant difference in influx of inflammatory cells between the 5 mouse strains (p=0.0074). 129S6 mice had a significant higher number of inflammatory cells in the infarct area compared to FVB and Swiss mice. (*: p<0.05) and Swiss (#: p<0.01) mice. A field is defined as 90.000 μm².* **B:** *Gelatin zymography demonstrating the activity of matrix metalloproteinases (MMP)-2 and -9 in myocardial infarct tissue obtained from 3 day old infarcts. Quantification of the latent forms of MMP-2 and MMP-9, expressed in intensity units (IOD), showed slightly higher latent-MMP-9 levels in 129S6 mice; however this did not reach statistical significance. Active MMP-levels were difficult to detect in these tissue samples. For full color illustrations, see page 159.*

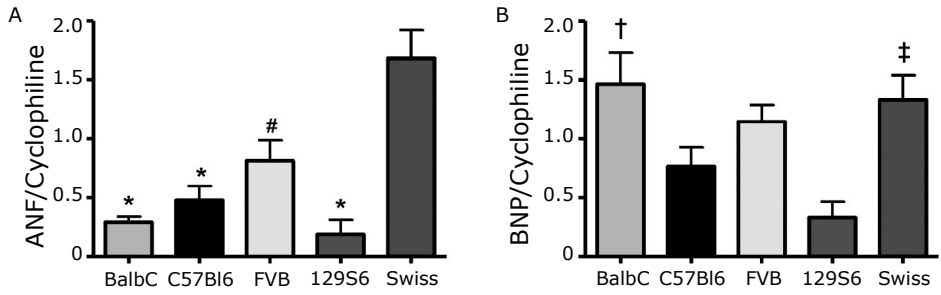

Figure 3.6 **Quantitative PCR characterization of ANF and BNP**

A: the ANF/cyclophiline ratio was significantly increased in Swiss mice compared to BalbC, C57Bl6, 129S6 (:p<0.001) and FVB mice (#:p<0.01). B: BNP/cyclophilin ratio was lowest in 129S6 mice and was significantly different from BalbC (†: p<0.01) and Swiss mice (‡p<005).*

Inflammatory cells in the infarct area

The number of inflammatory cells in the border zone of day 3 post-MI infarcts differed significantly between all five mouse strains (p=0.0074). The most prominent influx of inflammatory cells was observed in the 129S6 mice, which was significantly greater than in FVB mice (p<0.05) and Swiss mice (p<0.01) (Figure 3.5A).

MMP analysis

At day 3 post-MI the amount of latent MMP-2 was comparable in all strains (p=0.9424, Figure 5B). Latent MMP-9 levels were slightly elevated in 129S6 mice although this did not reach statistical significance (p=0.477). Active MMP-2 and MMP-9 levels were undetectable in day 3 post-MI samples.

Expression of ANF and BNP

ANF expression, normalized for the housekeeping gene cyclophilin, was significantly increased in Swiss mice compared to BalbC, C57Bl6, 129S6 (all p<0.001) and FVB mice (p<0.01). BNP expression, corrected for cyclophilin, was lowest in 129S6 mice and was significantly different from BalbC (p<0.01) and Swiss mice (p<0.05) (Figure 3.6).

DISCUSSION

The present study provides a unique insight into the effect of the genetic background on post-MI wound healing in five different mouse strains. The major observations in the present study were marked differences in the frequency of infarct rupture and in the magnitude of thinning of the infarct area. The latter was inversely related to the preservation of cardiac function.

In this study we observed a high frequency of infarct rupture in 129S6 mice. This is in accordance with findings of other studies, in which the incidence of infarct rupture in male 129Sv mice ranged from 59-82%.[77, 82] In one of these studies infarct rupture was associated with a higher density of regional inflammatory cells at the border zone of the infarct area and an increased MMP-9 expression.[82] MMP-9 is known to play an important role in the development of infarct rupture, both in mice and humans.[23, 73] In the present study, we did observe a significant increase in the number of inflammatory cells in the border zone of the infarct of 129S6 mice. Although there was a tendency towards increased MMP-9 levels in 129S6 mice at 3 days post-MI, the levels did not differ significantly from the other strains. This may be explained by the time window in which the experiments were done. We sacrificed animals at day 3 post-MI, so before the onset of infarct rupture. This implies that MMP-9 responsible for rupture of the infarct area has just started to be produced. We did not observe any differences in MMP-2 activity between the five mouse strains at day 3 post-MI. Others have described a role for MMP-2; targeted deletion of MMP-2 has been shown to reduce the incidence of infarct rupture.[24, 83] In these studies, MMP-2 upregulation occurred at day 4-7 post-MI, which is beyond our time point of sacrifice.[82, 84] Moreover, in human infarct rupture MMP-2 does not seem to play a role, as was observed for mice in the present study.[73] Furthermore, 129S6 mice also showed a significantly higher systolic blood pressure compared to the other mouse strains. In humans, high blood pressure is a risk factor for development of infarct rupture.[19] The elevated blood pressure in 129S6 mice is therefore likely to contribute to the increased frequency of infarct rupture observed in these mice.

Taken together, our observations indicate that 129S6 mice have an augmented inflammatory response compared to other mouse strains. The increased influx of inflammatory cells, combined with possible increase in MMP-9, may have weakened the extracellular matrix more in 129S6 than in other strains. Combined with the high systolic blood pressure, this may contribute to the high incidence of infarct rupture in 129S6 mice. It has been suggested that infarct rupture in humans may occur due to hypertension and increased local left ventricular wall stress; administration of beta-blockers and/or angiotensin converting enzyme inhibitors might prevent rupture.[19]
In the present study, cardiac function of mice from five different strains was followed up to 4 weeks after MI. Swiss and BalbC mice had the worst cardiac function after MI. They showed high systolic and end diastolic volumes and marked reductions in ejection fraction and fractional shortening. This was associated with significant infarct thinning without compensatory hypertrophy of the septum. The elevated BNP levels and lung weight/body weight ratios at 28 days post-MI suggest that these mice were progressing into heart failure. Remarkably, however, Swiss and BalbC mice were the mice with the highest survival

rates in our study. This raises an interesting parallel with the current pharmacotherapy of heart failure in which administration of a beta-blocker and/or ACE inhibitor, drugs that depress cardiac function, reduce the morbidity in heart failure patients[85] and increase the time of survival.[63, 86]

Secondary thinning of the infarct area between day 14 and 28 was marked in BalbC, FVB and Swiss, but absent in C57Bl6 and 129S6. This was paralleled by the highest number of myofibroblasts at 14 days after MI in the latter two groups. The role of myofibroblasts has been well established in wound healing in the skin, where the myofibroblasts align perpendicular to the wound rim.[49] The contractile properties of the myofibroblasts bring the wound margins in closer proximity, a phenomenon which is known as wound contraction and which reduces the scar size.[49] The reduction in size is stabilized by extracellular matrix deposition and subsequently the myofibroblasts disappear from the scar area.[44] However, unlike wound healing in the skin,[50] myofibroblasts persist for up to 20 years in well-healed human infarcts[13] suggesting a sustained role for myofibroblasts in the maintenance of the infarct area and prevention of secondary dilatation in the beating heart which is under repetitive stress.

The present study shows profound effects of the genetic background on the wound healing process post-MI in mice. This raises the question whether the genetic background of mice used in a study is optimal to investigate the effect of a specific genetic modification or whether some effects remain unnoticed due to the use of a specific genetic background.[74, 87] Furthermore, when planning a study, either to test the effect of genetic modification or e.g. a pharmacological intervention on infarct healing, guidelines would be helpful to chose the optimal mouse strain. The present study provides novel insights into the effect of the genetic background on infarct healing that can help researchers to determine which mouse strain is most suitable to study a certain aspect of infarct healing (Table 3.4).

- To study strategies to prevent infarct rupture, 129S6 and –to a lesser extent- C57Bl6 are the models of choice. These mice show a high frequency of infarct rupture with characteristics that resemble infarct rupture in humans. Therefore these mouse strains should be the first choice in studies aiming at testing genetic or pharmacological interventions to reduce the incidence of infarct rupture.

- To study heart failure post-MI, BalbC and Swiss are the preferred models. These strains clearly show reduced cardiac performance, combined with increases in BNP levels and increases in lung weight, resembling the symptoms observed in human heart failure patients.

- To study infarct thinning, BalbC, FVB and Swiss are best suitable. These strains have relatively few myofibroblasts at 14 days post-MI which may explain the more profound secondary dilatation of the infarct area in these strains. Therefore, these models are well-suited to study interventions aiming at the preservation of myofibroblasts in the infarct area. Moreover, their low frequency of infarct rupture and poor cardiac function make them the strain of choice to study the effect of therapies on infarct healing.

- If a model with preserved cardiac function after MI is needed, one should choose between C57Bl6, 129S6 or FVB. Obviously, 129S6 and –to a lesser extent- C57Bl6 have the disadvantage that a significant number of animals will be lost due to infarct rupture. This leaves FVB as the strain of choice for this kind of experiments.

Table 3.4 Overview of mouse model characteristics post MI

	Survival	infarct rupture	signs of heart failure	Dilatation of infarct	secondary hypertrophy	cardiac function	hemodynamics post-MI	good model to study
BalbC	+	–	+	+	–	–	+/–	heart failure
C57Bl6	+/–	+/–	–	–	+/–	+	+	infarct healing
FVB	+/–	+/–	–	+	+	+	+/–	infarct healing
129S6	–	+	–	–	+/–	+	+	prevention of infarct rupture
Swiss	+	+/–	+	+	+/–	–	–	heart failure

Limitations of the study

In order to limit the number of variables, we used young (10-12 weeks old) male mice in this study. It is well known that gender has a major influence on the outcome of experimental studies, including studies on infarct healing.[88] Male mice have a higher rate of infarct rupture[77, 89] and poorer cardiac function with maladaptive remodeling compared to female mice.[89] Furthermore, remodeling post-MI is dependent on the age of the mice.[90] Because most of the studies on the effect of genetic alterations on cardiac remodeling post-MI use young adult male mice, we have limited our study to this subgroup. However, we can not exclude that the results may be different when mice with other characteristics are used.

Increased Matrix Metalloproteinase-8 and -9 Activity in Patients with Infarct Rupture after Myocardial Infarction

4

Cardiovasculair Pathology 2009; 18:37-43.

ABSTRACT

Background: Infarct rupture is a usually fatal complication of myocardial infarction (MI), for which no molecular mechanism has been described in humans. Experimental evidence in mouse models suggests that the degradation of the extracellular matrix by matrix metalloproteinases (MMPs) plays an important role in infarct rupture. The present study was designed to study the role of MMP-2, -8 and -9 in human infarct rupture.

Methods: Heart samples were obtained from patients who died from infarct rupture and control MI patients. The MMP activity was determined by zymography and quantitative immunocapture activity assay. TIMP-1 levels were measured and immunohistochemistry for MMP-2 and MMP-9 was performed.

Results: The amounts of both total and active MMP-8 and MMP-9 were significantly higher in ruptured infarct tissue than in control MI tissue, but no differences in MMP-2 activity were observed. Furthermore, the number of inflammatory cells was significantly higher in the ruptured infarcts than in control infarcts.

Conclusions: These data suggest that increased MMP-8 and -9 activity in the infarct area, caused by a more prominent infiltration of inflammatory cells, contribute to infarct rupture in humans.

INTRODUCTION

Infarct rupture is a life-threatening complication of myocardial infarction (MI), which usually occurs in the first week after acute MI.[91-95] Rupture is most frequent when the infarct is located in the left ventricular free wall,[91] causing almost instantaneous death due to cardiac tamponade.[96] Infarct rupture accounts for up to 10% of the mortality from acute MI.[94, 97] The only clinical parameters that are generally associated with infarct rupture include transmural infarction, first episode of MI and a poor collateral circulation.[98, 99] However, little is known about the molecular mechanisms that lead to infarct rupture in humans.

The progress in transgenic technology has fuelled research on mechanisms of infarct rupture in mice. These studies have shown that inhibition of plasminogen activation[22, 23, 100] or targeted deletion of matrix metalloproteinase (MMP)-2[24, 83] or MMP-9[23] reduces the incidence of infarct rupture in mice. Similar results have been observed using pharmacological inactivation of MMP-2.[83] The combined results of these mouse studies suggest that excessive degradation of the extracellular matrix in the infarct area can lead to infarct rupture. However, there is a paucity of data in humans, evaluating the possible role of these molecules in infarct rupture.

The present study was undertaken to evaluate the possible contribution of matrix metalloproteinases to infarct rupture in humans. We focused on MMPs associated with inflammatory processes, such as MMP-2, MMP-8 and -9. We analyzed the amounts of both the active and latent forms of MMPs in a unique set of samples obtained from ruptured human infarcts and compared them to infarcts of similar age that did not rupture. Since overexpression of tissue inhibitor of metalloproteinase-1 (TIMP-1) has been shown to protect against infarct rupture in mice,[23] we also assessed the TIMP-1 levels in human infarcts. In addition, we evaluated the extent of inflammatory cells in the infarct area.

METHODS

Tissue selection

Collection, storage and use of human heart tissue and patient data were performed in agreement with the "Code for Proper Secondary Use of Human Tissue in the Netherlands" (http://www.fmwv.nl). In this study, a set of samples of left ventricular (LV) tissue was obtained at autopsy, snap-frozen in liquid nitrogen and stored at –80 °C until further use. LV samples from 10 patients who died from infarct rupture (age 52 to 87 years; 8 males, 2 females) were included, as well as LV samples from 10 control MI patients who suffered from MI but died from causes other than infarct rupture (age 48 to 86 years; 4 males, 6 females).

The two groups were matched according to postinfarction survival times. The infarct area (identified by nitroblue tetrazolium (NBT) staining) was present at different anatomical locations as indicated in Table 4.1. Samples from both the infarct area and a non-infarcted area of the LV were collected from all patients. There was no significant difference in the time between death and autopsy between the two groups (rupture: 22.6±6.1 hours, control MI: 19.6±5.1 hours). For more patient data we refer to Table 4.1.

To expand our findings with immunohistochemistry, an additional set of tissue samples, which were formalin fixed and paraffin embedded, was investigated. Infarct age was determined by histological analysis of haematoxylin and eosin-stained sections according to previously described criteria.[3] Inflammatory cells were identified by cytological characteristics and counted in four randomly chosen fields (90.000 µm2 per field) of the border zone in 6 ruptured and 6 non-ruptured control infarcts.

Zymography

Protein was isolated from four 20 µm frozen tissue sections obtained from a subgroup of 6 ruptured and 6 control MI patients (see above) as previously described.[22] MMP activity was visualized using zymography, as previously described.[11] Briefly, gelatin (final concentration of 0.66 mg/ml) was added to a 10% standard Laemmli[79] acrylamide polymerization mixture. Ten µg (for MMP-2 analysis) or 1 µg (for MMP-9 analysis) of non-denatured protein was loaded per lane(80). A protein standard with proven MMP-2 and -9 activity was loaded on each gel as a control. Following electrophoresis, gels were rinsed two times 15 minutes in 2.5% Triton X-100 and incubated overnight at 37 ^{0}C in substrate buffer (50 mmol/L Tris HCl pH 8.5, 5 mmol/L $CaCl_2$, and 0.02% NaN_3). After incubation, gels were stained with 0.1% Coomassie Blue R 250 in acetic acid: methanol:water (1:4:5) and destained in the same solvent. The zones of proteolytic activity were visualized as clear bands against a dark background. The gels were digitized and analyzed with image analysis software (Qwin version 3.4.0, Leica, Cambridge, UK). The integrated optical density of the individual bands was determined and normalized against the value of a standard sample that was run on every gel.

MMP immunocapture activity assay

Total and active MMP-2, -8 and -9 were measured in 10 infarct rupture and 10 control MI patients, using the Biotrak MMP-activity assay (Amersham/GE Healthcare, Buckinghamshire, UK) according to manufacturer's instructions. In short: MMP-activity was analyzed in cardiac tissue homogenates using the proform of a detection enzyme that is activated by captured active MMP into an active detection enzyme. The amount of active MMP was determined directly using this specific capture step. In order to measure the total MMP content,

MMP in its pro-form was activated using p-Aminophenylmercuric Acetate.[101, 102] Protein samples were isolated as described above. MMP activity was expressed in units/ml, in which a unit is defined as the extinction at 405 nm per time-unit in a two-step reaction (ΔA_{405}*1000/t^2).

TIMP-1 levels were measured in protein samples from ruptured and control MI patients using the human TIMP-1 ELISA kit (R&D Systems, Minneapolis, MN, USA) according to the manufacturer's instructions. TIMP-1 levels are expressed in ng/ml.

Immunohistochemistry

Histological sections (4 µm) were cut from paraffin-embedded tissue from all patients, mounted on glass slides coated with 3-aminopropyltriethoxysilane (APTS, Sigma-Aldrich, St. Louis MO, USA) and dried overnight in an incubator at 37 °C. The sections were deparaffinated in xylene, rehydrated and endogenous peroxidase was blocked by incubation in methanol containing 0.3% H_2O_2 for 15 minutes, followed by rinsing with Tris buffered saline, pH 7.5 (TBS). For antigen retrieval of MMP-9, a microwave pretreatment step was needed: these sections were treated by boiling in 0.01 M citrate buffer (pH 6.0) for 10 minutes in a microwave (750 Watt) and allowed to cool down for 15 minutes at room temperature (RT). Mouse monoclonal antibodies, raised against human MMP-2 and MMP-9 (Merck Biosciences, Darmstadt Germany) were used. Sections were incubated with the primary antibodies for 1 hour at RT in the following dilutions: MMP-2 (1:20) and MMP-9 (1:30). After washing with TBS, biotinylated sheep anti-mouse IgG (Amersham, dilution 1:250) was applied to each section and incubated for 1 hour at RT. Subsequently, sections were washed and incubated with alkaline phosphatase coupled ABC reagent (DAKO, Glostrup, Denmark) for 30 min at RT. Alkaline phosphatase activity was visualized using New Fuchsin substrate (BioGenex, San Ramon, CA, USA), resulting in a red precipitate. The sections were counterstained with hematoxilin, dehydrated and aqueously mounted.

Table 4.1 Overview of patient data

	M:F	Age	MI localization			MI age	Hypertension	Diabetes	Thrombolysis	CABG/ PTCA	Previous MI
			Posterior	Anterior	Lateral						
Infarct Rupture	8:2	67±10	4/10	5/10	1/10	1-6 days	2/10	2/10	1/10	4/10	1/10
Control MI	4:6	70±13	5/10	4/10	1/10	1-6 days	1/10	1/10	0/10	6/10	10/10

CABG=coronary artery bypass graft, PTCA=percutaneous transluminal coronary angioplasty

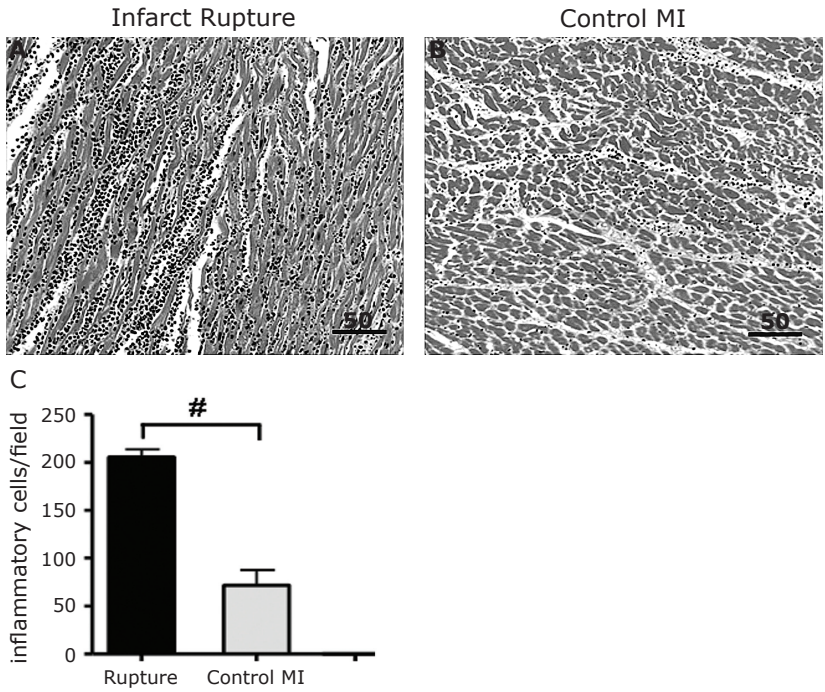

Figure 4.1 **Histological analysis of inflammatory cells in infarct rupture and control MI patients**

Representative images of H&E staining of the MI border zone in infarct rupture patients (A) and control MI patients (B). (C) Quantitative analysis of the inflammatory cells showed a significant increase in infarct rupture patients compared to control MI patients (P < 0.001). A field is defined as 90.000 μm². Scale bar length is indicated in μm. For full color illustration, see page 160.

Statistical analysis

All data are presented as means±SEM. Statistical analysis was performed using a Mann-Whitney U test; a P-value <0.05 was considered to indicate statistical significance.

RESULTS

Inflammatory cells in the infarct area

Inflammatory cells were counted in the border zones of both infarct rupture and control MI samples. In each section 4 randomly selected fields of the border zone (90.000 μm² each) were analyzed. Massive influx of inflammatory cells was observed in the ruptured infarcts (Figure 4.1A). In the control MI patients (Figure 4.1B) the influx of inflammatory cells was approximately one third of the level in the ruptured infarcts. (P < 0.001). (Figure 4.1C)

MMP analysis

The amounts of both latent and active MMP-2 and MMP-9 in samples from ruptured infarcts were compared to samples of age-matched infarcts obtained from control MI patients by zymography (Figure 4.2A). The amount of latent MMP-2 was similar in both groups, but the amount of active MMP-2 tended to be somewhat higher in the ruptured infarcts, although this did not reach statistical significance (p=0.18) (Figure 4.2B). Latent MMP-9 levels were significantly elevated in rupture samples compared to infarct tissue obtained from the control MI patients ($p<0.05$), and the active MMP-9 levels were more than 2-fold higher in rupture samples ($p<0.05$) (Figure 4.2B).

To confirm and expand these findings, the amounts of total and active MMP-2, MMP-8 and MMP-9 were determined in an MMP activity assay. The amounts of both total and active MMP-8 and -9 were 1.8 to 8.4 fold higher ($p<0.05$) in rupture samples compared to control MI samples (Figure 4.3A, B). In contrast, total and active MMP-2 did not significantly differ between the two groups (Figure 4.3A-B). In addition, the amount of TIMP-1, determined by ELISA and expressed in ng/ml (Figure 4.3C), demonstrated a more than 2-fold increase in infarct rupture patients compared to control MI patients ($p<0.05$).

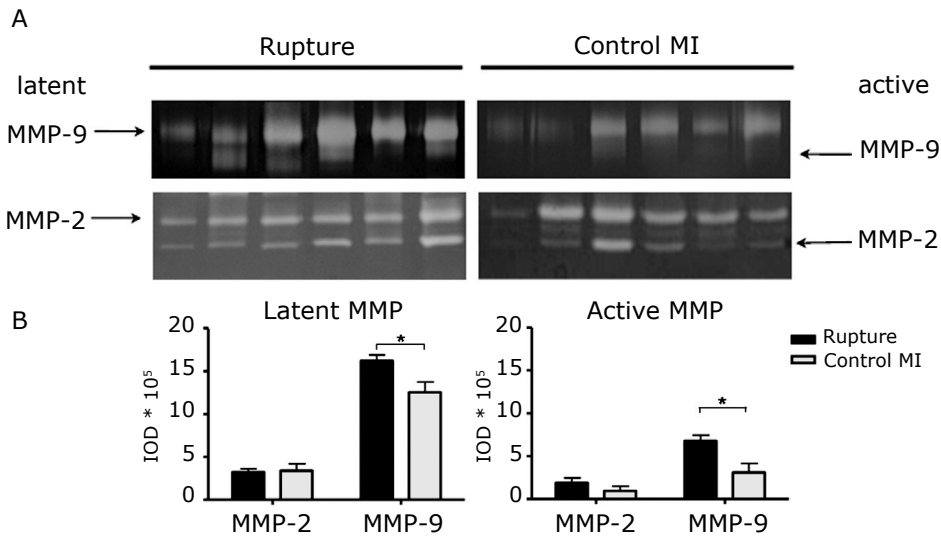

Figure 4.2 **Zymographic analysis of MMP-2 and MMP-9 in infarct rupture and control myocardial infarction patients**

*(A) Gelatin zymography demonstrating the MMP activity in myocardial infarct tissue obtained from infarct rupture patients and control MI patients. The two top bands represent the latent and active form of MMP-9, respectively, whereas the two lower bands represent the latent and active form of MMP-2. (B) Quantification of the latent and active forms of MMP-2 and MMP-9 on zymography, expressed in intensity units (IOD). Both latent and active MMP-9 are significantly higher in the infarct rupture patients compared to control MI patients. *: p<0.05*

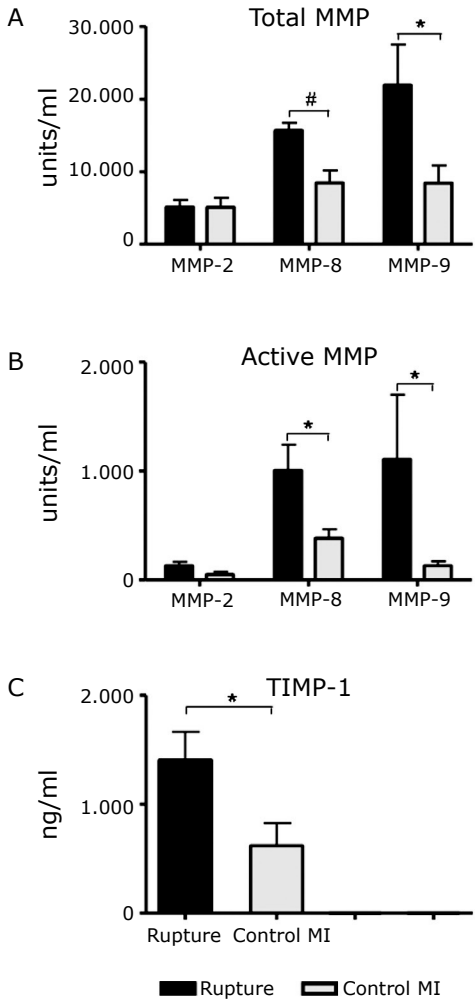

Figure 4.3 **MMP activity**

*MMP activity assay; total (A) and active (B) MMP-2, MMP-8 and MMP-9 are expressed as units per ml. Total and active MMP-2 are not significantly different between ruptured and control MI. However, both total and active MMP-8 and MMP-9 are significantly higher in the infarct rupture group. *: P<0.05, #: P< 0.01 (C) TIMP-1 levels, expressed in ng/ml, are significantly higher in infarct rupture patients compared to control MI patients. #: p<0.05*

MMP localization in the infarct rupture and control MI group

MMP-2 immunoreactivity was mainly observed in vital cardiomyocytes (Figure 4.4A,B), but also in smooth muscle cells, fibroblast-like cells, endothelial cells and inflammatory cells. Necrotic cardiomyocytes, identified by the absence of nuclei, lacked immunoreactivity for MMP-2 (Figure 4.4A,C). No differences were observed in MMP-2 staining between the infarct rupture patients and the control MI patients.

MMP-9 was localized in and around the inflammatory cells both in the infarct rupture and control MI group (Figure 4.5A-D). However, in the infarct rupture group (Figure 4.5A,B) the number of positive cells and the staining intensity of MMP-9 appeared to be higher than in the control MI group (Figure 4.5C,D). This observation corroborates the increased amounts of MMP-9 in both zymography and activity assays as well as the higher number of inflammatory cells in the infarct rupture group.

DISCUSSION

To identify molecular mechanisms associated with infarct rupture in humans, we evaluated MMP-2, -8, -9 and TIMP-1 in myocardial specimens from victims of infarct rupture and compared them to infarct zones from uncomplicated MI. Total and active MMP-8 and -9 were significantly elevated, suggesting a possible role of matrix dissolution preceding rupture. Since remote areas of myocardium in patients with infarct rupture do not demonstrate upregulation of MMP activity

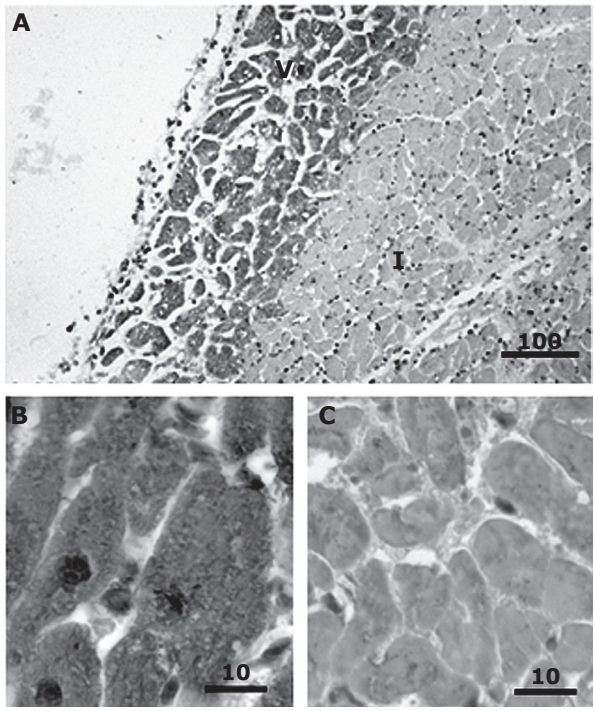

Figure 4.4 Representative images of immunohistochemical staining for MMP-2

MMP-2 was mainly present in vital (V) cardiomyocytes (A-B) and decreased in ischemic (I) cardiomyocytes (A,C). MMP-2 immunoreactivity showed the same pattern in ruptured and control MI. Scale bar length is indicated in μm. For full color illustration, see page 160.

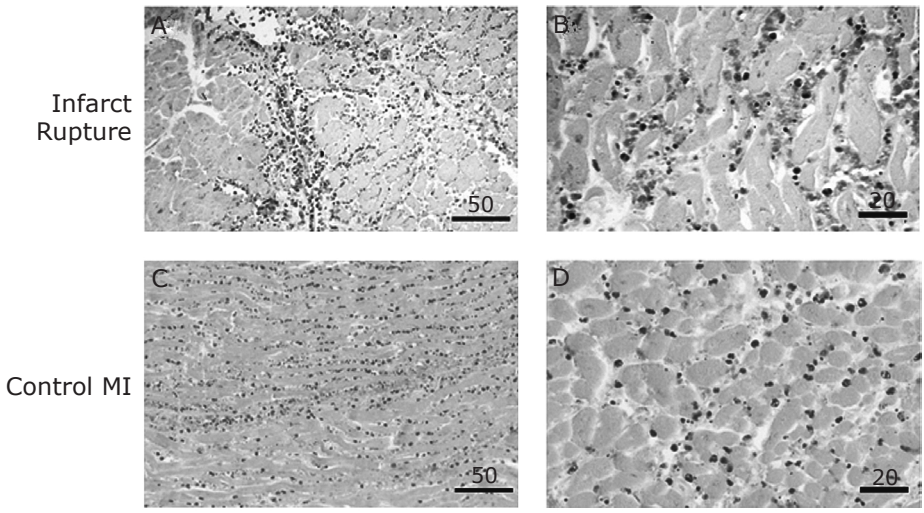

Figure 4.5 Representative images of immunohistochemical staining for MMP-9

MMP-9 was mainly present in inflammatory cells (Figure 4.5A-D). Infarct rupture patients (Figure 4.5A-B) showed more abundant staining than control MI patients (Figure 4.5C-D). Scale bar length is indicated in μm. For full color illustration, see page 161.

(data not shown), and inflammation around the infarct area is significantly more intense, it is likely that MMP upregulation is secondary to inflammation. The cause of the increased inflammatory response is currently subject of investigation in our lab.

Infarct rupture typically occurs in the first week after a transmural MI. The first days after MI are characterized by an inflammatory response, migrating from the border zone to the center of the infarct area in approximately 14 days following MI. This inflammatory response is followed by the formation of granulation tissue, which starts not earlier than 5 days after MI.[83, 97] Therefore, the main constituents of 1-4 day old infarcts are necrotic cardiomyocytes, embedded in their original matrix, and inflammatory cells. The wound healing response after MI requires a delicately controlled proteolysis of the necrotic debris in the infarct area: too little proteolysis will hamper the progression of wound healing and too much proteolysis will deteriorate the integrity of the infarct area.[23] MMPs play a central role in proteolysis within the infarct zone and therefore were subject of this study.

The relationship between infarct rupture and activity of different members of the MMP family has been studied in mouse models. Either genetic or pharmacological inhibition of MMP-2 has been shown to protect against infarct rupture in

mice.[24, 83] This has been attributed to a reduced macrophage infiltration of the infarct area, leading to a delayed post-MI remodeling.[83] An increased MMP-9 activity in ruptured infarcts has also been reported in animal studies.[22, 23, 84, 103] The activity of MMP-9 increased as early as 1 day after MI and reached a maximum at 2-4 days after MI in mice,[84] suggesting a link with neutrophil infiltration of the infarct area.[3] Moreover, MMP-9 gene ablation protected against infarct rupture in mice.[23] Another member of the MMP family, known to be produced by inflammatory cells like neutrophils and macrophages, is MMP-8.[100, 104, 105] Although a role for MMP-8 in infarct rupture has not been reported to date, it is a likely candidate to contribute because of the increased influx of inflammatory cells in ruptured infarcts.

In the present study, the activity of MMP-8 and -9 in ruptured infarcts was significantly increased. However, no increase in MMP-2 activity was observed, which is in disagreement with the protective role of MMP-2 inhibition in animal models.[24, 83] This may reflect a difference in the pathophysiology of infarct rupture between mice and men. Previous studies in humans have used indirect measurement of MMP-levels, either in pericardial fluid[106] or plasma,[107] to study MMP-levels during infarct healing and rupture in humans. In pericardial fluid, both MMP-2 and -9 were upregulated after acute myocardial infarction, but only MMP-9 was further elevated in a subgroup suffering from ventricular septum rupture.[106] The profile of MMP-8 and -9 expression reported here is in agreement with increased plasma levels of MMP-8 and -9, reported earlier, in patients after myocardial infarction although infarct rupture was not addressed in that study.[107] However, it is to be noted that these studies only reported the latent forms of MMP due to the indirect nature of the sample collection. In the present study, MMP activity was determined directly in the source tissue, allowing separate analysis of latent and active MMPs.

The localization of MMP-2 and -9 was determined using immunohistochemistry. MMP-2 immunoreactivity was observed in the cardiomyocytes, whereas MMP-9 immunoreactivity was confined to the inflammatory cells in the infarct area. Because MMP-8 is well known to be expressed in neutrophils and macrophages,[100, 105] these observations indicate that the MMPs produced by the inflammatory cells may play a major role in infarct rupture. Elevated numbers of inflammatory cells in ruptured infarcts have previously been reported[84] and were confirmed in the present study. Furthermore, we cannot rule out that latent MMPs, present in the interstitium are activated and also contribute to tissue proteolysis, although we expect this contribution to be of minor importance.

The activity of MMP has to be tightly regulated to prevent excessive matrix degradation. Members of the family of tissue inhibitors of metalloproteinases (TIMPs) can inhibit MMP activity. We determined the amount of TIMP-1, which

can inhibit a broad spectrum of MMPs by binding to active MMP, providing a localized regulation of MMP activity. TIMP-1 has previously been shown by our group to be upregulated after MI.[100] We observed a significant upregulation of TIMP-1 in the ruptured infarcts compared to control infarcts in the present study. Although this observation may seem contra-intuitive, the increased TIMP-1 levels apparently can not effectively counteract the increased MMP activity in the ruptured infarcts. Upregulation of TIMPs has also been demonstrated in other inflammatory processes, like multiple sclerosis.[108] Moreover, TIMP-1 increases when macrophages are activated with cytokines or LPS in vitro.[109, 110] Alternatively, TIMP-1 may prolong the life span of inflammatory cells in the tissue by specific blockade of their transmigration and by inhibiting their spontaneous apoptosis. In acute pyelonephritis, these entrapped and activated inflammatory cells excessively destroy the extracellular matrix.[111] A similar mechanism may contribute to the increased inflammation and MMP-activity in infarct rupture.

One of the limitations of this study is the matching between ruptured patients and control MI patients. (see Table 4.1). The limited number of cases prevented a full match with respect to gender. Furthermore, patients with infarcts at different anatomical locations were included. However, the study was designed to match for postinfarction survival time in order to allow a fair comparison in MMP activity levels post-MI. Another limitation of the study is the timing of rupture of the included patients. The "classic" ruptures, as included in this study, occur at day 4-10 post-MI. Nowadays, with the advent of thrombolytic therapy, there is an increase in early ruptures, within the first day(s) post-MI. It is known that the timing of thrombolytic therapy is very critical, leading to a decrease in cardiac rupture when administered early, but an increase in the risk of cardiac rupture when administered late after the onset of MI.[112] In the present study only one patient who received thrombolytic therapy was included. Therefore we cannot conclude that upregulation of MMP-8 and -9 activity is also responsible for trombolysis-induced early infarct rupture.

In conclusion, we report an increase in both latent and active MMP-8 and -9 in human ruptured infarcts, compared to control infarcts at the same time after MI. No difference in MMP-2 activity was observed, although this MMP also has been associated with infarct rupture in mouse models. The increased amounts of MMP-8 and -9 were likely produced by larger numbers of inflammatory cells in the ruptured infarcts compared to controls. These observations in humans may help develop therapeutic tools for this life-threatening complication of MI.

Acknowlegements
We thank Jos B.G. Paquay, Peter M. Lijnen, Denise van Hezik, Maria Vlieks and the residents of the Department of Pathology for their help in collecting human tissue samples.

Defective Intercellular Adhesion Complex in Myocardium Predisposes to Infarct Rupture in Humans

5

Journal of the American College of Cardiology 2008;51:2184-92

ABSTRACT

Objective: To evaluate intercellular adhesion complex proteins in myocardium in human infarct rupture.

Background: Infarct rupture, a fatal complication of myocardial infarction (MI), has been attributed to a defective cell adhesion complex in a transgenic mouse model.

Methods: Heart samples were collected from autopsies from infarct rupture and control (non-rupture) MI patients. Both infarcted and remote areas were included. Cell adhesion proteins including αE-catenin, β-catenin, γ-catenin, and N-cadherin were characterized by immunohistochemistry and immunoblotting. Genetic analysis was undertaken to evaluate mutations and polymorphisms in the αE-catenin gene. In addition, infarct rupture was studied in transgenic mice heterozygous for αE-catenin C-terminal deficiency, mimicking the situation in human infarct rupture patients.

Results: No αE-catenin was detected in 70% of remote samples of infarct rupture hearts compared to 20% in control MI by immunohistochemistry. The immunoblot analysis confirmed a significant reduction in remote areas, and complete absence of αE-catenin in infarct areas from infarct rupture patients. No mutation or polymorphism of the αE-catenin gene was discovered. Other cell adhesion proteins were not significantly affected in remote areas of infarct rupture hearts. Three-fourths of the heterozygous αE-catenin C-terminal truncated mice died of infarct rupture, compared to one-fourth of the wild type littermates.

Conclusions: The data show a reduced expression and defective localization of αE-catenin in the intercalated disc region in patients dying of infarct rupture. The mechanism of lower expression of αE-catenin remains to be elucidated.

INTRODUCTION

Although generally considered to be a rare complication of acute myocardial infarction (MI), myocardial infarct rupture remains a common cause of death,[91, 93] and accounts for approximately 10% of mortality.[94, 97] Rupture is most frequent when the infarct area is located in the ventricular free wall[91] and nearly always results in sudden death from massive blood loss into the pericardium, causing cardiac tamponade.[91, 95] Most infarct ruptures occur within the first week of MI,[94, 95] usually after transmural, first, or anterior MI, and in the setting of poor collateral circulation.[99, 113] Little is known about the molecular mechanisms of infarct rupture.

Recently, the role of defective intercellular adhesion complexes has been implicated, based on an increased incidence of infarct rupture in mice lacking the αE-catenin gene.[25] αE-catenin protein is a component of the cadherin/catenin cell adhesion complex, which mediates cell adhesion in many cell types.[114] Loss of cell adhesion molecules has been associated with metastasis in many human cancers,[115] underscoring their role in cell adhesion. In myocardium, these cell adhesion complexes are located in the intercalated disks,[116] and a weakened cardiomyocyte adhesion could facilitate inflammatory cell infiltration. Increased inflammatory cell influx and consequent upregulation and activation of matrix metalloproteinases have previously been reported to be associated with infarct rupture in animal studies[19, 100] and in humans.[117]

The present study was undertaken to evaluate the role of cadherin and catenin proteins, especially αE-catenin, in patients dying of infarct rupture. In this case control study, we performed biochemical and immunohistochemical characterization of the adhesion complex proteins and compared with age matched postmortem myocardial tissue specimens obtained from MI patients dying of causes other than infarct rupture (control MI). The adhesion complex proteins were characterized in both infarcted and remote areas. The analysis of the αE-catenin gene was also performed to identify mutations or polymorphisms. In addition, to mimic these observations in an animal model, we studied the impact of MI in transgenic mice heterozygously deficient for the C-terminal part of αE-catenin and found a higher incidence of infarct rupture compared to their wild type littermates.

METHODS

Myocardial tissue specimens

Collection, storage and use of human heart tissue and patient data were undertaken in compliance with the "Code for Proper Secondary Use of Human

Table 5.1 Characteristics of pateints included in this study

	Infarct rupture		Control MI	
	Prospective (n=10)	Retrospective (n=10)	Prospective (n=10)	Retrospective (n=10)
Men:women	8:2	4:6	4:6	5:5
Age (years)	67±10	75±6	70±13	75±7
MI localization				
Posterior	4	3	5	4
Anterior	5	7	4	4
Lateral	1	0	1	2
MI age	1-6 days	1-6 days	1-6 days	3-216 months
One-vessel disease	5	6	2	1
Thrombolysis	1	1	0	0
Rescue PCI	4	2	4	1
CABG*	0	0	1	6
Smoker	5	1	1	2
Diabetes	1	3	2	3
Hypertension	3	3	3	4
Previous MI	1†	3†	2	10‡

**None of the coronary artery bypass grafts (CABGs) were performed in the acute phase of myocardial infarction (MI); †Small and nontransmural MI; ‡Selected for previous, well-healed, transmural MI; PCI=percutaneous coronary intervention*

Tissue in the Netherlands" (http://www.fmwv.nl). For the present study, the post-mortem myocardial tissue specimens were collected in 40 patients with MI, 20 with infarct rupture and 20 without rupture (control MI). For each patient, samples from the infarct area and from remote myocardial region were obtained (Table 5.1).

For the prospective part of the study, myocardial samples were obtained at autopsy (collected from 2001 to 2006). Part of the samples were snap frozen in liquid nitrogen, part was formalin fixed. Left ventricular (LV) myocardial samples were collected from 10 patients who died of infarct rupture (age 52 to 87 years; 8 males, 2 female) (infarct rupture group). For comparison, LV samples were also collected from 10 MI patients who suffered from MI 3-7 days before death but died from causes other than infarct rupture (age 48 to 86 years; 4 males, 6 females; control group). The two groups were similar according to post-MI survival times. Also, there was no significant difference in the time lapsed between death and autopsy between the two groups (rupture: 22.6 ± 6.1 hours, control MI: 19.6 ± 5.1 hours). The frozen tissue samples were stored at –80 °C and subsequently used for Western blotting and DNA isolation. The formalin-fixed

tissues were embedded in paraffin, and the sections stained with hematoxylin and eosin to estimate the infarct age. In addition, all formalin-fixed tissue specimens were used for immunohistochemical staining for catenin and cadherin family proteins.

For the retrospective part of the study, myocardial tissue samples were obtained from Maastricht Pathology Tissue Collection registry; autopsies were performed between 1996-2000). After review of the clinical histories, paraffin-embedded tissue samples from different areas of the heart were obtained from 10 patients, who had died of infarct rupture. The age of the patients (4 males and 6 females) ranged from 63 to 84 years; all 10 patients had sustained rupture of the LV free wall in the index episode and had no evidence of previous transmural MI. In addition, post-mortem myocardial specimens were also collected from 10 control patients (5 males and 5 females) who had suffered from transmural MI in past, but had died of unrelated causes. These patients revealed pathological evidence of an old-infarct with adequate infarct healing. The age of these patients ranged from 63 to 85 years and was similar with the patients in the infarct rupture group.

Immunohistochemistry

From paraffin-embedded tissue, 4 μm-thick sections were cut, mounted on glass slides coated with 3-aminopropyltriethoxysilane (APTS, Sigma-Aldrich, St. Louis MO, USA) and dried overnight in an incubator at 37 °C. The sections were deparaffinated in xylene, rehydrated and endogenous peroxidase was blocked by incubation in methanol containing 0.3% hydrogen peroxide for 15 minutes, and rinsed with PBS. For antigen retrieval of β-catenin, γ-catenin and N-cadherin, sections were boiled twice for 5 minutes in 10 mmol/L citrate buffer (pH 6.0). For αE-catenin, sections were boiled in citrate buffer for 10 minutes at 110 °C in an autoclave. The following primary antibodies were used: β-catenin monoclonal antibody (dilution 1:500, Transduction Labs, Lexington KY, USA), γ-catenin polyclonal antibody (dilution 1:50, Santa Cruz Biotechnology, Santa Cruz, California) and pan-cadherin monoclonal antibody (dilution 1:250, Sigma). This pan-cadherin antibody was raised against the C-terminal cadherin sequence, which is common in many cadherins including N-cadherin, the main cardiac form. Immunohistochemistry for αE-catenin was performed using two different polyclonal antibodies raised against the C-terminal part of the αE-catenin protein (dilutions 1:50, Santa Cruz and 1:100 Neomarkers, Fremont CA, USA, respectively). All sections were incubated overnight with the antibody at 4 °C. The following secondary antibodies were used: biotinylated multilink Swine-anti goat, -mouse and -rabbit (dilution 1:400, DAKO, Glostrup, Denmark) and rabbit-anti goat (dilution 1:600, DAKO). The Vectastain ABC kit (Vector, Burlingame CA, USA) was used according to the manufacturer's instructions to visualize the

binding of the primary antibodies. Sections were briefly counterstained with hematoxylin before mounting with Entellan (Merck, Darmstadt, Germany).

Four sections per patient, obtained from different parts of the heart, were analyzed in a blinded way by two independent observers. The sections were included into one of three categories: detectable staining of intercalated discs (ICD) in three or more sections per patient (+), detectable staining of ICD in one or two sections per patient (±), or no detectable staining of ICD (-).

Western blotting

For Western blotting, samples of the frozen heart tissue were placed in 500 µl ice-cold Laemmli buffer (6.6% Glycerol, 1.5% SDS, 41.5 mmol/L Tris/HCl pH=8.0) and homogenized with a PRO200 tissue homogenizer (PRO Scientific, Oxford CT, USA). After sonication and centrifugation, the supernatant was collected and protein content was measured using the BCA protein Assay (Pierce Biotechnology Inc., Rockford IL, USA). Ten µg of total protein was denatured by boiling in Laemmli sample buffer (Biorad, Hercules CA, USA), separated on a 10% SDS-PAGE gel[118] and transferred onto a Hybond C nitrocellulose membrane (Amersham Biosciences, Little Chalfont, UK). After blocking (5% nonfat dry milk (Biorad), 0.1% Tween in TBS) for 1 hour, membranes were incubated overnight at 4 °C with primary antibodies directed against α-catenin 1:3000 (Sigma-Aldrich, St. Louis, Missouri, USA) and α-tubulin (H-300) 1:500 (Santa Cruz, Santa Cruz CA, USA) for loading control. For this part of the study we were unable to use the αE-catenin antibodies that were used for immunohistochemistry, because these antibodies failed to produce a distinct band in our Western blot assay. The α-catenin antibody from Sigma is known to cross-react with both αE and αN-catenin, but since the latter subtype of α-catenin is not present in the heart the observed band represents αE-catenin. Anti-rabbit IgG (PI 1000) 1:5000, (Vector labs Inc., Burlingame, California, USA) was used as the secondary antibody and the membranes were developed using the Supersignal West Pico chemiluminescence kit (Pierce). Images of the blots were analyzed with image analysis software (Qwin, Leica, Cambridge, UK).

DNA isolation, PCR amplification and sequencing

In order to sequence the 16 coding exons of αE-catenin (*CTNNA1*, MIM:*116805), DNA was isolated from snap-frozen tissue samples from remote parts of the hearts of both infarct rupture patients and control MI patients. In total, we included tissue from 3 patients who died of infarct rupture and 3 patients who suffered from recent MI (3-7 days post-MI) but died from causes other than infarct rupture. DNA was isolated from the tissue samples using the Dneasy Tissue kit, (Qiagen, Hilden, Germany) according to the manufacturer's instructions.

Tabel 5.2 **Primers used for PCR and sequencing of αE-catenin (CTNNA1, Ensembl id no. ENST00000302763)**

Exon	Forward primer	Reverse primer	Ta (°C)
1	TGCCTGACTGACTTTTTGTTTCTT	GGCCTGTGCTATAGAACCATGTTA	56
2	TTTTAAAAGAATAACTTAATCTTGCTGTCTTT	CCACAAAAAAAATCTTCAAACACTG	57
3	GTGCATGAAATATACAAAGTTTGGATTAT	GCCAGTAGCAATCTTCCTGTGA	55
4	GGATGCCATCTTCTTTACAGACCT	CACAGAATGAGTTTTTCCCTCTAGATAG	64
5	AGAGTGCTCCAATTTCTTGTTTTATTTAC	GGGATGGTCAAGAGCTGGAA	57
6	AAGAAGGGAACAGAGATGAGTACTAACA	CTCCTCATCCATAAATATCTTACTTCAAAG	55
7	AATGCTCATCTCTTTTCCTTTTATCC	AAACAATCAGCACTTTCATCCAGA	55
8	AGTCTACCGTAAGCTTCATTAGATTTAAGTG	TGCCTACAAGTCAATGAAACTGC	55
9	TTCCTTAGCAGTCAAAAGAGAAAAATC	CCTCATCTCCACTTGAATCAAAATT	55
10	TGCATGTAAGACAAAGCCATGAC	GCAGTGTTTGCCCATTAATACAACT	55
11	GCTTACAGTTGCCACCTTTTCAT	GGTGGCCTGCCTCACTGA	63
12	AGCTGAGTGATTCAGGGAGGG	GAATGACGCATTGCTCAAGTTT	61
13	ATGTGTCTGACCTGTGATCTTTGTCT	AATACTGAGGGTGTTTTCCTGGAA	61
14	ATTCTTGGCTAATGCACTCTGAGA	GAAGAAAGTAGCCCCTGTGCAG	61
15	TCTTCTTTTTCTACTCCAACTGTGAGG	CCAGGAGGAGCTTGGAGACC	55
16	GCCAGGCCAGGATACTTGGT	GGTCAGCACGTTCCCACTG	64

*also used as sequence primer

PCR was performed in 25 µl reactions using PuReTaq Ready-To-Go PCR beads (Amersham). Both forward and reverse primers were used in a concentration of 10 µM (See Table 5.2). PCR reactions were performed in the Biorad I-cycler (Biorad). The PCR products were identified on a 1% agarose gel and purified using the High pure PCR purification kit (Roche diagnostics GmbH, Mannheim, Germany) according to the manufacturer's instructions.

Cycle sequencing was performed using the BigDye Terminator v3.1 cycle sequencing kit (Applied Biosystems, Foster City CA, USA) according to manufacturer's instructions. The forward primers of the PCR reactions were used as sequencing primers (see Table 5.2). In a 20 µl reaction volume, 3.2 pmol primer was added. The products of the sequence reactions were purified by ethanol precipitation and analyzed using an ABI Prism 3100 genetic analyzer (Applied Biosystems).

Experimental myocardial infarction in αE-catenin deficient mice, tissue collection and processing

Animals

Heterozygous αE-catenin C-terminal deficient mice were created using a gene trap strategy in R1 embryonic stem cells, which were a kind gift of Dr. P. Gruss, Germany. These embryonic stem cells where injected into C57Bl6 blastocysts to

generate αE-catenin deficient mice. In these mice, the mutation eliminates the carboxyl-terminal third of the protein and induces a complete loss of function phenotype.[119] Since homozygous mice die in the blastocyst stage,[119] we only used adult, male heterozygous mice (n=9) and compared them to their wildtype littermates (n=11). All experiments were conducted according to institutional guidelines and conformed to the guide of the care and use of laboratory animals published by the National Institutes of Health.

Experimental myocardial infarction
Experimental Myocardial infarction was induced as described previously.[78] Briefly, all mice received Buprenorphine 0.1 mg/kg subcutaneously as pain medication before surgery. Mice were anaesthetised using 3-4% Isoflurane, which was gradually decreased to 1.5-2.5% during surgery. The trachea was intubated to allow positive pressure respiration with room air (1.5 ml, 70/min). A ligature (6-0 prolene) was tied around the main left coronary artery after opening the skin, the left 4th intercostal space and the pericardial sac. Chest and skin were closed with 5-0 silk sutures.

Tissue collection
Mice were scheduled to be sacrificed 7 days after MI. Half of the heart was snap frozen into liquid nitrogen and stored at -80 °C until further use. The other half was formalin fixed and paraffin embedded for immunohistochemistry. Ten mice died of acute rupture between 3 to 5 days, and the tissue samples were collected similarly. The same protocol for Western blotting was used as described for human tissue.

Statistical analysis
All data are presented as means±SEM. Statistical analysis was performed using a two-way ANOVA with 1 repeated measures factor with Bonferroni posthoc-test as applicable. For analysis of the semiquantitative immunohistochemistry data, a Chi-square test was performed. Survival was analyzed by a Kaplan Meier curve with a log-rank test for differences between groups. A P-value <0.05 was considered to indicate statistical significance. Graphpad Prism 4 software (Graphpad Software, Inc., San Diego, CA) was used for statistical analysis.

RESULTS

Immunohistochemical localization of cellular adhesion motifs
To analyze the localization characteristics of the cell adhesion complex in infarcted and remote myocardium, immunohistochemistry was performed using antibodies specific for various cadherin and catenin family proteins in both prospectively and retrospectively collected tissue samples. In the infarct area we observed

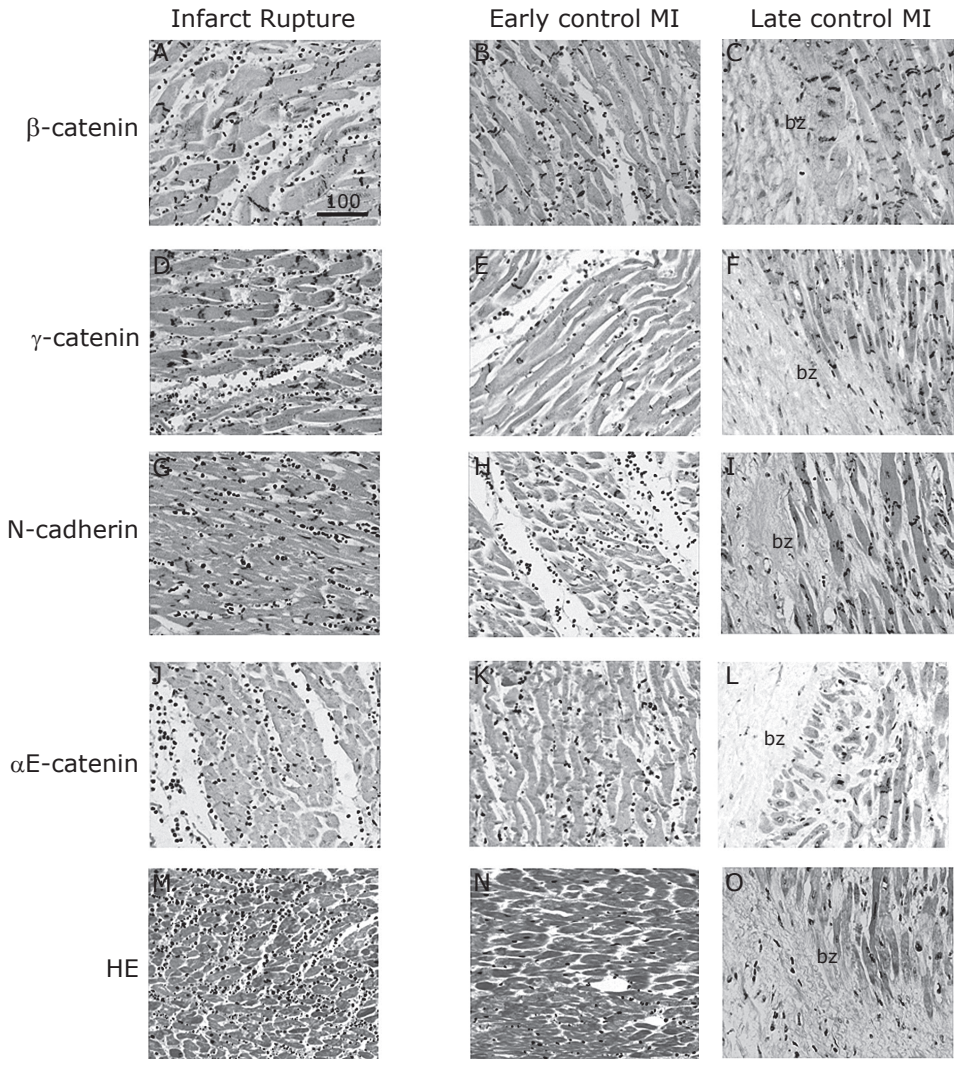

Figure 5.1 **Immunohistochemical characterization of cell adhesion complex proteins in the infarct area**

Representative microphotographs of immunostaining for β-catenin (A-C), γ-catenin (D-F), N-cadherin (G-I) and αE-catenin (J-L) in the infarct area of ruptured hearts (A,D,G,J), early (B,E,H,K) and late (C,F,I,L) control infarcts. A similar staining intensity for β-catenin, γ-catenin and N-cadherin was observed in the intercalated disk regions of the cardiomyocytes in infarct rupture and the two control MI groups. αE-catenin staining was undetectable in the infarct area of infarct rupture patients (J). However, staining was observed in the early control infarcts (K) as also in the border zone (bz) of late control MI's (L). Panel M-O shows H&E staining of the infarct area of ruptured patients (M), characterized by the necrotic cardiomyocytes and the massive influx of inflammatory cells. H&E staining of an early control MI (N) and the border zone of a late control MI (O) are also shown. Scale bar length is indicated in μm. For full color illustration, see page 162.

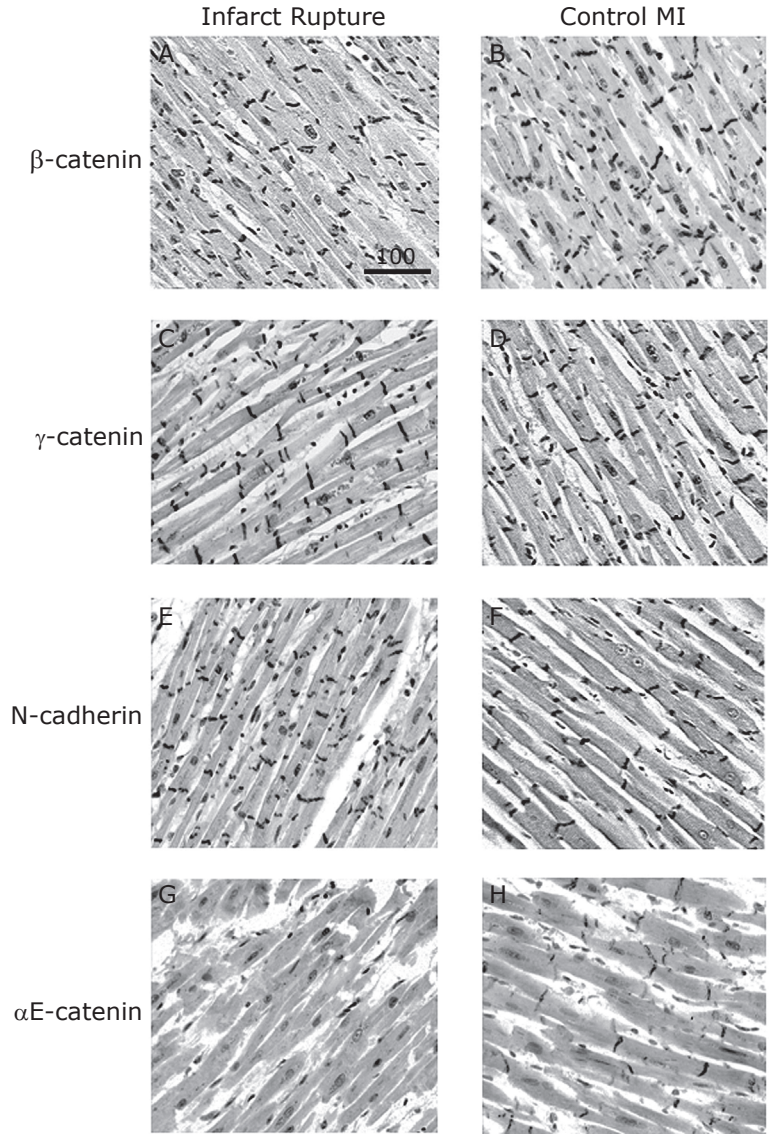

Figure 5.2 **Immunohistochemical characterization of cell adhesion complex proteins in the remote area**

Representative images of immunostaining for β-catenin (A, B), γ-catenin (C, D), N-cadherin (E, F) and αE-catenin (G,H) in remote parts of ruptured hearts (A,C,E,G) and control MI hearts without rupture (B,D,F,H). Abundant and similar staining for β-catenin, γ-catenin and N-cadherin was observed in the intercalated disk regions of the cardiomyocytes in infarct rupture and control MI groups. For αE-catenin, abundant staining of intercalated disks between cardiomyocytes was observed in the control MI hearts (H). On the contrary, 90% of the patients from the infarct rupture group showed either weak or no detectable aE-catenin staining (G). Scale bar length is indicated in μm. For full color illustration, *see page 163.*

Table 5.3 **Immunohistochemical distribution of adhesion complex proteins in myocardial specimens obtained from patients with and without infarct rupture**

	Control MI (n=20)			Infarct Rupture (n=20)		
Detectable Staining (%)	+	±	–	+	±	–
β-catenin	100			100		
γ-catenin	100			100		
Pan-cadherin	80	20		80	20	
αE-catenin	60	20	20	10	20	70

Detectable staining of the intercalated disc region was designated as + or ±, when staining was observed in ≥3 or 1-2 sections respectively, per 4 sections examined. Immunohistochemical staining was designated as (-) when no detectable staining was observed in all 4 sections.

staining for β-catenin (Figure 5.1A-B), γ-catenin (Figure 5.1D-E) and N-cadherin (Figure 5.1G-H) in the cardiomyocytes of both infarct rupture and early control MI patients. In contrast, no immunohistochemical staining for αE-catenin was observed in the infarct area of the infarct rupture patients (Figure 5.1J), whereas this staining was present in the early control MI group (Figure 5.1K). In the late control MI group, we detected staining with all four antibodies in surviving cardiomyocytes in the border zone of the infarct (Figure 5.1C,F,I,L). The H&E stained sections showed necrotic cardiomyocytes with increased numbers of inflammatory cells in the infarct area of infarct rupture patients (Figure 5.1M). To analyze whether the lack of αE-catenin in the infarct rupture patients was acquired or already present prior to infarction, we analyzed the remote areas with all four antibodies (Figure 5.2). β-Catenin (Figure 5.2A-B), γ-catenin (Figure 5.2C-D) and N-cadherin (Figure 5.2E-F) showed abundant presence within the intercalated disks in the remote myocardial regions of both the infarct rupture patients and control MI patients. No differences were observed between these two groups (see Table 5.3).

The results of immunohistochemical analyses of the remote myocardium with αE-catenin antibodies (raised against the C-terminal part of αE-catenin, obtained from Sant Cruz) are shown in Figure 5.2G-H. In 70% of infarct rupture patients, no αE-catenin staining was observed in the intercalated disks in remote region, whereas in 20% the staining was found to be low. In contrast, only in 20% of the control MI patients no αE-catenin could be demonstrated in the remote region (Table 5.3), a statistically significant difference ($p < 0.0001$). To confirm these findings, we used another antibody directed towards the C-terminal part of αE-catenin (obtained from Neomarkers). The latter αE-catenin antibody yielded results similar to those obtained with the Santa Cruz antibody (data not shown).

Western blotting

For semi-quantitative assessment of αE-catenin protein expression in infarct rupture and control MI patients, in both infarct and remote areas, we performed Western blotting (Figure 5.3) on the prospectively collected tissue samples. In the remote areas, densitometric analysis showed large amounts of αE-catenin in control MI patients. The expression was almost three-fold lower in the infarct rupture patients ($p<0.01$). In the infarct areas of the control MI group a slight, non-significant reduction in αE-catenin was detected compared to the remote areas of the same patients. In contrast, αE-catenin expression was almost completely absent in the infarct zone of infarct rupture patients (Figure 5.3A).

We also performed Western blotting for β-catenin (Figure 5.3B), γ-catenin (Figure 5.3C) and N-cadherin (Figure 5.3D). The remote tissue from both the infarct rupture and control MI patients demonstrated similar amounts of these cell adhesion molecules. Also, no significant difference was observed in β-catenin, γ-catenin and N-cadherin content in the infarct area of infarct rupture patients compared to control MI patients. Furthermore, in the infarct rupture group β-catenin, γ-catenin and N-cadherin all decreased significantly in the infarct area compared to remote myocardium.

Sequencing

To evaluate potential mutations or polymorphism of the αE-catenin gene in the infarct rupture patients that could lead to expression of a dysfunctional protein i.e. unable to localize to the intercalated discs, we sequenced each of the 16 coding exons of αE-catenin (*CTNNA1*) in 3 infarct rupture and 3 control MI patients with transmural infarcts. Although more than 20 SNPs have been described for the αE-catenin gene, we only observed a single SNP in exon 16 (rs1059110, G to A) in this study. In the rupture group we observed the following variants: one patient was GG, one patient was GA and one patient was AA. In the control group two patients were GG and one patient was AA. Based on these limited results, we conclude that there is no evidence for a role of this SNP in infarct rupture.

αE-catenin in experimental myocardial infarction

Heterozygous αE-catenin C-terminal deficient mice were used to study the effect of reduced αE-catenin content on infarct rupture, to mimic clinical scenario in ruptured MI patients. After induction of MI, only 25% of the heterozygous mice were alive 7 days post MI, as compared to 75% of their wild type littermates (see Figure 5.4A). All mice died of infarct rupture, diagnosed by massive blood loss in the thoracic cavity. Kaplan Meier analysis demonstrated significantly higher mortality in the heterozygous mice ($p=0.038$). Interestingly, no evidence of spontaneous heart muscle disease was obtained in non-infarcted heterozygous mice up to 70 weeks after birth (data not shown).

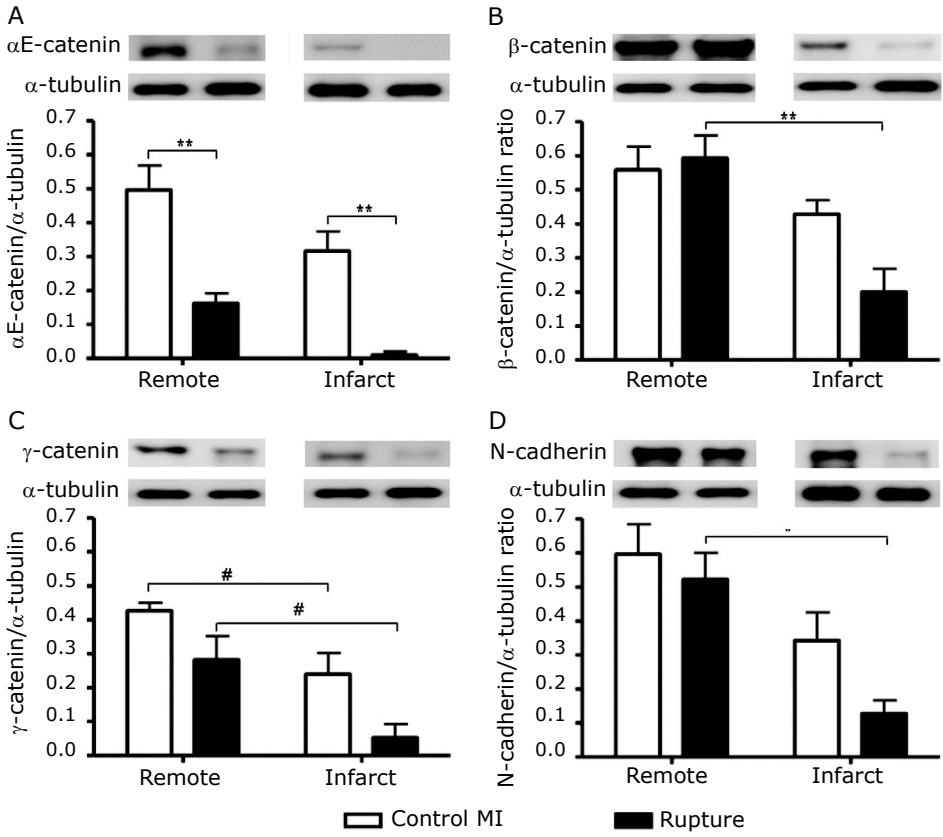

Figure 5.3 **Immunoblotting studies for characterization of cell adhesion complex proteins**

*Upper panel: representative Western blots of tissue obtained from infarct rupture patients and control MI patients, both from remote (non-ischemic) and infarct areas. A: αE-catenin, B: β-catenin, C: γ-catenin and D: N-cadherin; α-tubulin was used for normalization of the samples. Lower panel: Quantitative analysis of adhesion complex proteins, expressed as protein/α-tubulin ratio. Significantly less αE-catenin was detected in the remote area of infarct rupture patients (n=10) compared to control MI patients (n=10). In the infarct area, αE-catenin was undetectable in the infarct rupture group but readily detectable in the control MI group. Similar levels of β-catenin, γ-catenin and N-cadherin were observed in the remote areas of infarct rupture and control MI groups, although more extensive degradation of these proteins was detected under ischemic conditions. #p<0.05, *p<0.01, **p<0.001*

Immunohistochemical characterization revealed less intense staining of the intercalated disks in the heterozygous mice compared to wild type littermates (Figure 5.4C). On the contrary, other components of the cell adhesion complex proteins revealed no differences between wild type and transgenic mice (data

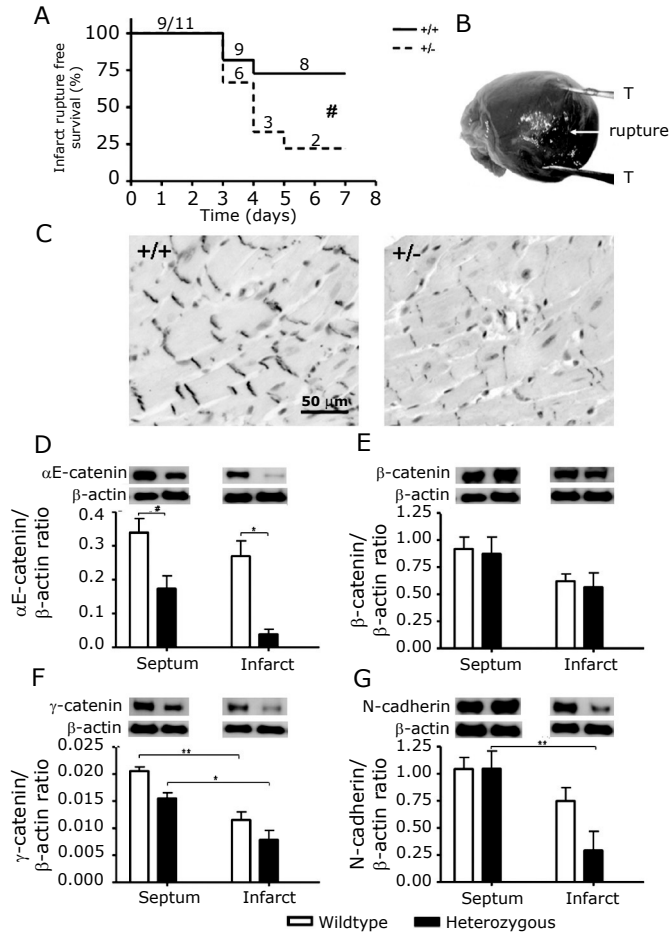

Figure 5.4 **Heterozygous αE-catenin C-terminal deficient mice show susceptibility to infarct rupture post-myocardial infarction**

*A: Kaplan Meier curve analysis of heterozygous αE-catenin C-terminal deficient mice (n=9) showed significantly lower rupture-free survival post MI (#: p=0.038) compared to their wildtype littermates (n=11). B: Macroscopic image of infarct rupture (T=tweezers). The arrow points at the tear in the infarct area, showing the blood loss through the ventricular wall. C: Representative images of Immunohistochemical analysis of αE-catenin, showing less intense staining of the intercalated disks in the heterozygous mice compared to wildtype littermates. D-G: Upper panels: Representative Western blot analysis for αE-catenin (D), β-catenin (E), γ-catenin (F) and N-cadherin (G) in heterozygous C-terminal αE-catenin deficient mice and their wildtype littermates, both from septum (non-ischemic) and infarct tissue; β-actin was used for normalization of the samples. Lower panels: Quantitative analysis of adhesion complex proteins, expressed as protein/β-actin ratio, demonstrating significantly lower αE-catenin in mice heterozygously deficient for C-terminally truncated αE-catenin (n=9) compared to their wildtype littermates (n=11). The other cell adhesion proteins were unaffected, although N-cadherin showed more degradation under ischemic conditions in the heterozygous mice. #p<0.05, *p<0.01, **p<0.001* *For full color illustration, see page 164.*

not shown). Similarly, Western blotting also demonstrated a significant decrease in αE-catenin protein expression in the heterozygous mice compared to their wild type littermates (Figure 5.4D; $P<0.05$). The reduction of αE-catenin in the heterozygous mice was similar to that observed in the infarct rupture patient group. Other adhesion complex proteins in the transgenic mice remained unaffected (Figure 5.4E-G). After MI however, a reduced γ-catenin and N-cadherin expression was observed in the infarct zone of the heterozygous mice, compared to uninfarcted tissue obtained from interventricular septum ($p<0.01$).

DISCUSSION

Characterization of the cell adhesion complex proteins in the myocardial specimens obtained from infarct rupture patients demonstrates a significantly reduced expression of αE-catenin and a lack of localization of this protein in the intercalated disks of both the infarct area and the remote, non-ischemic parts of infarct rupture hearts. These observations suggest that infarct rupture patients have an intrinsic defect in their cell adhesion complex which may have little effect on normal cardiac function, but may predispose the myocardium to rupture after transmural MI. The defective expression and localization of adhesion complex protein is not determined genetically. We sequenced the 16 exons that form the entire coding region of αE-catenin in infarct rupture patients and compared these sequences to those obtained from control MI group. A single SNP was observed, however this SNP was not consistently linked to the infarct rupture group. Therefore, mutations that affect αE-catenin at the protein level are unlikely to explain its reduced amounts and lack of localization in infarct rupture patients. However, this does not rule out that αE-catenin mutations that affect mRNA splicing and stability are present in infarct rupture patients. These mutations have been shown to reduce the stability of the cadherin/catenin complex in human cancer cells.[115] Unfortunately, mRNA obtained from postmortem tissue samples is severely damaged and cannot be used to study this hypothesis.

Interestingly, phosphorylation of the Tyr^{148} residue of α-catenin has been shown to enhance its interaction with β-catenin at the adherens junction.[120] Moreover, several phosphorylation sites on β-catenin ($Tyr^{142, 489, 654}$) and cadherin ($Ser^{684, 686, 692}$) have been proposed to play a role in the formation of the adherens junction complex.[114, 121, 122] Analysis of the effect of these posttranslational modifications on cell adhesion complex formation in cardiomyocytes and their relation to infarct rupture is desirable.

To test the role of defective adhesion protein complex in infarct rupture in an animal model, we used mice heterozygous for C-terminal truncated αE-catenin. Deletion studies have shown that the C-terminus is required for strong cell ad-

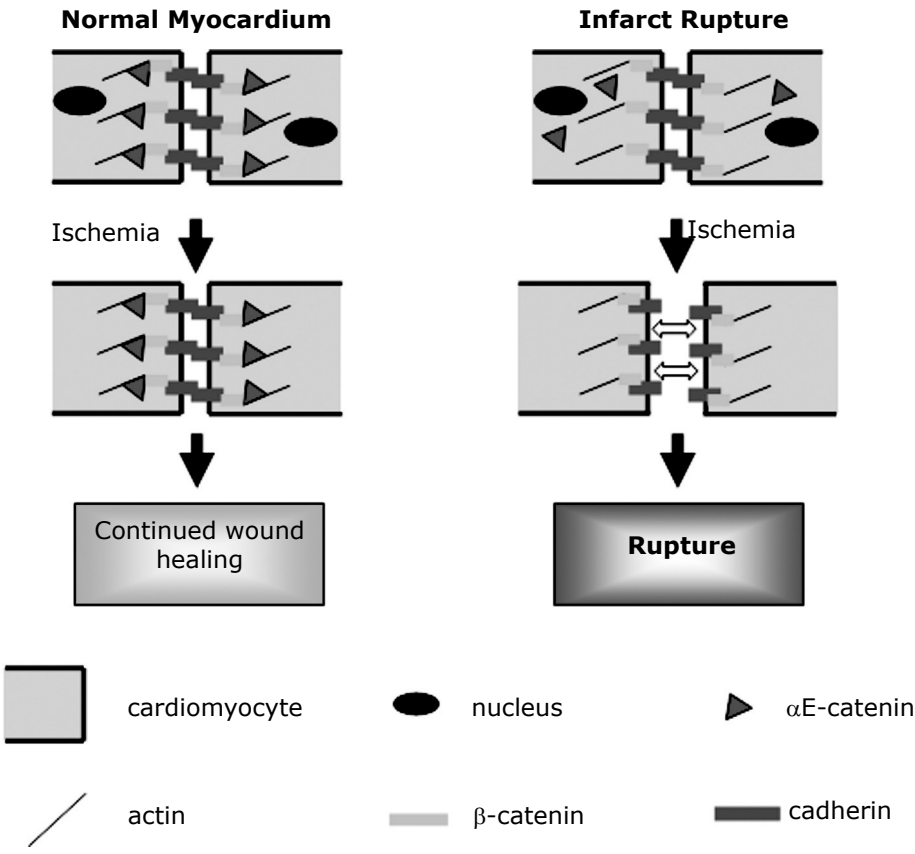

Figure 5.5 **Cartoon depicting the role of a defective intercellular adhesion complex in infarct rupture in humans**

In the left part of the cartoon, the normal components of the cell adhesion complex of cardiomyocytes from patients with normal infarct healing are shown. In the uninjured cardiomyocytes of normal hearts, αE-catenin is localized in the intercalated disks. Ischemia induces death of the cardiomyocytes in the infarct area, as shown by the loss of their nucleus. However, the integrity of the infarct area is sufficiently preserved by the adhering cardiomyocytes, and the wound healing and granulation tissue formation continue. As shown in the right side of the cartoon, αE-catenin is not localized in the intercalated disks of the cardiomyocytes in rupture-prone hearts. After ischemia, this abnormal cell adhesion complex causes the dead cardiomyocytes in the infarct area to loosen up their connections, causing further deterioration of the integrity of the infarct area and subsequently leading to infarct rupture. For full color illustration, see page 165.

hesion.[123] The immunohistological and Western blotting characteristics of the cell adhesion molecules in these mice were remarkably similar to those observed in human infarct rupture victims: Significantly reduced αE-catenin expression was observed localized to intercalated disk region in remote myocardium in comparison to normal expression and distribution of other components of the cell adhesion complex (β-catenin, γ-catenin and N-cadherin). Induction of MI in these mice resulted in a significantly higher frequency of infarct rupture than their wild type littermates. Interestingly, when not exposed to cardiac ischemia these heterozygous mice did not show any signs of cardiac malfunction for up to 70 weeks of age.

The alterations in the cell adhesion complex, observed in the infarct rupture patients and animals, seems to affect the integrity of myocardial skeleton in the infarct area, even though most of the cardiomyocytes are necrotic (Figure 5.5). A reduced cardiomyocyte adhesion could facilitate the migration of inflammatory cells into the infarct area, explaining the high numbers of these cells reported in ruptured infarcts; attendant upregulation and activation of proteolytic enzymes may further facilitate infarct rupture.[19, 117, 124]

Conclusions: The present study demonstrates that a decreased αE-catenin cell adhesion protein expression and localization predispose to infarct rupture. The results of this study lead to the hypothesis that infarct rupture is associated with an abnormality of the cell adhesion complex of the cardiomyocytes. Further research on the mechanisms that control the localization of cell adhesion molecules in the intercalated disks will be needed to better understand this proposed molecular mechanism of infarct rupture.

Acknowledgements
We thank Prof. Dr. F. van Roy, Ghent University, Belgium, for his helpful comments and suggestions. We also thank Dr. Jos B.G. Paquay for his help in collecting human tissue samples. Embryonic stem cells from αE-catenin C-terminal deficient mice were a kind gift of Dr. P. Gruss, Germany.

Molecular Imaging of Interstitial Alterations in Remodeling Myocardium after Myocardial Infarction

6

Journal of the American College of Cardiology 2008;52:2017-28

ABSTRACT

Objectives. To evaluate interstitial alterations in myocardial remodeling using a radiolabeled Cy5.5-RGD imaging peptide (CRIP) that targets myofibroblasts.

Background. Collagen deposition and interstitial fibrosis contribute to cardiac remodeling and heart failure (HF) after myocardial infarction (MI). Evaluation of myofibroblastic proliferation should provide indirect evidence of the extent of fibrosis.

Methods. Of the 46 Swiss-Webster mice, MI was induced in 41 by coronary artery occlusion and 5 were used unmanipulated. Of the 41 mice, 6, 6, and 5 received intravenous Tc-99m labeled CRIP for microSPECT-CT imaging after 2, 4, and 12 weeks of MI; 8 received captopril or captopril with losartan up to 4 weeks after MI. Scrambled CRIP was used 4 weeks after MI in 6 mice; the remaining 10/46 mice received unradiolabeled CRIP for histological characterization.

Results. Maximum CRIP uptake was observed in the infarct area; quantitative uptake (percent injected dose per gram, %ID/g) was highest at 2 weeks (2.75±0.19%), followed by 4 (2.26±0.04%), and 12 (1.74±0.11%) weeks compared to unmanipulated mice (0.59±0.09%). The uptake was higher at 12 weeks in the remote areas. The uptake was histologically traced to myofibroblasts. Captopril alone (1.78±0.16%) and with losartan (1.13±0.14%) significantly reduced tracer uptake; scrambled CRIP (0.74 ± 0.07%) was similar to CRIP uptake in normal myocardium.

Conclusions. Radiolabeled CRIP allows for noninvasive visualization of interstitial alterations during cardiac remodeling, and is responsive to anti-angiotensin treatment. If proven clinically feasible, such a strategy would help identify post-MI patients likely to develop heart failure.

INTRODUCTION

Heart failure (HF) is evolving as one of the most important cardiovascular health problems worldwide. In the United States alone, approximately 5 million people suffer from manifest heart failure and over 500000 new cases are diagnosed every year.[125] The syndrome of HF post-MI is characterized by a relentless course of myocardial remodeling and functional deterioration,[30, 32, 126] which continues to occur even after the initial causative injury has abated.[4, 127] In addition to replacement fibrosis in the region of myocardial infarction (MI), the interstitial fibrosis in the non-infarcted myocardium significantly contributes to adverse remodeling and heart failure (HF).[52] In fact, presence of fibrosis remote from the infarct zone accounts for two-thirds of the fibrous tissue in the cardiomyopathic heart.[52, 128-130] The magnitude of myocardial fibrosis is correlated to the extent of ventricular dysfunction.[131] It is conceivable that an ability to noninvasively detect the process of myocardial fibrosis would allow assessment of likelihood of evolution of HF after MI.

The collagen production and fibrosis in the myocardium is associated with myofibroblastic proliferation.[127] Myofibroblasts demonstrate upregulation of angiotensin receptors and integrin moieties, which in turn may promote collagen genes and reduce metalloproteinase genes.[70] Such effects of integrin upregulation are prevented by abrogation of autocrine TGF-β signaling.[70] The RGD probes (peptides containing the arginine-glycine-aspartate motif) that bind to integrins such as $\alpha v\beta 3$ have been used to identify neovascularization in post-infarct animal models.[132] Since integrin $\alpha v\beta 3$ is associated with the supermature focal adhesions on the cell membrane of myofibroblasts, we hypothesized that appropriately labeled RGD probe should identify myofibroblasts in post-infarct myocardium.[56] In addition, scrutiny of the pro-collagen I sequence revealed RGD binding domains, such as DDX, and could also constitute a target for RGD-based imaging. Therefore, uptake of RGD probe should indirectly represent the rate of fibrogenesis or collagen deposition.

In the present study, we used Cy5.5-RGD imaging peptide (CRIP) labeled with technetium-99m (Tc), for feasibility of imaging the process of active myocardial fibrosis in a murine model of post-MI ventricular dysfunction. The noninvasive imaging ability of the radiolabled probe was compared with echocardiographic parameters of left ventricular geometric changes and pathological characterization of interstitial alterations. The fluorescent moiety of the targeting peptide allowed better histological characterization of the probe localization. An antibody against the fluorescent moiety of CRIP was used to immuno-electronmiroscopically trace the localization of CRIP. In addition, in vitro experiments were performed for characterization of the CRIP binding to mature and pro-collagen.

METHODS

Experimental Myocardial Infarction in Mice

The experimental protocol was approved by the Institution Animal Care and Use Committee of the University of California, Irvine, School of Medicine. In 41 adult Swiss Webster male mice (age: 4 months; body weight: ~50 g) MI was induced, under pentobarbital (75 mg/kg) and isoflurane gas anesthesia (2.0–3.0%) using a stereomicroscope (Leica MZ FL III, Leica, Switzerland). For this purpose, animals were placed on a heating pad in supine position, endotracheal intubation was performed under direct laryngoscopy and mechanical ventilation was maintained with a small animal respirator (Harvard Apparatus; tidal volume = 250 µl, rate = 210 breaths/min). After thoracotomy, the lateral branch of LCA was ligated with a 6.0-prolene suture 3 to 4 mm below the tip of left atrium. Successful ligation was verified by visual inspection of the LV apex for myocardial blanching indicating interruption in coronary flow. The chest and skin were closed in layers with 5.0-silk sutures. Animals were gradually weaned from the respirator.

For the evaluation of serial changes in collagen synthesis by radiolabeled CRIP imaging, animals were divided into groups as 2 weeks (n= 6), 4 weeks (n= 6) and 12 weeks (n= 5) after infarction (Table 6.1). Two groups of 4 animals each were treated with either captopril (60 mg/kg/day) alone or in combination with losartan (captopril 30 mg/kg/day, losartan 10 mg/kg/day) dissolved in the drinking water, to evaluate if molecular imaging with CRIP would allow determination of efficacy of therapeutic intervention. Five unmanipulated control mice were subjected to CRIP imaging for comparison with the infarcted mice after a 4-week wait. In addition, 6 animals, 4 weeks after MI, were imaged with Tc-labeled scrambled peptide (scrambled CRIP, AH-112298) to ensure the specificity of CRIP. In the remaining 10 mice, non-radiolabeled CRIP was used for pathological characterization of the target using fluorescence microscopy and immunoelectron microscopy.

Echocardiography

All animals were subjected to extensive echocardiographic studies for the assessment of myocardial infarct size, LV cavity dimensions and ventricular function.

Table 6.1 **Classification of animals used in the study**

Probe	Label	Control	2 weeks	4 weeks	12 weeks	4 weeks Captopril	4 weeks C+L*
Cy5.5RGD	Tc	5	6	6	5	4	4
Cy5.5RGD	-	-	10	-	-	-	-
Cy5.5scrambled	Tc	-	-	6	-	-	-

** C+L: Captopril and losartan*

Echocardiographic examination was performed under 2% isoflurane anesthesia for the assessment of infarct size, left ventricular (LV) cavitary dimensions and ventricular function before nuclear imaging. Echocardiograms were recorded with a commercially available ultrasound system (Sequoia™, Siemens) using a 14-MHz linear probe (15L8, Siemens) (MountainView, CA). An advanced high frame rate imaging technique, acoustic capture (Paragon®, Siemens), was adopted for image acquisition allowing temporal resolution of 8-10 msec (frame rate, 100-120 per s). B-mode images of LV parasternal long-axis and parasternal short-axis views at base, mid and apical LV levels were digitally stored as movie loops in 2-3 cardiac cycle length. Still images of LV M-mode as well as pulsed wave Doppler spectrum of mitral valve inflow and aortic valve forward flow were acquired at a sweep of 100 mm/s. Infarct area and LV area were measured by tracing endocardial borders on long axis images, and infarct-to-LV ratio was calculated. LV wall thicknesses and cavity dimensions were measured on LV M-mode spectrum as recommended by the American Society of Echocardiography guidelines,[133] followed by calculation of % fractional shortening and ejection fraction.

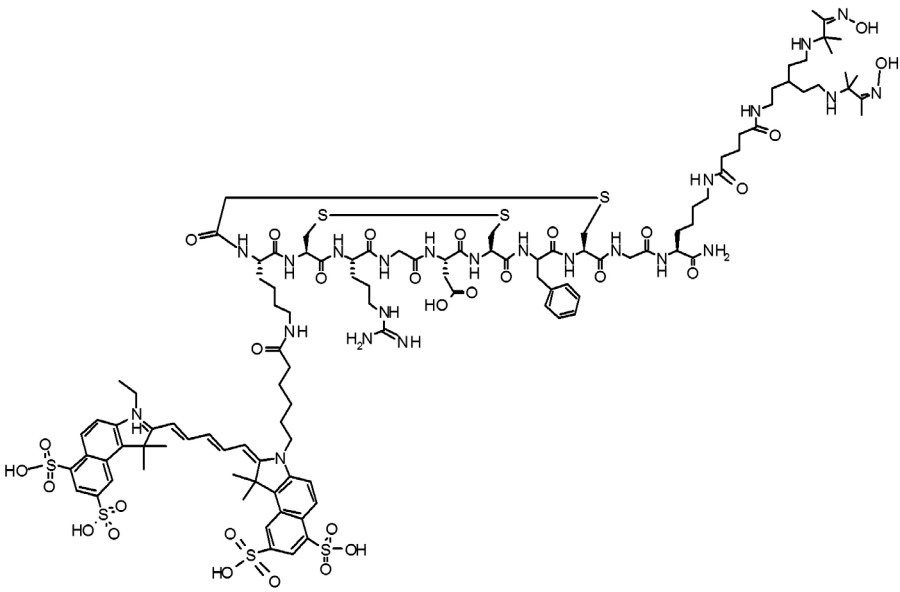

Figure 6.1 The structure and manipulation of CRIP

CRIP is a 2.5 kD, 10 amino acid-peptide, which contains an RGD-motif and has a bi-cyclic structure formed by a disulfide bridge and a thioether bridge. It is conjugated to both a fluorescent cyanine dye (Cy5.5) and the chelating agent cPN216 for radiolabeling with technetium-99m; the dye moiety and the chelating agent are conjugated through the lysine side-chain at the N- and C-terminal ends, respectively. For the preparation of scrambled CRIP, the order of the amino acids in CRIP was mixed so the sequence did not express the RGD-motif. The dye and the chelating agent were conjugated similarly (not shown).

CRIP and Scrambled CRIP: Structure and Radiolabeling

CRIP and scrambled CRIP were the kind gift of GE Healthcare, AS, Oslo, Norway. CRIP (AH110863, Figure 6.1) is a 2.5 kD peptide conjugated to both a fluorescent cyanine dye Cy5.5, and the chelating agent cPN216; the latter is linked for radiolabeling of the peptide with technetium-99m. The peptide comprises 10 amino acids, contains an RGD-motif, and has a bi-cyclic structure formed by a disulfide and a thioether bridge. The dye moiety and the chelating agent are conjugated to the peptide via the side-chain of lysine residue at the N- and C-terminal ends, respectively. A scrambled version of CRIP (AH-112298) was also prepared, where the order of the amino acids in CRIP has been altered so that the sequence does not express an RGD-motif. The dye and the chelating agent are conjugated at the same positions.

For radiolabeling, 50 µg of tracer was dissolved in 50 µl of MeOH and then added to freeze dried kit. 1.0 ml of $^{99m}TcO_4^-$ was added to the compound and left at room temperature for 20-30 min. Radiolabeling was confirmed by instant thin-layer chromatography with radiopurity of more than 90%. For nuclear imaging, 170±2.5 MBq (4.6±0.1 mCi) of Tc-CRIP was injected through the tail vein and imaging was performed after 3.5 hours.

Micro-SPECT Imaging with Tc-CRIP and Micro-CT

Radionuclide imaging was performed using a dual-head micro single-photon emission computed tomography (SPECT) gamma camera with micro-CT (X-SPECT, Gamma Medica, Inc., Northridge, CA) under isoflurane anesthesia. In vivo micro-SPECT images of the heart were acquired in 64×64 scaffold, 32 steps at 120 sec per step on 140 keV photopeak of ^{99m}Tc with 15% window using a low-energy high-resolution, pinhole collimator. After SPECT acquisition, micro-CT images were acquired without moving the mice. The micro-CT used an X-ray tube operating at 50 kVp and 0.6 mA, and images were acquired for 0.5 sec per view for 256 views in 360° rotation. The micro-SPECT images were converted to 256×256 scaffold and fused with micro-CT studies, allowing simultaneous scintigraphic and anatomic information in all tomographic scans in three different axes. After in vivo imaging, animals were sacrificed with an overdose of pentobarbital (150 mg/kg). Hearts were carefully explanted and planar images of the ex-vivo heart were acquired for 15 min in 128×128 matrix using a low-energy, high-resolution, pinhole collimator. Thereafter, hearts were cut into 3 bread-loaf slices (infarct, peri-infarct, and remote regions), using a mouse heart matrix (Zivic laboratories, Inc). The quantitative radiotracer uptake was determined by a gamma scintillation counter (1480 Wizard 3"; Wallac Co., USA). Biodistribution studies for the lung, liver, spleen, and kidney uptake were also undertaken.

Histopathological Characterization of Myocardial Specimens

After the nuclear imaging studies, the apical (predominantly containing infarct tissue), mid myocardium (peri-infarct) and basal (predominantly containing non-infarcted remote tissue) myocardial slices were washed in PBS, fixed over night with 4% paraformaldehyde in PBS (pH 7.4 at 4°C) and stored in PBS with 0.02% sodium azide at 4°C until used. The specimens were further processed by dehydration in a graded series of ethanol for paraffin-embedding. The blocks were cut in 5 μm sections, transferred to vectabond reagent treated slides (Vector SP-1800), dried overnight and stored until ready for use.

Masson's trichrome staining was used to determine infarct size. After deparaffinization and rehydration, sections were placed in working Weigert's iron hematoxylin for 10 minutes and tepid water rinsed for 10 minutes. Tissue sections were then incubated in Biebrich Scarlet-Acid Fuchsin Solution for 5 minutes, differentiated in Phosphotungstic-Phosphomolybdic Acid for 5 minutes and stained in Aniline Blue for 8 minutes. After rinsing with 1% Gallic Acedic Acid (GAA), sections were dehydrated and mounted in permanent mount medium.

Sirius Red staining eliminates cytoplasmic staining, revealing thin septa and collagen fibers clearly and enabling quantitative morphometric measurements. Sections were treated in 0.2% aqueous phosphomolybdic acid for 5 min and subsequently incubated for 60 min with 0.1% Sirius Red F3BA (C.I. 35780, Polysciences, Northhampton, UK) in saturated picric acid and washed for 2 min with 0.01 N HCL. Sections were rinsed in 70% ethanol for 30 seconds, then dehydrated, mounted with cover-slip and the amount of collagen was quantified,[23] The quality of collagen fibers was further investigated by Sirius red polarization microscopy, allowing semi-quantification of the mature, thick, tightly packed orange/red fibers and the newly formed, thin, loosely assembled yellow/green fibers.[134-137]

Alpha smooth muscle actin (ASMA) was used to determine myofibroblasts in the infarct area. After deparaffinization, rehydration and blocking of endogenous peroxidase, sections were incubated for 2 hours at room temperature using anti-alpha smooth muscle actin (ASMA monoclonal antibody, Sigma, dilution 1:2000). After washing in PBS, sections were incubated with secondary antibody (rabbit anti mouse HRP, DAKO, 1:500) for 1 hour at room temperature. Sections were briefly counterstained with haematoxylin.

Fluorescence microscopy

For localization of the target sites for CRIP, non-radiolabeled probe was injected intravenously in animals with 2 week old MI. After 3.5 hours, mice were sacrificed and hearts were excised. Frozen section of 5 μm were cut and rehydrated in PBS. Sections were incubated for 2 hours at room temperature using anti-

ASMA antibody (Sigma, 1:2000). After washing in PBS, sections were incubated with secondary antibody for 1 hour at room temperature (donkey anti-mouse IgG FITC, Jackson ImmunoResearch Europe, Newmarket, Suffolk, UK). Sections were examined using a Nikon Eclipse E-800 microscope.

In vitro studies for CRIP binding

Modified ELISA assays were developed for defining the interaction of CRIP and collagen I and III (Sigma Aldrich). In addition, a procollagen-I peptide was custom constructed containing a DDX sequence (H2N-GPP-GKN-G***DD***-***G***EA-GKP-GR-COOH). This sequence is common for mouse and human procollagen-I. The analysis was conducted using a Biacore 3000 system (Biacore, GE Healthcare, Uppsala, Sweden), that enabled the detection of noncovalent interactions between CRIP and procollagen I peptide in real time applying the physical principle of surface plasmon resonance. The analysis involved immobilization of synthetic peptide sequence on sensor chips CM5, followed by assessment of soluble CRIP or scrambled CRIP to the immobilized ligand. The change in refractive index at the chip surface layer as the soluble components associated with the ligand and subsequently dissociated, was expressed as resonance units (RU). To compensate for nonspecific background binding, an unmodified control surface was used. The change in resonance units at this surface was subtracted from the change in resonance units at the ligand surface.

Immuno electron microscopy

Immuno electron microscopy was performed according to previously described methods.[138] In short: hearts were perfused with 0.2% glutaraldehyde in 2% paraformaldehyde and 0.1M phosphate buffer (PB), pH 7.4. Hearts were excised and stored for 60 min in the above mentioned solution before storage in 1% paraformaldehyde and 0.1 M PB, pH 7.4 at 4 °C for at least 24 hours. Tissue samples were stored in 2.3 M sucrose in 0.1 M PB, sections were cut and placed on a grid in methyl cellulose/2.3 M sucrose solution (1:1). Anti-cyanine antibody was used (Acris antibodies, Hiddenhausen, Germany) to untrastructurally trace CRIP localization. After protein A gold labeling, sections were examined using a Philips CM100 microscope (Eindhoven, The Netherlands).

Statistical Analysis

All data are represented as mean±sem. To determine the statistical significance of differences in quantitative scintigraphic data, echocardiographic parameters, and histopathologic observations, 1-way ANOVA was performed followed by post-hoc Bonferonni test for multiple comparisons. Correlations were determined using linear regression analysis. Due to the small number of mice in each group, the assumptions of the 1-way ANOVA and linear regression models should be regarded as exploratory rather than definitive. P values < 0.05 were considered as statistically significant.

RESULTS

CRIP: Target Affinity and Localization Characteristics

The probe localization characteristics were determined by fluorescence microscopy of myocardial tissue sections of hearts explanted 2 weeks after MI from animals injected with (non radiolabeled) CRIP (Figure 6.2). The uptake was predominantly observed in the myocardial infarct zone. Colocalization of ASMA in the same cells as CRIP positive cells by fluorescence microscopy suggested probe specificity for myofibroblasts. Similarly, immuno electron microscopic examination was performed wherein intravenously administered CRIP in 2-week old infarcts was localized by immunogold labeled anti-Cy antibody. The uptake was confirmed in the myofibroblasts, which were ultra structurally identified by the presence of large amounts of rough endoplasmic reticulum. A small amount of internalized CRIP was seen within the myofibroblasts. No uptake of the probe was observed in the collagen fibers. In vitro binding assays revealed CRIP uptake by activated $\alpha v\beta 3/5$ with an affinity of 1-3nM, but not by typical collagen receptors such as $\alpha 1\beta 1$ or $\alpha 5\beta 1$ or platelet receptor $\alpha IIb\beta 3$. Also, CRIP did not bind to mature collagen type I or III fibers. However, a specific noncovalent interaction of CRIP was observed with custom-made DDX-sequence containing pro-collagen I peptide. (Figure 6.2)

Table 6.2 Echocardiographic parameters of LV remodeling and function

	Normal	MI			4 weeks post-MI	
Parameter	Control	2 Weeks	4 Weeks	12 Weeks	Captopril°	C+L°
n	5	6	6	5	4	4
HR (bpm)	386±25	476±16*	406±24$^{\#}$	405±24$^{\#}$	324±15	376±76
MI (%)	0	47±5*	48±4*	47±4*	38±8	31±7
LVDd (cm)	0.46±0.01	0.53±0.01*	0.49±0.02	0.6±0.02$^{*\#\dagger}$	0.5±0.04	0.5±0.03
LVDs (cm)	0.29±0.01	0.48±0.01*	0.44±0.03*	0.51±0.03*	0.4±0.05	0.39±0.05
FS (%)	38±2	11±1*	11±2*	14±3*	29±5†	24±6
EF (%)	74±2	27±3*	29±4*	34±5*	41±4	47±7

Data are presented as mean±SD. BW: body weight, HR: heart rate, LV: left ventricle, MI: myocardial infarction/LV areax100%, LVD: LV diameter (s: systolic, d: diastolic), FS: fractional shortening, EF: ejection fraction, C+L: captopril+losartan, *p<0.05 vs normal control, # p<0.05 vs 2 weeks, † P<0.05 vs 4 weeks, °treatments groups were statistically compared with 4 weeks post-MI

Radionuclide Imaging with Tc-CRIP

The infarct size in all untreated animals was similar (Table 6.2). The left ventricular cavity dimensions (both end systolic and end-diastolic) were greater at 2, 4 and 12 weeks post-MI, and the % fractional shortening and ejection fraction decreased post-MI compared to normal control animals. In vivo micro-SPECT imaging demonstrated Tc-CRIP uptake in the infarct area (Figure 6.3). The use of micro-CT identified precise localization of the radioactivity in the cardiac region and allowed differentiation of the uptake in apical myocardium from the radiotracer sequestration in the liver. The ex vivo planar images of the explanted heart specimens confirmed the results of in vivo imaging and demon-

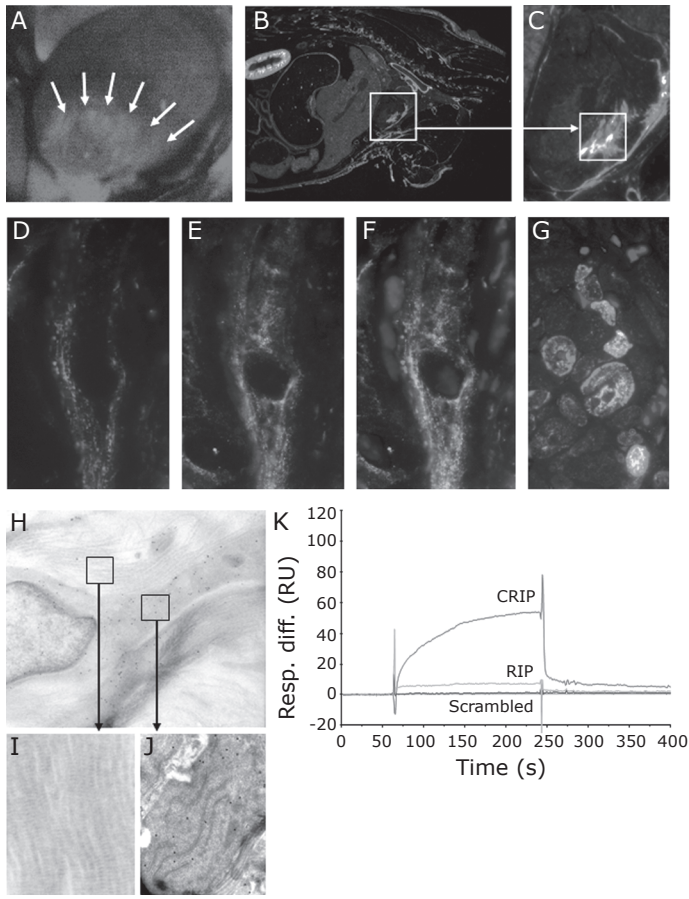

Figure 6.2 **Characterization of target binding of CRIP**

Probe targeting was evaluated 3.5 H after intravenous administration of CRIP in 2-week post-MI animals. The localization of the Cy5.5 fluorescence (red) was clearly observed in the infarct and peri-infarct zone in vivo (A, arrowheads). A 30-micron whole mouse slice demonstrates myocardial uptake of the probe (B, square); intense uptake is seen in the kidney which serves as the route of excretion. (C), Magnification of the area enclosed by the square in (B) demonstrates fluorescent probe localization in the subendocardium. (D-E) For further characterization of the probe targets, we correlated the uptake of intravenously administered CRIP in 2 week post-MI animals (red, D) with concurrent staining of the sections by anti-ASMA antibody (green, E), colocalization is shown by overlay (F) The localization of CRIP was observed in spindle shaped myofibroblasts in the infarct area. CRIP and ASMA colocalization is seen in transversely sectioned myofibroblasts in (G). For immuno EM, similarly intravenously administered CRIP was traced by gold labeled anti-cy antibody (black immunogold partikels 10 nm). CRIP clearly localized with myofibroblasts (H), containing characteristic abundance of rough endoplasmatic reticulum (I). No uptake was seen in mature collagen fibers (J). (K) shows sensograms (Biacore 3000 instrument) obtained with CRIP and scrambled CRIP exposure to a surface with a immobilized peptide sequence H2N-GPP-GKN-GDD-GEA-GKP-GR-COOH, aa221-240 from procollagen-I. In addition, RGD imaging peptide without Cy5.5 dye was also used in the experiment (RIP). The higher RU values for CRIP than RIP is due to the higher molecular weight of CRIP. For full color illustration, see page 166.

strated maximum uptake in infarct and border zone. Minimal increase in uptake was seen in the remote area (Figure 6.4). In contrast to CRIP, scrambled CRIP did not show uptake in the infarcted myocardium, showing that CRIP uptake is RGD-dependent and specific. Similarly, no Tc-CRIP uptake was seen in the unmanipulated hearts.

The uptake in the infarcted region was maximum in the 2-week old MI. There was statistically significant reduction in uptake in 4 and 12-week old infarcts (Figure 6.4). The quantitative Tc-CRIP uptake in the myocardial tissue specimens was calculated and represented as percent injected dose per gram (%ID/g) of tissue. It can be presumed that the quantitative uptake represents the extent of the process of myocardial fibrosis. As observed in the in vivo and ex vivo images, the maximum radiotracer uptake was observed in the infarcted myocardium (%ID/g: 2.75±0.19%) at 2 weeks which was 5-fold higher than the control myocardial specimens (0.59±0.09%; $p<0.0001$) (Figure 6.4B). This uptake was significantly higher compared to 4 (2.26±0.04%; $p<0.0038$) and 12 (1.74±0.11%; $p<0.0001$) weeks after MI. The CRIP uptake in the remote myocardium was higher than in the control myocardial specimens and increased significantly by 12 weeks (1.04±0.06%), as compared to control myocardial specimens (0.68±0.07%; $p=0.001$). The uptake in the infarct area had no correlation with MI size determined either by akinetic echo segments or Masson

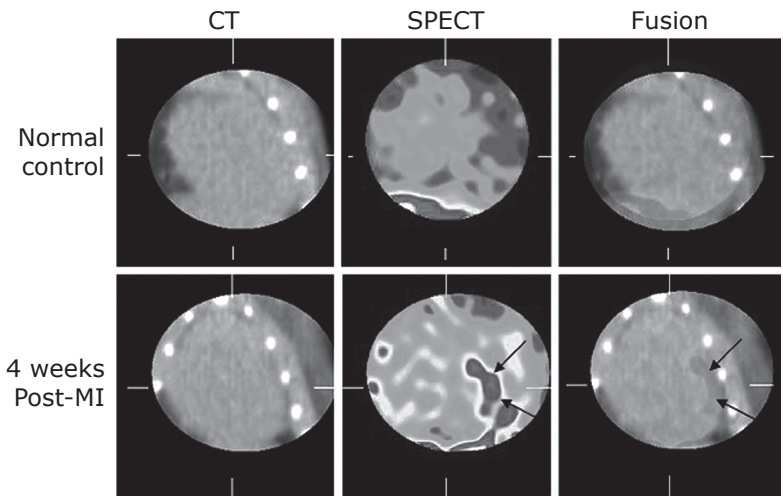

Figure 6.3 **In vivo microCT, microSPECT and fusion images in frontal projection in unmanipulated control and 4-week post-MI animals 3H after radiolabeled CRIP administration**

No uptake of Tc-CRIP was observed in the unmanipulated animal (top row). On the other hand, intense anterior uptake is seen in the infarcted mouse (bottom row). The cardiac localization is confirmed in the CT fusion image. For full color illustration, see page 167.

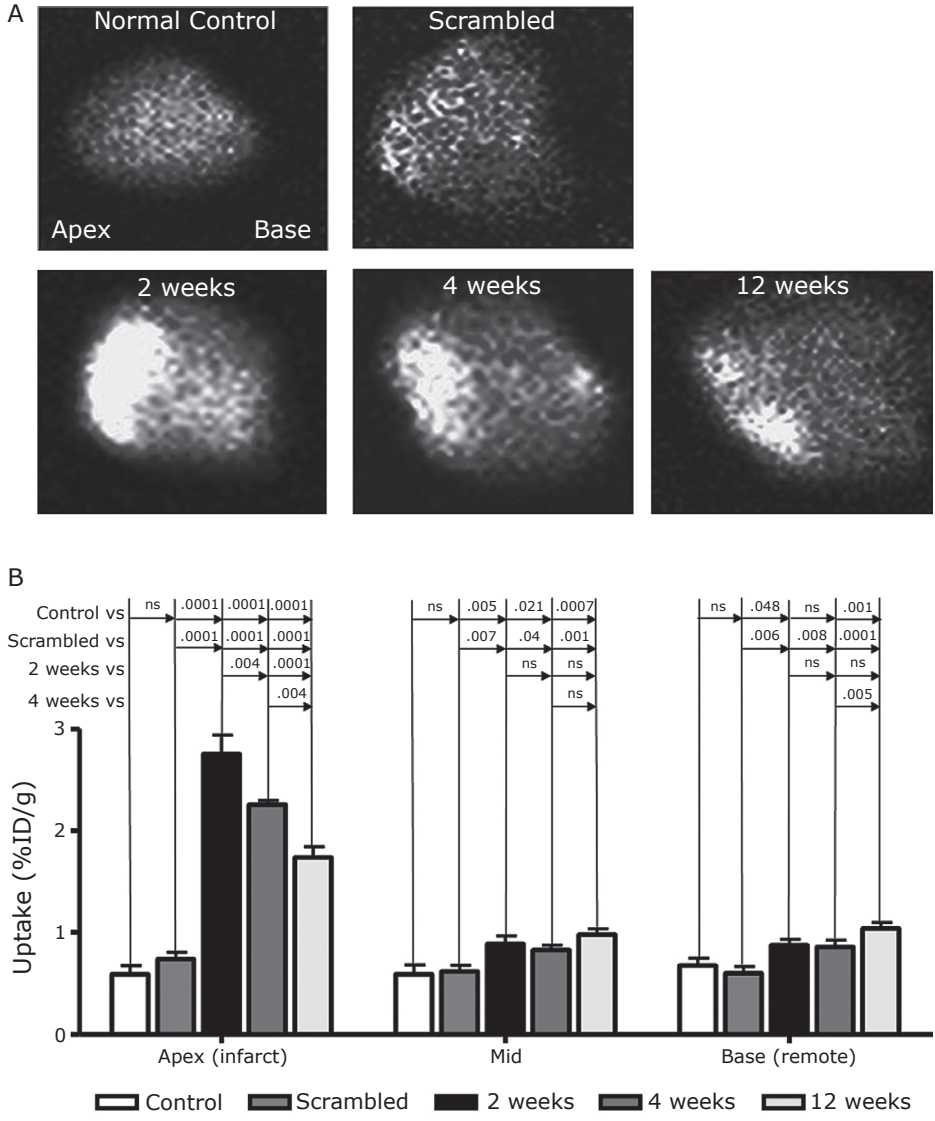

Figure 6.4 **Ex vivo images of the explanted hearts in control and post-MI animals with radiolabeled CRIP and scrambled CRIP**

A. Ex Vivo Images. Control heart with RGD probe and 4-week post-MI heart with scrambled sequence show no radiotracer uptake. On the other hand, intense CRIP uptake is seen in 2-week post-MI animal. The uptake in the infarcted area was highest in mice 2 weeks after MI, followed by 4, and 12 weeks after MI. B. Quantitative Tc-CRIP uptake in the infarct (apex), peri-infarct (mid), and remote (base) areas. The %ID/g uptake in the infarct area is highest in mice 2 weeks after MI, followed by 4, and 12 weeks after MI. On the other hand, the uptake in peri-infarcted and remote areas shows trends towards higher uptake from 2 to 12 weeks after MI. No uptake of scrambled peptide was seen in the infarct zone. Quantitative data confirmed the findings of ex vivo images. For full color illustration, see page 168.

trichrome staining (r=-0.17, -0.12 respectively; p=ns). The nontarget organ distribution of Tc-CRIP demonstrated kidney to be the major organ of radiation burden (and excretion), (see Table 6.3). The tracer clearance was fast and only 8% of the tracer could be recovered in the circulation at 2 hours as compared to 5 minutes after administration; CRIP T½ was calculated as 28 minutes.

Two additional groups of 4 animals each were treated with either captopril alone or in combination with losartan. Upon ultrasound examination, the neurohumoral antagonists prevented ventricular dilation and preserved ventricular function (Table 6.2). The CRIP uptake at 4 weeks after MI, was significantly reduced after captopril (1.78±0.16%, p=0.0004) or captopril+losartan (1.13±0.14%, p=0.0001) treatment compared to untreated animals (Figure 6.5).

Table 6.3 Tracer Uptake (%ID/g) in organs and blood

Group	Blood	Lung	Liver	Spleen	Kidney
Sham	0.82±0.06	1.42±0.18	4.90±1.26	1.51±0.18	9.60±0.56
2 weeks	1.00±0.11	2.75±0.61	3.91±0.47	1.89±0.23	11.93±1.15
4 weeks	1.06±0.10	2.26±0.25	2.85±0.53	2.02±0.31	10.29±1.31
12 weeks	0.98±0.13	1.81±0.33	2.26±0.27	1.63±0.12	9.21±0.63

Histopathological Assessment

The histological sections demonstrated large infarcts involving the anterior LV wall (Figure 6.6); infarct size was similar in all animals. Over the 3 months following infarction, LV wall demonstrated significant thinning and the extent of inflammation gradually subsided. Myofibroblasts, expressing alpha smooth muscle actin, were present at 2 weeks post MI in the infarct area and decreased over time. The replacement and interstitial collagen was analyzed by picrosirius red polarization microscopy of myocardial specimens (Figure 6.7) obtained from infarct and remote regions. Although the total collagen content in the infarct region remained similar over time, the thin, newly formed (yellow-green) collagen fibers reduced and correlated with the radiotracer uptake (r^2=0.34; p=0.05) (Figure 6.7A,C,E). In the remote region, the overall collagen deposition was markedly lower as compared to the infarct region (Figure 6.7A-B). However, both collagen content and (yellow-green) thin collagen fibers increased substantially in the remote region over time (Figure 6.7D). There was a direct correlation between tracer uptake and the thin collagen fiber deposition (r^2=0.45; p=0.001) (Figure 6.7F). The direct correlation of CRIP uptake with ASMA-positive myofibroblasts and thin collagen fibers suggests that collagen production is decreased in the infarct zone over time.

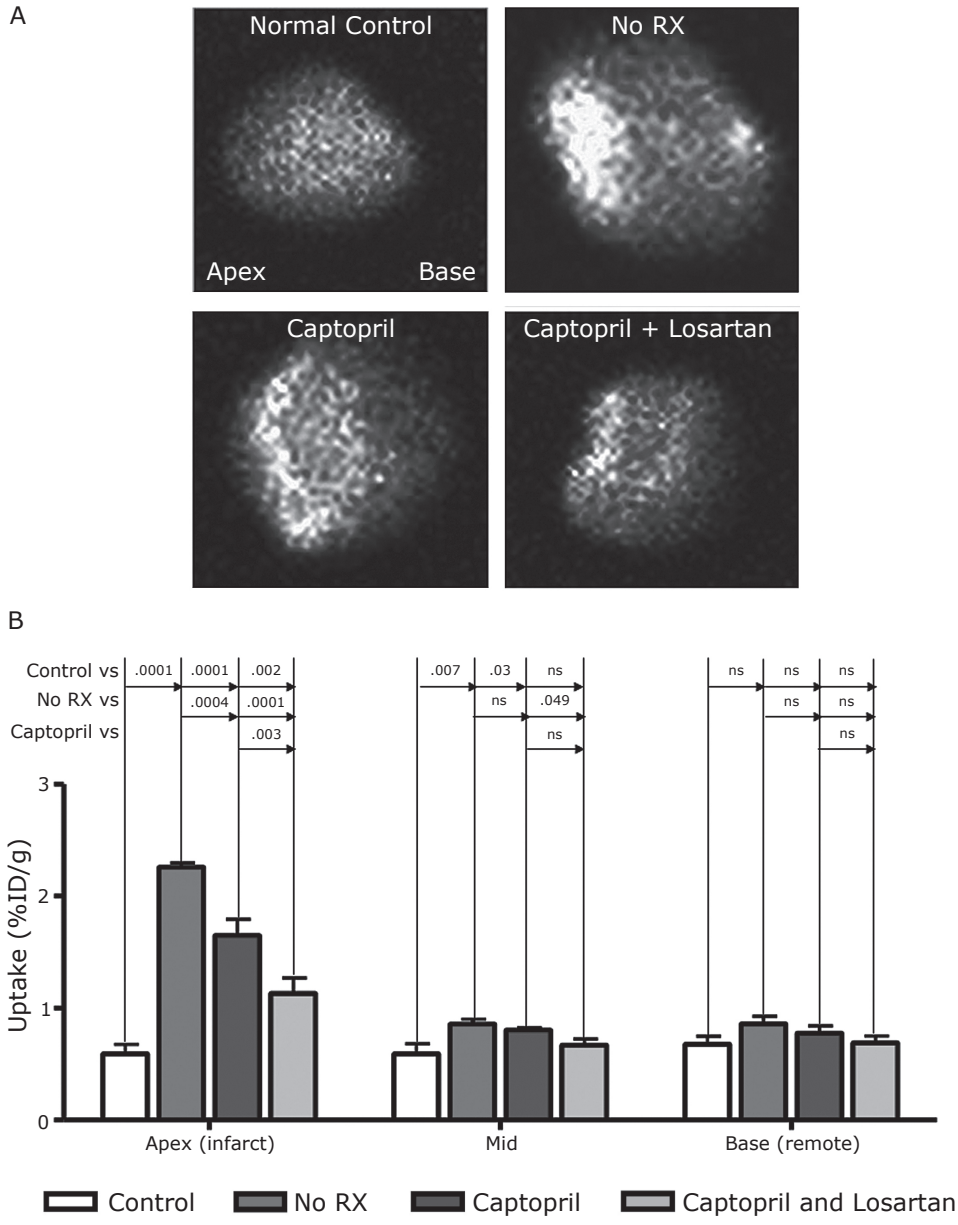

Figure 6.5 **Radiolabeled CRIP uptake after anti-angiotensin therapy in post-MI animals**

A. Ex Vivo Images 4 weeks post-MI. In 4-week post-MI animals, captopril treatment alone and in combination with losartan demonstrates significantly lower radiotracer uptake as observed in gamma images of the ex vivo explanted hearts. B. Quantitative Tc-CRIP uptake was significantly lower after therapeutic intervention in infarcted and nonsignificantly lower in non-infarcted areas. For full color illustration, see page 169.

DISCUSSION

The present study demonstrates the feasibility of noninvasive assessment of interstitial alterations in post-infarction ventricular myocardium by technetium-99m labeled CRIP. The lack of binding of scrambled CRIP (which carries a deranged RGD-motif) confirms that the CRIP binding is RGD-dependent and specific. Fluorescence and immunoelectron microscopy confirmed the binding of CRIP to the myofibroblasts. The CRIP uptake paralleled newly formed, thin, yellow-green collagen fiber production, suggesting that the CRIP uptake should indirectly represent the rate of collagen deposition. CRIP did not bind to the mature collagen fibers.

The uptake of CRIP in the infarct area was significantly higher at 2 weeks compared to 4 or 12 weeks after MI; the uptake almost completely resolved by 52 weeks in the infarct area (data not shown). The time-response curve of CRIP uptake in post MI hearts may parallel the expression dynamics of $\alpha v\beta 3$, as observed in hepatic stellate cells.[139] Myofibroblasts evolve and are activated by inflammatory cytokines elicited in the area following the insult. Collagen and other matrix molecules are produced and integrins are upregulated to attach the cells to the matrix for survival and proliferation. The expression of $\beta 3$ integrins is associated with angiogenesis in the peri-infarct zone and peaks around 7 days after MI as part of the remodeling process. Subsequently as inflammation resolves, collagen fibrils are cross linked by tranglutaminase activity and no more ligands are available for avb3 binding and the cells disappear through apoptosis or anoxis.[139] Therefore, after 12 month there are large amounts of collagen but no more integrins for CRIP to bind to; in other words, there is fibrosis but little fibrogenesis or myofibroblasts in mouse infarcts. However, since myofibroblasts have been reported up to 20 years after MI in well-healed human infarcts,[13] the binding characteristics of CRIP may be more favorable in humans than rodent hearts.
Unlike the infarcted zone, the CRIP uptake in the remote myocardium was higher at 12 weeks. It is well established that alterations in interstitial collagen can significantly influence the size and shape of the cardiac chamber as well as ventricular function and hence ventricular remodeling.[140] Excessive collagen deposition or pathological fibrosis contributes to LV dysfunction and poor prognosis in MI patients by inducing myocardial stiffness, promoting development of arrhythmias and adversely affecting systolic function.[141]

The myocardium contains an endogenous RAS system, and activation of renin-angiotensin-aldosterone axis results in cardiac fibroblast proliferation and fibrosis.[59, 142] This response is transduced by AT1 receptors which are far more abundant on cardiac fibroblasts than on myocytes.[143] Angiotensin II acts through the upregulation of additional fibrogenic growth factors, which mediate or augment

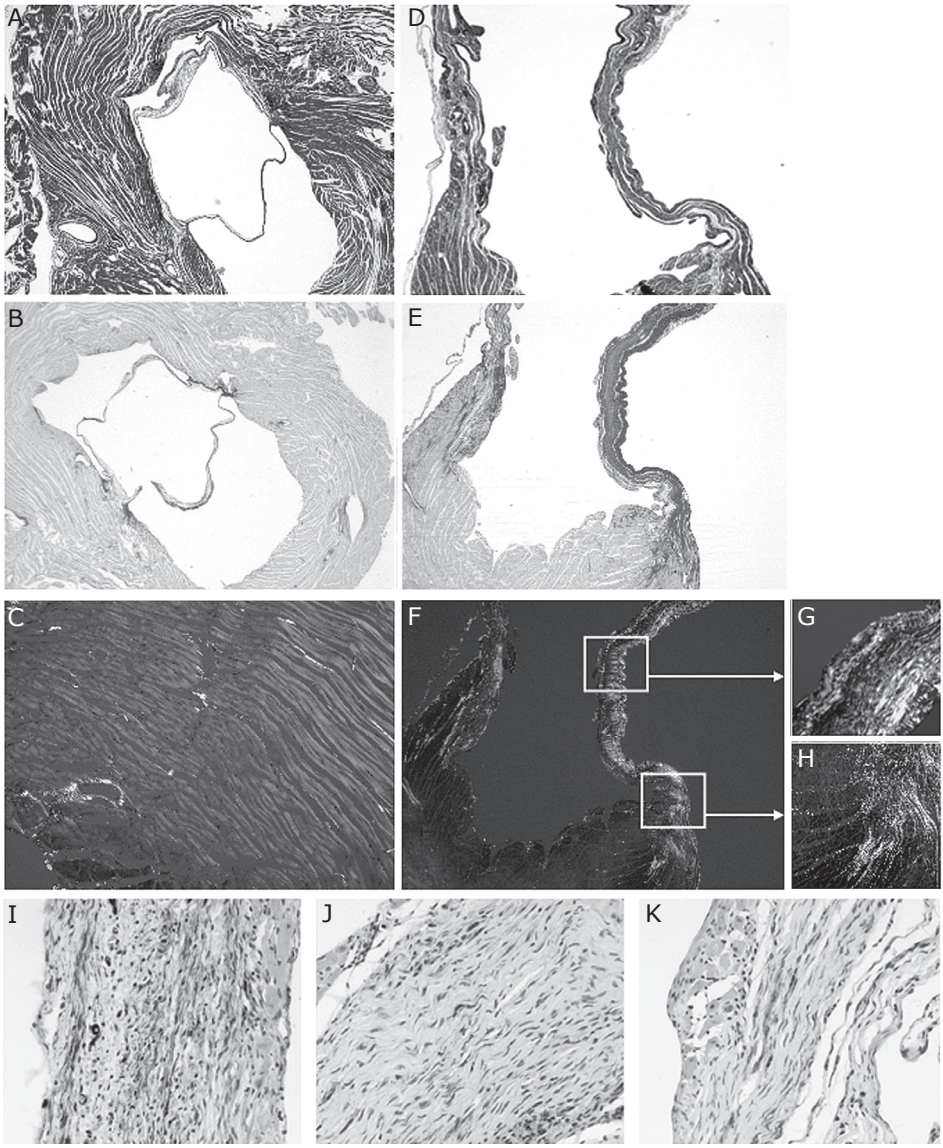

Figure 6.6 Histological assessment of control heart and 4 weeks post MI

Masson's trichrome (A,D) and Picro Sirius Red (B,E) staining, and Sirius Red staining with polarized light (C, F-H) in remote (A-C) and infarct center or border regions (D-H) in a heart 4 weeks after MI. The remote area is from the base of the heart as indicated by the enclosed mitral valve. The remote region shows minimal fibrosis (A) and collagen deposition (B,C). On the other hand, the infarct region shows significant wall thinning and fibrosis (D) with evidence of collagen deposition (E,F). The two areas from (F) are magnified to demonstrate collagen deposition in infarct center (G) and infarct border (H). Immunohistochemical characterization with anti-ASMA antibody (brown) of the infarct zone at 2 (I), 4 (J) and 12 (K) weeks reveal progressive decrease in the number of myofibroblasts over time. For full color illustration, see page 170.

the effects of angiotensin II, including TGFβ1. Upregulation of angiotensin production, AT1 receptors and increased collagen mRNA in myofibroblasts is associated with healing infarct scars,[144] and anti-angiotensin therapy may inhibit myocardial remodeling. The uptake of the Tc-CRIP was markedly reduced by captopril alone and more so in combination with losartan. Although angiotensin II levels decrease initially with ACE inhibitor therapy,[145, 146] their levels may rise gradually over time due to alternative conversion pathways. Therefore, a combination therapy of an ACE inhibitor with an angiotensin receptor blocker (ARB) acts synergistically and may benefit greater than either agent used alone. The present study demonstrated relatively superior effect of combination therapy in reduction of fibrogenesis compared to captopril therapy alone. Although OPTIMAAL and VALIANT studies did not substantiate the concept of combination therapy in post MI patients,[147, 148] ValHeFT and CHARM studies have demonstrated the superior efficacy of combination therapy in reduction of morbidity in heart failure patients with (CHARM Addition)[85] or without (ValHeFT)[63] improvement in survival. Since both agents are known to favorably alter the prognosis in patients with heart failure and the present study demonstrates decrease in collagen deposition after captopril±losartan treatment, it is possible that the decrease in collagen deposition is a favorable phenomenon. Alternatively, we hypothesize that the impact of anti-angiotensin therapy on the infarct zone may be relatively lower as compared to the remote region, wherein all collagen formation may get abrogated. As such, evaluation of the impact of therapy at 12 weeks could have offered more information.

Since LV remodeling post-MI is the leading cause of heart failure and is a determinant of morbidity and mortality,[30, 149] it is important to predict the likelihood of occurrence of cardiac remodeling. It is possible to detect the occurrence of collagen formation post-MI by measuring procollagen I and III in serum. The measurements of these markers have been shown to provide independent information pertaining to left ventricular function[150, 151] and survival[152, 153] in patients with heart failure. However, these markers are not specific and may not be of value in patients with other conditions associated with collagen formation such as arthritis.[154] The potential value of radiolabeled CRIP is its ability to noninvasively localize at the site of interstitial alterations and collagen formation in the myocardium, and therefore may provide information about evolution of heart failure. Our pilot clinical study with a radiolabeled RGD peptide in patients at 3 and 8 weeks after MI has shown the feasibility of interstitial imaging. In these patients, 1-year follow-up magnetic resonance imaging study confirmed the extent of fibrosis detected earlier by the radiolabeled RGD uptake.[155]

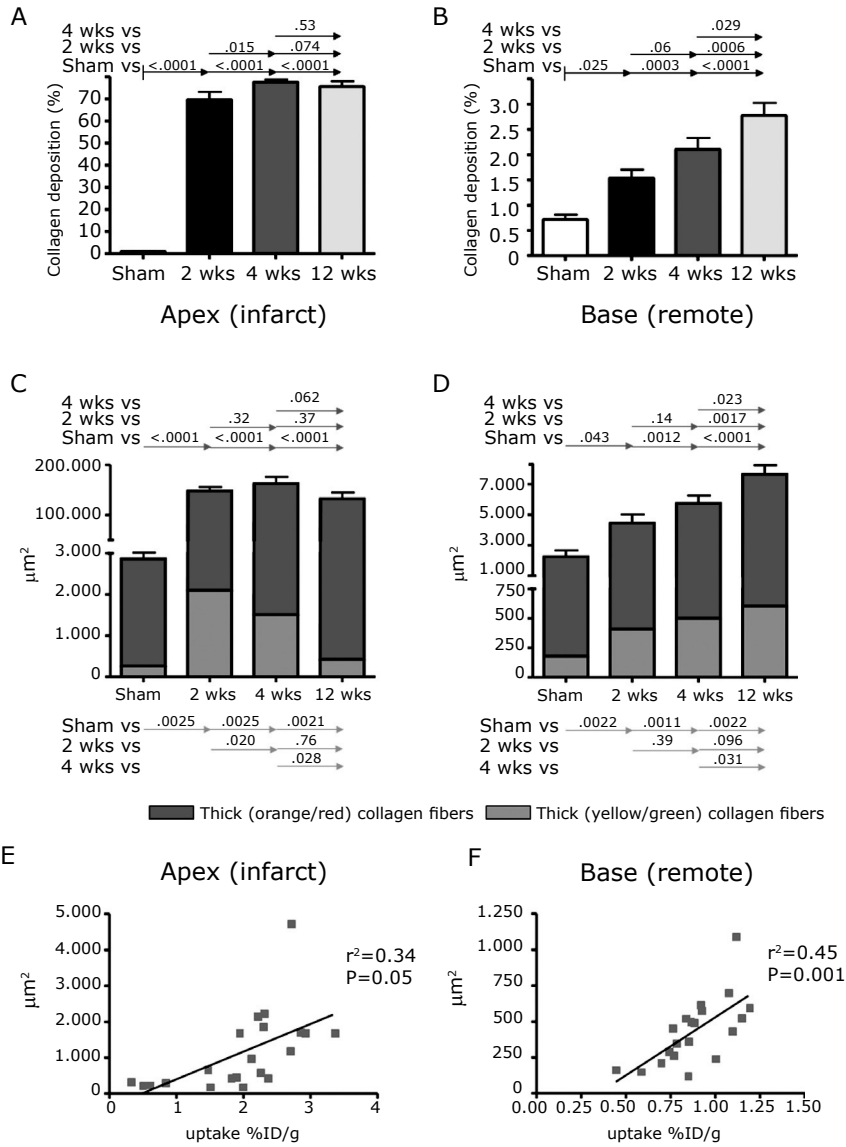

Figure 6.7 **Collagen fiber analysis in remote and infarct regions**

The total collagen content in the infarcted area (A) remains similar with the passage of time, whereas it increases significantly in the remote region (B). Further characterization of the collagen fibers by polarization reveals that the thin or new collagen fibers (green) decreased in the infarct region (suggestive of cessation of collagen production and maturation of the collagen fibers) (C) and increased substantially in the remote area (D) (suggesting ongoing production of the new collagen with increasing total collagen content). The prevalence of new collagen fibers paralleled the CRIP uptake and demonstrated a significant direct correlation, both in infarct and remote zone (E, F). For full color illustration, see page 171.

Acknowledgments
We thank Hans Duimel for his help with the immuno electron microscopy. Susanne van den Borne was supported by a grant from the Van Walree Fund of the Royal Netherlands Academy of Arts and Sciences. Johan Verjans was partially supported by the DiPalma-Brodsky research grant to Dr. Narula. CRIP and scrambled CRIP were kindly provided to Dr. Narula by GE Healthcare, Oslo, Norway.

7

Molecular Imaging for Efficacy of Pharmacologic Intervention in Myocardial Remodeling

Journal of the American College of Cardiology:
Cardiovascular Imaging 2009;2:187-198

ABSTRACT

Objectives: Employing molecular imaging techniques, we examined interstitial alterations during post-myocardial infarction (MI) remodeling and assessed the efficacy of anti-angiotensin and anti-mineralocorticoid intervention, alone and in combination.

Background: The antagonists of the renin-angiotensin-aldosterone axis restrict myocardial fibrosis and cardiac remodeling after MI, and contribute to improved survival. Radionuclide imaging with technetium-99m-labeled Cy5.5 RGD imaging peptide (CRIP) targets myofibroblasts and indirectly allows monitoring of the extent of collagen deposition post-MI.

Methods: 99mTc-CRIP was intravenously administered for gamma imaging after 4 weeks of experimental MI in 63 Swiss-Webster mice and in 6 unmanipulated (disease control) mice. Of 63 animals, 50 were treated with captopril (C), losartan (L), spironolactone (S) alone, or in combination (CL, SC, SL, and SCL) for 4 weeks; 8 (treatment control) mice received no treatment. In all animals, echocardiography was performed for infarct size determination and development of cardiac remodeling. Hearts were characterized histopathologically for the presence of myofibroblasts, and thick and thin collagen fiber deposition.

Results: Acute MI size was similar in all groups. The quantitative CRIP percent injected dose per gram uptake was highest in the infarct area of untreated control mice (2.30±0.05%), and decreased significantly in animals treated with one agent (C,L or S; 1.71±0.08%; $p=0.0002$). Addition of two (CL, SC, or SL 1.31±0.08%; $p<0.0001$) or three agents (SCL; 1.16±0.11%; $p<0.0001$) demonstrated further reduction in tracer uptake. Decrease in echocardiographic LV function, strain and rotation parameters, as well as histologically-verified deposition of thin collagen fibers was significantly reduced in treatment groups, and correlated with CRIP uptake.

Conclusions: Radiolabeled CRIP allows evaluation of the efficacy of neurohumoral antagonists post-MI and reconfirms superiority of combination therapy. If proven clinically, molecular imaging of the myocardial healing process may help plan an optimal treatment for patients susceptible to heart failure.

INTRODUCTION

Upregulation of the renin-angiotensin-aldosterone axis after myocardial infarction (MI) contributes to the process of cardiac remodeling and hence evolution of heart failure.[156-159] Although this remodeling process is initiated by myocyte loss, interstitial and myocytic alterations continue to occur inexorably even after the initial injury has abated.[3, 4, 160] Anti-angiotensin,[62, 64, 161] and anti-aldosterone[162] treatments effectively control this process, and delays or prevents the development of heart failure.[65, 163-165] These therapeutic interventions reduce the extent of interstitial collagen deposition, which is considered to be the basis of their efficacy.[156, 157] Combination of these agents has been shown to be more effective than the solitary agents.[61, 63]

The efficacy of pharmacologic intervention in a clinical milieu is variable, and it is desirable to define optimal use of anti-remodeling agents for individual patients. While pharmacogenomics has been proposed as an important determinant of such a strategy,[166, 167] the role of phenotypic characterization by novel imaging methods is also being explored.[159] It has recently been reported that the extent of new collagen deposition can be assessed by molecular imaging employing technetium-99m-labeled Cy5.5-RGD-imaging peptide (CRIP).[71] Through RGD-based targeting, CRIP binds to the myofibroblasts in the healing infarct and correlates with the extent of new collagen deposition after experimental MI.[71] In our preliminary experiment we proposed that such imaging strategy may have a role in identifying the impact of a therapeutic intervention on collagen deposition and hence the efficacy of the therapy. In the present study, we evaluated the effect of an angiotensin converting enzyme inhibitor (ACE-I), an angiotensin receptor blocker (ARB), and a selective aldosterone receptor antagonist (SARA), individually and in combination, on infarct healing, employing CRIP imaging.

METHODS

The present study was performed in 69 Swiss-Webster mice. Of these, myocardial infarction was produced in 63 mice by occlusion of the left coronary artery (LCA). Echocardiograms were obtained before and after coronary occlusion to demonstrate the basal LV dimensions and function, and the infarct size. Of the 63 infarcted mice, 20 mice received a single agent intervention (1Rx); 8, 6 and 6 animals were started on spironolactone (S), captopril (C), losartan (L), respectively. 22 of 63 animals received dual therapy (2Rx); 6, 8, and 8 were started on a combination of captopril + losartan (CL), spironolactone + captopril (SC) or spironolactone + losartan (SL), respectively. 8 of 63 post-MI animals received a combination of three neurohumoral antagonists (3Rx, spironolactone + captopril + losartan (SCL) (Table 7.1). Eight post-MI animals did not receive any pharmacologic agent and served as treatment controls (No Rx) and 5 post-MI animals

Table 7.1 **Various treatment groups, dosage schedules and quantitative 99mTc-CRIP uptake**

		Dose			Infarct		Remote	
Group	Spironolactone	Captopril	Losartan	N	%ID/g	p	%ID/g	p
Control#	-	-	-	6	0.590±0.09	†	0.677±0.07	ns
No Rx	-	-	-	8	2.302±0.05	*	0.921±0.08	ns
S	20 mg/kg/day	-	-	8	1.798±0.15	*†	0.903±0.08	ns
C	-	60 mg/kg/day	-	6	1.718±0.13	*†	0.867±0.10	ns
L	-	-	20 mg/kg/day	6	1.576±0.11	*†	0.752±0.07	ns
CL	-	30 mg/kg/day	10 mg/kg/day	6	1.374±0.22	*†	0.783±0.11	ns
SC	20 mg/kg/day	60 mg/kg/day	-	8	1.280±0.15	*†	0.786±0.06	ns
SL	20 mg/kg/day	-	20 mg/kg/day	8	1.293±0.11	*†	0.821±0.13	ns
SCL	20 mg/kg/day	60 mg/kg/day	20 mg/kg/day	8	1.157±0.11	*†	0.796±0.08	ns

#The quantitative CRIP uptake in control animals was obtained from the myocardial specimen corresponding to infarct and remote regions of post-MI animals. *p<0.05 to <0.0001 compared with control animals. †p<0.05 to 0.0001 compared with No Rx-treated animals.

received a scrambled version of the imaging peptide (sCRIP) to serve as tracer controls. In addition, 6 unmanipulated animals were included in the imaging protocol as disease control animals. After 4 weeks, all animals again underwent echocardiographic examination for the characterization of the remodeling process and received Tc-99m labeled CRIP intravenously. 3.5 hours after CRIP administration, hearts were explanted and ex vivo imaging was performed using a microSPECT camera. The hearts were then sectioned into three cross-sectional bread loaf slices to represent apical (predominantly infarct), middle and the basal (predominantly remote) areas. All samples were gamma-counted for quantitative CRIP (and sCRIP) uptake. Subsequently, all myocardial specimens were processed for histopathological characterization, particularly the extent of myofibroblastic proliferation, and thick and thin collagen fiber deposition.

Experimental Myocardial Infarction in Mice

This Experimental protocol was approved by the Institutional Animal Care and Use Committee of the University of California Irvine School of Medicine. In 63 adult Swiss Webster male mice (age, 3 months; body weight, ~50 g), the lateral branch of the LCA was ligated under Pentobarbital (75 mg/kg i.p.) and gas anesthesia (2.0–3.0% isoflurane) to induce MI. Briefly, animals were first placed on a heating pad, in the supine position. Endotrachial intubation was performed under direct laryngoscopy and mechanical ventilation maintained with a small animal respirator (Harvard Apparatus; tidal volume = 250 µl, rate = 210 breaths/min). After thoracotomy, the lateral branch of the LCA was ligated at the root with a 6.0-prolene suture. Successful ligation was verified by visual inspection of myocardial blanching and akinesis or dyskinesis of the apical segment. The chest cavity was closed in layers with 6.0-silk, and the skin closed with 4.0-silk sutures. Animals were gradually weaned from the respirator. Six of the 69 mice were left unmanipulated as disease control mice for comparison with the post-MI mice.

Treatment Protocols after Myocardial Infarction in Mice

Spironolactone (Innovative Research of America, Sarasota, FL) was administered via a subcutaneous pellet, releasing 1 mg/day, placed under the skin on the back, immediately after MI surgery. Captopril (Sigma, St Louis, MO) and Losartan (kind gift of Merck, Rahway, NJ) were administered in the drinking water in a concentration of 60 mg/kg/day and 20 mg/kg/day, respectively. When combination of anti-angiotensin therapy was given, the dosages were halved. The animals received the intervention for 4 weeks starting on the post-MI day 0 (Table 7.1).

Echocardiography

Echocardiographic studies were performed in all mice for the evaluation of left ventricular dimensions and function. All animals underwent three echocardiographic studies; performed at baseline level, immediately after MI, and the last study was performed at 4 weeks post-MI, just before CRIP imaging. Mice were anesthetized with 2% isoflurane, and echocardiograms were made (Sequoia, Siemens, Mountviews, CA) using a 14-MHz linear probe (15L8, Acuson). An advanced high frame rate imaging technique (Paragon®, Siemens, Mountviews, CA) was adopted to increase temporal resolution at a frame rate of 120 fps. B-mode images of LV parasternal long-axis, parasternal short-axis, and apical views were digitally acquired at 2-3 cardiac cycle lengths. Images of LV short-axis were standardized at three levels, base, mid and apex. M-mode imaging was unified according to the American Society of Echocardiography guidelines for measurements of wall thickness, chamber dimensions, and functional parameters.[133] Infarction area (A_{inf}) and LV area (A_{LV}) were measured by tracing relative endocardial borders respectively on the long-axis images. Myocardial infarction percentage (MI%) was calculated as A_{inf}/A_{LV}x100. LV cavity dimensions, ejection fraction (EF), strain and rotation were calculated.

Radionuclide Imaging with ^{99m}Tc-CRIP

CRIP (AH110863, kind gift of GE Healthcare/Amersham Health AS, Oslo, Norway) is a 2.5 kD peptide conjugated to both a fluorescent cyanine dye Cy5.5, and the chelating agent cPN216; which is linked for radiolabeling of the peptide with technetium-99m. The peptide comprises 10 amino acids, contains an RGD-motif, and has a bi-cyclic structure formed by a disulfide and a thioether bridge. The dye moiety and the chelating agent are conjugated to the peptide by the side-chains of lysine residues at the N- and C-terminal ends, respectively. CRIP, by RGD-based targeting, binds to myofibroblasts,[71] and is labeled with Technetium-99m for radionuclide imaging. For radiolabeling, 50 µg of CRIP was dissolved in 50 µL of MeOH and then added to freeze dried kit. 1.0 ml of $^{99m}TcO_4^-$ was added to the compound and left at room temperature for 20-30 min. Instant thin-layer chromatography confirmed radiopurity of more than 90%. 3.7±0.02 mCi (137±0.7 MBq) of ^{99m}Tc-CRIP was injected intravenously through the tail

vein. At 3.5 hours after CRIP administration, mice were sacrificed with an overdose of pentobarbital (150 mg/kg i.p.). Hearts were carefully dissected and planar images of *ex vivo* hearts were acquired for 15 min in 128 × 128 matrix using a low-energy, high-resolution pinhole collimator, mounted in a dual-head micro single-photon emission computed tomography (SPECT) gamma camera (X-SPECT, Gamma Medica, Inc., Northridge, CA). Thereafter, hearts were cut into apical, middle and basal slices. The quantitative ^{99m}Tc-CRIP uptake was determined with a gamma scintillation counter (1480 Wizard 3"; Wallac Co.). CRIP biodistribution and radiation burden to lung, liver, spleen, and kidney was also determined.

Histological Evaluation of Myocardial Specimens

After completion of the nuclear studies the three broad-loaf slices were washed in PBS, fixed in 4% paraformaldehyde in PBS over 24 hours, processed and embedded in paraffin and 4 µm sections were prepared. After deparaffinization and rehydration, sections were stained with haematoxylin & eosin, Masson's trichrome and picro-sirius red. After deparaffinization and rehydration, sections were placed in working Weigert's iron hematoxylin for 10 minutes and tepid water rinsed for 10 minutes for Masson's trichrome staining. Tissue sections were then incubated in Biebrich Scarlet-Acid Fuchsin Solution for 5 minutes, differentiated in Phosphotungstic-Phosphomolybdic Acid for 5 minutes and stained in Aniline Blue for 8 minutes. After rinsing with 1% Gallic Acedic Acid (GAA), sections were dehydrated and mounted in permanent mount medium.

For picro-sirius red, sections were incubated for 5 min with 0.2% aqueous phosphomolybdic acid and subsequently incubated for 90 min with 0.1% sirius red F3BA (C.I. 35780, Polysciences, Northhampton, UK) in saturated aqueous picric acid and washed for 2 min with 0.01 M HCl. Sections were then dehydrated and mounted with cover-slip. The relative collagen areas in the infarcted, and remote areas, were determined under a microscope (×200) coupled to a computerized morphometry system (Quantimet, Leica, Cambridge, UK). The quality of collagen fibers was further investigated by Sirius red polarization microscopy, allowing quantification of the thick, tightly packed, more mature orange/red fibers and the newly formed, thin, loosely assembled yellow/green fibers.[134, 135] Approximately 4-5 fields per section were analyzed in the myocardium.

Alpha smooth muscle actin (ASMA) was used to determine myofibroblasts in the infarct area. After deparaffinization, rehydration and blocking of endogenous peroxidase, sections were incubated for 2 hours at room temperature using anti-alpha smooth muscle actin (ASMA monoclonal antibody, Sigma, dilution 1:2000). After washing in PBS, sections were incubated with secondary antibody (rabbit anti mouse HRP, DAKO, 1:500) for 1 hour at room temperature. Sections were briefly counterstained with haematoxylin. ASMA area was quan-

tified by Quantimet analysis in 4-5 fields per section. ASMA uptake was only counted for myofibroblasts and care was taken not to include ASMA uptake observed in vasculature.

Statistical Analysis

Data are presented as mean±sem. Quantitative radiotracer uptake was calculated as percent total injected dose per gram (%ID/g) of tissue. Radiotracer uptake and echocardiographic measurements were expressed as mean ± standard deviation. Based on our previous study,[71] CRIP uptake was reduced by >25% in the captopril group compared to the untreated group, and in combination treatment (losartan plus captopril) compared to single therapy (captopril alone) group; as such we propose that having at least 6 mice per group is sufficient to detect, with at least 90% power and alpha=0.01, reductions in the uptake of CRIP of at least 25% in treated compared to untreated animals, or 2 vs. 1 agent groups. This confirms that our current study is well-powered. To determine the statistical significance of differences among 1 Rx, 2 Rx and 3 Rx treatment groups, one-way ANOVA followed by post-hoc Bonferroni's test for multiple comparisons was used. The correlation between the quantitative tracer uptake and echocardiographic parameters or histological characteristics was evaluated by linear regression analysis. P values < 0.05 were considered as statistically significant.

RESULTS

^{99m}Tc-CRIP Uptake and Pharmacologic Intervention

Maximum CRIP uptake was observed in the infarct zone of the untreated post-MI mice. CRIP uptake was substantially reduced in the treated animals (Table 7.1; Figure 7.1A); no CRIP uptake was seen in the unmanipulated hearts. Scrambled CRIP, which has a deranged RGD sequence, did not show uptake in the infarcted myocardium, and demonstrated that CRIP uptake is RGD-dependent and specific.

The quantitative CRIP uptake in the myocardial tissue specimens was calculated and represented as percent injected CRIP dose per gram (%ID/g) of myocardial tissue. CRIP uptake in the infarcted area was observed to be the highest in the untreated MI group (No Rx; 2.30±0.05%). There was a significant reduction in CRIP uptake in the infarct area in all treated animals (1.46±0.06%) compared to the untreated animals ($p<0.0001$). The reduction of uptake was significant even when the animals were treated with a single neurohumoral antagonist (1Rx, 1.71±0.08%, $p=0.0002$) (Figure 7.1B). Each agent was independently effective; spironolactone (1.80±0.15%; $p=0.0011$), captopril (1.72±0.13%; $p=0.0059$) and losartan (1.58±0.11%; $p<0.0001$) (Table 7.1).

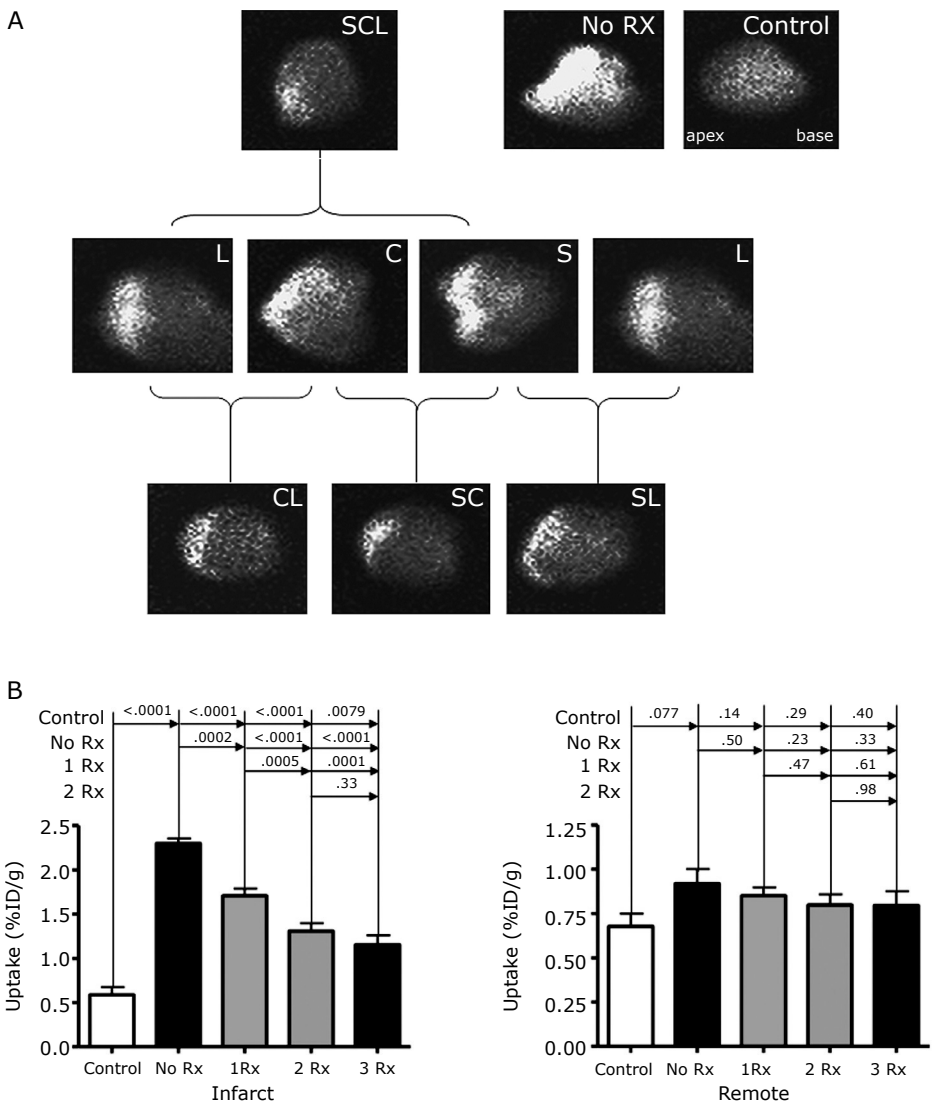

Figure 7.1 **Radiolabeled CRIP uptake after neurohumoral antagonist treatment in post-MI animals**

A. Disease control (unmanipulated) heart with RGD probe shows no radiotracer uptake in ex vivo image of the heart. On the other hand, intense CRIP uptake is seen in 4-week untreated (no Rx) post-MI animals (upper panel, right). The uptake in the infarcted area is reduced after neurohumoral treatment with solitary agents and combination therapy (middle and lower panels). Losartan (L) images are displayed twice (middle panel) for the convenience of comparison. C= captopril, S= spironolactone. B. Quantitative Tc-CRIP uptake in the infarct (apex, above) and remote (base, below) areas. The %ID/g uptake in the infarct area is highest in untreated mice, followed by treatment with one (1Rx), two (2Rx) and three (3Rx) agents, respectively. On the other hand, the uptake in the remote area shows no significant differences between treated and untreated animals. Quantitative data confirmed the findings of ex vivo images. For full color illustration, see page 172.

Use of two neurohumoral antagonists (2Rx, 1.31±0.09%) influenced the uptake to a greater extent than a single agent (1Rx, 1.71±0.08%) treatment (p=0.0005) (Figure 7.1B). Uptake with various combinations was as follows; CL (1.37±0.22%; p<0.0001), SC (1.28±0.15%; p<0.0001), and SL (1.29±0.11%; p<0.0001) (Table 7.1). Combination of all 3 agents further reduced the CRIP uptake (3Rx, 1.16±0.11%) in the infarct area (Figure 7.1B). The decrease in CRIP uptake in triple treated animals was significantly lower than one agent treatment (p=0.0001), but was statistically insignificantly reduced compared to two-agent therapy (p=0.33) (Figure 7.1).

CRIP uptake in the remote myocardium was increased, although statistically insignificantly, in the untreated post-MI animals (0.92±0.08) as compared to the unmanipulated control animals with no infarcts (0.68±0.07, p=0.07) (Figure 7.1B). The tracer uptake was minimally reduced in the treated groups. It seems that we would need a longer study to observe a statistically significant resolution of tracer uptake in response to therapeutic intervention (Table 7.1). We believe so because our previous study demonstrated that an increase in CRIP uptake in the remote area occurred only at 12 weeks after MI.[71]

Echocardiographic examination and remodeling characteristics

As shown in Table 7.2, initial MI size was similar in all animal groups. Over the 4-week follow-up period, there was a reduction in LV ejection fraction in untreated post-MI (30±3%) animals compared to unmanipulated disease control animals (64±2%, p<0.0001). Neurohumoral antagonists significantly prevented the functional loss (EF 44±1%), compared to untreated animals p=0.0016). Similar to LV ejection fraction, there was a significant decrease in the myocardial strain development in untreated animals (-4.59±0.7 unit %) compared to unmanipulated (-12.00±0.9unit %) animals (p<0.0001); loss of myocardial strain was significantly prevented by treatment with neurohumoral agents (-8.04±0.3 unit %, p=0.0005). The strain development in 1Rx (-7.17±0.5 unit %, p=0.0126), 2Rx (-8.28±0.5unit %, p=0.0011) and 3Rx (-9.33±0.56 unit %, p<0.0001) groups was better preserved compared to the untreated control group. However, the preservation of strain development did not reach statistical significance on comparison of 1Rx vs. 2Rx (p=0.1304), or 2Rx vs. 3Rx (p=0.2530) agents; 3Rx was statistically significantly better than the 1Rx intervention (p=0.0168). The results of loss of apical rotation or counterclockwise twist of the LV were similar to the loss of strain development. The rotation in all (0.55±0.03°, p<0.0001), 1Rx (0.49±0.04°, p=0.0006), 2Rx (0.57±0.04°, p<0.0001) and 3Rx (0.63±0.06°, p<0.0001) groups was preserved compared to the untreated control group. However, once again, the prevention of rotational loss did not reach statistical significance on comparison of 1Rx vs. 2Rx (p=0.1684), or 2Rx vs. 3Rx (p=0.3601) agents; 3Rx was statistically significantly better than the 1Rx intervention (p=0.0481). The LV ejection

Table 7.2 Overview echo data

		Control	no RX	S	C	L	CL	SC	SL	SCL
n		6	8	8	6	6	6	8	8	8
Day 0	BW (g)	46±1	45±3	53±2	46±4	53±6	42±3	48±2	47±1	48±2
	MI(%)	0	41±2*	41±3*	39±5*	42±11*	40±3*	40±3*	41±3*	43±3*
4 weeks	LVIDd (cm)	0.46±0.01	0.55±0.03*	0.52±0.03*	0.52±0.02*	0.50±0.02	0.5±0.03	0.52±0.02	0.51±0.02	0.50±0.01
	LVIDs (cm)	0.30±0.01	0.46±0.04*	0.46±0.04*	0.41±0.03*	0.41±0.02*	0.40±0.04*	0.43±0.03*	0.43±0.02*	0.44±0.03*
	EF (%)	64±2	30±3*	39±4*	43±2*†	47±4*†	44±6*†	43±4*†	47±5*†	44±3*†
	Strain (unit %)	-12.0±0.9	-4.6±0.7*	-6.9±0.9*	-7.7±0.7*†	-7.0±1.1*	-7.3±1.3*†	-8.0±0.5*†	-9.1±0.9*†‡	-9.3±0.6*†‡
	Rotation (°)	1.85±0.06	0.22±0.04*	0.48±0.07*†	0.50±0.04*†	0.50±0.08*†	0.53±0.09*†	0.54±0.05*†	0.62±0.07*†	0.63±0.06*†

*p<0.05 to <0.0001 compared with control mice. †p<0.05 to <0.001 compared with untreated mice (no Rx). ‡p<0.05 compared with spironolactone, BW = body weight; C= captopril; CL = captopril and losartan; EF = ejection fraction; L= losartan; LVIDd= left ventricular diastolic dimension; LVIDs = left ventricular systolic dimension; MI = myocardial infarction; S = spironolactone; SC = spironolactone and captopril; SCL = spironolactone, captopril and losartan; SL = spironolactone and losartan

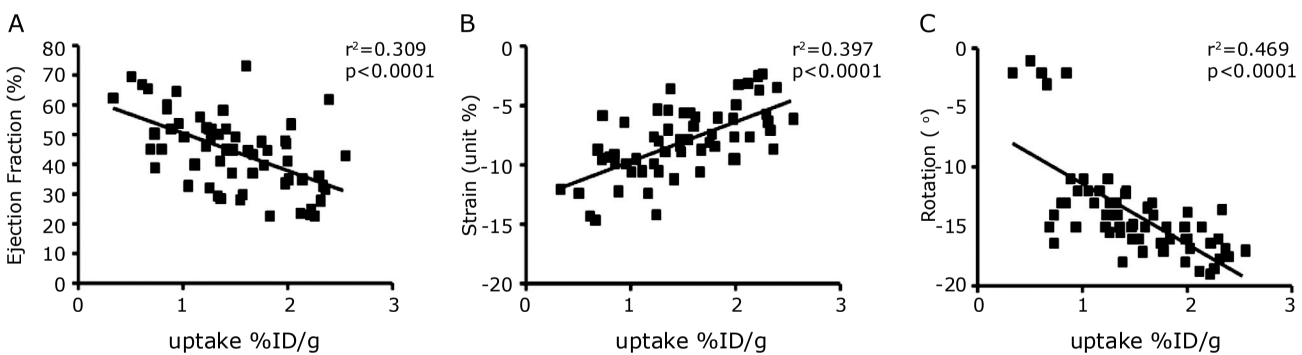

Figure 7.2 Correlation of radiolabeled CRIP uptake and echocardiographic parameters of remodeling in all animals

A significant correlation between CRIP uptake and LV ejection fraction (A), myocardial strain (B) and apical counterclockwise rotation (C) is observed.

fraction, strain development and rotation correlated with %ID/g CRIP uptake (r^2=0.309, 0.397 and 0.469, respectively; p<0.0001, <0.0001 and <0.0001) (Figure 7.2)

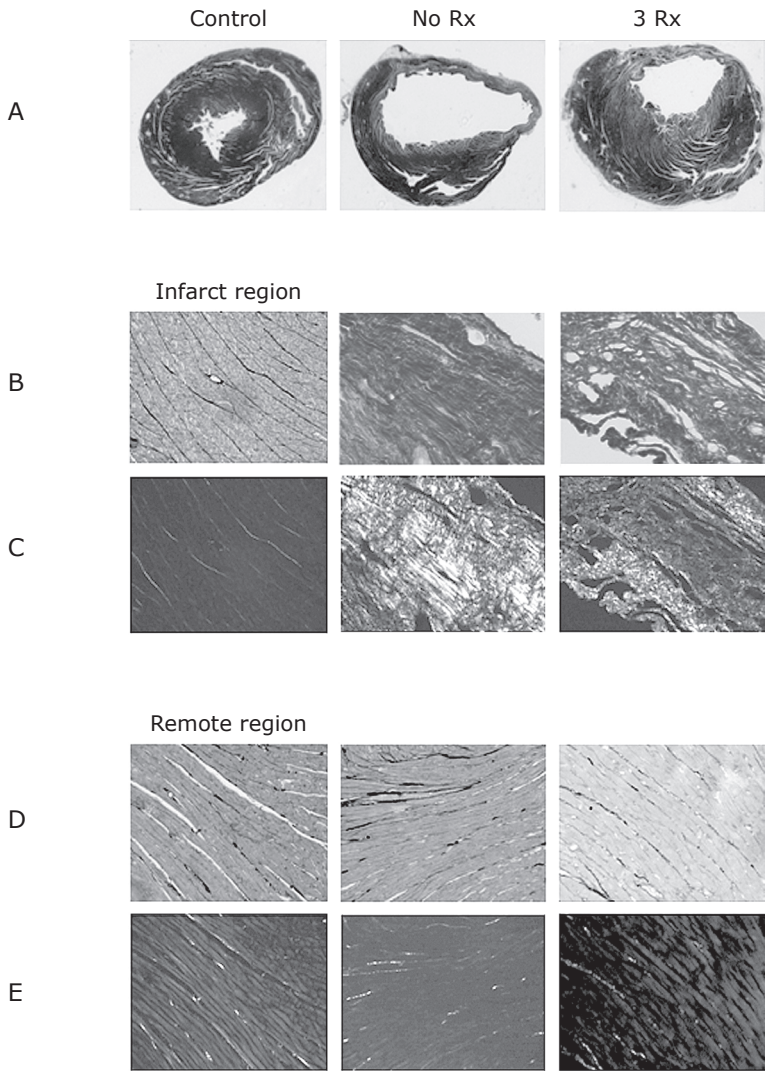

Figure 7.3 **Histopathological characterization of the treated and untreated animals**

Masson's trichrome staining was performed for infarct localization in control, untreated and treated animals (A). In addition, histological staining was performed with picro sirius red to demonstrate collagen deposition, which on polarized light allowed identification of the quality of collagen, in the infarct (B,C) and remote regions (D,E). The left column presents control animals, middle column shows untreated animals (no Rx) and the right column shows animals treated with 3Rx neurohumoral antagonists (SCL). The remote region shows minimal fibrosis and collagen deposition (D). On the other hand, infarct region shows significant wall thinning (A) and fibrosis with evidence of substantial collagen deposition in untreated animals (B, NoRx). 3Rx treated animals show reduced fibrosis (A, SCL) and collagen deposition (B, SCL) in the infarcted area. The Sirius staining under polarized light provides distinction of thick red-orange and thin yellow-green collagen fibers in the infarct region (C). For full color images, *see page 173.*

Histologic characterization of infarct and remote myocardium and correlation with CRIP uptake

Masson's trichrome and picro sirius red staining (Figure 7.3) of the myocardial slices allowed the assessment of total collagen content, and the composition in thick and thin collagen fibers. The percent collagen content in the infarcted area in untreated animals was 79±1%, which reduced substantially in the treated animals (66±1%, $p<0.0001$) (Figure 7.4A, Table 7.3). The collagen content decreased in animals treated with 1Rx (71±2%, $p=0.006$), 2Rx (64±1%, $p<0.0001$), or 3Rx (65±2%, $p=0.0008$) agents (Figure 7.4A). The results were similar for the yellow-green collagen fiber deposition in the infarcted myocardium suggesting decrease in new or thin collagen fiber synthesis (Figure 7.4C). The new, thin collagen fibers correlated with CRIP uptake in the infarct ($r^2=0.5475$, $p<0.0001$) (Figure 7.4E). In the remote region, the overall collagen deposition was markedly lower as compared to the infarct region. The collagen content of the untreated remote myocardium (NoRx, 2.1±0.2%) was significantly higher than the unmanipulated hearts (0.73±0.1%, $p<0.0001$)(Figure 7.4B). A marked decrease in collagen content and yellow-green collagen fiber deposition was observed in the remote region after treatment (Figure 7.4D, Table 7.3); collagen content in treated animals was not different from unmanipulated animals. There was a direct correlation between tracer uptake and thin collagen fiber deposition in the remote region ($r^2=0.3473$; $p<0.0001$) (Figure 7.4F).

We performed ASMA staining for quantification of the myofibroblasts (Figure 7.5A). The ASMA positive area was substantially larger in the untreated animals (NoRx, 6.11±2.6 μm^2) compared to the unmanipulated animals (0.007±0.01 μm^2, $p=0.013$). Treatment with 1Rx (4.91±0.8 μm2, $p=0.51$), 2Rx (2.22±1.0 μm^2, $p=0.037$) or 3Rx (1.54±0.5 μm^2, $p=0.039$) interventions substantially restricted the myofibroblast prevalence (Figure 7.5B, Table 7.3). There was a directly proportional relationship between CRIP uptake and ASMA positive area ($r^2=0.5828$, $p<0.0001$) (Figure 7.5C).

Table 7.3 **The extent of collagen deposition and myofibroblast count in various animal groups**

	Infarct				Remote		
Group	Collagen (%)	YG (mm^2)	OR (mm^2)	ASMA (mm^2)	Collagen (%)	YG (mm^2)	OR (mm^2)
Control	0.90±0.06†	221±32†	2430±164†	0†	0.73±0.07†	170±27†	2052±274†
No Rx	79.3±1.4*	2343±230*	190026±19520*	6.1±2.6*	2.11±0.22*	571±83*	5234±527*
S	70.9±1.5*†	1452±206	157337±10096*	4.0±1.6	1.32±0.32†	323±109†	3181±795†
C	71.3±3.1*†	1591±139*	165676±11887*	6.1±1.2*	1.29±0.17†	328±42†	3139±526†
L	70.1±3.0*†	1849±293*	145112±25166*	4.5±0.3	1.31±0.10†	304±38†	3155±314†
CL	68.2±2.8*†	2304±370*	137198±14136*†	4.2±2.4	1.17±0.31†	298±75†	2950±807†
SC	61.3±2.4*†	1545±402*	154679±15678*	1.3±1.0	1.12±0.12†	313±34†	3197±407†
SL	62.2±2.2*†	1248±354†	168002±10340*	0.7±0.1†	1.32±0.11†	342±24†	3873±347†
SCL	64.7±1.7*†	689±111†	159914±22116*	1.5±0.5†	1.12±0.14†	291±51†	3321±474†

*p<0.05 compared with control animals. †p<0.05 compared to No Rx treated animals, ASMA = alpha smooth muscle cells; OR = Orange-red; thick, crosslinked collagen fibers, YG = Yellow-green; thin, new collagen fibers

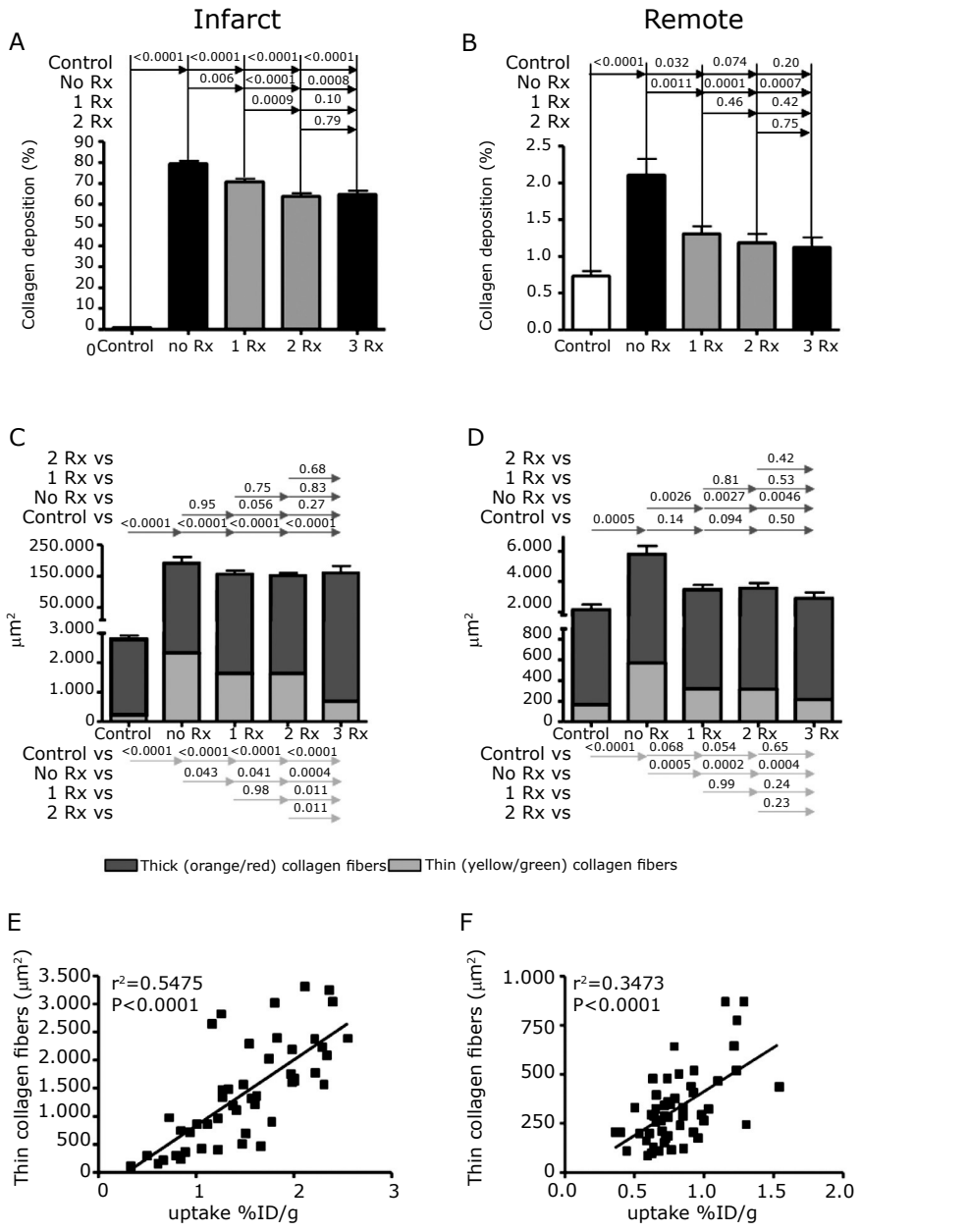

Figure 7.4 Collagen fiber deposition in infarct and remote regions

The total collagen content decreases with treatment in the infarcted (A), as well as the remote (B) areas. Further characterization of the collagen fibers by polarization reveals that the thin or new yellow-green collagen fibers decreased both in the infarct (C) and remote (D) regions after treatment. This indicates cessation of new collagen production and maturation of the collagen fibers after treatment. The prevalence of new collagen fibers paralleled the CRIP uptake and demonstrated a significant direct correlation, both in infarct (E) and remote (F) regions. For full color images, see page 174.

The direct correlation between radiotracer uptake and ASMA-positive myofibroblasts as well as radiotracer uptake and thin collagen fibers suggests that treatment with neurohumoral antagonists results in decreased new collagen production in the infarct zone.

DISCUSSION

Molecular imaging in myocardial remodeling

The present study employs molecular imaging of myofibroblasts during infarct healing. The radiotracer, CRIP, contains an RGD sequence, and binds to myofibroblasts through activated $\alpha v\beta 3/5$ integrins with an affinity of 1-3nM.[71] RGD is also known to commonly target the integrin expression associated with neoangiogenesis early after MI and macrophage influx during infarct healing. We have observed that after 2 weeks of infarct healing, myofibroblasts comprise a predominant target for RGD probes.[71] In addition, a specific noncovalent interaction of CRIP was also observed with custom-made DDX-sequence contained within pro-collagen I. The previous study using CRIP had demonstrated the feasibility of noninvasively imaging the extent of myofibroblasts prevalence in a post-MI mouse model.[71] The CRIP uptake receded over time in the infarct region with substantial resolution over 3 months after the myocardial injury. This previous report also demonstrated that the uptake was significantly reduced at 4 weeks upon treatment with captopril alone or in combination with losartan, and proposed that CRIP uptake could monitor the efficacy of neurohumoral antagonists and help identify the optimum level of therapeutic intervention.[71] A simultaneously conducted clinical study, using RGD-seeking peptide demonstrated the feasibility of molecular imaging early after MI.[155] The radiotracer uptake after MI predicted the extent of eventual magnetic resonance imaging-verified fibrosis after one year. Based on these results, the present study investigated the effect of various anti-remodeling agents, alone or in combination, on the extent of myocardial interstitial alterations. The present study demonstrated the efficacy of neurohumoral antagonists to reduce collagen formation/deposition in a 4-week post-MI mouse model. This study also reconfirmed that combination of two neurohumoral antagonists was superior to an individual agent used for intervention; three agents decreased the radiotracer uptake further albeit not significantly. The radiotracer uptake correlated closely with parameters of depressed myocardial mechanics, the quantitative prevalence of myofibroblasts and thin fiber collagen deposition. The data obtained in the present study corroborate with information provided by the estimation of collagen synthesis and fragmentation markers in the ser.[150, 151, 153] Procollagen type III amino-terminal peptide (PNIIIP) is decreased in chronic heart failure patients using anti-angiotensin and anti-aldosterone treatment.[152, 168]

What is the optimum therapy?

The clinical role of ACE-inhibitors, ARB, and SARA has been conclusively demonstrated in trials confirming the reduction in morbidity and mortality in patients with overt heart failure.[62-64,85,161,162] These agents also decrease the likelihood of developing heart failure in patients with asymptomatic decrease in LV ejec-

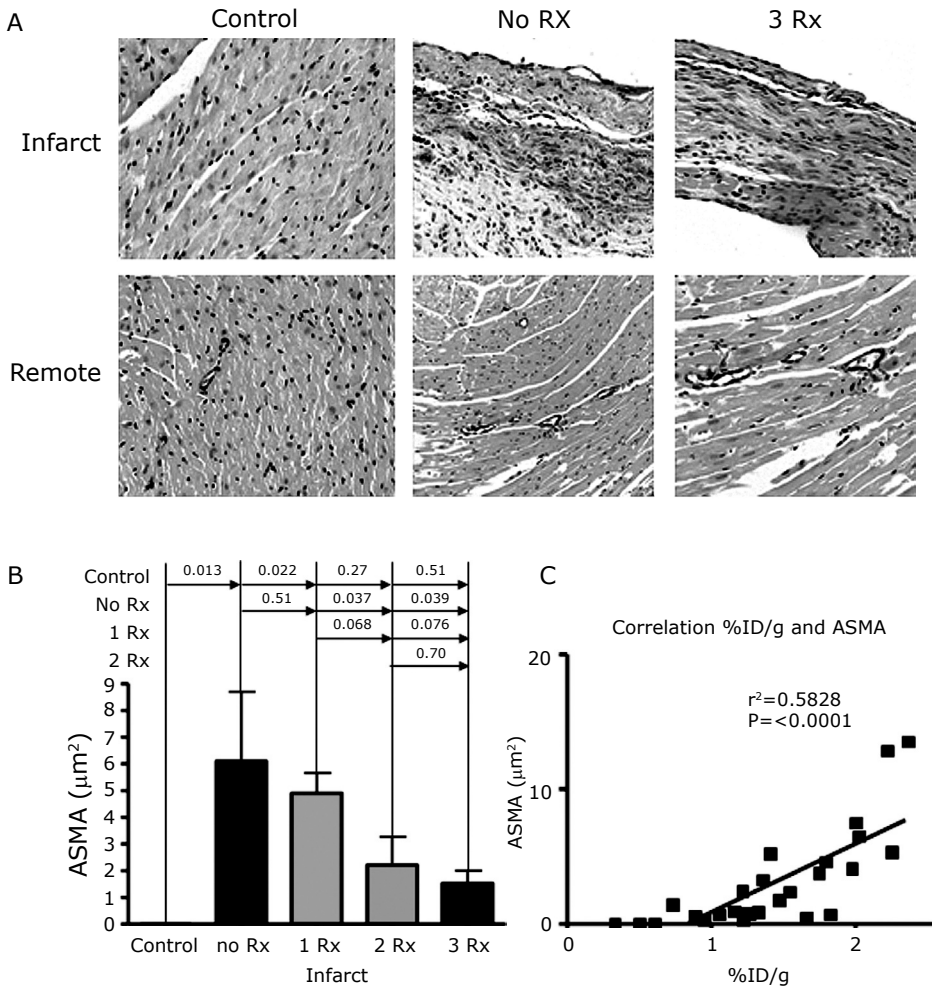

Figure 7.5 **Radiolabeled CRIP uptake and the prevalence of ASMA-verified myofibroblasts**

Immuohistochemical staining with ASMA antibody allowed quantitative assessment of myofibroblasts infiltration in the infarct and remote regions (A). The left column presents control animals, the middle column shows untreated animals (no Rx) and the right column shows 3Rx-animals (SCL). There is a marked decrease in number of myofibroblasts in the infarct region in 2Rx and 3Rx groups (B). There is a significant direct correlation between the extent of myofibroblasts and the CRIP uptake in infarct region (C). For full color images, see page 175.

tion fraction,[65, 164] as well as those predisposed to development of heart failure but normal LV ejection fraction.[163,169] It is also established that anti-angiotensin agents in combination are superior to any agent used alone. The combination of ACE-I with ARB in the presence of beta blockers ± aldosterone inhibitors reduces the combined endpoint of mortality[16] and hospitalization for worsening of heart failure.[63] The experimental data from the present study confirm the superior effect of combination of two agents. However, addition of the third agent did not decrease the uptake significantly. It is encouraging to observe the efficacy of an imaging agent to identify difference in infarct healing, which could be of translational clinical benefit.

Is lack of collagen deposition favorable?

The present study raises an important question about the relevance of decrease in collagen deposition in the post-infarct patients. Total abolition of collagen deposition, which has been evaluated in clodronate liposome treated animals (wherein infarct healing becomes defective with minimal collagen deposition and inefficient necrotic myocyte removal),[170] leads to higher tendency of aneurysmal formation and infarct rupture. On the other hand, direct myocardial injection of collagen in experimental infarcts leads to dense collagen deposition and prevents myocardial remodeling.[171] Such experiments suggest that the collagen deposition may not necessarily be harmful. On the other hand, the use of ACE-I or SARA allow reduction of collagen deposition as demonstrated by circulating collagen degradation products.[168] The present study demonstrated a decrease in collagen deposition with suppression of angiotensin-aldosterone axis. Since neurohumoral antagonists lead to favorable clinical outcomes, conceivably reduced collagen deposition should be of benefit. Although the present study is not capable of explaining these paradoxical observations, it is possible that predominant decrease of collagen content observed in the remote myocardium in the present study, and the collagen fiber maturation (to thick fibers) observed in the infarct region may contribute to a more balanced healing.

Conclusions: The present study demonstrates that CRIP imaging allows for the evaluation of the efficacy of anti-remodeling therapy. It also reconfirms the superiority of combination therapy over a solitary use of neurohumoral antagonists. If proven clinically, molecular imaging of the remodeling processes could facilitate individualizing the treatment for patients susceptible to heart failure.

Acknowledgments

The imaging agents (CRIP and sCRIP) were kindly provided by GE healthcare, and Losartan was a kind gift of Merck & Co.

Susanne van den Borne was partially supported by a grant from the Netherlands Heart Foundation (2006R013).

General Discussion

GENERAL DISCUSSION AND CONCLUSIONS

Myocardial infarction is a frequent cardiovascular event in the Western world. Due to improved clinical management, acute mortality post-MI has been reduced and more patients enter the phase of cardiac wound healing. In this thesis we investigated myocardial infarct healing and focused on complications of the wound healing process, in particular infarct rupture and heart failure due to dilatation.

Infarct rupture

The results of mouse studies suggest that excessive degradation of the extracellular matrix in the infarct area can lead to infarct rupture, since targeted deletion of matrix metalloproteinases (MMP)-2[24,83] or MMP-9[23] reduces the incidence of infarct rupture post-MI, while overexpression of tissue inhibitor of metalloproteinase-1 (TIMP-1) has been shown to protect against infarct rupture.[23] The role of defective intercellular adhesion complexes has also been implicated, as an increased incidence of infarct rupture has been reported in mice lacking the αE-catenin gene.[25] However, molecular mechanisms involved in infarct rupture in humans have not been described so far. We hypothesized that cell adhesion molecules, especially αE-catenin, and upregulation of MMP's are also involved in the process of infarct rupture in humans.

In the studies described in chapter 4 and 5 we investigated the levels of MMP-2, -8 and -9, TIMP-1 and αE-catenin in cardiac tissue samples from patients who died of infarct rupture post-MI. We found significantly elevated total and active levels of MMP-8 and MMP-9 secondary to an augmented inflammatory response in these tissue samples compared to matched non-ruptured control MI samples (chapter 4). Furthermore, we observed a reduced expression and defective localization of αE-catenin in the intercalated disks of uninjured cardiomyocytes in the same infarct rupture patients (chapter 5). These results could be mimicked in an animal model with reduced αE-catenin expression, where three-fourths of the heterozygous αE-catenin C-terminal truncated mice died of infarct rupture, compared to one-fourth of the wildtype littermates. These results suggest that weakened cardiomyocyte adhesion, due to reduced expression and mislocalization of αE-catenin, facilitates increased inflammatory cell infiltration. Based on the results in mice and men, our working model is that the increased inflammatory cell influx, resulting from a defective cell adhesion complex, and the subsequent upregulation and activation of MMP-8 and -9 affect the integrity of the extracellular matrix, thereby facilitating infarct rupture. This working model is depicted in Figure 8.1.

In chapter 3 we studied the effect of genetic background on wound healing post-MI. In this extensive experimental study, examining five different mouse

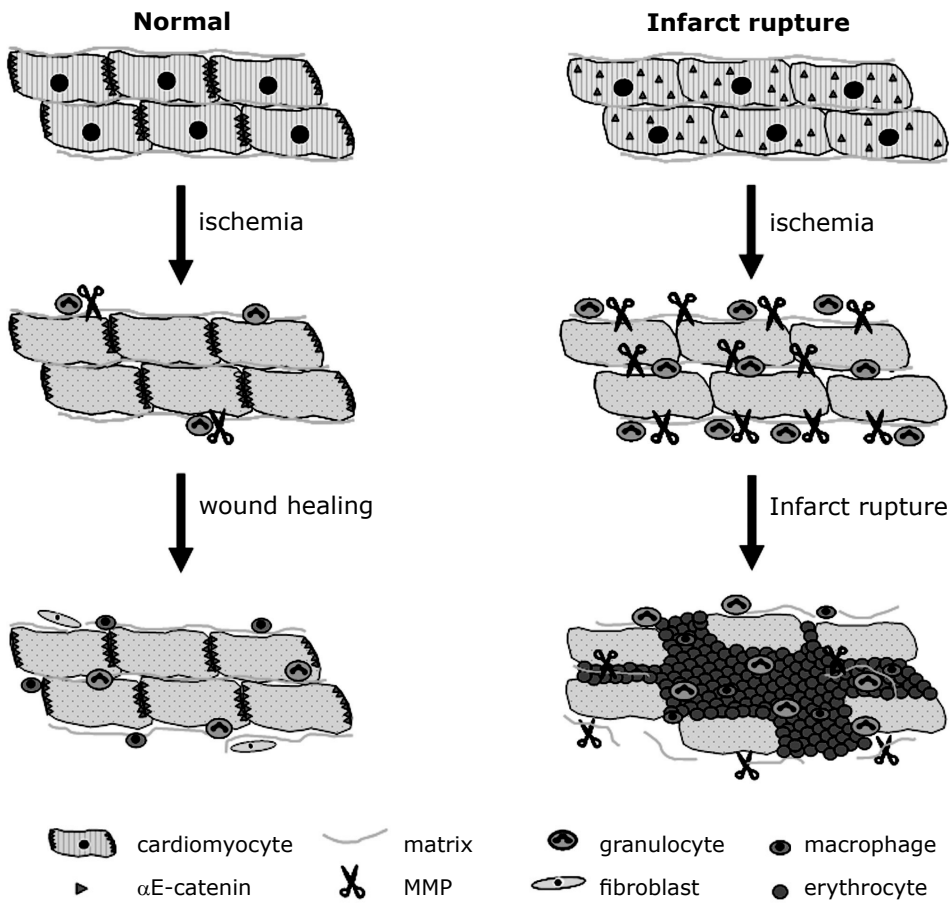

Figure 8.1 **Cartoon of molecular mechanisms that can lead to infarct rupture in humans**

In the left part of the cartoon, the wound healing post-MI in patients with normal infarct healing is shown whereas the right part of the cartoon focuses on the defective wound healing as proposed in infarct rupture patients. In the uninjured cardiomyocytes of normal hearts, αE-catenin is localized in the intercalated disks. Ischemia induces death of the cardiomyocytes in the infarct area, as shown by the loss of their nuclei. However, apparently the adhering cardiomyocytes still can form an effective barrier against inflammatory cells and ventricular blood. In the normal heart, the wound healing will commence and granulation tissue will replace the dead cardiomyocytes, taking over the barrier function against the ventricular blood. In the rupture-prone heart, however, αE-catenin is reduced and poorly localized in the intercalated disks of the cardiomyocytes. After ischemia, this abnormal cell adhesion complex causes the dead cardiomyocytes in the infarct area to loosen up their connections, giving access to more inflammatory cells. The MMPs deposited by these inflammatory cells induce extensive degradation of the extracellular matrix in the infarct area, causing further deterioration of the integrity of the infarct area and subsequently leading to infarct rupture. For full color image, see page 176.

strains, it became clear that infarct rupture frequency in mice is highly dependent on genetic background. Infarct rupture occurred in 62% of 129S6 mouse, whereas only 5% of BalbC mice died of infarct rupture. The high incidence of infarct rupture was associated with high systolic blood pressure and an increased influx of inflammatory cells. However, although MMP-9 was slightly increased at day 3 post-MI, there were no significant differences in MMP-levels between the five mouse strains. A possible explanation could be the timing of tissue collection. At day three of the experiment, when we measured MMP-activity, none of the mice had ruptured, suggesting that MMP activity had not yet fully developed. Furthermore, as only 62% of these mice develop infarct rupture, this further reduces the average MMP level in this group.

Heart failure

Ischemic heart disease is the leading cause of chronic heart failure in the Western world.[27] After MI, the heart undergoes a complex process of structural and molecular remodeling, which is beneficial at first, and contributes to the maintenance of the cardiac output. However, the remodeling can become deleterious, marked by ventricular dilatation, infarct wall thinning, replacement and interstitial fibrosis with a corresponding progressive impairment of the contractile function, leading to heart failure.[30] About 22% of male and 46% of female patients suffering from MI will develop heart failure within 6 years.[27] The prevalence of heart failure is similar in black and white males; however, in black women the prevalence of heart failure is higher than in white women and it is even higher than in males.[27] This suggests the involvement of genetic and gender factors in human heart failure. It is of paramount importance to detect patients at risk of heart failure as soon as possible in order to start optimal treatment and decrease the risk of clinical symptoms of heart failure. We hypothesized that molecular imaging is a tool to study heart failure development and the effects of heart failure treatment post-MI in order to prevent the clinical syndrome of heart failure.

As the genetic background turned out to be an important determinant of cardiac dilatation and heart failure, we studied the development of heart failure post-MI in five different mouse strains in chapter 3. Cardiac dilatation was most marked in Swiss mice and was associated with reduced ejection fraction and cardiac contractility. Furthermore, these mice showed secondary dilatation of the infarct area between 14 and 28 days post-MI, which was paralleled by a low number of myofibroblasts in the infarct area at day 14 post-MI. Myofibroblasts are important in wound healing post-MI, depositing replacement collagen in the infarct area to create a strong scar and can be anticipated to prevent secondary dilatation by their contractile properties. However, post-MI there are also changes in the remote zone, far away from the infarct. Interstitial fibrosis deposited in the remote zone increases mechanical stiffness and contributes to diastolic and

systolic dysfunction.[34] In this respect we hypothesize that the cardiac myofibroblast, and consequently fibrotic remodeling, is a predictive marker for heart failure, which makes it a suitable candidate for molecular imaging. Hence, in chapter 6 we evaluated interstitial alterations in myocardial remodeling in the mouse using a radiolabeled Cy5.5-RGD imaging peptide (CRIP) that targets the myofibroblasts. The maximum uptake was observed at 2 weeks post-MI in the infarct region and it decreased gradually by week 12; uptake in the remote areas only exceeded baseline values at 12 weeks. The uptake was histologically traced to the myofibroblasts. This study demonstrated the feasibility of noninvasive imaging of interstitial changes during cardiac remodeling.

In chapter 7 we used the same technique to asses the efficacy of anti-angiotensin and anti-mineralocorticoid intervention. Myofibroblasts express AT1 receptors and it is known that activation of the endogenous RAAS system in the myocardium results in cardiac fibroblast proliferation and fibrosis.[34] Indeed, we found that radiolabeled CRIP allows evaluation of the efficacy of neurohumoral antagonists in cardiac remodeling post-MI and that it is sensitive enough to detect therapy-induced alterations in the cardiac interstitium. We also reconfirmed the superiority of combination therapy: clinical trials have shown that ACE inhibitors with ARB's or aldosterone antagonists improve the outcome in survivors post-MI.[63, 168] CRIP imaging offers a novel tool for assessing efficacy of heart failure therapy, allowing individualized monitoring and optimization of pharmacotherapy.

Outlook

Molecular imaging is a rapidly developing technique that aims to visualize biological and physiological processes of disease in a repetitive and non-invasive way. After unraveling the molecular pathway of infarct rupture in humans, one can imagine the advantage of molecular imaging in detecting patients post-MI who are at risk of infarct rupture. It can be speculated that αE-catenin would be a good marker to detect patients at risk of infarct rupture, since the decreased expression and mislocalization is likely to be present even before the onset of ischemia. However, αE-catenin is present inside the cell which makes it technically harder to detect. Furthermore, infarct rupture patients still do have αE-catenin, albeit at lower levels. Whether molecular imaging techniques will be sensitive enough to detect the decrease in αE-catenin remains to be determined. If so, patients admitted with a transmural MI can be screened immediately post-MI for lower αE-catenin levels or mislocalization. Other possible targets will be MMP's or inflammatory cells. In a mouse model, MMP-2 and -9 has already been imaged using a near-infrared fluorescent probe[172] or a ^{99m}Tc-labeled MMP-probe,[173] indicating that MMP targeting post-MI is feasible. However, imaging MMP activity may be too late in the process since increased activated MMP's already lead to rupture. Therefore, imaging inflammatory cells is a more logical approach. This

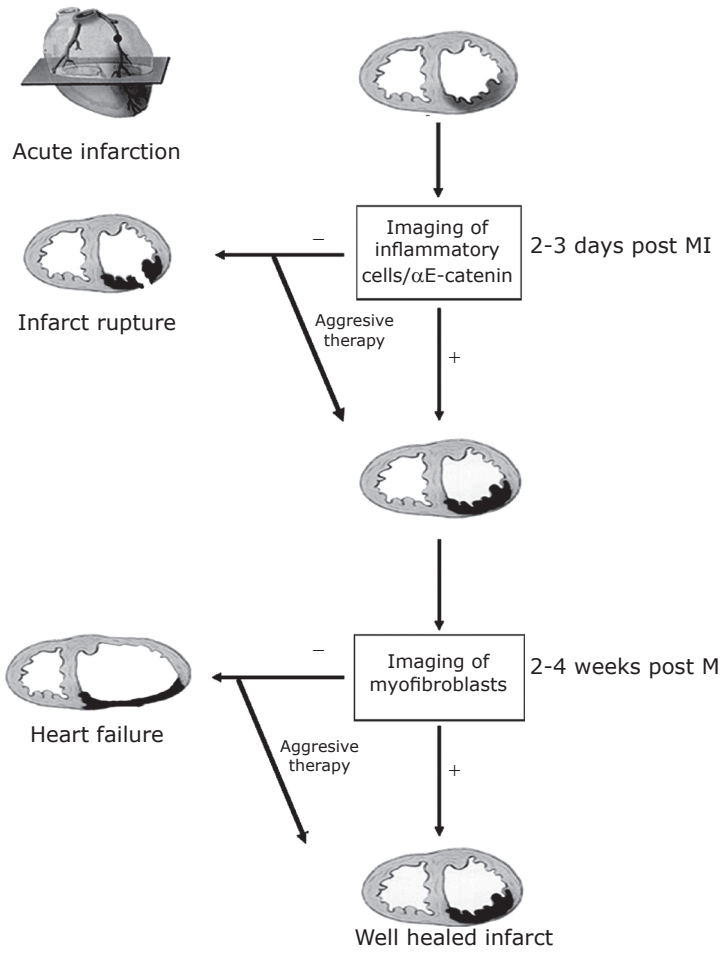

Figure 8.2 **Implementation of molecular imaging strategies in the clinical management of MI patients**

After 2-3 days post-MI polymorphonuclear leukocytes infiltrate the infarcted area. At this time, when the infarct wall is at its weakest, the infarct area may rupture, often leading to sudden death. Imaging inflammatory cells or αE-catenin at this time would allow identification of patients at risk of infarct rupture, as indicated by (-) in the cartoon. Timely identification will allow administration of aggressive therapy in order to prevent infarct rupture. When low levels of inflammatory cells or high αE-catenin levels are detected the risk of infarct rupture is low as indicated by (+) in the cartoon. In the hearts that do not rupture, there is matrix remodeling and granulation tissue formation that by 3 weeks includes removal of necrotic debris, mononuclear cell infiltration, increased numbers of myofibroblasts and capillaries, and an increase in collagen deposition. Imaging the myofibroblasts at this time point would identify patients at risk of developing heart failure post-MI, as indicated by the (-) in the cartoon. Aggressive treatment at an early phase may prevent heart failure development and lead to a well healed infarct. Patients with sufficient myofibroblasts in the infarct area, as indicated by (+) in the cartoon have a low risk of heart failure and are likely to develop a well healed scar. Figure adapted from: E. Creemers and J. Cleutjens.

can be accomplished by imaging of for instance myeloperoxidase activity by MRI. Myeloperoxidase is produced by inflammatory cells and can serve as a surrogate marker for the extent of tissue inflammation in myocardial infarction.[174] Screening patients with a transmural MI for an increased inflammatory response would allow identification of patients at risk of infarct rupture. These patients can be treated with aggressive β-blockade to decrease the cardiac work load or even be sedated for the first 10 days post-MI. During that time granulation tissue can form and the risk of rupture is reduced (See Figure 8.2).

For heart failure it is a different story. The impact of heart failure, both in patient burden and cost of medical treatment, is very high. The estimated direct and indirect cost of heart failure in the United States for 2008 is 34.8 billion dollars.[27] In the Netherlands the yearly costs for heart failure patients are between 136 and 455 million euro's.[175] As a result of the increasing number of survivors post-MI, hence increasing incidence of heart failure, and the lack of a cure for this condition, it is of utmost importance to detect patients at risk of heart failure before the disease becomes clinically manifest. In that way they can be treated optimally in order to prevent symptomatic heart failure (See Figure 8.2).

Although BNP and Galactin-3 are good markers for heart failure, they are measured in plasma rather than directly in the heart. Furthermore, we would like to detect the risk of heart failure as early as possible, preferably before plasma BNP and Galactin-3 plasma levels are elevated. Our pre-clinical studies showed a potential value of CRIP in its ability to non-invasively localize the site of interstitial alterations and collagen formation in the myocardium, and therefore may provide information about the evolution of heart failure. Furthermore it allowed the evaluation of the efficacy of anti-remodeling therapy. If corroborated clinically, molecular imaging of remodeling processes could detect patients at risk for heart failure at an early stage and could facilitate individualizing the treatment for patients susceptible for heart failure. A clinical pilot study with a radiolabeled RGD peptide in patients 3 and 8 weeks post-MI has shown the feasibility of imaging interstitial alterations. In these patients, 1-year follow-up magnetic resonance imaging confirmed the extent of fibrosis detected in the early stage by radiolabeled RGD peptide.[155]

In conclusion, alterations in the cadherin/catenin cell adhesion complex may lead to weakened cardiomyocyte adhesion, allowing excessive inflammatory cell infiltration and subsequent MMP activation, which is presented as a novel molecular mechanism for infarct rupture post-MI in humans. These observations provide novel insights to develop diagnostic tools for infarct rupture. Furthermore, the feasibility of myofibroblast imaging may serve as an early marker for heart failure development. If proven clinically, this molecular imaging technique

of the myocardial infarct healing process may identify patients at risk for heart failure at an early stage and may help plan an optimal treatment regimen for patients susceptible for heart failure.

9

References

Summary

Samenvatting

Full Color Illustrations

REFERENCES

1. Murray CJ, Lopez AD. Mortality by cause for eight regions of the world: Global Burden of Disease Study. Lancet 1997;349:1269-76.
2. Cleutjens JP. The role of matrix metalloproteinases in heart disease Cardiovasc Res 1996;32:816-21.
3. Cleutjens JP, Blankesteijn WM, Daemen MJ, Smits JF. The infarcted myocardium: simply dead tissue, or a lively target for therapeutic interventions. Cardiovasc Res 1999;44:232-41.
4. Volders PG, Willems IE, Cleutjens JP, Arends JW, Havenith MG, Daemen MJ. Interstitial collagen is increased in the non-infarcted human myocardium after myocardial infarction. J Mol Cell Cardiol 1993;25:1317-23.
5. Antman EM, Braunwald E. Acute myocardial infarction. In: Heart disease, a textbook of cardiovascular medicine. Braunwald E, editor. Philadelphia: WB Saunders Company; 2001. p. 1114-231.
6. Soonpaa MH, Daud AI, Koh GY, et al. Potential approaches for myocardial regeneration. Ann N Y Acad Sci 1995;752:446-54.
7. Haunstetter A, Izumo S. Apoptosis: basic mechanisms and implications for cardiovascular disease. Circ Res 1998;82:1111-29.
8. Lagrand WK, Niessen HW, Wolbink GJ, et al. C-reactive protein colocalizes with complement in human hearts during acute myocardial infarction. Circulation 1997;95:97-103.
9. Matsumori A, Furukawa Y, Hashimoto T, et al. Plasma levels of the monocyte chemotactic and activating factor/monocyte chemoattractant protein-1 are elevated in patients with acute myocardial infarction. J Mol Cell Cardiol 1997;29:419-23.
10. Sturk A, Hack CE, Aarden LA, Brouwer M, Koster RR, Sanders GT. Interleukin-6 release and the acute-phase reaction in patients with acute myocardial infarction: a pilot study. J Lab Clin Med 1992;119:574-9.
11. Cleutjens JP, Kandala JC, Guarda E, Guntaka RV, Weber KT. Regulation of collagen degradation in the rat myocardium after infarction. J Mol Cell Cardiol 1995;27:1281-92.
12. Tyagi SC, Campbell SE, Reddy HK, Tjahja E, Voelker DJ. Matrix metalloproteinase activity expression in infarcted, noninfarcted and dilated cardiomyopathic human hearts. Mol Cell Biochem 1996;155:13-21.
13. Willems IE, Havenith MG, De Mey JG, Daemen MJ. The alpha-smooth muscle actin-positive cells in healing human myocardial scars. Am J Pathol 1994;145:868-75.
14. Willems IE, Arends JW, Daemen MJ. Tenascin and fibronectin expression in healing human myocardial scars. J Pathol 1996;179:321-5.
15. Bishop JE, Laurent GJ. Collagen turnover and its regulation in the normal and hypertrophying heart. Eur Heart J 1995;16 Suppl C:38-44.
16. Chien KR. Stress pathways and heart failure. Cell 1999;98:555-8.
17. Olivetti G, Melissari M, Balbi T, Quaini F, Sonnenblick EH, Anversa P. Myocyte nuclear and possible cellular hyperplasia contribute to ventricular remodeling in the hypertrophic senescent heart in humans. J Am Coll Cardiol 1994;24:140-9.
18. Brilla CG, Janicki JS, Weber KT. Impaired diastolic function and coronary reserve in genetic hypertension. Role of interstitial fibrosis and medial thickening of intramyocardial coronary arteries. Circ Res 1991;69:107-15.

19. Wehrens XH, Doevendans PA. Cardiac rupture complicating myocardial infarction. Int J Cardiol 2004;95:285-92.
20. Birnbaum Y, Chamoun AJ, Anzuini A, Lick SD, Ahmad M, Uretsky BF. Ventricular free wall rupture following acute myocardial infarction. Coron Artery Dis 2003;14:463-70.
21. Batts KP, Ackermann DM, Edwards WD. Postinfarction rupture of the left ventricular free wall: clinicopathologic correlates in 100 consecutive autopsy cases. Hum Pathol 1990;21:530-5.
22. Creemers E, Cleutjens J, Smits J, et al. Disruption of the plasminogen gene in mice abolishes wound healing after myocardial infarction. Am J Pathol 2000;156:1865-73.
23. Heymans S, Luttun A, Nuyens D, et al. Inhibition of plasminogen activators or matrix metalloproteinases prevents cardiac rupture but impairs therapeutic angiogenesis and causes cardiac failure. Nat Med 1999;5:1135-42.
24. Hayashidani S, Tsutsui H, Ikeuchi M, et al. Targeted deletion of MMP-2 attenuates early LV rupture and late remodeling after experimental myocardial infarction. Am J Physiol Heart Circ Physiol 2003;285:H1229-35.
25. Sheikh F, Chen Y, Liang X, et al. alpha-E-catenin inactivation disrupts the cardiomyocyte adherens junction, resulting in cardiomyopathy and susceptibility to wall rupture. Circulation 2006;114:1046-55.
26. Katz AM. The cardiomyopathy of overload: an unnatural growth response. Eur Heart J 1995;16 Suppl O:110-4.
27. Rosamond W, Flegal K, Furie K, et al. Heart disease and stroke statistics--2008 update: a report from the American Heart Association Statistics Committee and Stroke Statistics Subcommittee. Circulation 2008;117:e25-146.
28. Weisman HF, Bush DE, Mannisi JA, Weisfeldt ML, Healy B. Cellular mechanisms of myocardial infarct expansion. Circulation 1988;78:186-201.
29. Gaasch WH. Diagnosis and treatment of heart failure based on left ventricular systolic or diastolic dysfunction. Jama 1994;271:1276-80.
30. Pfeffer MA, Braunwald E. Ventricular remodeling after myocardial infarction. Experimental observations and clinical implications. Circulation 1990;81:1161-72.
31. Weissleder R, Mahmood U. Molecular imaging. Radiology 2001;219:316-33.
32. Opie LH, Commerford PJ, Gersh BJ, Pfeffer MA. Controversies in ventricular remodelling. Lancet 2006;367:356-67.
33. Schocken DD, Benjamin EJ, Fonarow GC, et al. Prevention of heart failure: a scientific statement from the American Heart Association Councils on Epidemiology and Prevention, Clinical Cardiology, Cardiovascular Nursing, and High Blood Pressure Research; Quality of Care and Outcomes Research Interdisciplinary Working Group; and Functional Genomics and Translational Biology Interdisciplinary Working Group. Circulation 2008;117:2544-65.
34. Brown RD, Ambler SK, Mitchell MD, Long CS. The cardiac fibroblast: therapeutic target in myocardial remodeling and failure. Annu Rev Pharmacol Toxicol 2005;45:657-87.
35. Wynn TA. Cellular and molecular mechanisms of fibrosis. J Pathol 2008;214:199-210.
36. Kalluri R, Neilson EG. Epithelial-mesenchymal transition and its implications for fibrosis. J Clin Invest 2003;112:1776-84.
37. Zeisberg EM, Tarnavski O, Zeisberg M, et al. Endothelial-to-mesenchymal transition contributes to cardiac fibrosis. Nat Med 2007;13:952-61.

38. Bucala R, Spiegel LA, Chesney J, Hogan M, Cerami A. Circulating fibrocytes define a new leukocyte subpopulation that mediates tissue repair. Mol Med 1994;1:71-81.
39. Tomasek JJ, Gabbiani G, Hinz B, Chaponnier C, Brown RA. Myofibroblasts and mechano-regulation of connective tissue remodelling. Nat Rev Mol Cell Biol 2002;3:349-63.
40. Squires CE, Escobar GP, Payne JF, et al. Altered fibroblast function following myocardial infarction. J Mol Cell Cardiol 2005;39:699-707.
41. Hinz B, Gabbiani G. Mechanisms of force generation and transmission by myofibroblasts. Curr Opin Biotechnol 2003;14:538-46.
42. Serini G, Bochaton-Piallat ML, Ropraz P, et al. The fibronectin domain ED-A is crucial for myofibroblastic phenotype induction by transforming growth factor-beta1. J Cell Biol 1998;142:873-81.
43. Wang J, Chen H, Seth A, McCulloch CA. Mechanical force regulation of myofibroblast differentiation in cardiac fibroblasts. Am J Physiol Heart Circ Physiol 2003;285:H1871-81.
44. Gabbiani G. The myofibroblast in wound healing and fibrocontractive diseases. J Pathol 2003;200:500-3.
45. Virag JI, Murry CE. Myofibroblast and endothelial cell proliferation during murine myocardial infarct repair. Am J Pathol 2003;163:2433-40.
46. Foo IT, Naylor IL, Timmons MJ, Trejdosiewicz LK. Intracellular actin as a marker for myofibroblasts in vitro. Lab Invest 1992;67:727-33.
47. Muro AF, Chauhan AK, Gajovic S, et al. Regulated splicing of the fibronectin EDA exon is essential for proper skin wound healing and normal lifespan. J Cell Biol 2003;162:149-60.
48. Hinz B, Phan SH, Thannickal VJ, Galli A, Bochaton-Piallat ML, Gabbiani G. The myofibroblast: one function, multiple origins. Am J Pathol 2007;170:1807-16.
49. Gabbiani G, Hirschel BJ, Ryan GB, Statkov PR, Majno G. Granulation tissue as a contractile organ. A study of structure and function. J Exp Med 1972;135:719-34.
50. Desmouliere A, Redard M, Darby I, Gabbiani G. Apoptosis mediates the decrease in cellularity during the transition between granulation tissue and scar. Am J Pathol 1995;146:56-66.
51. Sun Y, Kiani MF, Postlethwaite AE, Weber KT. Infarct scar as living tissue. Basic Res Cardiol 2002;97:343-7.
52. Beltrami CA, Finato N, Rocco M, et al. Structural basis of end-stage failure in ischemic cardiomyopathy in humans. Circulation 1994;89:151-63.
53. Eyden B. The myofibroblast: a study of normal, reactive and neoplastic tissues, with an emphasis on ultrastructure. J Submicrosc Cytol Pathol 2007:7-166.
54. Blankesteijn WM, Essers-Janssen YP, Verluyten MJ, Daemen MJ, Smits JF. A homologue of Drosophila tissue polarity gene frizzled is expressed in migrating myofibroblasts in the infarcted rat heart. Nat Med 1997;3:541-4.
55. Rosenkranz S, Flesch M, Amann K, et al. Alterations of beta-adrenergic signaling and cardiac hypertrophy in transgenic mice overexpressing TGF-beta(1). Am J Physiol Heart Circ Physiol 2002;283:H1253-62.
56. Hinz B. Masters and servants of the force: the role of matrix adhesions in myofibroblast force perception and transmission. Eur J Cell Biol 2006;85:175-81.
57. Smith-Mungo LI, Kagan HM. Lysyl oxidase: properties, regulation and multiple functions in biology. Matrix Biol 1998;16:387-98.

58. Hong HH, Uzel MI, Duan C, Sheff MC, Trackman PC. Regulation of lysyl oxidase, collagen, and connective tissue growth factor by TGF-beta1 and detection in human gingiva. Lab Invest 1999;79:1655-67.
59. Weber KT. Extracellular matrix remodeling in heart failure: a role for de novo angiotensin II generation. Circulation 1997;96:4065-82.
60. Harada K, Sugaya T, Murakami K, Yazaki Y, Komuro I. Angiotensin II type 1A receptor knockout mice display less left ventricular remodeling and improved survival after myocardial infarction. Circulation 1999;100:2093-9.
61. Pfeffer MA, Swedberg K, Granger CB, et al. Effects of candesartan on mortality and morbidity in patients with chronic heart failure: the CHARM-Overall programme. Lancet 2003;362:759-66.
62. Pitt B, Poole-Wilson PA, Segal R, et al. Effect of losartan compared with captopril on mortality in patients with symptomatic heart failure: randomised trial--the Losartan Heart Failure Survival Study ELITE II. Lancet 2000;355:1582-7.
63. Cohn JN, Tognoni G. A randomized trial of the angiotensin-receptor blocker valsartan in chronic heart failure. N Engl J Med 2001;345:1667-75.
64. Effects of enalapril on mortality in severe congestive heart failure. Results of the Cooperative North Scandinavian Enalapril Survival Study (CONSENSUS). The CONSENSUS Trial Study Group. N Engl J Med 1987;316:1429-35.
65. Effect of enalapril on survival in patients with reduced left ventricular ejection fractions and congestive heart failure. The SOLVD Investigators. N Engl J Med 1991;325:293-302.
66. Verjans JWH, Lovhaug D, Narula N, et al. Noninvasive imaging of angiotensin receptores after myocardial infarction. J Am Coll Cardiol- Cardiovascular imaging 2008;1:354-62.
67. Hunt SA. ACC/AHA 2005 guideline update for the diagnosis and management of chronic heart failure in the adult: a report of the American College of Cardiology/American Heart Association Task Force on Practice Guidelines (Writing Committee to Update the 2001 Guidelines for the Evaluation and Management of Heart Failure). J Am Coll Cardiol 2005;46:e1-82.
68. Szabo Z, Speth RC, Brown PR, et al. Use of positron emission tomography to study AT1 receptor regulation in vivo. J Am Soc Nephrol 2001;12:1350-8.
69. Dilsizian V, Eckelman WC, Loredo ML, Jagoda EM, Shirani J. Evidence for tissue angiotensin-converting enzyme in explanted hearts of ischemic cardiomyopathy using targeted radiotracer technique. J Nucl Med 2007;48:182-7.
70. Asano Y, Ihn H, Yamane K, Jinnin M, Mimura Y, Tamaki K. Increased expression of integrin alpha(v) beta3 contributes to the establishment of autocrine TGF-beta signaling in scleroderma fibroblasts. J Immunol 2005;175:7708-18.
71. van den Borne SW, Isobe S, Verjans JW, Petrov A, Lovhaug D, Li P, et al. Molecular Imaging of interstitial alterations in remodeling myocardium after myocardial infarction. J Am Coll Cardiol. 2008;51:2184-92.
72. Verjans JW, Wolters SL, Lax M, et al. Imaging αvβ3/β5 Integrin Upregulation In Patients After Myocardial Infarction. Circulation 2007;116-II:3288.
73. van den Borne SW, Cleutjens JP, Hanemaaijer R, et al. Increased matrix metalloproteinase-8 and -9 activity in patients with infarct rupture after myocardial infarction. Cardiovasc Pathol 2009; 18:37-43.
74. Linder CC. Genetic variables that influence phenotype. Ilar J 2006;47:132-40.

75. Hoover-Plow J, Shchurin A, Hart E, et al. Genetic background determines response to hemostasis and thrombosis. BMC Blood Disord 2006;6:6.
76. Majid A, He YY, Gidday JM, et al. Differences in vulnerability to permanent focal cerebral ischemia among 3 common mouse strains. Stroke 2000;31:2707-14.
77. Gao XM, Xu Q, Kiriazis H, Dart AM, Du XJ. Mouse model of post-infarct ventricular rupture: time course, strain- and gender-dependency, tensile strength, and histopathology. Cardiovasc Res 2005;65:469-77.
78. Lutgens E, Daemen MJ, de Muinck ED, Debets J, Leenders P, Smits JF. Chronic myocardial infarction in the mouse: cardiac structural and functional changes. Cardiovasc Res 1999;41:586-93.
79. Laemmli UK. Cleavage of structural proteins during the assembly of the head of bacteriophage T4. Nature 1970;227:680-5.
80. Tyagi SC, Matsubara L, Weber KT. Direct extraction and estimation of collagenase(s) activity by zymography in microquantities of rat myocardium and uterus. Clin Biochem 1993;26:191-8.
81. van de Schans VA, van den Borne SW, Strzelecka AE, et al. Interruption of Wnt signaling attenuates the onset of pressure overload-induced cardiac hypertrophy. Hypertension 2007;49:473-80.
82. Fang L, Gao XM, Moore XL, et al. Differences in inflammation, MMP activation and collagen damage account for gender difference in murine cardiac rupture following myocardial infarction. J Mol Cell Cardiol 2007;43:535-44.
83. Matsumura S, Iwanaga S, Mochizuki S, Okamoto H, Ogawa S, Okada Y. Targeted deletion or pharmacological inhibition of MMP-2 prevents cardiac rupture after myocardial infarction in mice. J Clin Invest 2005;115:599-609.
84. Tao ZY, Cavasin MA, Yang F, Liu YH, Yang XP. Temporal changes in matrix metalloproteinase expression and inflammatory response associated with cardiac rupture after myocardial infarction in mice. Life Sci 2004;74:1561-72.
85. McMurray JJ, Ostergren J, Swedberg K, et al. Effects of candesartan in patients with chronic heart failure and reduced left-ventricular systolic function taking angiotensin-converting-enzyme inhibitors: the CHARM-Added trial. Lancet 2003;362:767-71.
86. Dargie HJ. Effect of carvedilol on outcome after myocardial infarction in patients with left-ventricular dysfunction: the CAPRICORN randomised trial. Lancet 2001;357:1385-90.
87. Gerlai R. Gene-targeting studies of mammalian behavior: is it the mutation or the background genotype? Trends Neurosci 1996;19:177-81.
88. Du XJ. Gender modulates cardiac phenotype development in genetically modified mice. Cardiovasc Res 2004;63:510-9.
89. Cavasin MA, Tao Z, Menon S, Yang XP. Gender differences in cardiac function during early remodeling after acute myocardial infarction in mice. Life Sci 2004;75:2181-92.
90. Bujak M, Kweon HJ, Chatila K, Li N, Taffet G, Frangogiannis NG. Aging-related defects are associated with adverse cardiac remodeling in a mouse model of reperfused myocardial infarction. J Am Coll Cardiol 2008;51:1384-92.
91. Julian DG. Why do patients die after myocardial infarction? J Cardiovasc Pharmacol 1991;18:S80-2.
92. McMullan MH, Maples MD, Kilgore TL, Jr., Hindman SH. Surgical experience with left ventricular free wall rupture. Ann Thorac Surg 2001;71:1894-8; discussion 1898-9.
93. Pretre R, Benedikt P, Turina MI. Experience with postinfarction left ventricular free wall rupture. Ann Thorac Surg 2000;69:1342-5.

94. Reeder GS. Identification and treatment of complications of myocardial infarction. Mayo Clin Proc 1995;70:880-4.
95. Stout B, Ferrell L, Wray T, Mayes C. Myocardial rupture. Your patient's survival may depend on you. Postgrad Med 1991;90:115-22.
96. Antman EM, Braunwald E. Acute myocardial infarction. Heart disease, a textbook of cardiovascular medicine. In: Braunwald E, editor. Philadelphia: WB Saunders&Co;1997. p.1184-268.
97. Davis N, Sistino JJ. Review of ventricular rupture: key concepts and diagnostic tools for success. Perfusion 2002;17:63-7.
98. Olsen EGJ. Ischemic disease of the myocardium and its complications. In: Silver MD, editor. Cardiovascular Pathology. New York: Churchill Livingstone; 1983. p. 671-717.
99. Pasotti M, Prati F, Arbustini E. The pathology of myocardial infarction in the pre and post interventional era. Heart 2006;92(11):1552-6.
100. Creemers EE, Cleutjens JP, Smits JF, Daemen MJ. Matrix metalloproteinase inhibition after myocardial infarction: a new approach to prevent heart failure? Circ Res 2001;89:201-10.
101. Chapman RE, Scott AA, Deschamps AM, et al. Matrix metalloproteinase abundance in human myocardial fibroblasts: effects of sustained pharmacologic matrix metalloproteinase inhibition. J Mol Cell Cardiol 2003;35:539-48.
102. Hanemaaijer R, Visser H, Konttinen YT, Koolwijk P, Verheijen JH. A novel and simple immunocapture assay for determination of gelatinase-B (MMP-9) activities in biological fluids: saliva from patients with Sjogren's syndrome contain increased latent and active gelatinase-B levels. Matrix Biol 1998;17:657-65.
103. Creemers EE, Davis JN, Parkhurst AM, et al. Deficiency of TIMP-1 exacerbates LV remodeling after myocardial infarction in mice. Am J Physiol Heart Circ Physiol 2003;284:H364-71.
104. Van Lint P, Libert C. Matrix metalloproteinase-8: cleavage can be decisive. Cytokine Growth Factor Rev 2006;17:217-23.
105. Herman MP, Sukhova GK, Libby P, et al. Expression of neutrophil collagenase (matrix metalloproteinase-8) in human atheroma: a novel collagenolytic pathway suggested by transcriptional profiling. Circulation 2001;104:1899-904.
106. Kameda K, Matsunaga T, Abe N, et al. Increased pericardial fluid level of matrix metalloproteinase-9 activity in patients with acute myocardial infarction: possible role in the development of cardiac rupture. Circ J 2006;70:673-8.
107. Webb CS, Bonnema DD, Ahmed SH, et al. Specific temporal profile of matrix metalloproteinase release occurs in patients after myocardial infarction: relation to left ventricular remodeling. Circulation 2006;114:1020-7.
108. Bar-Or A, Nuttall RK, Duddy M, et al. Analyses of all matrix metalloproteinase members in leukocytes emphasize monocytes as major inflammatory mediators in multiple sclerosis. Brain 2003;126:2738-49.
109. Ardans JA, Economou AP, Martinson JM, Jr., Zhou M, Wahl LM. Oxidized low-density and high-density lipoproteins regulate the production of matrix metalloproteinase-1 and -9 by activated monocytes. J Leukoc Biol 2002;71:1012-8.
110. Saren P, Welgus HG, Kovanen PT. TNF-alpha and IL-1beta selectively induce expression of 92-kDa gelatinase by human macrophages. J Immunol 1996;157:4159-65.

111. Chromek M, Tullus K, Lundahl J, Brauner A. Tissue inhibitor of metalloproteinase 1 activates normal human granulocytes, protects them from apoptosis, and blocks their transmigration during inflammation. Infect Immun 2004;72:82-8.
112. Honan MB, Harrell FE, Jr., Reimer KA, et al. Cardiac rupture, mortality and the timing of thrombolytic therapy: a meta-analysis. J Am Coll Cardiol 1990;16:359-67.
113. Olsen EGJ. Ischemic disease of the myocardium and its complications. In: Silver MD, ed. Cardiovascular pathology. 2nd edition ed. New York: Churchill Livingstone, 1983:671-717.
114. Lilien J, Balsamo J. The regulation of cadherin-mediated adhesion by tyrosine phosphorylation/dephosphorylation of beta-catenin. Curr Opin Cell Biol 2005;17:459-65.
115. Hirohashi S, Kanai Y. Cell adhesion system and human cancer morphogenesis. Cancer Sci 2003;94:575-81.
116. Severs NJ. The cardiac gap junction and intercalated disc. Int J Cardiol 1990;26:137-73.
117. van den Borne SWM, Cleutjens JPM, Hanemaaijer R, et al. Increased MMP-8 and -9 activity in patients with infarct rupture after myocardial infarction. Cardiovasc Pathol accepted for publication.
118. Laemmli U. Cleavage of structural proteins during the assembly of the head of bacteriophage T4. Nature 1970;227:680-685.
119. Torres M, Stoykova A, Huber O, et al. An alpha-E-catenin gene trap mutation defines its function in preimplantation development. Proc Natl Acad Sci U S A 1997;94:901-6.
120. Burks J, Agazie YM. Modulation of alpha-catenin Tyr phosphorylation by SHP2 positively effects cell transformation induced by the constitutively active FGFR3. Oncogene 2006;25:7166-79.
121. Harris TJ, Peifer M. Decisions, decisions: beta-catenin chooses between adhesion and transcription. Trends Cell Biol 2005;15:234-7.
122. Brembeck FH, Schwarz-Romond T, Bakkers J, Wilhelm S, Hammerschmidt M, Birchmeier W. Essential role of BCL9-2 in the switch between beta-catenin's adhesive and transcriptional functions. Genes Dev 2004;18:2225-30.
123. Imamura Y, Itoh M, Maeno Y, Tsukita S, Nagafuchi A. Functional domains of alpha-catenin required for the strong state of cadherin-based cell adhesion. J Cell Biol 1999;144:1311-22.
124. Birnbaum Y, Fishbein MC, Blanche C, Siegel RJ. Ventricular septal rupture after acute myocardial infarction. N Engl J Med 2002;347:1426-32.
125. Thom T, Haase N, Rosamond W, et al. Heart disease and stroke statistics--2006 update: a report from the American Heart Association Statistics Committee and Stroke Statistics Subcommittee. Circulation 2006;113:e85-151.
126. Pfeffer JM, Pfeffer MA, Braunwald E. Influence of chronic captopril therapy on the infarcted left ventricle of the rat. Circ Res 1985;57:84-95.
127. Cleutjens JP, Blankesteijn WM, Daemen MJ, Smits JF. The infarcted myocardium: simply dead tissue, or a lively target for therapeutic interventions. Cardiovasc Res 1999;44:232-41.
128. Massie BM, Conway M. Survival of patients with congestive heart failure: past, present, and future prospects. Circulation 1987;75:IV11-9.
129. Gerdes AM, Capasso JM. Structural remodeling and mechanical dysfunction of cardiac myocytes in heart failure. J Mol Cell Cardiol 1995;27:849-56.
130. Francis GS, McDonald KM. Left ventricular hypertrophy: an initial response to myocardial injury. Am J Cardiol 1992;69:3G-7G; discussion 7G-9G.

131. Heeneman S, Cleutjens JP, Faber BC, et al. The dynamic extracellular matrix: intervention strategies during heart failure and atherosclerosis. J Pathol 2003;200:516-25.
132. Meoli DF, Sadeghi MM, Krassilnikova S, et al. Noninvasive imaging of myocardial angiogenesis following experimental myocardial infarction. J Clin Invest 2004;113:1684-91.
133. Schiller NB, Shah PM, Crawford M, et al. Recommendations for quantitation of the left ventricle by two-dimensional echocardiography. American Society of Echocardiography Committee on Standards, Subcommittee on Quantitation of Two-Dimensional Echocardiograms. J Am Soc Echocardiogr 1989;2:358-67.
134. Whittaker P, Kloner RA, Boughner DR, Pickering JG. Quantitative assessment of myocardial collagen with picrosirius red staining and circularly polarized light. Basic Res Cardiol 1994;89:397-410.
135. MacKenna DA, Omens JH, McCulloch AD, Covell JW. Contribution of collagen matrix to passive left ventricular mechanics in isolated rat hearts. Am J Physiol 1994;266:H1007-18.
136. Szendroi M, Vajta G, Kovacs L, Schaff Z, Lapis K. Polarization colours of collagen fibres: a sign of collagen production activity in fibrotic processes. Acta Morphol Hung 1984;32:47-55.
137. Andrade GB, Riet-Correa F, Montes GS, Battlehner CN, Saldiva PH. Dating of fibrotic lesions by the Picrosirius-polarization method. An application using the lesions of Lechiguana (bovine focal proliferative fibrogranulomatous panniculitis). Eur J Histochem 1997;41:203-9.
138. Liou W, Geuze HJ, Slot JW. Improving structural integrity of cryosections for immunogold labeling. Histochem Cell Biol 1996;106:41-58.
139. Zhou X, Jamil A, Nash A, et al. Impaired proteolysis of collagen I inhibits proliferation of hepatic stellate cells: implications for regulation of liver fibrosis. J Biol Chem 2006;281:39757-65.
140. Jugdutt BI, Amy RW. Healing after myocardial infarction in the dog: changes in infarct hydroxyproline and topography. J Am Coll Cardiol 1986;7:91-102.
141. Whittaker P, Boughner DR, Kloner RA. Role of collagen in acute myocardial infarct expansion. Circulation 1991;84:2123-34.
142. Pfeffer JM, Fischer TA, Pfeffer MA. Angiotensin-converting enzyme inhibition and ventricular remodeling after myocardial infarction. Annu Rev Physiol 1995;57:805-26.
143. Gray MO, Long CS, Kalinyak JE, Li HT, Karliner JS. Angiotensin II stimulates cardiac myocyte hypertrophy via paracrine release of TGF-beta 1 and endothelin-1 from fibroblasts. Cardiovasc Res 1998;40:352-63.
144. Sun Y, Weber KT. Infarct scar: a dynamic tissue. Cardiovasc Res 2000;46:250-6.
145. Schieffer B, Wirger A, Meybrunn M, et al. Comparative effects of chronic angiotensin-converting enzyme inhibition and angiotensin II type 1 receptor blockade on cardiac remodeling after myocardial infarction in the rat. Circulation 1994;89:2273-82.
146. Wollert KC, Drexler H. The kallikrein-kinin system in post-myocardial infarction cardiac remodeling. Am J Cardiol 1997;80:158A-161A.
147. Dickstein K, Kjekshus J. Effects of losartan and captopril on mortality and morbidity in high-risk patients after acute myocardial infarction: the OPTIMAAL randomised trial. Optimal Trial in Myocardial Infarction with Angiotensin II Antagonist Losartan. Lancet 2002;360:752-60.
148. Pfeffer MA, McMurray JJ, Velazquez EJ, et al. Valsartan, captopril, or both in myocardial infarction complicated by heart failure, left ventricular dysfunction, or both. N Engl J Med 2003;349:1893-906.

149. White HD, Braunwald E. Applying the open artery theory: use of predictive survival markers. Eur Heart J 1998;19:1132-9.
150. Poulsen SH, Host NB, Jensen SE, Egstrup K. Relationship between serum amino-terminal propeptide of type III procollagen and changes of left ventricular function after acute myocardial infarction. Circulation 2000;101:1527-32.
151. Radovan J, Vaclav P, Petr W, et al. Changes of collagen metabolism predict the left ventricular remodeling after myocardial infarction. Mol Cell Biochem 2006;293:71-8.
152. Zannad F, Radauceanu A. Effect of MR blockade on collagen formation and cardiovascular disease with a specific emphasis on heart failure. Heart Fail Rev 2005;10:71-8.
153. Cicoira M, Rossi A, Bonapace S, et al. Independent and additional prognostic value of aminoterminal propeptide of type III procollagen circulating levels in patients with chronic heart failure. J Card Fail 2004;10:403-11.
154. Kotaniemi A, Risteli J, Aho K, Hakala M. Increased type I collagen degradation correlates with disease activity in reactive arthritis. Clin Exp Rheumatol 2003;21:95-8.
155. Verjans JW, Wolters SL, Lax M, et al. Imaging avb3/b5 Integrin Upregulation in Patients After Myocardial Infarction. Circulation 2007;116-II:3288.
156. Weber KT, Brilla CG. Pathological hypertrophy and cardiac interstitium. Fibrosis and renin-angiotensin-aldosterone system. Circulation 1991;83:1849-65.
157. Weber KT, Anversa P, Armstrong PW, et al. Remodeling and reparation of the cardiovascular system. J Am Coll Cardiol 1992;20:3-16.
158. Pitt B. Aldosterone blockade in patients with systolic left ventricular dysfunction. Circulation 2003;108:1790-4.
159. Shirani J, Narula J, Eckelman WC, Narula N, Dilsizian V. Early imaging in heart failure: exploring novel molecular targets. J Nucl Cardiol 2007;14:100-10.
160. Anversa P, Capasso JM. Cardiac hypertrophy and ventricular remodeling. Lab Invest 1991;64:441-5.
161. Cohn JN, Johnson G, Ziesche S, et al. A comparison of enalapril with hydralazine-isosorbide dinitrate in the treatment of chronic congestive heart failure. N Engl J Med 1991;325:303-10.
162. Pitt B, Zannad F, Remme WJ, et al. The effect of spironolactone on morbidity and mortality in patients with severe heart failure. Randomized Aldactone Evaluation Study Investigators. N Engl J Med 1999;341:709-17.
163. Yusuf S, Sleight P, Pogue J, Bosch J, Davies R, Dagenais G. Effects of an angiotensin-converting-enzyme inhibitor, ramipril, on cardiovascular events in high-risk patients. The Heart Outcomes Prevention Evaluation Study Investigators. N Engl J Med 2000;342:145-53.
164. Pfeffer MA, Braunwald E, Moye LA, et al. Effect of captopril on mortality and morbidity in patients with left ventricular dysfunction after myocardial infarction. Results of the survival and ventricular enlargement trial. The SAVE Investigators. N Engl J Med 1992;327:669-77.
165. Pitt B, Remme W, Zannad F, et al. Eplerenone, a selective aldosterone blocker, in patients with left ventricular dysfunction after myocardial infarction. N Engl J Med 2003;348:1309-21.
166. McNamara DM, Holubkov R, Janosko K, et al. Pharmacogenetic interactions between beta-blocker therapy and the angiotensin-converting enzyme deletion polymorphism in patients with congestive heart failure. Circulation 2001;103:1644-8.

167. Small KM, Wagoner LE, Levin AM, Kardia SL, Liggett SB. Synergistic polymorphisms of beta1- and alpha2C-adrenergic receptors and the risk of congestive heart failure. N Engl J Med 2002;347:1135-42.
168. Zannad F, Alla F, Dousset B, Perez A, Pitt B. Limitation of excessive extracellular matrix turnover may contribute to survival benefit of spironolactone therapy in patients with congestive heart failure: insights from the randomized aldactone evaluation study (RALES). Rales Investigators. Circulation 2000;102:2700-6.
169. Yusuf S, Teo KK, Pogue J, et al. Telmisartan, ramipril, or both in patients at high risk for vascular events. N Engl J Med 2008;358:1547-59.
170. van Amerongen MJ, Harmsen MC, van Rooijen N, Petersen AH, van Luyn MJ. Macrophage depletion impairs wound healing and increases left ventricular remodeling after myocardial injury in mice. Am J Pathol 2007;170:818-29.
171. Dai W, Wold LE, Dow JS, Kloner RA. Thickening of the infarcted wall by collagen injection improves left ventricular function in rats: a novel approach to preserve cardiac function after myocardial infarction. J Am Coll Cardiol 2005;46:714-9.
172. Chen J, Tung CH, Allport JR, Chen S, Weissleder R, Huang PL. Near-infrared fluorescent imaging of matrix metalloproteinase activity after myocardial infarction. Circulation 2005;111:1800-5.
173. Su H, Spinale FG, Dobrucki LW, et al. Noninvasive targeted imaging of matrix metalloproteinase activation in a murine model of postinfarction remodeling. Circulation 2005;112:3157-67.
174. Nahrendorf M, Sosnovik D, Chen JW, et al. Activatable magnetic resonance imaging agent reports myeloperoxidase activity in healing infarcts and noninvasively detects the antiinflammatory effects of atorvastatin on ischemia-reperfusion injury. Circulation 2008;117:1153-60.
175. Reitsma JB, Mosterd A, Koek HL. Hart- en vaatziekten in Nederland 2002, cijfers over ziekte en sterfte. Nederlandse Hartstichting 2002;november.

9

SUMMARY

The process of myocardial infarct healing is very complex and can lead to several complications. The present thesis focuses on two common complications of myocardial infarction, associated with the healing process. The first complication is infarct rupture, which occurs in the early phase post-MI, typically between 3-6 days after the infarction. It is a usually lethal complication of acute MI for which no adequate treatment is available. Risk factors for infarct rupture are a transmural infarction, first infarction and a poor collateral circulation. Animal experiments have shown a role for matrix metalloproteinases and cell adhesion proteins in the development of infarct rupture. However, molecular mechanisms involved in infarct rupture in humans have not been described so far. The first hypothesis of this thesis is that cell adhesion molecules, especially αE-catenin, and upregulation of MMP's are involved in the process of infarct rupture in humans.

The second complication related to wound healing post-MI is heart failure, a condition in which the heart is unable to provide sufficient cardiac output to meet the metabolic and oxygen demands of the peripheral tissues. Due to the advances in diagnosis and management of the acute phase of MI, the prevalence of patients with manifest heart failure increases. Most available treatment strategies alleviate the symptoms, but none of the current therapies is able to cure heart failure. Therefore the only rational therapy for heart failure is to prevent its development. This illustrates the utmost importance to develop strategies for early detection of individuals at risk to develop heart failure so that early prevention and treatment may be initiated. This leads to the second hypothesis of this thesis; molecular imaging is a tool to study the process of heart failure and the effects of heart failure treatment post-MI.

In **chapter 2** an overview is given of literature describing the process of myocardial infarct healing with a focus on the role of the myofibroblast. Furthermore, molecular targets in the myofibroblasts amenable to imaging are described as well as experimental studies attempting to image the myofibroblasts.

In **chapter 3** we studied infarct healing post-MI in different mouse strains that are frequently used in cardiovascular research, in order to study the effect of the genetic background on the outcome of these studies. In five different mouse strains (BalbC, C57Bl6, FVB, 129S6 and Swiss) myocardial infarction was induced and infarct healing was studied. Infarct rupture, typically occurring at 3-6 days post-MI, was most frequent in 129S6 mice (62%), followed by C57Bl6 (36%), FVB (29%), Swiss (23%) and BalbC (5%). The high incidence of infarct rupture in 129S6 mice correlated with elevated systolic blood pressure and an increased influx of inflammatory cells at day 3 post-MI. Acute heart failure was

observed in 28% of FVB mice in the first week post-MI, but was rare in other groups. Cardiac dilatation was most marked in Swiss mice with a more than 3-fold increase in end-systolic volume compared to sham, and was least prominent in 129S6 mice. The dilatation correlated with decreased hemodynamic measurements and a decreased ejection fraction. Secondary thinning of the infarct area between day 14 and 28 was significant in BalbC, FVB and Swiss, but absent in C57Bl6 and 129S6. We concluded that the outcome of infarct healing in mice is strongly dependent on genetic background. Therefore, results from studies on pharmacological or genetic interventions in which different mouse strains were used should be compared with caution. The results of the present study allowed us to provide guidelines for the choice of a mouse strain that is most suitable to study a certain aspect of infarct healing.

Since it is known from literature that matrix metalloproteinases (MMP's) play an important role in the development of infarct rupture post-MI in mice, we studied the role of these MMPs in post mortem heart samples of patients who died of infarct rupture post-MI (**chapter 4**). We observed an increased MMP-8 and MMP-9 activity in the infarct area, probably caused by a more prominent infiltration of inflammatory cells in the border zone of the infarct, which is likely to contribute to infarct rupture in humans.

Furthermore, we studied the role of cellular adhesion proteins in post-mortem heart samples of patients who died of infarct rupture post-MI (**chapter 5**). We observed a reduced expression and defective localization of αE-catenin in the intercalated disk region in infarct rupture patients. The mechanism of lower expression of αE-catenin remains to be elucidated. A diminished adhesion of the cardiomyocytes may facilitate the infiltration of inflammatory cells into the infarct area, leading to excessive MMP activity and subsequently to infarct rupture and thus may provide a molecular mechanism for infarct rupture post-MI in humans.

The next two chapters of this thesis focused on molecular imaging of myofibroblasts to visualize cardiac remodeling post-MI. In **chapter 6** we evaluated interstitial alterations in myocardial remodeling using a radiolabeled Cy5.5-RGD imaging peptide (CRIP) that targets the myofibroblasts. Maximum CRIP uptake was observed in the infarct area with the highest uptake at 2 weeks post-MI, followed by 4 and 12 weeks compared to unmanipulated animals. In the remote areas the uptake was not significantly different from control values at 2 and 4 weeks, but the uptake increased significantly at 12 weeks post-MI. The uptake was traced to the myofibroblasts and correlated with the extent of collagen deposition. We conclude that radiolabeled CRIP allows for noninvasive visualization of interstitial alterations during cardiac remodeling.

In **chapter 7** we investigated whether this imaging probe can detect the efficacy of pharmacological intervention after MI. Antagonists of the renin-angiotensin-aldosteron axis restrict myocardial fibrosis and cardiac remodeling post-MI and contribute to improved survival. Since the activating effect of Angiotensin II on myofibroblast proliferation and activity is well established, interference in the RAAS system can be anticipated to affect myofibroblast number and activity. Therefore, evaluation of myofibroblasts should provide indirect evidence of the extent of fibrosis and the efficacy of therapy. We induced MI in mice and treated them with captopril, losartan or spironolactone alone or in combination for 4 weeks post-MI. The CRIP uptake was highest in untreated control animals and decreased significantly in animals treated with one agent. Treatment with two or three agents demonstrated a further reduction in tracer uptake. We concluded that radiolabeled CRIP allows evaluation of the efficacy of neurohumoral antagonists post-MI and reconfirms superiority of combination therapy.

In conclusion, in this thesis alterations in the cadherin/catenin cell adhesion complex and the subsequent excessive inflammatory response are presented as a novel molecular mechanism for infarct rupture post-MI in humans. These observations provide novel insights to develop diagnostic tools for prevention of infarct rupture. Furthermore, the feasibility of myofibroblast imaging as an early marker for heart failure development is demonstrated. If proven clinically, this molecular imaging technique of the myocardial infarct healing process may identify patients at risk for heart failure at an early stage and may help plan an optimal treatment regimen for patients susceptible for heart failure.

9

SAMENVATTING

Het proces van wondgenezing na een myocard infarct (MI) is erg complex en kan leiden tot diverse complicaties. In dit proefschrift richten we ons op twee veelvoorkomende complicaties na myocard infarct die geassocieerd zijn met het wondgenezingsproces. De eerste complicatie is infarctruptuur, een complicatie die optreedt in de eerste fase na MI, meestal binnen 3-6 dagen na het infarct. Aangezien er geen adequate behandeling mogelijk is, sterven de meeste patiënten aan een infarctruptuur. Infarctruptuur is geassocieerd met een transmuraal infarct, een eerste episode van een myocard infarct en een slechte collaterale circulatie. Dierexperimenten hebben een rol voor matrix metalloproteinases (MMP's) en celadhesie eiwitten aangetoond in de ontwikkeling van infarctruptuur. Echter, er zijn geen moleculaire mechanismen beschreven die de ontwikkeling van infarctruptuur in mensen verklaren. De eerste hypothese van dit proefschrift is dat in de humane situatie celadhesie moleculen, met name αE-catenin, en een opregulatie van MMP's betrokken zijn bij het proces van infarctruptuur.

Een tweede complicatie die gerelateerd is aan wondgenezing na een myocard infarct is hartfalen. Dit is een conditie waarbij het hart onvoldoende output kan leveren om aan de metabole en zuurstof behoefte van de perifere weefsels te voldoen. Door de vermindering van de acute sterfte na een myocard infarct is het aantal patiënten dat een infarct overleeft, en daardoor kans heeft om hartfalen te ontwikkelen, gestegen. De beschikbare behandelingen verlichten de symptomen van hartfalen, maar kunnen hartfalen niet genezen. Het is uitermate belangrijk om nieuwe technieken te ontwikkelen zodat patiënten met een risico op hartfalen in een vroeg stadium kunnen worden opgespoord, nog voordat de patiënt klachten heeft. Hierdoor kan de behandeling in een heel vroeg stadium worden gestart en kan de ontwikkeling van de symptomen van hartfalen worden tegengegaan. Dit leidt tot de tweede hypothese van dit proefschrift; moleculaire beeldvorming is een techniek om het proces van hartfalen te bestuderen en kan tevens de effecten van de behandeling van hartfalen in kaart brengen.

In **hoofdstuk 2** wordt een literatuuroverzicht gegeven van het proces van wondgenezing na myocardinfarct met een focus op de myofibroblasten. Verder worden moleculaire targets beschreven die gebruikt zouden kunnen worden voor imaging en wordt een overzicht gegeven van experimentele studies waarin is getracht om myofibroblasten te imagen.

In **hoofdstuk 3** hebben we infarctgenezing na MI bestudeerd in verschillende muizenstammen die veelvuldig in cardiovasculair onderzoek worden gebruikt. Het doel was de effecten van de genetische achtergrond op de resultaten van deze studies te bestuderen. Vijf verschillende muizen stammen (BalbC, C57Bl6, FVB, 129S6 and Swiss) werden geïncludeerd, MI werd geïnduceerd en infarct

genezing werd bestudeerd. Infarctruptuur werd waargenomen tussen 3-6 dagen na MI en trad het meest frequent op in 129S6 muizen (62%), gevolgd door C57Bl6 (36%), FVB (29%), Swiss (23%) en BalbC (5%). De hoge incidentie van infarctruptuur in de 129S6 muizen was geassocieerd met een hoge systole bloeddruk en een grotere influx van ontstekingscellen op dag 3 na MI. Acuut hartfalen werd gezien in 28% van de FVB muizen in de eerste week na MI, maar kwam zelden voor in de andere groepen. Cardiale dilatatie was het meest uitgesproken in Swiss muizen, met een meer dan 3-voudige stijging in het eind systole volume in vergelijking met sham geopereerde muizen. De dilatatie correleerde met een verminderde contractie en relaxatie van het hart en een lagere ejectiefractie. Cardiale dilatatie kwam het minste voor in 129S6 muizen. Secondaire dilatatie van het infarct tussen dag 14 en 28 na MI trad op in BalbC, FVB en Swiss muizen, maar was afwezig in C57Bl6 en 129S6. Uit de bevindingen in hoofdstuk 3 concluderen we dat de infarct heling na MI in muizen sterk afhankelijk is van hun genetische achtergrond. Voorzichtigheid is geboden bij het vergelijken van resulaten die zijn verkregen in verschillende muizenstammen. Verder bieden de uitkomsten een richtlijn voor het kiezen van een geschikte muizenstam om bepaalde aspecten van cardiale remodelering na MI te bestuderen.

Uit de literatuur is bekend dat in experimentele muismodellen matrix metalloproteinases (MMP's) een belangrijke rol spelen in de ontwikkeling van infarctruptuur na MI. In **hoofdstuk 4** bestudeerden we de rol van deze MMP's in post-mortem hartweefsel van patiënten die waren overleden aan een infarctruptuur. De resulaten van deze studie laten zien dat een verhoogde activiteit van MMP-8 en MMP-9 in het infarctgebied, veroorzaakt door een grotere influx van ontstekingscellen, leidt tot infarctruptuur in mensen.

In **hoofdstuk 5** bestudeerden we de rol van cel adhesie eiwitten in post-mortem hart weefsel van patiënten die waren overleden aan infarct ruptuur na MI. De resultaten lieten een verminderde expressie zien van αE-catenine in patiënten overleden aan infarctruptuur. Tevens bleek dat bij deze patiënten minder αE-catenin in de intercalairschijven aanwezig was en dat dit eiwit dus niet goed gelokaliseerd is in de hartspiercel. Alhoewel het precieze mechanisme dat leidt tot een lagere expressie van αE-catenin nog verder onderzocht moet worden, is op basis van de resultaten uit hoofdstuk 4 en 5 een mogelijk mechanisme beschreven dat kan leiden tot infarctruptuur na MI in mensen, en dat als startpunt kan dienen voor de ontwikkeling van (preventieve) geneesmiddelen.

Hoofdstukken 6 en 7 van dit proefschrift richten zich op moleculaire imaging van myofibroblasten om zodoende de cardiale remodelering na MI in beeld te brengen. In **hoofdstuk 6** hebben we gekeken naar interstitiële veranderingen tijdens remodelering van het myocard. Hiervoor hebben we gebruik gemaakt van een radioactief gelabeled Cy5.5-RGD imaging peptide (CRIP) dat aan my-

ofibroblasten bindt. Maximale CRIP opname werd gezien in het infarct gebied met de hoogste opname 2 weken na MI, gevolgd door 4 en 12 weken na MI in vergelijking tot dieren zonder MI. De CRIP opname in het niet-geïnfarceerde restmyocard verschilde niet van controle waarden 2 en 4 weken na infarct maar was verhoogd op 12 weken na MI. De CRIP opname was gerelateerd aan het aantal myofibroblasten en correleerde met de hoeveelheid collagen depositie. Concluderend laat deze studie zien dat radioactief gelabeld CRIP interstitiële veranderingen gedurende cardiale remodelering op een niet-invasieve manier in kaart kan brengen.

In **hoofdstuk 7** hebben we gekeken of deze imaging probe de effecten van farmacologische interventies na MI kan detecteren. Antagonisten van de renine-angiotensine-aldosteron-as kunnen myocardiale fibrose en cardiale remodelering verminderen en leiden tot een verbeterde overleving. Aangezien myofibroblasten AT1 receptoren tot expressie brengen is het waarschijnlijk dat beïnvloeding van het RAAS system een effect heeft op de myofibroblasten. Imaging van myofibroblasten zou indirect de hoeveelheid fibrose moeten weergeven. Direct na infarcering werden de muizen 4 weken behandeld met captopril, losartan of spironolactone alleen of in combinatie. De CRIP opname was het hoogste in onbehandelde controle dieren en verminderde significant in de dieren die met monotherapie waren behandeld. Behandeling met twee of drie medicijnen liet een verdere reductie in probe opname zien. Concluderend liet deze studie zien dat radioactief gelabeled CRIP de mogelijkheid biedt om de effecten van farmacologische interventie te evalueren. Verder bevestigde deze studie de superioriteit van combinatie therapie in de behandeling van hartfalen.

Concluderend beschrijft dit proefschrift twee belangrijke complicaties van wondgenezing na een myocardinfarct. Enerzijds wordt een nieuw moleculair mechanisme beschreven voor infarctruptuur na MI in mensen. Anderzijds laat het een mogelijkheid zien om myofibroblasten te imagen als een vroege marker voor hartfalen. Als deze techniek klinisch wordt bewezen, zouden patiënten met een risico op hartfalen in een vroeg stadium kunnen worden gedetecteerd en kan een optimaal behandelplan voor deze patiënten worden opgesteld, om zodoende het ontstaan van hartfalen te voorkomen.

9

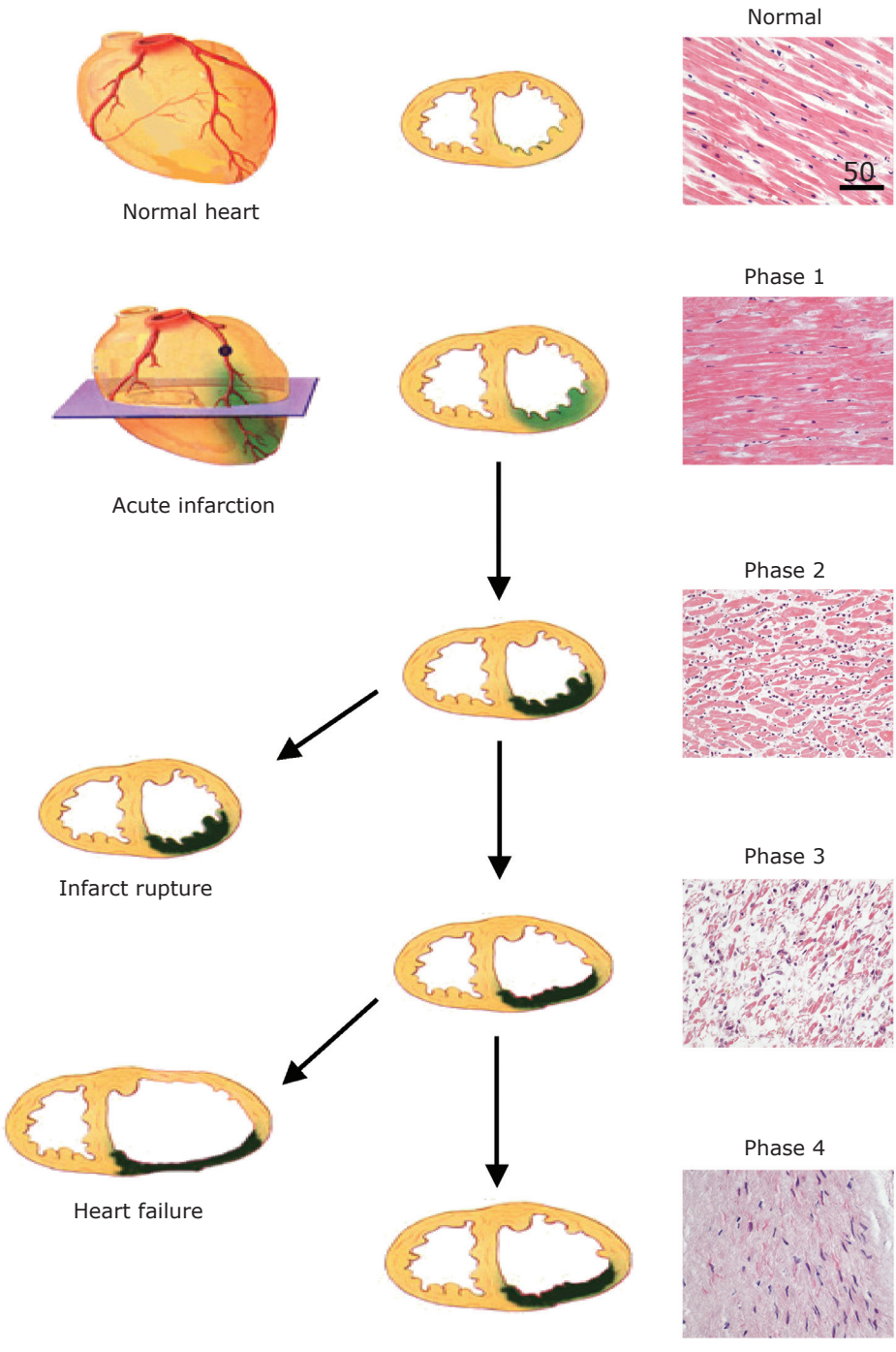
Normal
Normal heart
50
Phase 1
Acute infarction
Phase 2
Infarct rupture
Phase 3
Heart failure
Phase 4

Figure 1.1 The different phases of wound healing post-myocardial infarction

The top row shows a normal heart, a transverse heart section, and associated normal heart histology. Acute myocardial infarction occurs when there is occlusion of one of the coronary arteries (occlusion of the left anterior descending coronary artery is represented by a black dot over the artery). The first phase of the wound healing process (12-18 hours post-infarction) is characterized by eosinophilia and nuclear pyknosis (second row, far right panel). Between days 1 and 4 post infarction the nuclei may disappear and polymorphonuclear leukocytes infiltrate into the infarcted area with removal of necrotic fibers (third row, phase 2). At this time, when the infarct wall is weakest, the myocardium may rupture, often leading to sudden death. In the hearts that do not rupture, there is matrix remodeling and granulation tissue formation that by 3 weeks includes removal of necrotic debris, mononuclear cell infiltration, increased numbers of fibroblasts and capillaries, and an increase in collagen deposition (fourth row, phase 3). After three months, the infarcted region thins and is replaced by scar tissue (bottom row, phase 4). The remaining viable myocardium may remodel and become dysfunctional, leading to heart failure. Scale bar length is indicated in micrometers. Figure adapted from: E. Creemers and J. Cleutjens.

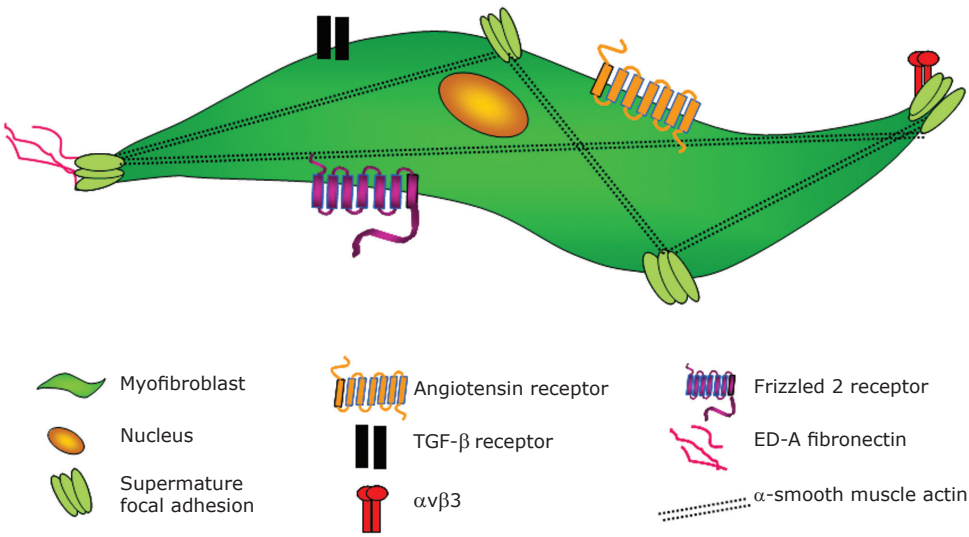

Figure 2.2 Potential targets for myofibroblast imaging

The myofibroblasts expresses several targets that might be of interest for molecular imaging. Angiotensin receptor, Frizzled-2 receptor and TGF-β receptors are reasonable candidates and easily accessible to targeting tracer molecules because of their extracellular localization. αvβ3 integrins are expressed in the supermature focal adhesions and may constitute yet another candidate. However, specificity and efficacy of these targets needs to be determined because these targets are presented on numerous other cell types.

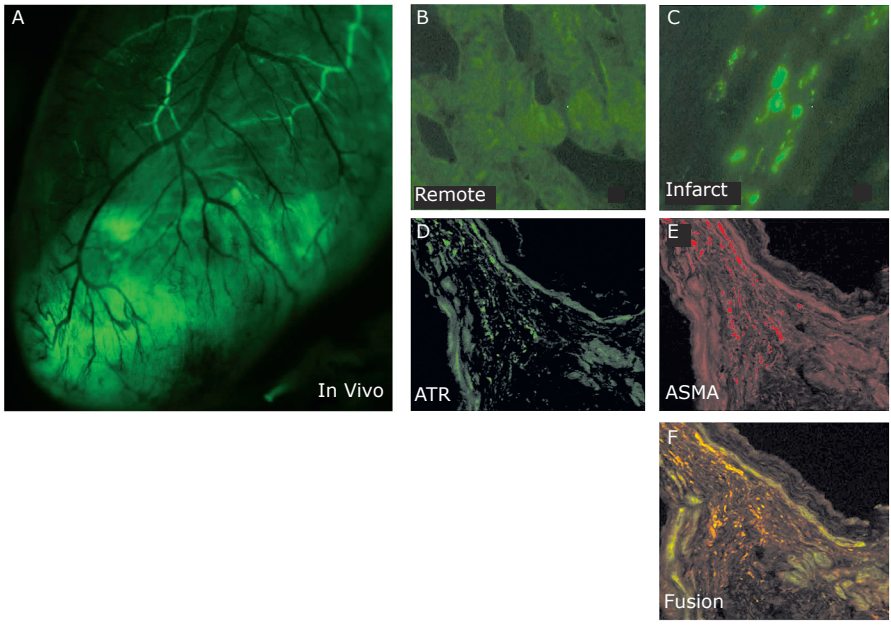

Figure 2.3 **Optical imaging of angiotensin receptors**

In vivo microscopic imaging shows a 3-week old myocardial infarction in a mouse model for myocardial infarction. After administration of green fluorescent angiotensin peptide analog (APA) increased uptake in the infarct area is observed (A). Sections show no uptake of APA in the remote zone (B) and clear uptake in non-myocytic cells in the infarct region (C). The angiotensin receptor positive cells (D, green), also stained positive for ASMA (E, red) showing colocalization (F, yellow) indicating that AT receptors are present on myofibroblasts.

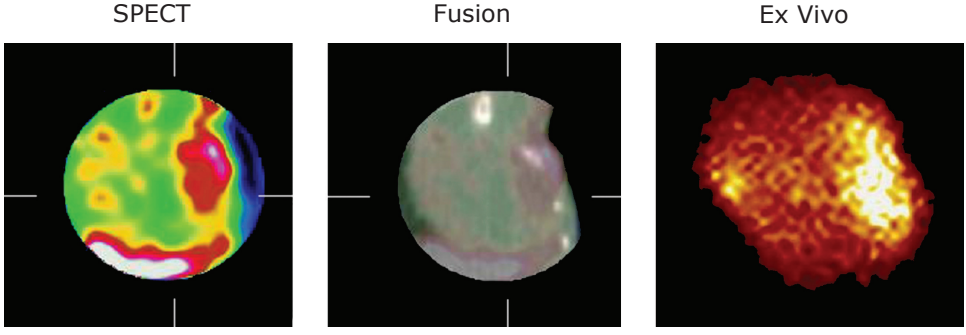

Figure 2.4 **In and Ex vivo images of radiolabeled CRIP imaging**

In vivo imaging with radiolabeled CRIP showed intense uptake in the infarct area two weeks post MI. The uptake decreased over time. The cardiac localization is confirmed in CT fusion image and ex vivo images.

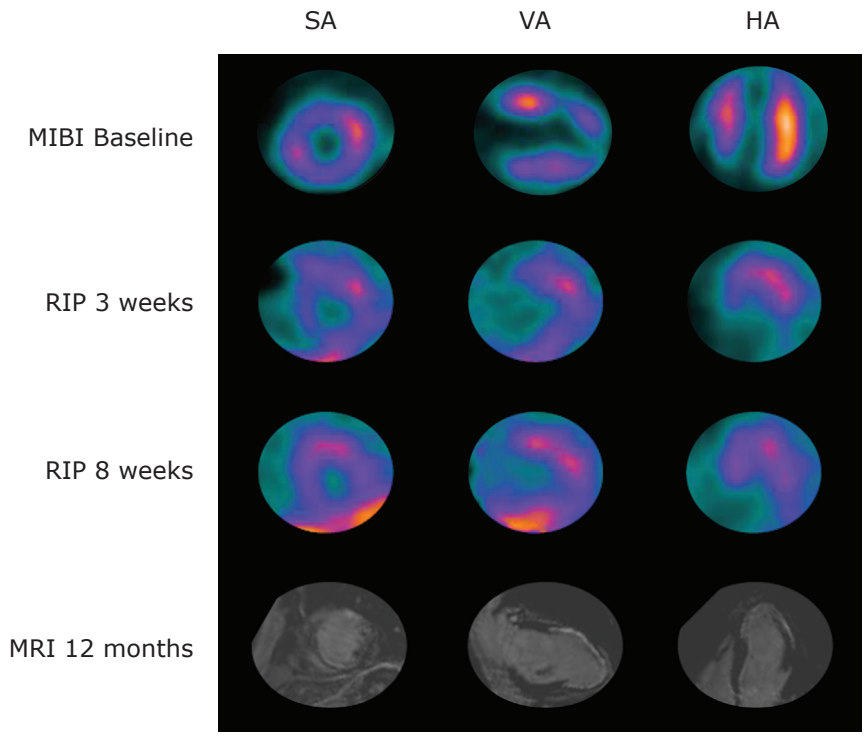

Figure 2.5 **MIBI at baseline, RIP imaging at 3 and 8 week post-MI and cardiac MRI 1 year post-MI**

The MIBI scan (first row) shows apical perfusion defects in the short axis (SA), vertical axis (VA) and horizontal axis (HA) at baseline. RIP imaging at 3 and 8 weeks post MI (row 2 and 3) show uptake corresponding to the infarct area and borderzone delineated by the MIBI scan. The cardiac MR one year post-MI shows scar formation corresponding to RIP uptake (row 4).

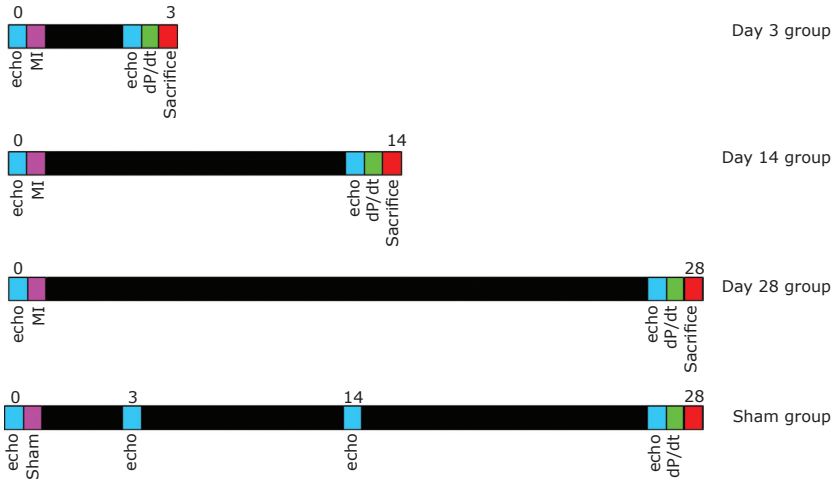

Figure 3.1 **Flow chart of the experimental protocols**

Of each mouse strain, mice were divided into 4 groups. All MI mice were subjected to baseline echocardiography, MI surgery and echo and hemodynamic measurements at the experimental time point. As a control, sham operated mice of every strain were used. They underwent echocardiography before MI and at day 3, 14 and 28. Hemodynamic measurements were executed at day 28.

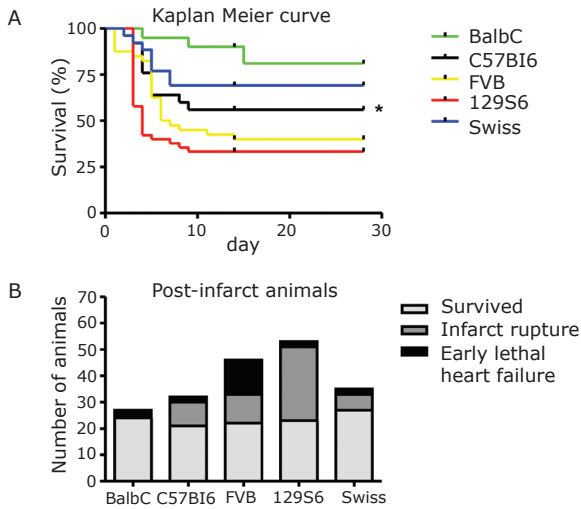

Figure 3.2 **Survival and causes of death between 5 different mouse strains**

A: *Kaplan Meier curve analysis of 5 different mouse strains showed significant differences in survival (p=0.004). BalbC mice showed the highest survival, 85% of these mice were still alive at day 28 post-MI. The BalbC mice were followed by Swiss (69%), C57Bl6 (56%) FVB (37%) whereas only 33% of the 129S6 mice were still alive at 28 days post-MI.* **B:** *The causes of death in the post-MI mice were infarct rupture and early heart failure in the first week post-MI. Of the 129S6 mice, 62% died of infarct rupture, as compared to only 5% of the BalbC mice. Death due to acute heart failure in the first week post-MI mainly occurred in the FVB mice (28%).*

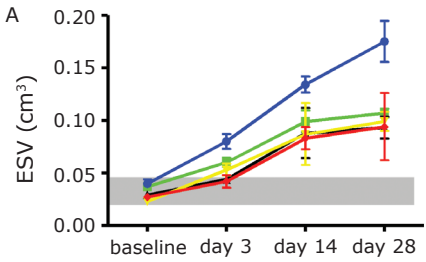

Strain			p-value
BalbC	>	C57Bl6	ns
BalbC	>	FVB	ns
BalbC	>	129S6	ns
C57Bl6	>	129S6	ns
FVB	>	C57Bl6	ns
FVB	>	129S6	ns
Swiss	>	BalbC	0.0001
Swiss	>	C57Bl6	<0.0001
Swiss	>	FVB	<0.0001
Swiss	>	129S6	<0.0001

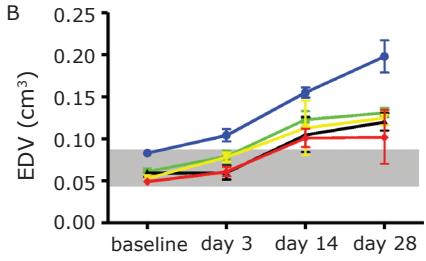

Strain			p-value
BalbC	>	C57Bl6	ns
BalbC	>	FVB	ns
BalbC	>	129S6	0.0128
C57Bl6	>	129S6	ns
FVB	>	C57Bl6	ns
FVB	>	129S6	ns
Swiss	>	BalbC	<0.0001
Swiss	>	C57Bl6	<0.0001
Swiss	>	FVB	<0.0001
Swiss	>	129S6	<0.0001

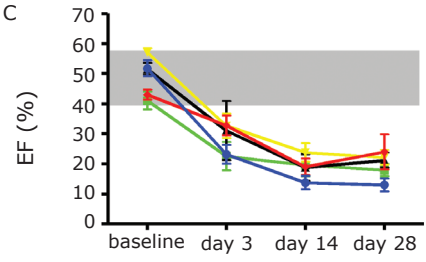

Strain			p-value
BalbC	>	Swiss	ns
C57Bl6	>	BalbC	0.0038
C57Bl6	>	129S6	ns
C57Bl6	>	Swiss	<0.0001
FVB	>	BalbC	0.0001
FVB	>	C57Bl6	ns
FVB	>	129S6	ns
FVB	>	Swiss	<0.0001
129S6	>	BalbC	0.0076
129S6	>	Swiss	0.0001

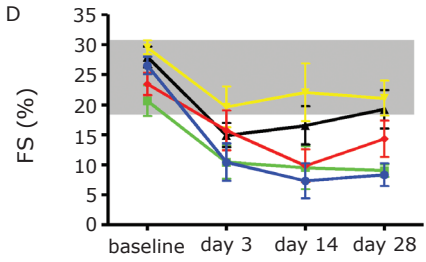

Strain			p-value
BalbC	>	Swiss	ns
C57Bl6	>	BalbC	0.0002
C57Bl6	>	FVB	ns
C57Bl6	>	129S6	ns
C57Bl6	>	Swiss	<0.0001
FVB	>	BalbC	<0.0001
FVB	>	129S6	0.0269
FVB	>	Swiss	<0.0001
129S6	>	BalbC	ns
129S6	>	Swiss	0.0320

Figure 3.3 **Echocardiographic measurements**

Echocardiographic measurements were performed in sham operated and in post-MI mice. The values measured at baseline in the sham operated mice remained similar over time and are represented by the grey rectangle. Post-MI, end systolic volume (ESV) and end diastolic volume (EDV) increased in all mouse strains, with the highest increase in Swiss mice (Fig. 3.3 A,B). The ejection fraction (EF) and fractional shortening (FS) decreased after MI surgery in all mouse strains with the highest decrease in Swiss and BalbC mice. BalbC (green), C57Bl6 (black), FVB (yellow), 129S6 (red), Swiss (blue).

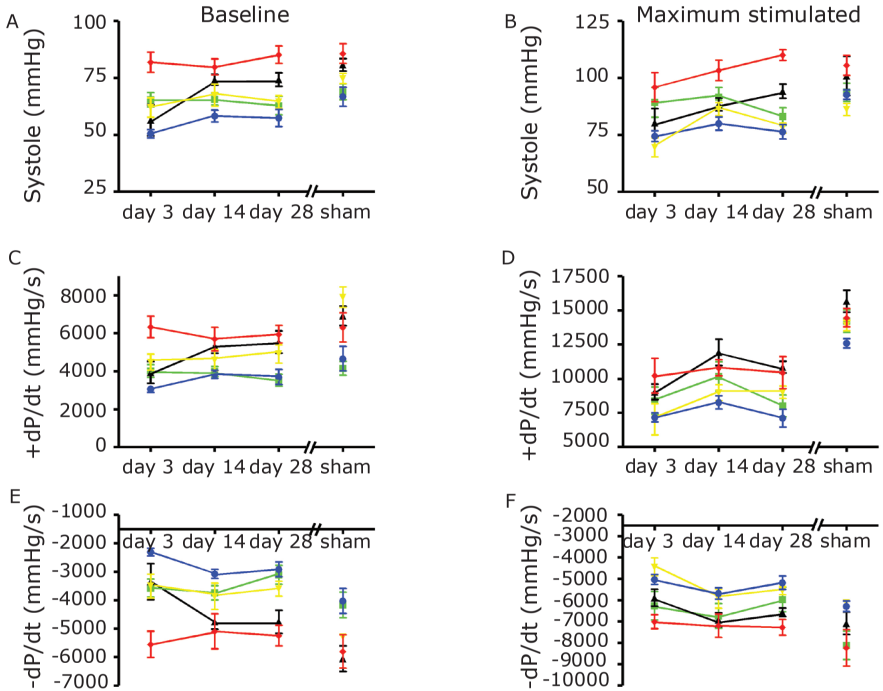

Strain		Strain	p-value
BalbC	>	FVB	ns
BalbC	>	Swiss	ns
C57Bl6	>	BalbC	ns
C57Bl6	>	FVB	0.0433
C57Bl6	>	Swiss	<0.0001
FVB	>	Swiss	ns
129S6	>	BalbC	<0.0001
129S6	>	C57Bl6	<0.0001
129S6	>	FVB	<0.0001
129S6	>	Swiss	<0.0001

Strain		Strain	p-value
BalbC	>	Swiss	ns
C57Bl6	>	BalbC	<0.0001
C57Bl6	>	FVB	ns
C57Bl6	>	Swiss	<0.0001
FVB	>	BalbC	0.0195
FVB	>	Swiss	<0.0001
129S6	>	BalbC	<0.0001
129S6	>	C57Bl6	ns
129S6	>	FVB	0.0028
129S6	>	Swiss	<0.0001

Strain		Strain	p-value
BalbC	>	C57Bl6	ns
BalbC	>	129S6	<0.0001
C57Bl6	>	129S6	0.0045
FVB	>	BalbC	ns
FVB	>	C57Bl6	0.0327
FVB	>	129S6	<0.0001
Swiss	>	BalbC	0.0256
Swiss	>	C57Bl6	<0.0001
Swiss	>	FVB	ns
Swiss	>	129S6	<0.0001

Figure 3.4 Hemodynamic measurements

Hemodynamic measurements were taken in sham-operated mice at day 28 and in post-MI mice either at day 3, 14 or 28 depending on the group. Hemodynamic measurements were taken under physiological (baseline) conditions (A,C,E) and after maximal stimulation with dobutamine (B, D, F). Results from the three-way ANOVA are presented in the tables. Systolic blood pressure was significantly higher in 129S6 mice compared to the other strains. Also, systolic blood pressure was significantly higher in C57Bl6 mice compared to FVB and Swiss mice (Figure 4A-B). The +dP/dt, a measurement of contraction strength, was highest in 129S6 mice and was significantly different from BalbC, FVB and Swiss mice. The lowest +dP/dt values were measured in Swiss mice (Figure 4C,D). The ventricular relaxation (−dP/dt), was best in 129S6 mice both at baseline and after maximum dobutamine stimulation. BalbC (green ■), C57Bl6 (black ▲), FVB (yellow ▼), 129S6 (red ◆), Swiss (blue ●).

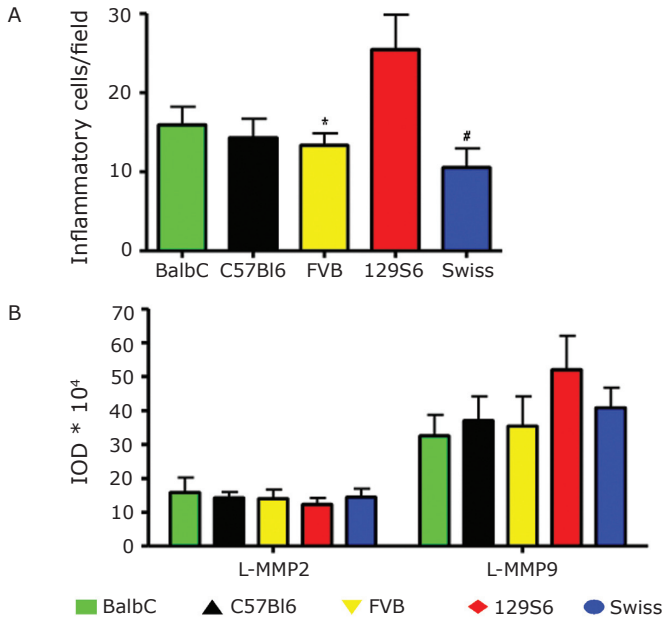

Figure 3.5 **Inflammatory cell influx and MMP-activity at day 3 post-myocardial infarction**

Inflammatory cells were counted at the infarct borderzone 3 days post-MI. **A:** *Quantitative analysis showed a significant difference in influx of inflammatory cells between the 5 mouse strains (p=0.0074). 129S6 mice had a significant higher number of inflammatory cells in the infarct area compared to FVB and Swiss mice. (*: p<0.05) and Swiss (#: p<0.01) mice. A field is defined as 90.000 μm².* **B:** *Gelatin zymography demonstrating the activity of matrix metalloproteinases (MMP)-2 and -9 in myocardial infarct tissue obtained from 3 day old infarcts. Quantification of the latent forms of MMP-2 and MMP-9, expressed in intensity units (IOD), showed slightly higher latent-MMP-9 levels in 129S6 mice; however this did not reach statistical significance. Active MMP-levels were difficult to detect in these tissue samples.*

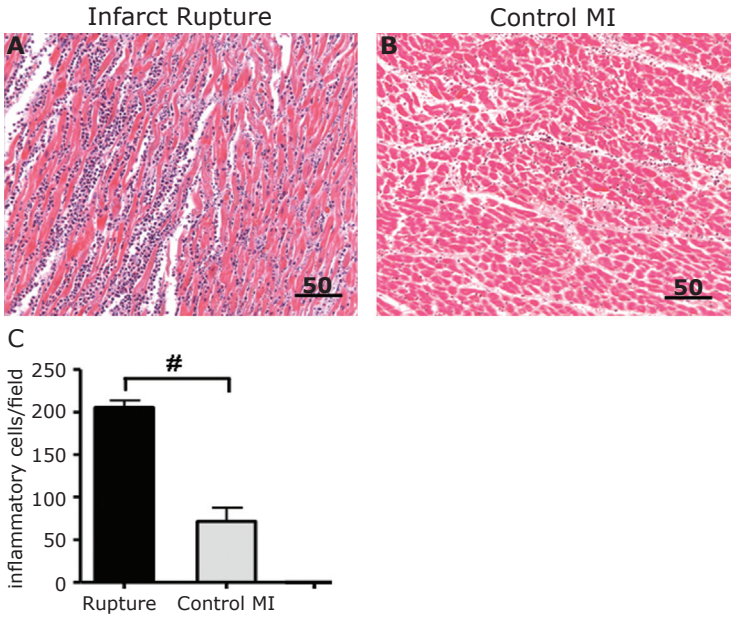

Figure 4.1 **Histological analysis of inflammatory cells in infarct rupture and control MI patients**

Representative images of H&E staining of the MI border zone in infarct rupture patients (A) and control MI patients (B). (C) Quantitative analysis of the inflammatory cells showed a significant increase in infarct rupture patients compared to control MI patients ($P < 0.001$). A field is defined as 90.000 μm^2. Scale bar length is indicated in µm.

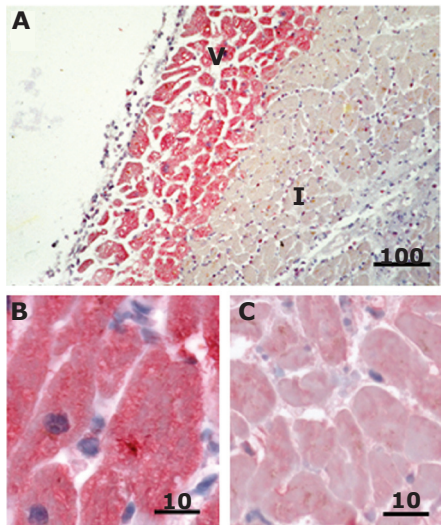

Figure 4.4 **Representative images of immunohistochemical staining for MMP-2**

MMP-2 was mainly present in vital (V) cardiomyocytes (A-B) and decreased in ischemic (I) cardiomyocytes (A,C). MMP-2 immunoreactivity showed the same pattern in ruptured and control MI. Scale bar length is indicated in µm.

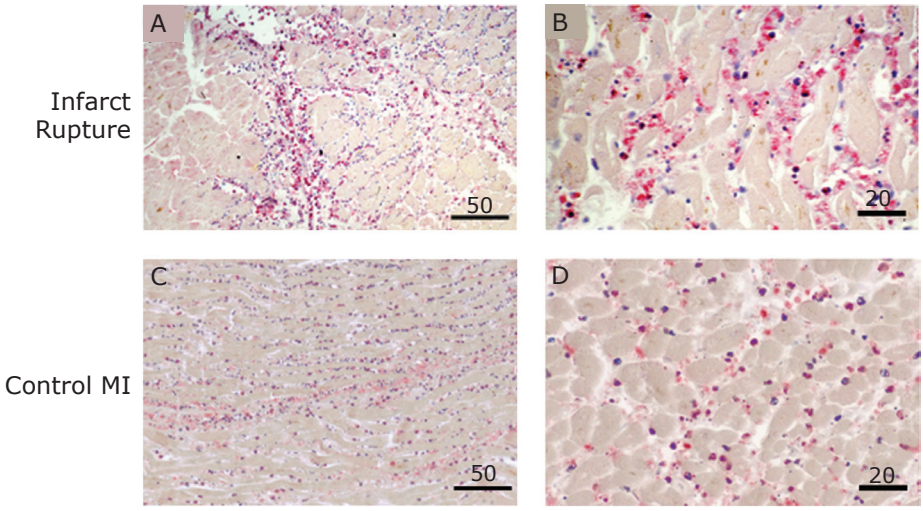

Figure 4.5 Representative images of immunohistochemical staining for MMP-9

MMP-9 was mainly present in inflammatory cells (Figure 4.5A-D). Infarct rupture patients (Figure 4.5A-B) showed more abundant staining than control MI patients (Figure 4.5C-D). Scale bar length is indicated in μm.

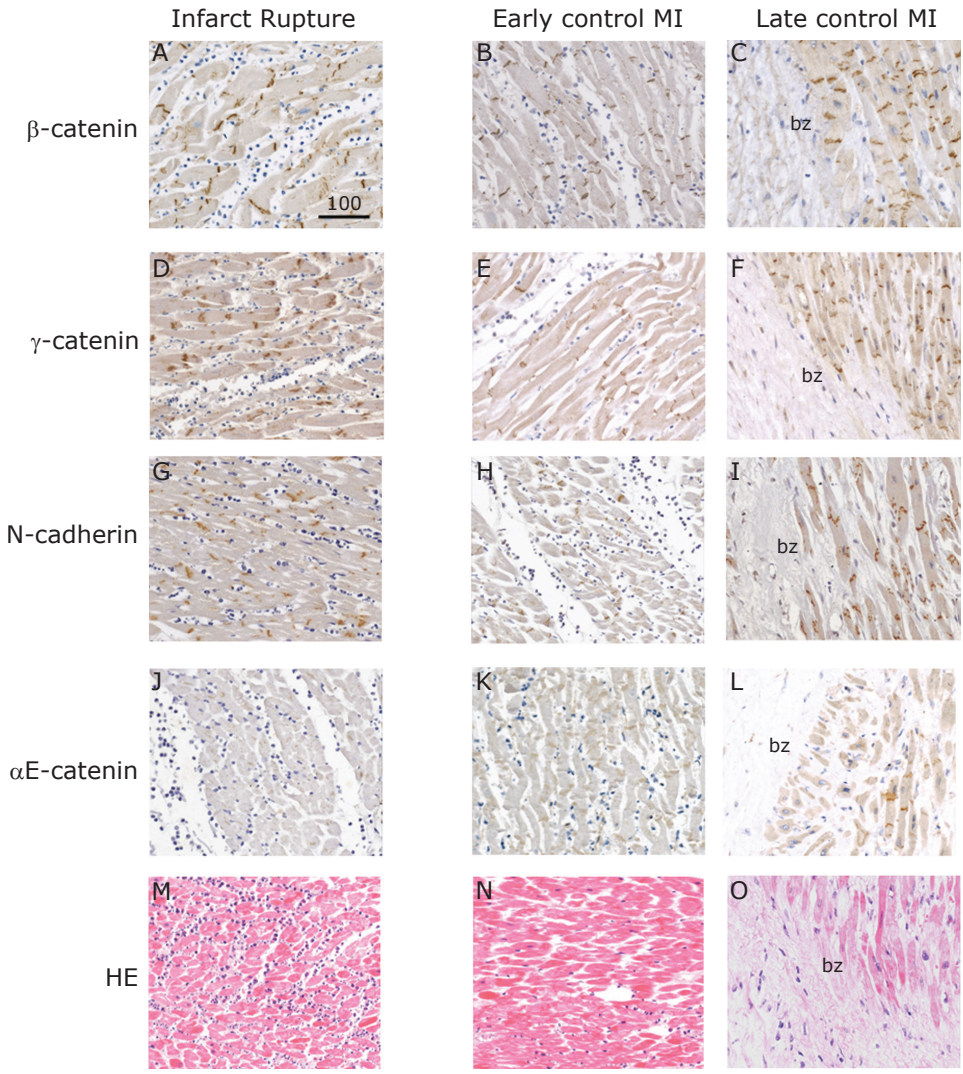

Figure 5.1 **Immunohistochemical characterization of cell adhesion complex proteins in the infarct area**

Representative microphotographs of immunostaining for β-catenin (A-C), γ-catenin (D-F), N-cadherin (G-I) and αE-catenin (J-L) in the infarct area of ruptured hearts (A,D,G,J), early (B,E,H,K) and late (C,F,I,L) control infarcts. A similar staining intensity for β-catenin, γ-catenin and N-cadherin was observed in the intercalated disk regions of the cardiomyocytes in infarct rupture and the two control MI groups. αE-catenin staining was undetectable in the infarct area of infarct rupture patients (J). However, staining was observed in the early control infarcts (K) as also in the border zone (bz) of late control MI's (L). Panel M-O shows H&E staining of the infarct area of ruptured patients (M), characterized by the necrotic cardiomyocytes and the massive influx of inflammatory cells. H&E staining of an early control MI (N) and the border zone of a late control MI (O) are also shown. Scale bar length is indicated in μm.

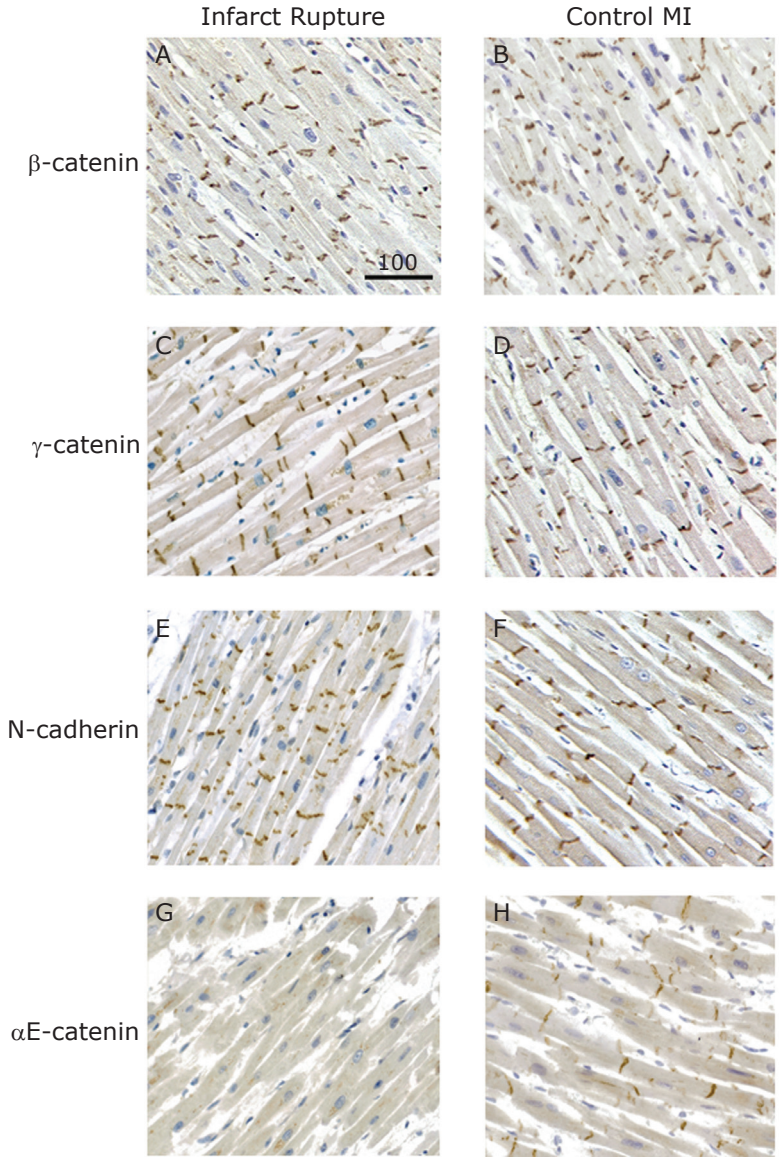

Figure 5.2 **Immunohistochemical characterization of cell adhesion complex proteins in the remote area**

Representative images of immunostaining for β-catenin (A, B), γ-catenin (C, D), N-cadherin (E, F) and αE-catenin (G,H) in remote parts of ruptured hearts (A,C,E,G) and control MI hearts without rupture (B,D,F,H). Abundant and similar staining for β-catenin, γ-catenin and N-cadherin was observed in the intercalated disk regions of the cardiomyocytes in infarct rupture and control MI groups. For αE-catenin, abundant staining of intercalated disks between cardiomyocytes was observed in the control MI hearts (H). On the contrary, 90% of the patients from the infarct rupture group showed either weak or no detectable aE-catenin staining (G). Scale bar length is indicated in μm.

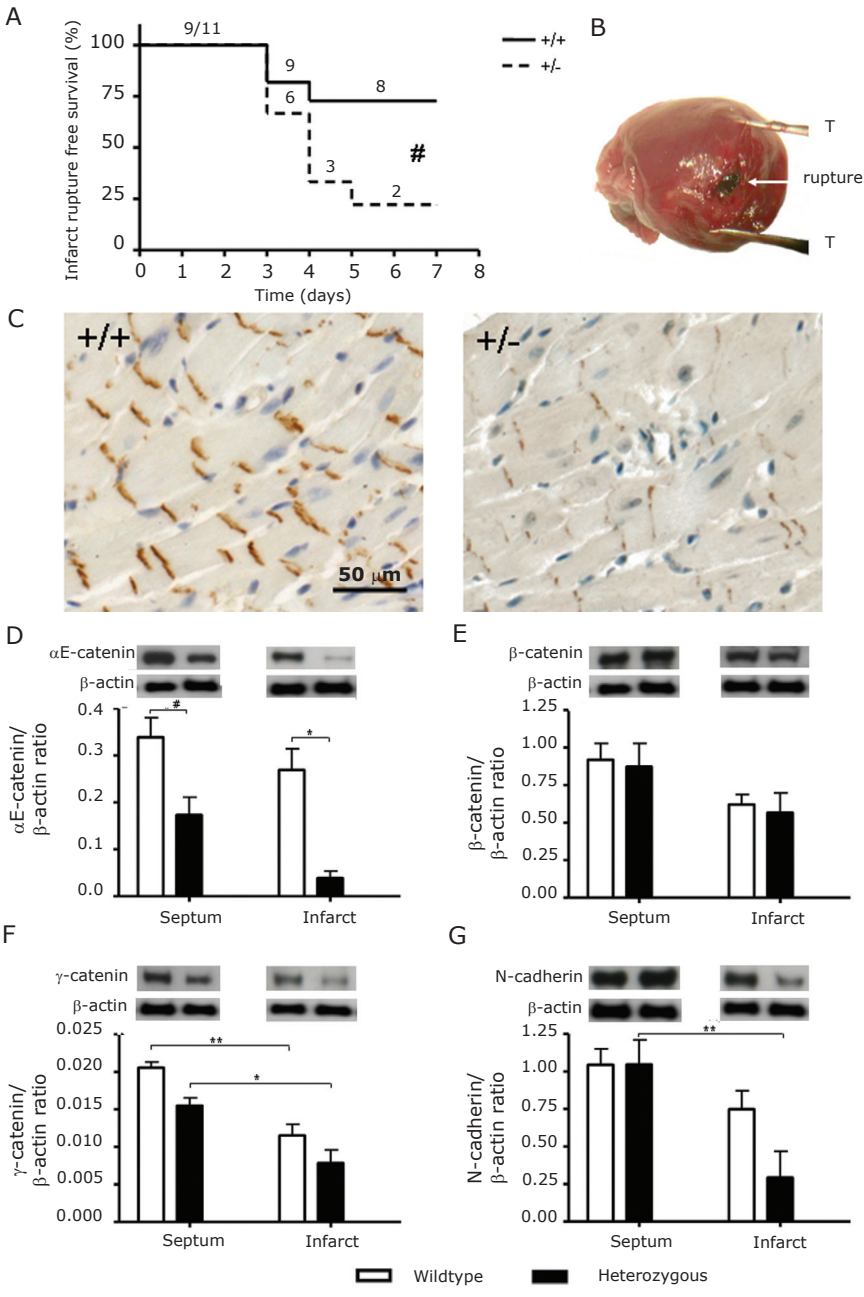
A
Infarct rupture free survival (%)
100
75
50
25
0
9/11
9
6
8
3
2
#
0 1 2 3 4 5 6 7 8
Time (days)
+/+
+/-
B
T
rupture
T
C
+/+
50 μm
+/-
D
αE-catenin
β-actin
αE-catenin/ β-actin ratio
0.4
0.3
0.2
0.1
0.0
#
*
Septum
Infarct
E
β-catenin
β-actin
β-catenin/ β-actin ratio
1.25
1.00
0.75
0.50
0.25
0.00
Septum
Infarct
F
γ-catenin
β-actin
γ-catenin/ β-actin ratio
0.025
0.020
0.015
0.010
0.005
0.000
**
*
Septum
Infarct
G
N-cadherin
β-actin
N-cadherin/ β-actin ratio
1.25
1.00
0.75
0.50
0.25
0.00
**
Septum
Infarct
Wildtype
Heterozygous

Figure 5.4 **Heterozygous αE-catenin C-terminal deficient mice show susceptibility to infarct rupture post-myocardial infarction**

*A: Kaplan Meier curve analysis of heterozygous αE-catenin C-terminal deficient mice (n=9) showed significantly lower rupture-free survival post MI (#: p=0.038) compared to their wildtype littermates (n=11). B: Macroscopic image of infarct rupture (T=tweezers). The arrow points at the tear in the infarct area, showing the blood loss through the ventricular wall. C: Representative images of Immunohistochemical analysis of αE-catenin, showing less intense staining of the intercalated disks in the heterozygous mice compared to wildtype littermates. D-G: Upper panels: Representative Western blot analysis for αE-catenin (D), β-catenin (E), γ-catenin (F) and N-cadherin (G) in heterozygous C-terminal αE-catenin deficient mice and their wildtype littermates, both from septum (non-ischemic) and infarct tissue; β-actin was used for normalization of the samples. Lower panels: Quantitative analysis of adhesion complex proteins, expressed as protein/β-actin ratio, demonstrating significantly lower αE-catenin in mice heterozygously deficient for C-terminally truncated αE-catenin (n=9) compared to their wildtype littermates (n=11). The other cell adhesion proteins were unaffected, although N-cadherin showed more degradation under ischemic conditions in the heterozygous mice. #p<0.05, *p<0.01, **p<0.001.*

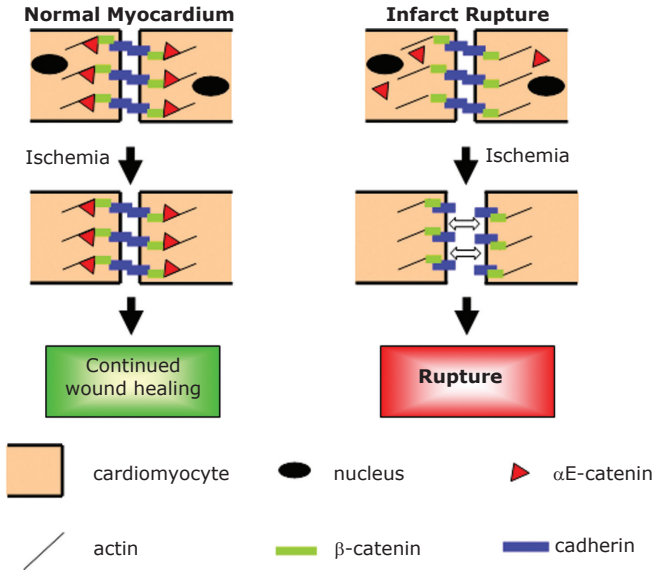

Figure 5.5 **Cartoon depicting the role of a defective intercellular adhesion complex in infarct rupture in humans**

In the left part of the cartoon, the normal components of the cell adhesion complex of cardiomyocytes from patients with normal infarct healing are shown. In the uninjured cardiomyocytes of normal hearts, αE-catenin is localized in the intercalated disks. Ischemia induces death of the cardiomyocytes in the infarct area, as shown by the loss of their nucleus. However, the integrity of the infarct area is sufficiently preserved by the adhering cardiomyocytes, and the wound healing and granulation tissue formation continue. As shown in the right side of the cartoon, αE-catenin is not localized in the intercalated disks of the cardiomyocytes in rupture-prone hearts. After ischemia, this abnormal cell adhesion complex causes the dead cardiomyocytes in the infarct area to loosen up their connections, causing further deterioration of the integrity of the infarct area and subsequently leading to infarct rupture.

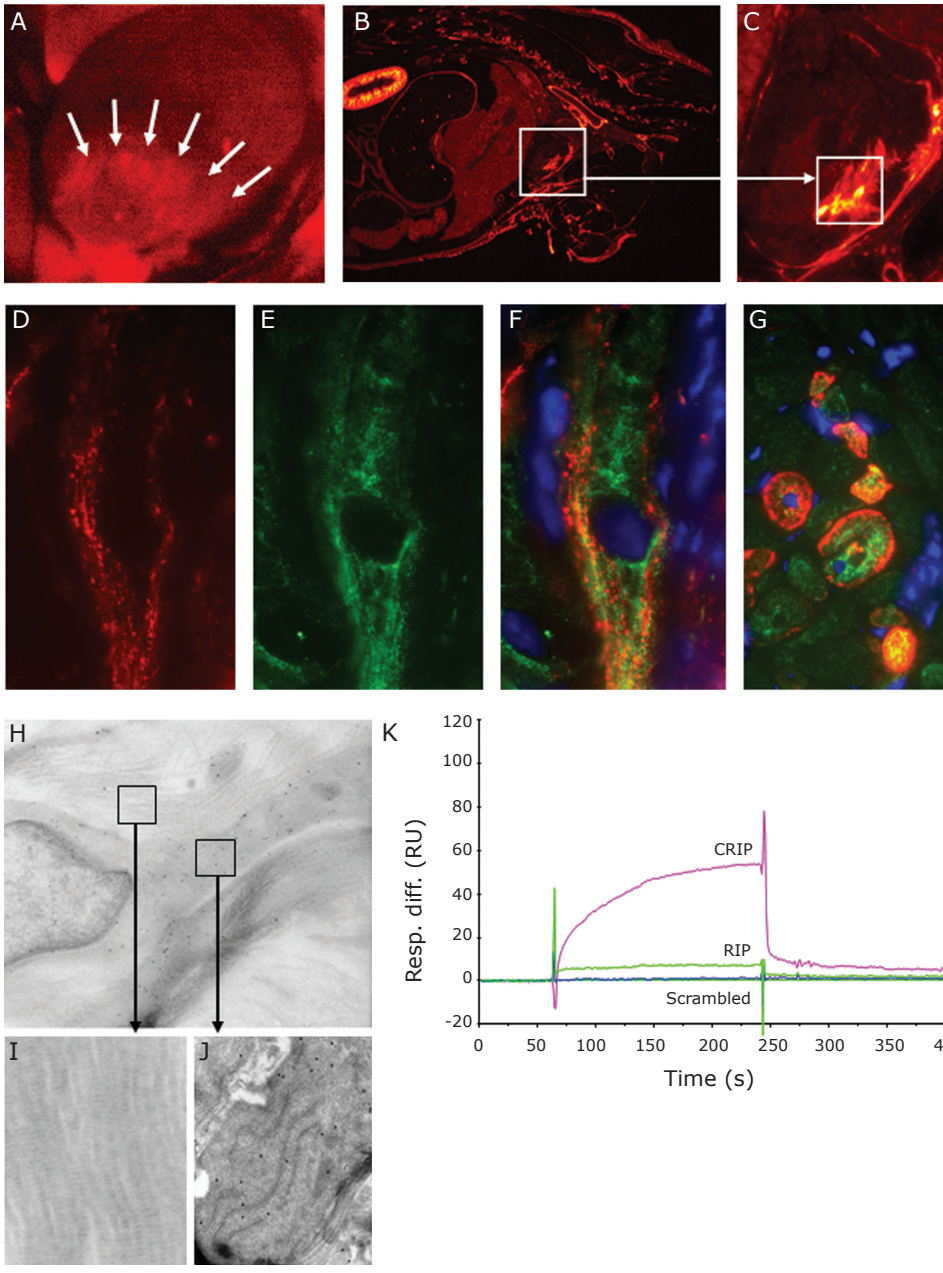
A
B
C
D
E
F
G
H
I
J
K
120
100
80
60
40
20
0
-20
Resp. diff. (RU)
CRIP
RIP
Scrambled
0
50
100
150
200
250
300
350
400
Time (s)

Figure 6.2 **Characterization of target binding of CRIP**

Probe targeting was evaluated 3.5 H after intravenous administration of CRIP in 2-week post-MI animals. The localization of the Cy5.5 fluorescence (red) was clearly observed in the infarct and peri-infarct zone in vivo (A, arrowheads). A 30-micron whole mouse slice demonstrates myocardial uptake of the probe (B, square); intense uptake is seen in the kidney which serves as the route of excretion. (C), Magnification of the area enclosed by the square in (B) demonstrates fluorescent probe localization in the subendocardium. (D-E) For further characterization of the probe targets, we correlated the uptake of intravenously administered CRIP in 2 week post-MI animals (red, D) with concurrent staining of the sections by anti-ASMA antibody (green, E), colocalization is shown by overlay (F) The localization of CRIP was observed in spindle shaped myofibroblasts in the infarct area. CRIP and ASMA colocalization is seen in transversely sectioned myofibroblasts in (G). For immuno EM, similarly intravenously administered CRIP was traced by gold labeled anti-cy antibody (black immunogold partikels 10 nm). CRIP clearly localized with myofibroblasts (H), containing characteristic abundance of rough endoplasmatic reticulum (I). No uptake was seen in mature collagen fibers (J). (K) shows sensograms (Biacore 3000 instrument) obtained with CRIP and scrambled CRIP exposure to a surface with a immobilized peptide sequence H2N-GPP-GKN-GDD-GEA-GKP-GR-COOH, aa221-240 from procollagen-I. In addition, RGD imaging peptide without Cy5.5 dye was also used in the experiment (RIP). The higher RU values for CRIP than RIP is due to the higher molecular weight of CRIP.

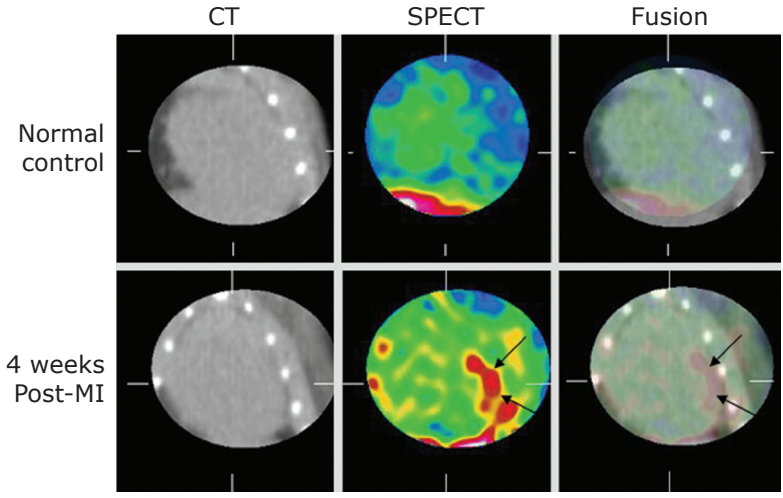

Figure 6.3 **In vivo microCT, microSPECT and fusion images in frontal projection in unmanipulated control and 4-week post-MI animals 3H after radiolabeled CRIP administration**

No uptake of Tc-CRIP was observed in the unmanipulated animal (top row). On the other hand, intense anterior uptake is seen in the infarcted mouse (bottom row). The cardiac localization is confirmed in the CT fusion image.

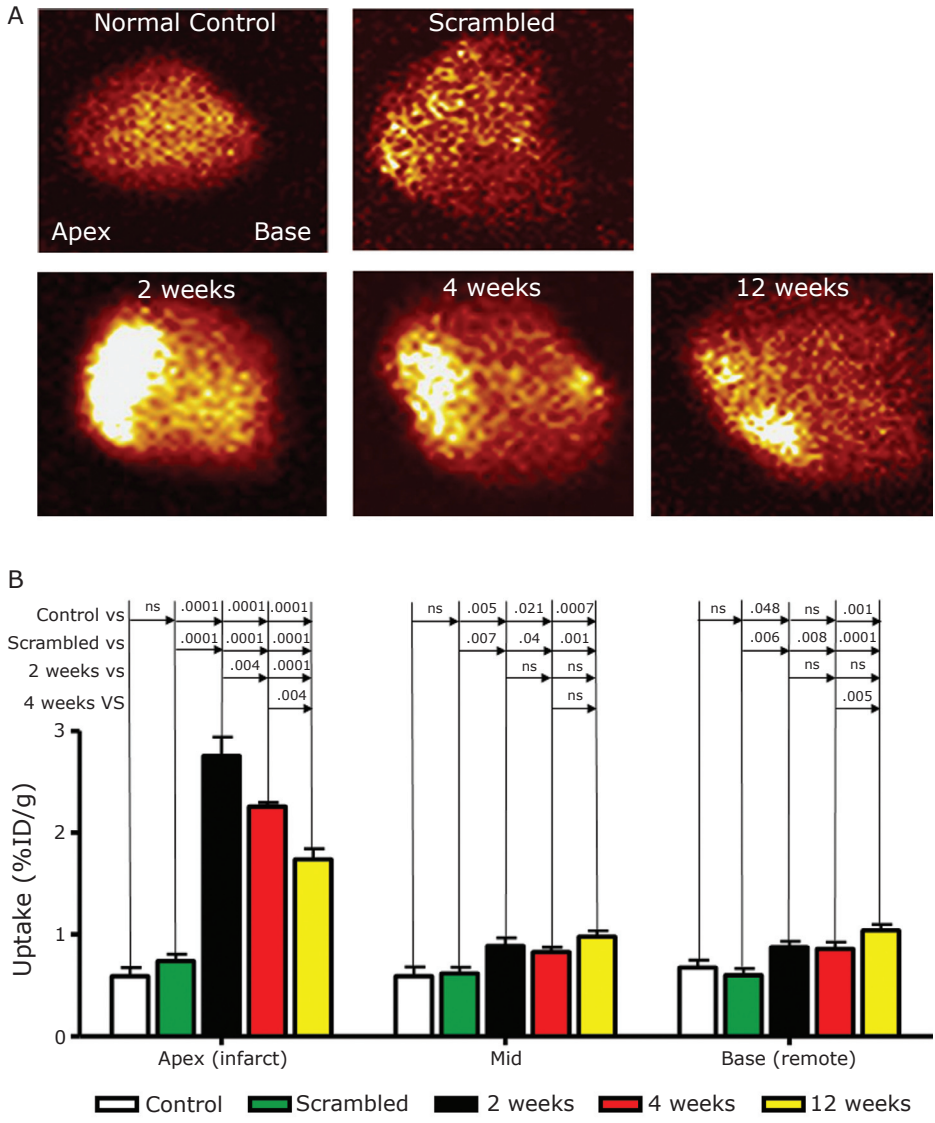

Figure 6.4 **Ex vivo images of the explanted hearts in control and post-MI animals with radiolabeled CRIP and scrambled CRIP**

A. Ex Vivo Images. Control heart with RGD probe and 4-week post-MI heart with scrambled sequence show no radiotracer uptake. On the other hand, intense CRIP uptake is seen in 2-week post-MI animal. The uptake in the infarcted area was highest in mice 2 weeks after MI, followed by 4, and 12 weeks after MI. B. Quantitative Tc-CRIP uptake in the infarct (apex), peri-infarct (mid), and remote (base) areas. The %ID/g uptake in the infarct area is highest in mice 2 weeks after MI, followed by 4, and 12 weeks after MI. On the other hand, the uptake in peri-infarcted and remote areas shows trends towards higher uptake from 2 to 12 weeks after MI. No uptake of scrambled peptide was seen in the infarct zone. Quantitative data confirmed the findings of ex vivo images.

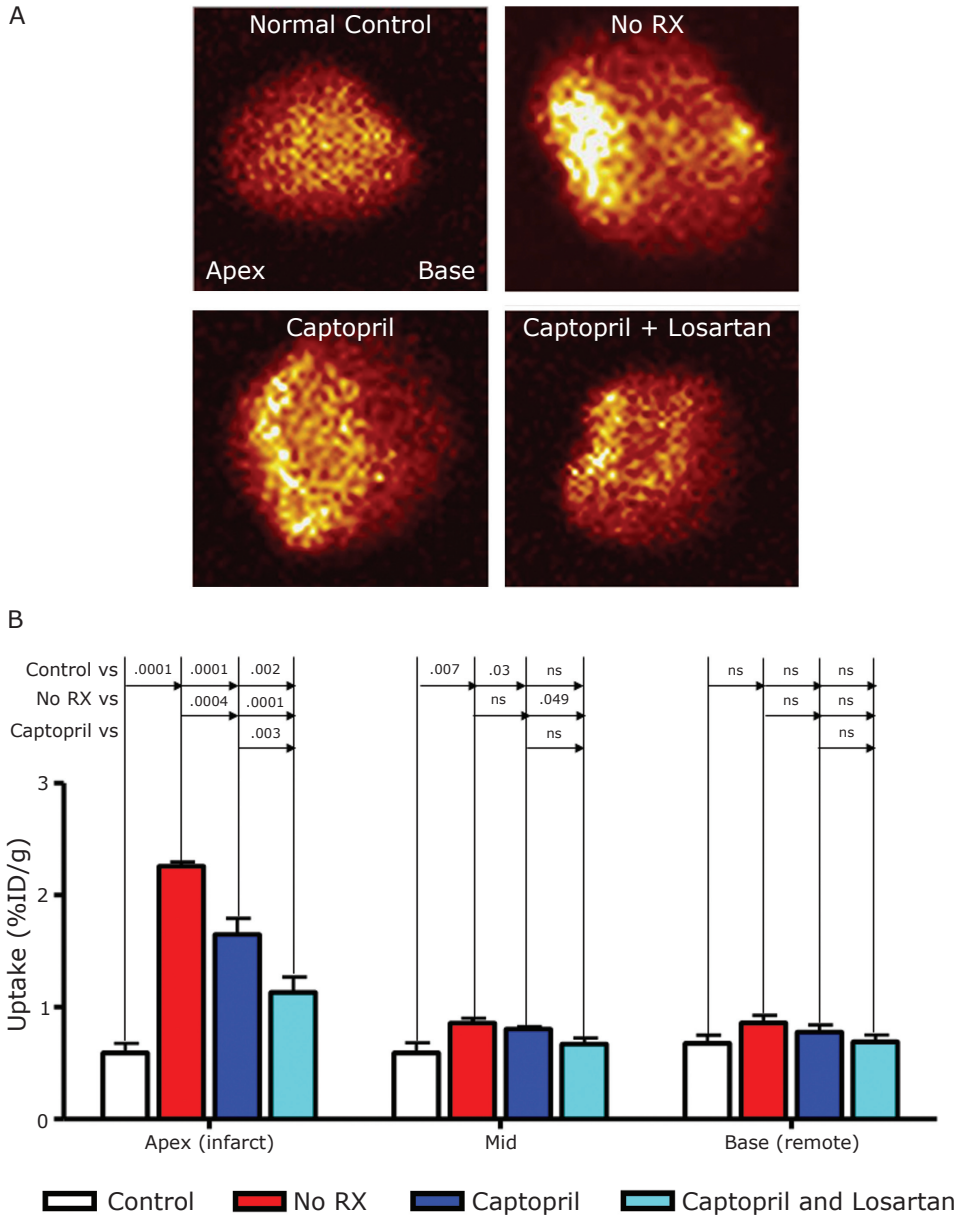

Figure 6.5 **Radiolabeled CRIP uptake after anti-angiotensin therapy in post-MI animals**

A. Ex Vivo Images 4 weeks post-MI. In 4-week post-MI animals, captopril treatment alone and in combination with losartan demonstrates significantly lower radiotracer uptake as observed in gamma images of the ex vivo explanted hearts. B. Quantitative Tc-CRIP uptake was significantly lower after therapeutic intervention in infarcted and nonsignificantly lower in non-infarcted areas.

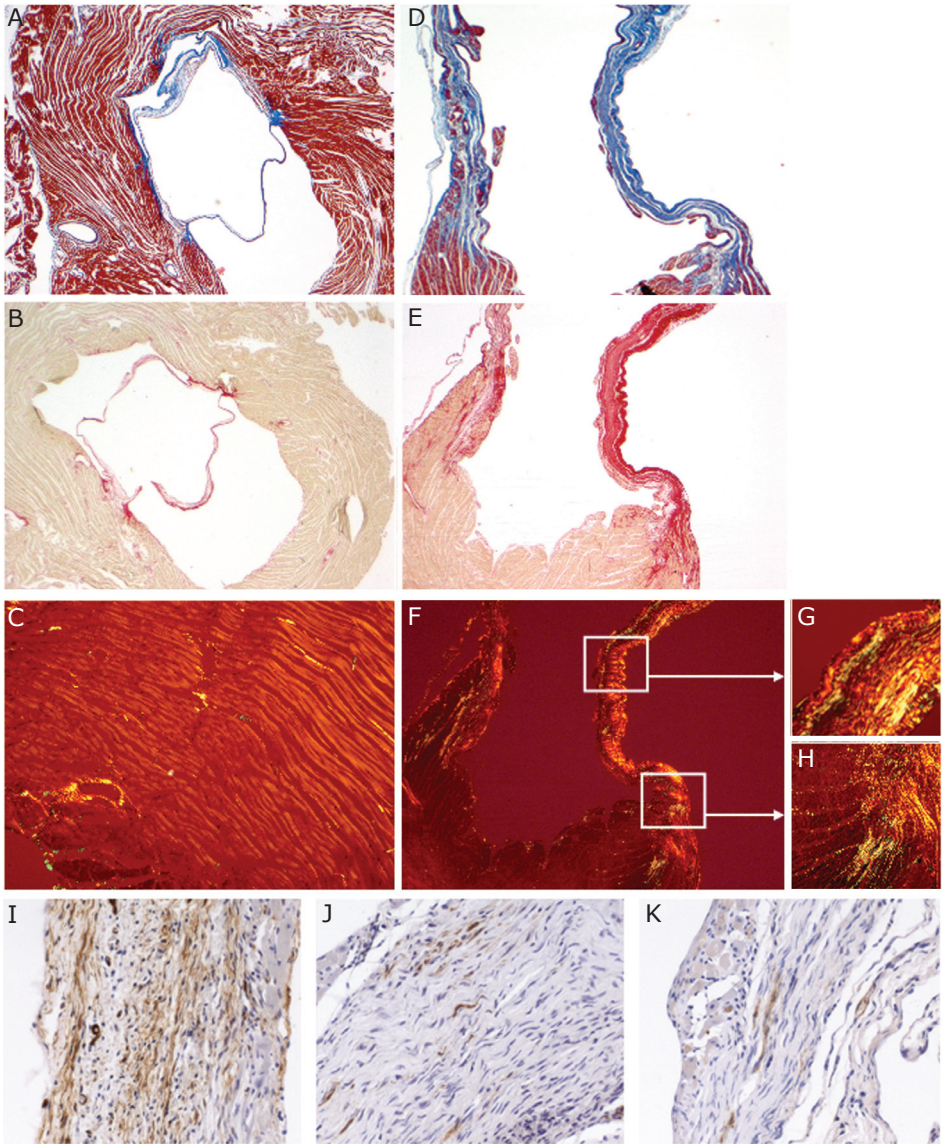

Figure 6.6 **Histological assessment of control heart and 4 weeks post MI**

Masson's trichrome (A,D) and Picro Sirius Red (B,E) staining, and Sirius Red staining with polarized light (C, F-H) in remote (A-C) and infarct center or border regions (D-H) in a heart 4 weeks after MI. The remote area is from the base of the heart as indicated by the enclosed mitral valve. The remote region shows minimal fibrosis (A) and collagen deposition (B,C). On the other hand, the infarct region shows significant wall thinning and fibrosis (D) with evidence of collagen deposition (E,F). The two areas from (F) are magnified to demonstrate collagen deposition in infarct center (G) and infarct border (H). Immunohistochemical characterization with anti-ASMA antibody (brown) of the infarct zone at 2 (I), 4 (J) and 12 (K) weeks reveal progressive decrease in the number of myofibroblasts over time.

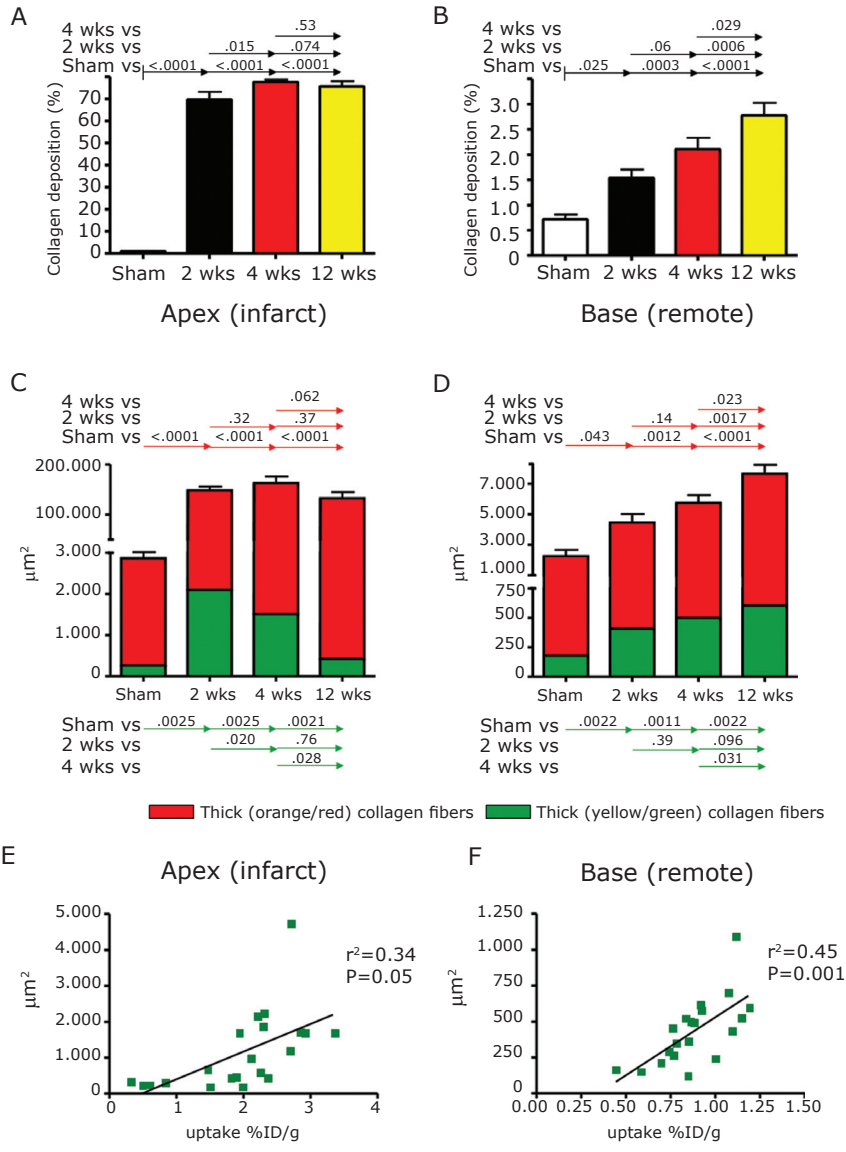

Figure 6.7 **Collagen fiber analysis in remote and infarct regions**

The total collagen content in the infarcted area (A) remains similar with the passage of time, whereas it increases significantly in the remote region (B). Further characterization of the collagen fibers by polarization reveals that the thin or new collagen fibers (green) decreased in the infarct region (suggestive of cessation of collagen production and maturation of the collagen fibers) (C) and increased substantially in the remote area (D) (suggesting ongoing production of the new collagen with increasing total collagen content). The prevalence of new collagen fibers paralleled the CRIP uptake and demonstrated a significant direct correlation, both in infarct and remote zone (E, F). For full color illustration, see page 171.

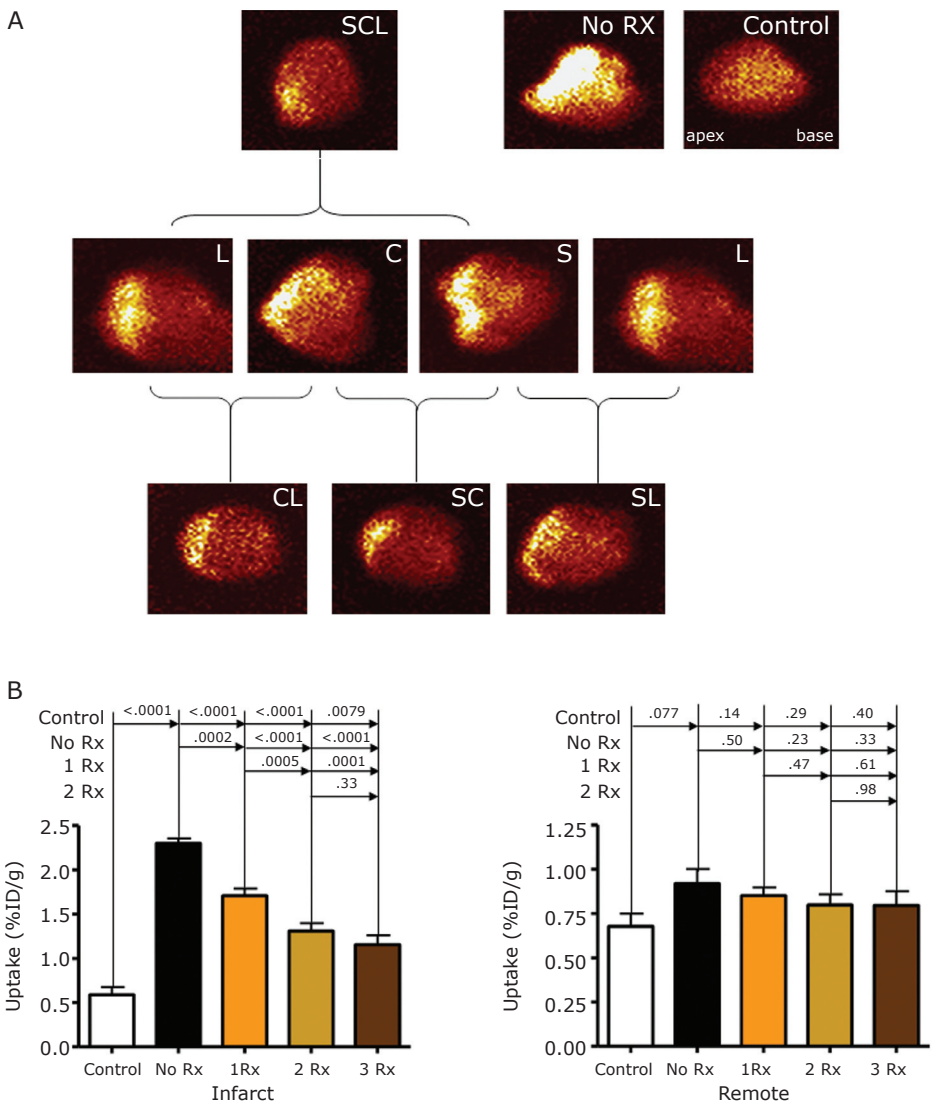

Figure 7.1 **Radiolabeled CRIP uptake after neurohumoral antagonist treatment in post-MI animals**

A. Disease control (unmanipulated) heart with RGD probe shows no radiotracer uptake in ex vivo image of the heart. On the other hand, intense CRIP uptake is seen in 4-week untreated (no Rx) post-MI animals (upper panel, right). The uptake in the infarcted area is reduced after neurohumoral treatment with solitary agents and combination therapy (middle and lower panels). Losartan (L) images are displayed twice (middle panel) for the convenience of comparison. C= captopril, S= spironolactone. B. Quantitative Tc-CRIP uptake in the infarct (apex, above) and remote (base, below) areas. The %ID/g uptake in the infarct area is highest in untreated mice, followed by treatment with one (1Rx), two (2Rx) and three (3Rx) agents, respectively. On the other hand, the uptake in the remote area shows no significant differences between treated and untreated animals. Quantitative data confirmed the findings of ex vivo images.

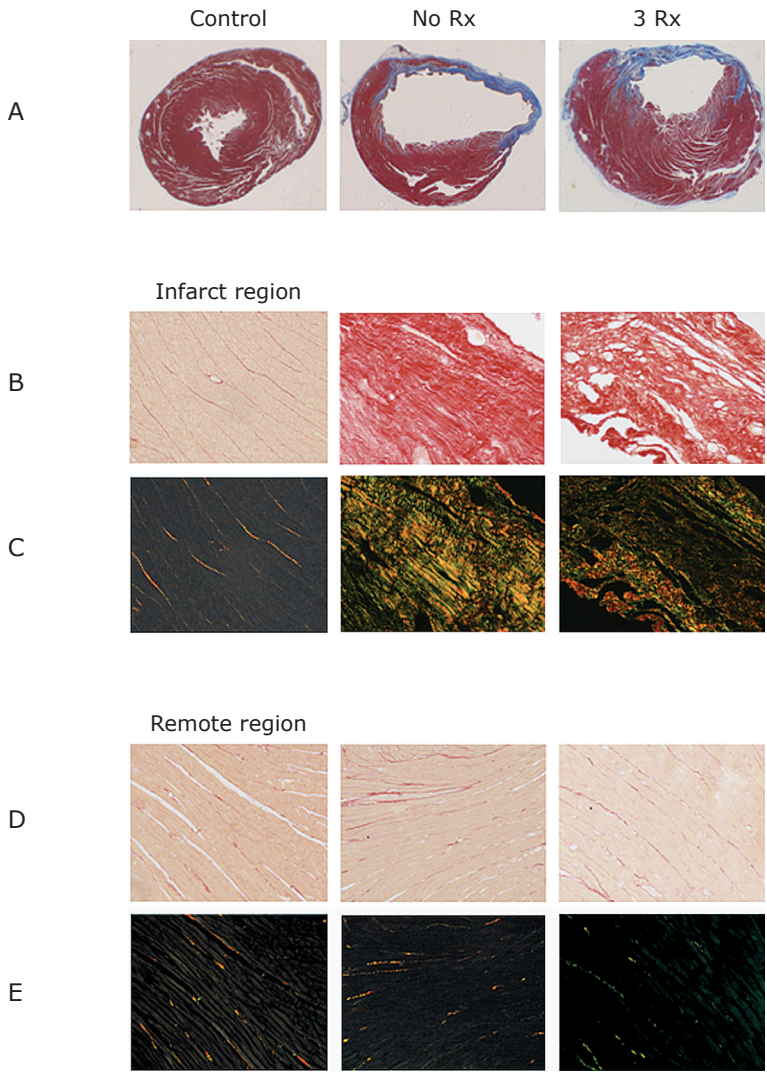

Figure 7.3 **Histopathological characterization of the treated and untreated animals**

Masson's trichrome staining was performed for infarct localization in control, untreated and treated animals (A). In addition, histological staining was performed with picro sirius red to demonstrate collagen deposition, which on polarized light allowed identification of the quality of collagen, in the infarct (B,C) and remote regions (D,E). The left column presents control animals, middle column shows untreated animals (no Rx) and the right column shows animals treated with 3Rx neurohumoral antagonists (SCL). The remote region shows minimal fibrosis and collagen deposition (D). On the other hand, infarct region shows significant wall thinning (A) and fibrosis with evidence of substantial collagen deposition in untreated animals (B, NoRx). 3Rx treated animals show reduced fibrosis (A, SCL) and collagen deposition (B, SCL) in the infarcted area. The Sirius staining under polarized light provides distinction of thick red-orange and thin yellow-green collagen fibers in the infarct region (C).

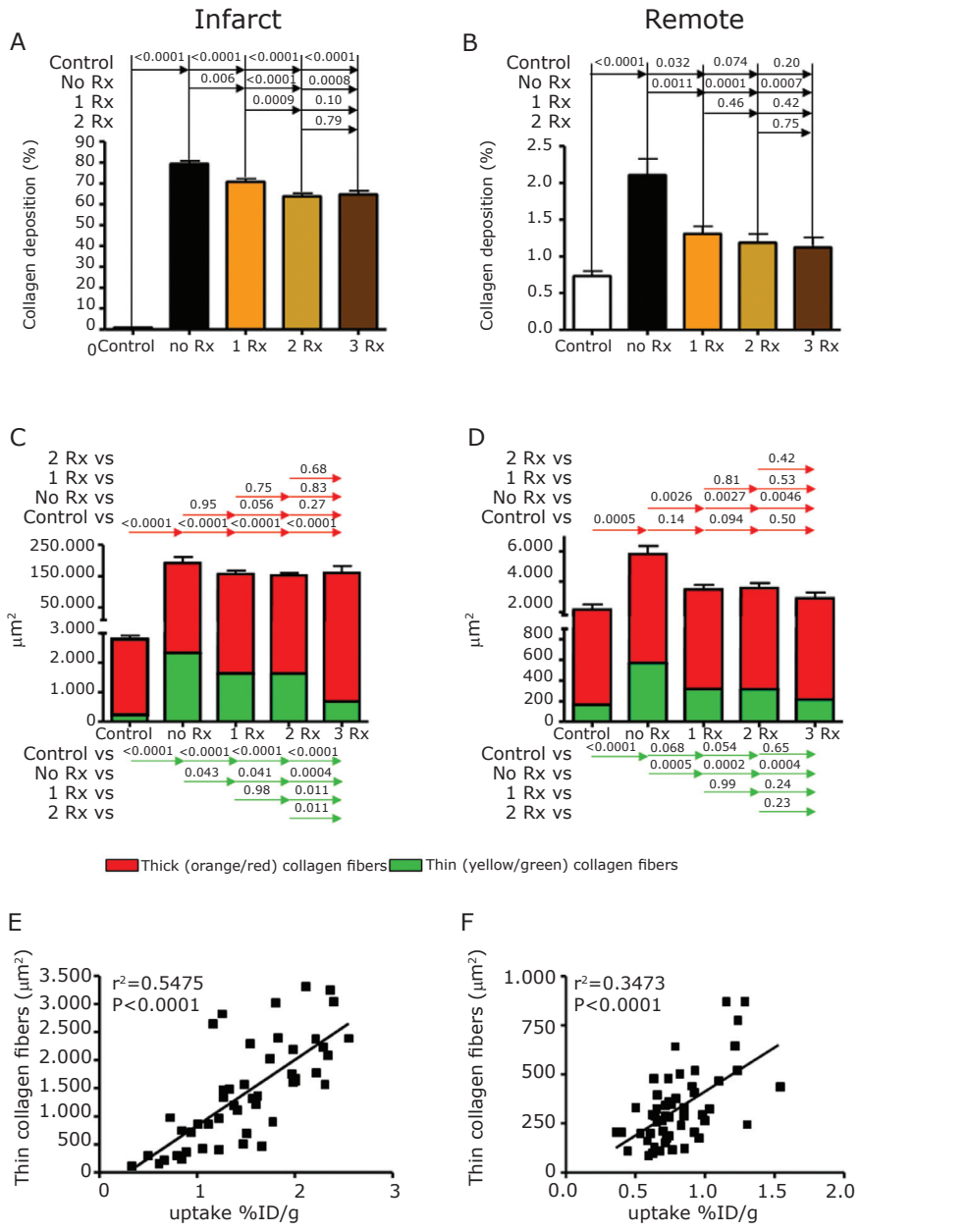

Figure 7.4 **Collagen fiber deposition in infarct and remote regions**

The total collagen content decreases with treatment in the infarcted (A), as well as the remote (B) areas. Further characterization of the collagen fibers by polarization reveals that the thin or new yellow-green collagen fibers decreased both in the infarct (C) and remote (D) regions after treatment. This indicates cessation of new collagen production and maturation of the collagen fibers after treatment. The prevalence of new collagen fibers paralleled the CRIP uptake and demonstrated a significant direct correlation, both in infarct (E) and remote (F) regions. For full color images, see page 174.

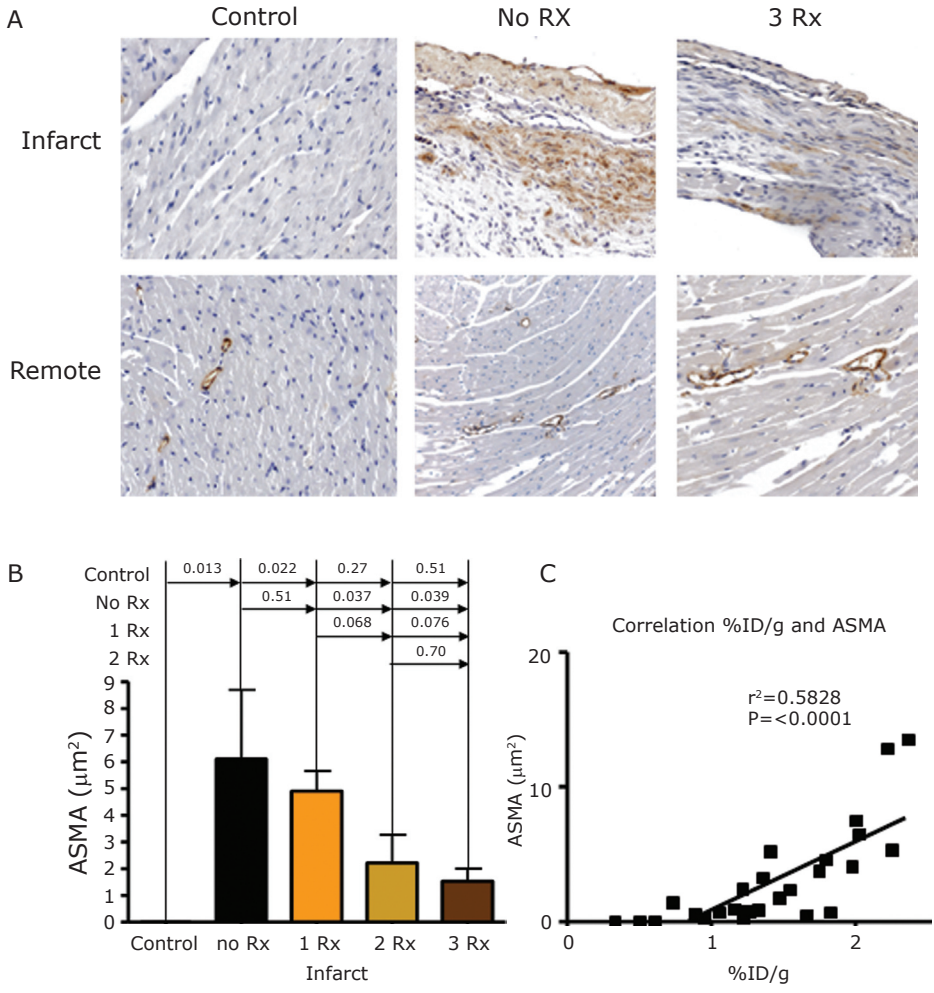

Figure 7.5 **Radiolabeled CRIP uptake and the prevalence of ASMA-verified myofibroblasts**

Immuohistochemical staining with ASMA antibody allowed quantitative assessment of myofibroblasts infiltration in the infarct and remote regions (A). The left column presents control animals, the middle column shows untreated animals (no Rx) and the right column shows 3Rx-animals (SCL). There is a marked decrease in number of myofibroblasts in the infarct region in 2Rx and 3Rx groups (B). There is a significant direct correlation between the extent of myofibroblasts and the CRIP uptake in infarct region (C).

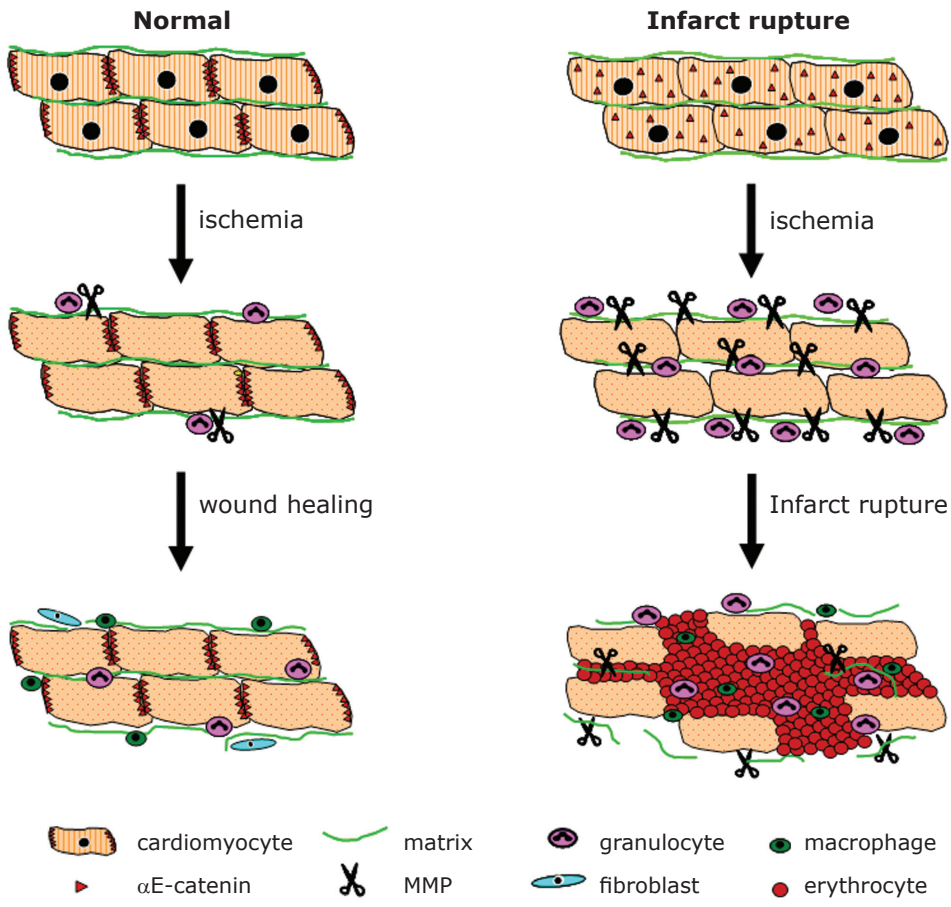

Figure 8.1 **Cartoon of molecular mechanisms that can lead to infarct rupture in humans**

In the left part of the cartoon, the wound healing post-MI in patients with normal infarct healing is shown whereas the right part of the cartoon focuses on the defective wound healing as proposed in infarct rupture patients. In the uninjured cardiomyocytes of normal hearts, αE-catenin is localized in the intercalated disks. Ischemia induces death of the cardiomyocytes in the infarct area, as shown by the loss of their nuclei. However, apparently the adhering cardiomyocytes still can form an effective barrier against inflammatory cells and ventricular blood. In the normal heart, the wound healing will commence and granulation tissue will replace the dead cardiomyocytes, taking over the barrier function against the ventricular blood. In the rupture-prone heart, however, αE-catenin is reduced and poorly localized in the intercalated disks of the cardiomyocytes. After ischemia, this abnormal cell adhesion complex causes the dead cardiomyocytes in the infarct area to loosen up their connections, giving access to more inflammatory cells. The MMPs deposited by these inflammatory cells induce extensive degradation of the extracellular matrix in the infarct area, causing further deterioration of the integrity of the infarct area and subsequently leading to infarct rupture.

DANKWOORD

Eindelijk is het dan zover, het proefschrift is af. Het is een intense periode geweest met vallen en opstaan, met vreugde en frustratie. Een periode waarin ik ontzettend veel heb geleerd. En dat had ik niet kunnen doen zonder een heleboel mensen die me met raad en daad hebben bijgestaan. Bij deze wil ik iedereen die in meer of mindere mate aan dit proefschrift heeft bijgedragen bedanken. Een aantal mensen wil ik hier even uitlichten.

Allereerst natuurlijk mijn promotores en copromotor. Professor Daemen; beste Mat, het is allemaal begonnen naar aanleiding van een student-assistentschap op de vakgroep Pathologie. Uit het onderzoek dat ik daar deed kwamen niet zo'n bijzondere resultaten, maar jij gaf me de mogelijkheid om me verder in het onderzoek te verdiepen in de vorm van een student-aio plaats. Ik ben je ontzettend dankbaar voor die kans en het uiteindelijke resultaat mag er zijn. Je positieve houding, interesse en humor, maar vooral ook je capaciteit om "spijkers met koppen te slaan" had ik soms heel hard nodig.

Professor Smits; beste Jos, graag wil ik je bedanken voor je vertrouwen en positieve houding. Er moeten momenten zijn geweest dat ook jij het somber in zag, maar daar heb je nooit iets van laten blijken. Je bleef me motiveren om door te gaan. Dank ook voor het kritisch nalezen van de manuscripten en het proefschrift. Je kennis van de Nederlandse taal is ongekend.

Dr. Blankesteijn; beste Matthijs, jij was mijn dagelijkse begeleider en je hebt het hele proces vanaf het begin gevolgd. Je hebt de gave om ingewikkelde materie heel duidelijk uit te leggen. Dit leidde regelmatig tot goede discussies waar weer nieuwe ideeen uit voort kwamen. Bedankt hiervoor. Ook de overige mensen van de moleculaire farmacologie mogen hier niet ontbreken. Marielle en Yvonne, bedankt voor de introductie in de moleculaire biologie. Jos P, bedankt voor je hulp met de weefselverzameling. Peter en Lily voor de oneindige hoeveelheid Western blots en QPCR's, Sanna en Cristel voor de gezelligheid, Hilde voor het vele regelwerk en de kletspraatjes en Sander voor alle expertise en gezelligheid die je met je meebracht.

Professor Narula; dear Jagat. I am very grateful for the opportunity of working with you at your lab at the University of California Irvine, USA. You are a true inspiration and a great mentor. Ten minutes of discussion with you leads to an explosion of ideas, each of which you approach with great enthusiasm. Thank you so much……for everything!
Artiom, Nezam, Han, Youping, Peng, Satoshi, Shin and Ai, thank you for al your help in the lab, the nice lunches and great diners.

Ook een woord van dank aan mijn beoordelingscommissie onder leiding van Prof. Crijns en verder bestaande uit Prof. Duncker, Prof. van Engelshoven, Prof. Ramaekers en Prof. van Roy voor de tijd die ze inversteerden in het lezen en beoordelen van mijn proefschrift.

Agnieszka, ontzettend bedankt voor het inzetten van alle dieren. Behalve dat je een fantastische operateur bent, beschik je ook over een goed organizatorisch talent. Ik kon de planning van de geac en het fokken van de dieren dan ook zonder problemen aan je overlaten. Ik heb met ontzettend veel plezier met je samengewerkt. Ook een woord van dank aan Peter, Jaques en Helma. Jullie waren altijd bereid om bij te springen en hebben menig dierexperiment voor me uitgevoerd. Jullie humoristische en nuchtere kijk op het onderzoek was heerlijk om even stoom af te blazen! Ben, bedankt voor al je uitleg en discussies omtrent de geac. Mensen van het CPV, ontzettend bedankt voor het verzorgen van de dieren.

Els, Mia, Mariëlle en Akke, bedankt voor de secretariële ondersteuning. Ger, jouw droge humor werkt erg relativerend. Fazzi, bedankt voor alle hulp met de kleuringen, de gezelligheid en je danscapriolen! Rob Hermans, wandelende encyclopedie, geen vraag was je te gek en wist je het antwoord niet meteen uit je mouw te schudden dan kwam een een tijdje later met een hele stapel literatuur. Ontzettend bedankt voor al je hulp en interesse. Lilian, jij bent altijd in voor een geintje en we hebben dan ook heel wat afgelachen samen. Een woord van dank aan alle oud-collega's en huidige AIO's en post-doc's, bedankt voor de prettige werksfeer!

Dan de MMIT academy onder leiding van Leo Hofstra en Chris Reutelingsperger. Op het moment dat mijn onderzoek op een dood punt zat hebben jullie me geadopteerd. Ik heb met ontzettend veel plezier met jullie samengewerkt. Jullie enthousiaste en vooral vrolijke en nuchtere manier van onderzoek doen werkt erg aanstekelijk. Bedankt voor alle kansen, de samenwerking met Dr. Narula, maar zeker ook de befaamde borrels, in Nederland, Belgie en the USA! Johan, bedankt voor de wetenschappelijke input, maar zeker ook voor de gezelligheid in Irvine, het laatse ritje in de Jeep was onvergetelijk! Reintje, de Cabo Cantina is niet hetzelfde zonder jou! Bedankt voor alle gezelligheid en de vele operaties. Nicole, bedankt dat je altijd voor me klaarstond, je hulp met de dieren en de leuke tijd in Irvine. DJ-Ward, CT koning, helaas geen dj op mijn feestje, bedankt voor de gezelligheid! Abdel, Bas, Sander, Froukje, Ewald, Heidi en Nico, bedankt voor alles!

Van de afdeling Pathologie wil ik graag Maria en Denise en alle arts-assistenten bedanken die hebben meegeholpen om weefsel te verzamelen. Verder een woord van dank aan Anique, bedankt voor de hulp met de immunohistochemie

en het snijden van de vele geac-coupes. Jack C, bedankt voor alle hulp bij het MMP werk en de Quantimet. Ton, bedankt voor de motiverende woorden en je interesse.

De cardio's; Mark, Blanche, Geert, Joost, Nard, Esther en Melissa. We hebben heel wat koffie met pindarotsjes weggewerkt, maar het meeste zijn toch de etentjes blijven hangen. Onder het genot van de beruchte rabarber champagne kwamen de tongen goed los;) Bedankt voor de leuke tijd en de fantastische stapavonden!

A word of thanks for GE Healthcare for providing the imaging agents. A special word of thanks goes to Dr. Lovhaug. Dear Dagfinn, thank you for all your help!

Prof Sussman, thank you for your hospitality in Cincinnati and for the introduction in the wonderful world of confocal microscopy.

Prof. van Roy, Steven en Barbara, heel erg bedankt voor de interessante discussies over catenines!

Een woord van dank aan mijn collega's van het OMC te Sittard. Ontzettend bedankt voor de kansen en voor de ruimte die jullie me gegeven hebben om dit proefschrift af te ronden.

Mijn paranimfen Veerle en Maarten. Veerle, als mede-AIO heb jij mijn onderzoek van dichtbij meegemaakt. Jij weet als geen ander hoe moeilijk het af en toe geweest is. Merciekes voor alle steun, de introductie in de vlaamse taal, de V&S cd, de congresbezoeken, de kilo's chocolade, dansen op de labtafel, de doorbikkel avonden en weekenden met de radio op 10, de vrolijke onderbroeken wedstrijd, maar vooral omdat je een fantastiche vriendin bent. Ik ben heel blij dat jij (voor het eerst relaxed) aan mij zijde zal staan. We made it!

Maarten, mijn andere paranimf. Ik heb een geweldige tijd met je gehad in Irvine, casual friday, tripjes in de cadillac (ik zal er niet over uitweiden, maar ik denk dat ik ALLES op de kaart van Starbucks heb geproeft), video avondjes op het lab of met een stinkende hond (hey, it wasn't me!). Daar naast ben je een enorm gedreven onderzoeker. Ik heb veel bewondering voor de manier waarop jij je in een onderwerp kunt vastbijten en hoe snel je thuis bent in de materie. Heel veel succes met de laatste loodjes!

Many thanks to the great friends I made during my stay in Irvine, they made me feel home in a foreign country. Brenda, Cristina, Sabina, Bindya, Marija, it was fanfreakintastic! I loved our trips and girls nights out. Let plan one again soon! Also many thanks to Raimon, little Andreu, Xevi & Asli, Eric, Roby, Sylvia, Anto

and M&M, Csaba and all the rest of Cat&Co and little Italy. Coming to Irvine is great, again and again!

Ik had dit proefschrift niet kunnen afronden zonder de hulp van mijn vrienden die voor de nodige ontspanning zorgden. Barbara, ook al woon je ver weg, je bleef erg betrokken. Je hebt geen idee hoe blij ik ben dat je weer terugkomt naar NL zodat we elkaar weer vaker kunnen zien en heerlijk kunnen kletsen. Patries, Juul, Birgit, Jen en Esther, ook al zijn we allemaal onze eigen weg gegaan, de keren dat we elkaar zien zij als vanouds. Bedankt voor jullie steun.

Muriel, ik ben ontzettend trots dat jij als eerste je Doctor bul behaald hebt. Je hebt ongelofelijk hard gewerkt. Ook al doen we compleet ander onderzoek, jij begrijpt me. Met jouw murrie-humor weet je me keer op keer weer op te vrolijken. Mieke, bedankt voor de heerlijke ontspannende middagen met je deugenietjes. Simone, snel weer een keertje slingers ophangen? Karlijn, bedankt voor je interesse, elke keer weer. Ai-pin, Pino, de bliksembezoekjes aan de coffee-lovers zijn super om even lekker bij te kletsen. Jessica, Tina, Aimee, bedankt voor de leuke etentjes en stapavonden.

Vito, carinyo, tan lluny pero alhora tan a prop. Thank you for your support, …… and so much more!

Monique, zussie, je hebt fantastisch werkt geleverd, het boekje ziet er dankzij jou prachtig uit. Bedankt ook voor de gastvrijheid, de weekendjes bij jou en Hendrik zijn heerlijk. Henkie, bedankt voor de gezelligheid en alle steun.

Pap en mam, ik kan jullie niet genoeg bedanken voor jullie onvoorwaardelijke steun en vertrouwen in mij. Altijd staan jullie voor me klaar. Het is steeds weer heerlijk om thuis te komen.

Susanne

CURRICULUM VITAE

Susanne W.M. van den Borne werd geboren op 14 februari 1976 te Tilburg. In 1994 behaalde zij haar VWO diploma aan het Sint Odulphus Lyceum in Tilburg. Van 1994 tot en met 1999 studeerde zij Gezondheidswetenschappen aan de Universiteit van Maastricht. Zij volgde de afstudeerrichting biologische gezondheidskunde, waarvoor zij in 1999 haar Masters diploma behaalde. In 1996 startte zij de studie geneeskunde aan dezelfde universiteit en behaalde in 2004 het artsdiploma (cum laude). Tijdens haar coschappen was zij reeds gestart als promovendus bij de vakgroep Farmacologie & Toxicologie onder begeleiding van Dr. W.M. Blankesteijn, Prof. J Smits en Prof. M. Daemen. In 2005 verkreeg zij een beurs van het Van Walree fonds van de KNAW, tevens ontving zij subsidie van de Nederlandse Hartstichting in 2006, beide voor een werkbezoek aan het laboratorium van Prof. J. Narula, Universiteit van California, Irvine, VS. Van 2006 tot 2008 werkte zij als projectcoördinator van het Euregional Platform for Assessment of Cancer Treatment aan de Universiteit Maastricht. Vanaf juli 2008 is zij werkzaam als arts-assistent in het Orbis Medisch Centrum te Sittard.

Susanne W.M. van den Borne was born on February 14th 1976 in Tilburg. She attended the Sint Odulphus Lyceum in Tilburg where she graduated in 1994. From 1994 till 1999 she studied biological health sciences at the University of Maastricht and obtained her MSc degree in 1999. In 1996 she started her medical training at the same university and obtained her medical degree in 2004 (cum laude). During her clinical internships she started as a PhD-student at the department of Pharmacology and Toxicology under supervision of Dr. W.M. Blankesteijn, Prof. J. Smits and Prof. M. Daemen. In 2005 she received a scholarship from the Van Walree fund of the KNAW and in 2006 from the Netherlands Heart Foundation, both to visit the laboratory of Prof. J. Narula, University of California Irvine, CA, USA. From 2006-2008 she worked as project coordinator of the Euregional Platform for Assessment of Cancer Treatment at Maastricht University. Since July 2008 she works as a resident at the Orbis Medical Center in Sittard.

LIST OF PUBLICATIONS

1. Veerle A.M. van de Schans, **Susanne W.M. van den Borne**, Agnieszka E. Strzelecka, Ben J.A. Janssen, Jos L.J. van der Velden, Ramon C.J. Langen, Antony Wynshaw-Boris, Jos F.M. Smits, W. Matthijs Blankesteijn. Interruption of Wnt Signaling Attenuates the Onset of Pressure Overload-Induced Cardiac Hypertrophy. Hypertension 2007;49:473-480.

2. Matthias Nahrendorf, Elena Aikawa, Jose-Luiz Figueiredo, Lars Stangenberg, **Susanne W. van den Borne**, W. Matthijs Blankesteijn, David E. Sosnovik, Farouc A. Jaffer, Ching-Hsuan Tung, Ralph Weissleder. Transglutaminase activity in acute infarcts predicts healing outcome and left ventricular remodeling: Implications for FXIII therapy and antithrombin use in myocardial infarction. European Heart Journal 2008;29(4):445-54

3. **Susanne W.M. van den Borne**, Peter M. Lijnen, Jack P.M. Cleutjens, Jos F.M. Smits, Mat J.A.P. Daemen, W. Matthijs Blankesteijn. A defective cell adhesion complex in cardiomyocytes predisposes to infarct rupture after myocardial infarction in humans. J. Am. Coll. Cardiol. 2008;51:2184-2192.

4. **van den Borne S.W.**, Isobe S, Verjans JW, Petrov A, Lovhaug D, Li P, Zandbergen HR, Ni Y, Frederik P, Zhou J, Arbo B, Rogstad A, Cuthbertson A, Chettibi S, Reutelingsperger C, Blankesteijn WM, Smits JF, Daemen MJ, Zannad F, Vannan MA, Narula N, Pitt B, Hofstra L, Narula J. Molecular imaging of interstitial alterations in remodeling myocardium after myocardial infarction. J Am Coll Cardiol 2008;52:2017-28.

5. **Susanne W.M. van den Borne**, Jack P.M. Cleutjens, Roeland Hanemaaijer, Esther E. Creemers, Jos F.M. Smits, Mat J.A.P. Daemen, and W. Matthijs Blankesteijn. Increased MMP-8 and -9 activation in patients with infarct rupture after acute myocardial infarction. Cardiovascular Pathology 2009;18:37-43.

6. **Susanne WM van den Borne**, Satoshi Isobe, H. Reinier Zandbergen, Peng Li, Artiom Petrov, Nathan D Wong, Shinichiro Fujimoto, Ai Fujimoto, Dagfinn Lovhaug, Jos FM Smits, Mat J.A.P. Daemen, W. Matthijs Blankesteijn, Chris Reutelingsperger, Faiez Zannad, Navneet Narula, Mani A. Vannan, Bertram Pitt, Leonard Hofstra, Jagat Narula. Molecular imaging for efficacy of pharmacologic intervention in myocardial remodeling. J Am Coll Cardiol Img 2009;2:187-98.

7. Zandbergen HR, Sharma UC, Gupta S, Verjans JW, **van den Borne S**, Pokharel S, van Brakel T, Duijvestein A, van Rooijen N, Maessen JG, Reutelingsperger C, Pinto YM, Narula J, Hofstra L. Macrophage depletion in hypertensive rats accelerated development of cardiomyopathy. J Cardiovasc Pharmacol Ther 2009 Jan 22. [Epub ahead of print]

8. **Susanne W.M. van den Borne**, W. Matthijs Blankesteijn, Dagfinn Lovhaug, Johan Verjans, Leonard Hofstra, and Jagat Narula. Molecular Imaging of Myocardial Remodeling: Targeting the Myofibroblasts. Review. Submitted

9. **Susanne W.M. van den Borne**, Veerle A.M. van de Schans, Agnieszka E. Strzelecka, Helena T.M. Vervoort-Peters, Peter M. Lijnen Jack P.M. Cleutjens, Jos F.M. Smits, Mat J.A.P. Daemen, Ben J.A Janssen, W. Matthijs Blankesteijn. Mouse strain determines the outcome of wound healing post-myocardial infarction. Submitted

10. Johan Verjans, **Susanne van den Borne**, Sander Wolters, Satoshi Isobe, Artiom Petrov, Ward Laufer, Michelle Lax, Dagfinn Lovhaug, Hendrikus Boersma, Gerrit Kemerink, Simon Schalla, Chris Reutelingsperger, Paul Gordon, Jaap Teule, Jagat Narula, Leo Hofstra. Molecular Imaging of Integrin Upregulation in Patients after Myocardial Infarction. Submitted

11. H. Reinier Zandbergen, Leo Hofstra, Ewald Dumont, Heidi Kenis, Johan Verjans, **Susanne van den Borne**, Francis D. Blankenberg, Nezam Haider, Artiom Petrov, Navneet Narula, Jagat Narula, Chris Reutelingsperger. Reversibility of phosphatydylserine externalization and apoptosis in the ischemic heart: implications for radionuclide imaging. Submitted